SYNTHETIC AND COMPUTATIONAL STUDIES OF ORGANOMETALLIC COMPLEXES CONTAINING LOW-COORDINATE GROUP 13 LIGANDS

Andrea Rossin

A thesis submitted to the University of Wales in accordance with the requirements for the degree of Doctor of Philosophy in the faculty of Science, Department of Chemistry, University of Wales, Cardiff.

September 2004

ProQuest LLC
789 East Eisenhower Parkway
P.O. Box 1346
Ann Arbor, MI 48106-1346

DECLARATION

This work has not previously been accepted in substance for any degree and is not being concurrently submitted in candidature for any degree.

Signed.....Andrea Rossler.....(candidate)

Date.....24 November '04.....

STATEMENT 1

This thesis is the result of my own investigations, except where otherwise stated.
Other sources are acknowledged by footnotes giving explicit references. A bibliography is appended.

Signed.....Andrea Rossler.....(candidate)

Date.....24 November '04.....

STATEMENT 2

I hereby give consent for my thesis, if accepted, to be available for photocopying and for inter-library loan, and for the title and summary to be made available to outside organisations.

Signed.....Andrea Rossler.....(candidate)

Date.....24 November '04.....

Abstract

The work presented in this thesis is concerned with synthetic and computational studies of low coordinate transition metal complexes of boron. New symmetrically bridged boryl complexes of iron and manganese have been prepared and characterised. Information obtained from spectroscopic and structural analyses, together with Density Functional theoretical studies, has been used to investigate the nature of the metal-boron bonds in these complexes. Development of the chemistry of related terminal analogues has also been undertaken. The M-B bonds present in these molecules can be considered mainly σ in character, with very little π contribution. Attempts to investigate the chemistry of base-stabilised boryl complexes, using PMe_3 and THF as Lewis bases, shows that, while PMe_3 adducts with haloboranes are very stable and do not react with metallic fragments, THF complexes give more promising results, especially when THF is also used as a solvent for the reaction. Substitution and abstraction chemistry of the new (mesityloxy)chloroborane $(MesO)BCl_2$ has been analysed. Replacement of the chlorine atom in $(\eta^5\text{-}C_5H_5)Fe(CO)_2[B(OMes)Cl]$ by other nucleophiles is possible, thereby generating new asymmetric boryl ligands. Chloride abstraction using $Na[BAr'_4]$ leads to the formation of the fluoroboryl complex $(\eta^5\text{-}C_5H_5)Fe(CO)_2[B(OMes)F]$ possibly via the putative terminal borylene $[(\eta^5\text{-}C_5R_5)(CO)_2Fe{=}B(OMes)]^+$. Oxidative addition of B-H, B-B and B-X bonds to both d-block (Rh, Pt) and p-block (In, Sn) metals as an alternative pathway to boryl complexes has also been examined. Unfortunately, while many of the reactions appear to give the expected products (on the basis of insitu NMR monitoring), purification difficulties have prevented the isolation of many of these species as pure compounds. DFT studies on terminal boron- aluminium- and gallium-containing complexes have been undertaken. Geometry optimisation, molecular orbital composition, bond dissociation energies and bond density partitioning have been investigated in order to probe the nature of the M=E bonds (E = B, Al, Ga) and the dependence of compound stability on both the ancillary metal-bound ligands and on the substituent of the group 13 diyl fragment. The examples considered were diyl complexes of general formula $[(\eta^5\text{-}C_5R_5)(L)_2M(EX)]^{n+}$, the "naked" bridging gallium complex $[\{(C_5Me_5)Fe(CO)_2\}_2Ga]^+$ and five gallium carbene complexes of first row transition metals (V, Mn, Fe, Co, Ni), featuring the heterocyclic ligand $\{:Ga[N(Ph)CH]_2\}^-$.

Contents

List of abbreviations used in the discussion

ADF	Amsterdam Density Functional
AO	Atomic orbital
Ar^f	3,5-bis(trifluoromethyl)phenyl
BCat	Catecholboryl -$BO_2C_6H_4$
B(tmg)	Trimethyleneglycolate boryl -$BO_2C_3H_6$
BDE	Bond dissociation energy
9-BBN	9-borabicyclo[3.3.1]nonane -BC_8H_{14}
B88	Becke 88 exchange functional
BP86	Becke 88 exchange plus Perdew 86 correlation functionals
BLYP	Becke 88 exchange plus Lee-Yang-Parr correlation functionals
B3	Becke three-parameter functional
^{n}Bu	Butyl -C_4H_9
^{t}Bu	*tert*-Butyl -$C(CH_3)_3$
bipy	2,2'-Bipyridine $(C_5H_4N)_2$
coe	Cyclooctene C_8H_{14}
CDA	Charge Decomposition Analysis
Cp	Cyclopentadienyl (C_5H_5)
Cp'	Methylcyclopentadienyl [$C_5(CH_3)H_4$]
Cp*	Pentamethylcyclopentadienyl [$C_5(CH_3)_5$]
Cy	Cyclohexyl -C_6H_{11}
Dppm	Bis(diphenylphosphino)methane $CH_2[P(C_6H_5)_2]_2$
Dppe	1,2-bis(diphenylphosphino)ethane $[P(C_6H_5)_2]CH_2$-$CH_2[P(C_6H_5)_2]$
Dppp	1,3-bis(diphenylphosphino)propane $[P(C_6H_5)_2]CH_2$-CH_2-$CH_2[P(C_6H_5)_2]$
Dppb	1,4-bis(diphenylphosphino)butane $[P(C_6H_5)_2]CH_2$-CH_2-CH_2-$CH_2[P(C_6H_5)_2]$
DMSO	Dimethylsulphoxide, $SO(CH_3)_2$
DFT	Density Functional Theory
ETS	Extended Transition State
Et	Ethyl -C_2H_5
ECP	Effective Core Potential

FMO	Fragment Molecular Orbital
Fp	$(\eta^5\text{-}C_5H_5)Fe(CO)_2$
Fp'	$[(\eta^5\text{-}C_5H_4(CH_3)]Fe(CO)_2$
Fp*	$[(\eta^5\text{-}C_5(CH_3)_5]Fe(CO)_2$
GGA	Generalised Gradient Approximation
GTO	Gaussian Type Orbital
HF	Hartree-Fock
LCAO-MO	Linear Combination of Atomic Orbitals - Molecular Orbitals
HOMO	Highest Occupied Molecular Orbital
IR	Infrared spectroscopy
Me	Methyl $-CH_3$
Mes	Mesityl (2,4,6-trimetylphenyl) $-C_6H_2(CH_3)_3$
MO	Molecular Orbital
nbn	Norbornene C_7H_{10}
NMR	Nuclear Magnetic Resonance
Ph	Phenyl $-C_6H_5$
^{i}Pr	Isopropyl $-CH(CH_3)_2$
PPN^+	Bis-(triphenylphosphoranylidene)ammonium $[(C_6H_5)_3P{=}N{=}P(C_6H_5)_3]^+$
PGTO	Primitive Gaussian Type Orbital
SOMO	Singly Occupied Molecular Orbital
SCF	Self Consistent Field
STO	Slater Type Orbital
THF	Tetrahydrofuran C_4H_8O
TMEDA	N,N,N',N'-tetramethylethylenediamine $(CH_3)_2N\text{-}CH_2\text{-}CH_2\text{-}N(CH_3)_2$
Wp	$(\eta^5\text{-}C_5H_5)W(CO)_3$
Wp'	$[(\eta^5\text{-}C_5H_4(CH_3)]W(CO)_3$
Wp*	$[(\eta^5\text{-}C_5(CH_3)_5]W(CO)_3$

Acknowledgments

...Once I read on someone's thesis that a PhD is a matter of endless thanking, and I believe it is very true. In every single day of my PhD time there was someone to thank for something, and the list of acknowledgments is really long. It is impossible for me to quote in a few lines all the names of people I would like to thank, but I will try anyway.

First, my supervisor Dr. Simon Aldridge, for all his ideas, guidance and motivation he provided during the last three years. I also thank him for all the practical things he taught me, for what he did for me at the beginning of my stay in Wales and for making me work with an "industrial" timetable, keeping the total number of my Italian coffee breaks under control! I still struggle to see him as a boss, because of our similar age, and I would rather remember him as a friend and a colleague.

Sincere thanks also to my "acquired second supervisor" Dr. David Willock, who helped me sailing the ocean of numbers and figures coming out of the ADF output files and disclosing the secrets lying under the cryptic Unix programming language. He adopted me as a student when I started the DFT calculations. I admire his reassuring approach to the theoretical problems, because even when the situation seemed tragic to me (very often I have to say), he has always found a way to sort things out. God bless him.

A very important part was played by all the people who were working with me in both the experimental and theoretical labs, with whom I shared a lot of funny moments, trying to forget about things that were not working. A big hug to Deborah Coombs/Kays, Richard (Riccardo) Calder, Miles Burrows, Rebecca Baghurst, Robert Strevens, Clare (Clara) Wastgaffe, Lisa (St)ratford, Amal Al-Fawaz, Christopher Bresner, Natalie (Olivia Newton) Bunn, Mark (Marco) Jones, Ruth Osiname, Rudy Coquet, Arturo Robertazzi, Farah Huque, Rajinder Mann and many others I will not name; they will always be with me. I also thank them for the English language "pearls of wisdom" they taught me, reminding me that there is not only the Queen's English to learn...

Coming to Wales was not only a job experience, but also a life adventure, and during this time I have stumbled across a lot of different people and cultures; each one has left me something to appreciate. The little (well, not so little now, but it really was three years ago) Italo-Spanish community I found in this place has been vital, and I want to thank all the friends coming from it: Silvio, Marco(I), Federica, Gerolamo, Maria, Nagore, Ziortza, Santiago, Claudia, Josè, Daniele, Javier, Txell, Elisenda, Carmela, Matteo, Caterina, Cristina, Rubén, Laura, Roberta, Deborha, Antonio, Marco(II), Pablo, Benjamin, Mariangeles, Tomàs. We spent so many hours together, complaining about the things of Italy and Spain that we miss in the UK!! I had some unforgettable times with them, and I wish them all the best for their future. To all the Spanish friends, thanks for teaching me Spanish, I will put it to good use.

A special thought for the housemates of 90 Newfoundland Road, the place where I settled down two weeks after I had arrived, and never left over three years time. How many memories of this house...living with Rosie, Nadine, Catherine, Nicola, "Kliff" Florent, Katja, Susannah, Nick, Steffan, Andy, Raùl and Fabrizio. Thanks for having been patient with me and my little obsessions...the consequences of a stressful student life!

Finally, the biggest thanks of all go to Mum, Dad and my sister Manuela, for their constant support and understanding and for having done all they could to make me lead a normal life in Wales (so different from Italy). I missed them a lot in Cardiff. I will be eternally grateful.

1 - Introduction

The chemistry of boron, the only non-metal of group 13, is characterised by a remarkable Lewis acidity, due to the fact that it possesses four valence orbitals (2s, $2p_x$, $2p_y$ and $2p_z$) but only three valence electrons available for bonding. Hence the tendency to form three-centre two-electron bonds (electron-deficient), especially with hydrogen. The large number of known boranes $[B_nH_m]^{x-}$ is an experimental verification of this. In its combinations with transition metals, boron displays a unique structural diversity, ranging from ionic to covalent and metallic bond types. Examples of these classes are metallic *borides* (binary compounds of general formula M_xB_y), with both boron-poor and boron-rich phases, *metallaboranes*[1] (formally derived from the parent boranes by replacing one or more boron atoms with metal atoms) and π *complexes* with boron-containing ligands derived from conjugated boron heterocycles (e.g. borole, boratabenzene, borazine)[2].

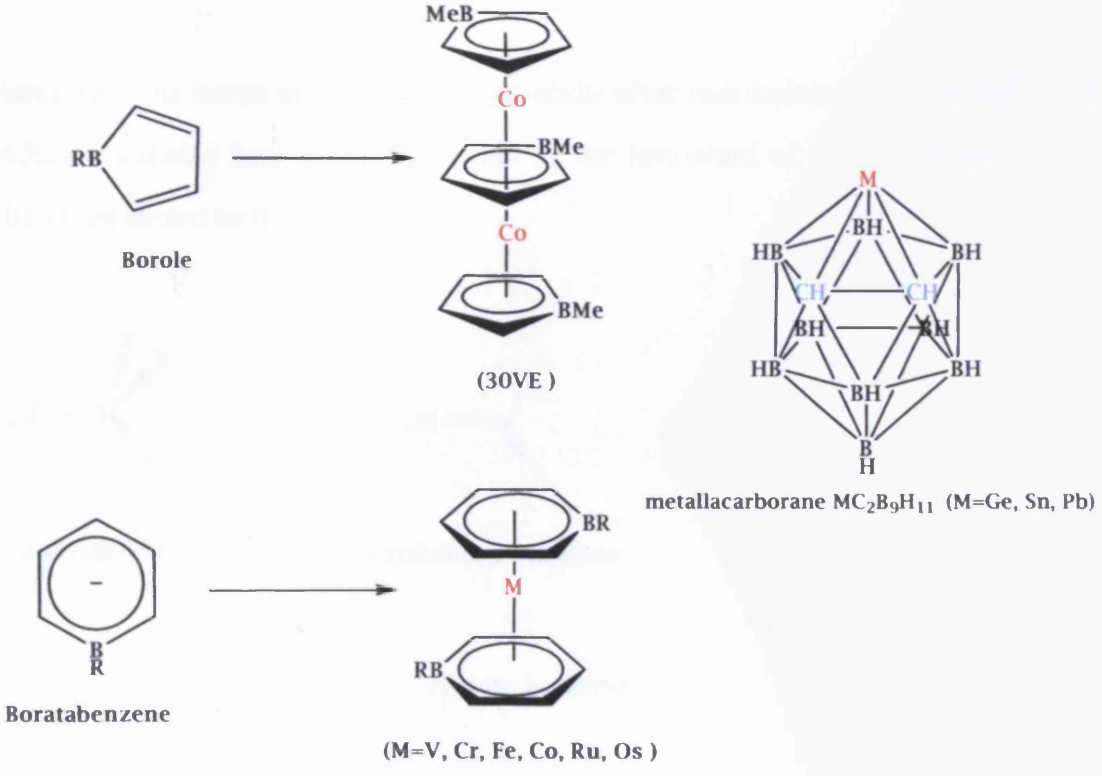

Figure 1 - Examples of boron organometallics

In addition to these classes of compounds, there is another well-established one, where the metal-boron interaction consists of an electron-precise two-centre two-electron bond. The

examples found in this category can be systematically classified according to the coordination number of boron and the number of metal-boron bonds: boryl complexes, containing a BR_2 mojety linked to a metal centre via single σ bond, terminal borylene complexes, where a BR fragment is linked to a single metal atom via either a double bond or a donor-acceptor interaction, and bridging borylene complexes, where the BR fragment forms two σ bonds with two or more different metal atoms.

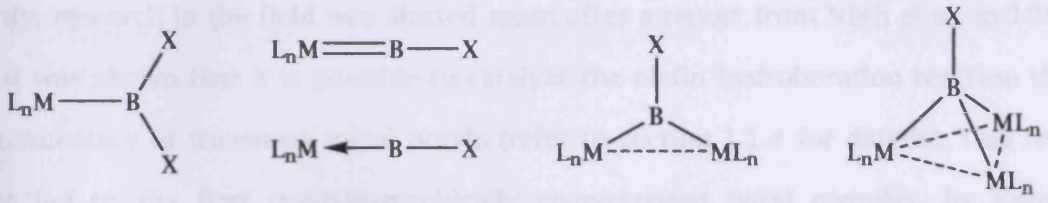

Boryl Terminal Borylene Bridging Borylenes

Figure 2 - Different coordination modes of low-valent boron containing ligands

Providing that the boron atom is still Lewis acidic after coordination, there is the possibility of adding a suitable base L, which results in the formation of base-stabilised boryls and borylenes, as shown in Figure 3.

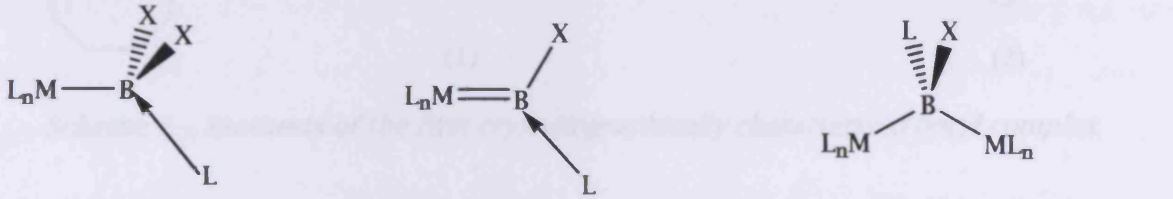

Base-stabilised boryl Base-stabilised borylene Base-stabilised bridging borylene

Figure 3 - Borylenes

1.1 - Transition metal boryl complexes [3]

1.1.1 - Historical overview

Among transition metal complexes of boron, the group of boryl compounds $L_nM\text{-}BX_2$ is the largest one, comprising more than 70 structurally authentic examples up to date. The very

first references to boryl complexes date back to the early 1960s, and Schmid reviewed the work done in the field 10 years later[4]. Several species derived from carbonylmetal and phosphine-carbonylmetal fragments were reported, including examples such as $(CO)_5Mn$-$B(NMe_2)_2$, $(\eta^5\text{-}C_5H_5)Fe(CO)_2\text{-}BCl_2$ and $(CO)_4(PPh_3)Mn\text{-}BPh_2$, but their identification was only based on IR and elemental analysis data. The lack of a crystallographic characterisation, together with contradictory ^{11}B-NMR data that has been reported by more recent investigations[5,6], casts considerable doubt on the correct formulation of these compounds. After a period of inactivity, research in the field was started again after a report from Nöth et al. in 1985[7], in which it was shown that it is possible to catalyse the olefin hydroboration reaction through the intermediacy of transition metal boryls (refer to section 1.1.4 for details). This renewed interest led to the first crystallographically characterised boryl complex, by Knorr and Merola in 1990[8]. *Mer*-Ir(H)(BCat)(Cl)$(PMe_3)_3$ 2 was obtained via oxidative addition of HBCat 1 at an iridium(I) centre.

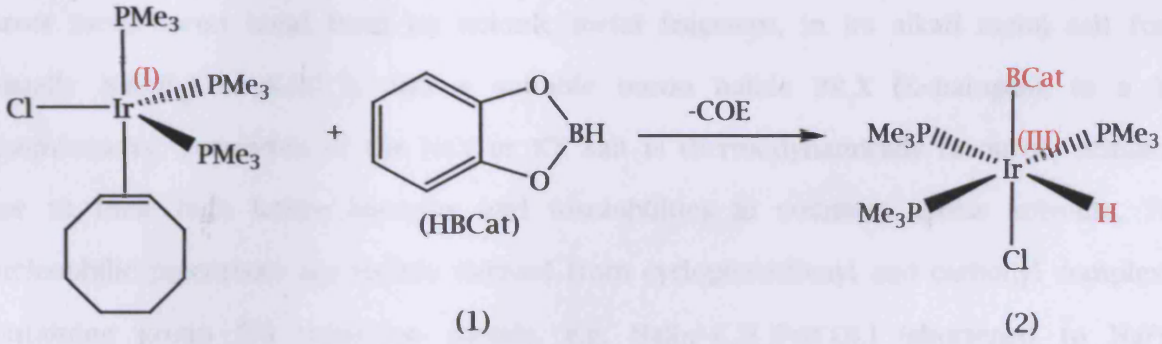

Scheme 1 – Synthesis of the first crystallographically characterised boryl complex

This compound contains the catecholboryl ligand (catecholate=1,2-dioxophenylene $O_2C_6H_4$-1,2), which is one of the most common boryl ligands, being found in ca. 50% of the structurally authenticated boryl complexes reported in the literature. Of relevance to this thesis is more recent research effort which has focused on the synthesis and characterisation of base-stabilised boryls, following the first example reported by Kawano et al. in 1999[9].

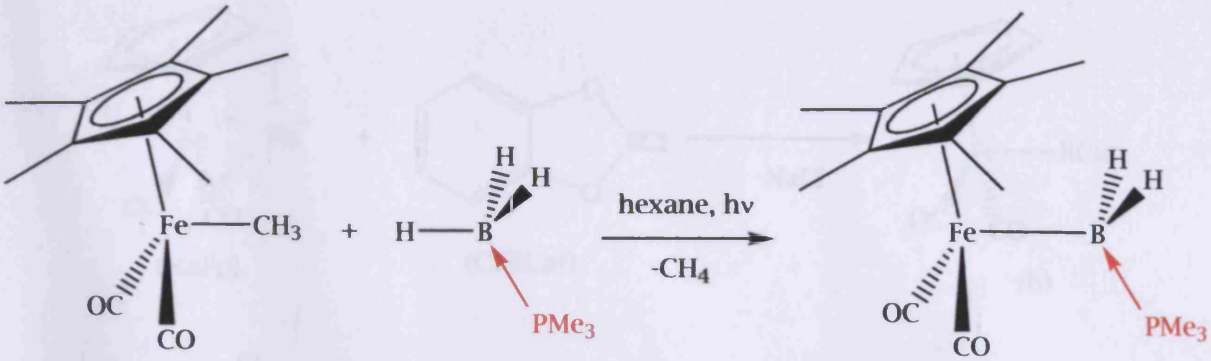

(3) (4) (5)

Scheme 2 – Synthesis of the base stabilised boryl $Cp^*Fe(CO)_2[BH_2.PMe_3]$ (5)

1.1.2 – Synthetic pathways to boryl- and base-stabilised boryl complexes

The main routes used to make boryl metal complexes are *metathesis* (salt elimination) and *oxidative addition* to low-valent metal centres. Metathesis consists of the formation of a direct metal-boron bond from an anionic metal fragment, in its alkali metal salt form (usually $Na(ML_n)$ or $K(ML_n)$), and a suitable boron halide BR_2X (X=halogen), in a 1:1 stoichiometry. Formation of the NaX or KX salt is thermodynamically favoured, primarily due to their high lattice energies and insolubilities in common apolar solvents. The nucleophilic precursors are mainly derived from cyclopentadienyl and carbonyl complexes containing group 5-8 transition metals, e.g. $Na[(\eta^5\text{-}C_5H_5)Fe(CO)_2]$ (shortened to NaFp), $Na[Mn(CO)_5]$, $Na[(\eta^5\text{-}C_5H_5)W(CO)_3]$ (NaWp), $K[(\eta^5\text{-}C_5H_5)_2TaH_2]$. The boron halide can contain a variety of peripheral substituents, and this methodology has also been extended to derivatives of diborane(4)[10] $X_2B\text{-}BX_2$ and of borazine (like 7)[11].

$$X\text{-}BR_2 + C^+ML_n^- \longrightarrow R_2B\text{-}ML_n + C^+X^-$$

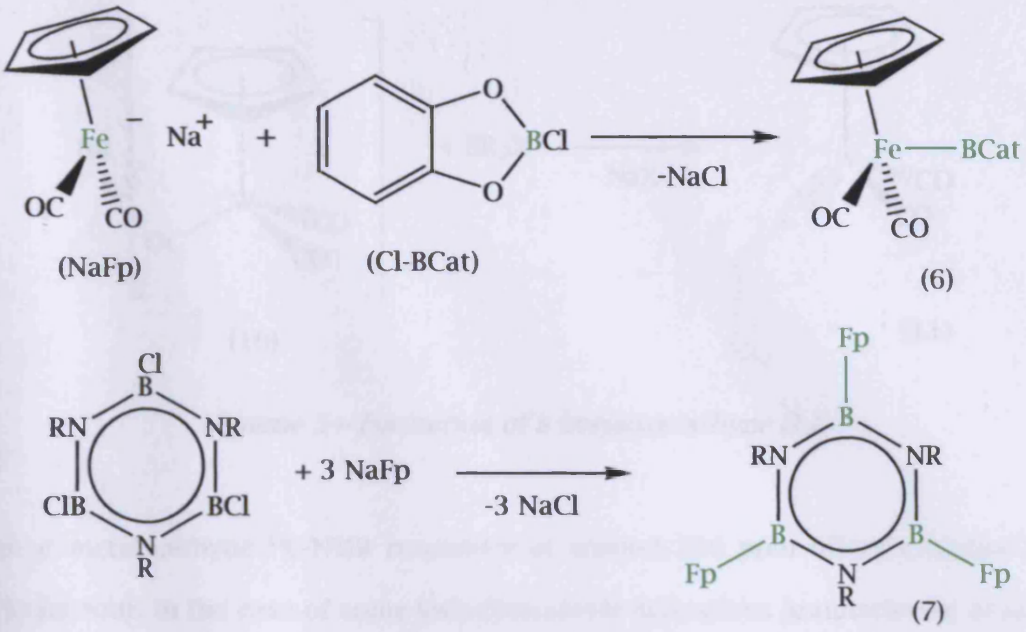

Scheme 3 – Examples of salt elimination reactions

If a *dianionic* metal fragment Na_2ML_n is used as a precursor, *bis-boryl* complexes can be obtained by the same method, by employing a 1:2 stoichiometry [12].

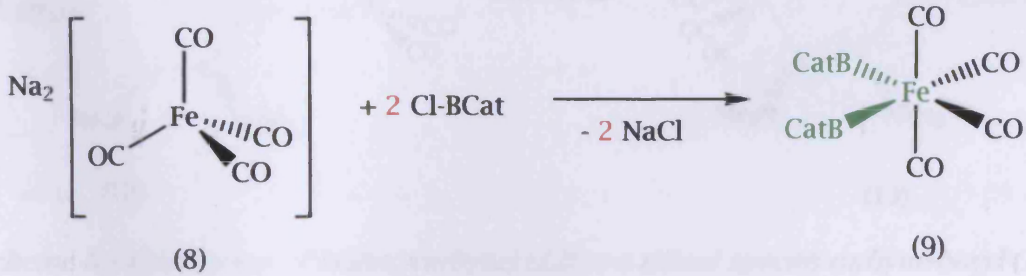

Scheme 4

It is not always the metal atom that is the most nucleophilic centre of the anion; in the case of the group 6 metal derivatives $Na[(\eta^5\text{-}C_5H_5)M(CO)_3]$ (M=Mo, W) there is spectroscopic and crystallographic evidence that the carbonyl oxygen atom also displays some nucleophilic character, leading to the formation of a *boryloxycarbyne* instead of a boryl complex[13].

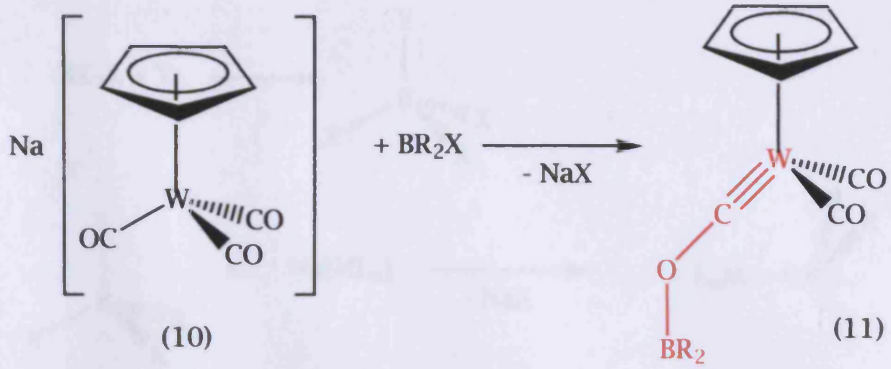

Scheme 5 – Formation of a boryloxycarbyne (11)

The typical metal carbyne ^{13}C-NMR resonance at around 250 ppm offers evidence for this type of behaviour. In the case of some iododiborane(4) derivatives Braunschweig *et al.*[13] have obtained crystal structures of the reaction products, which can be either of bis(oxycarbyne) nature or a "mixed" species, with both carbyne and boryl functionalities present.

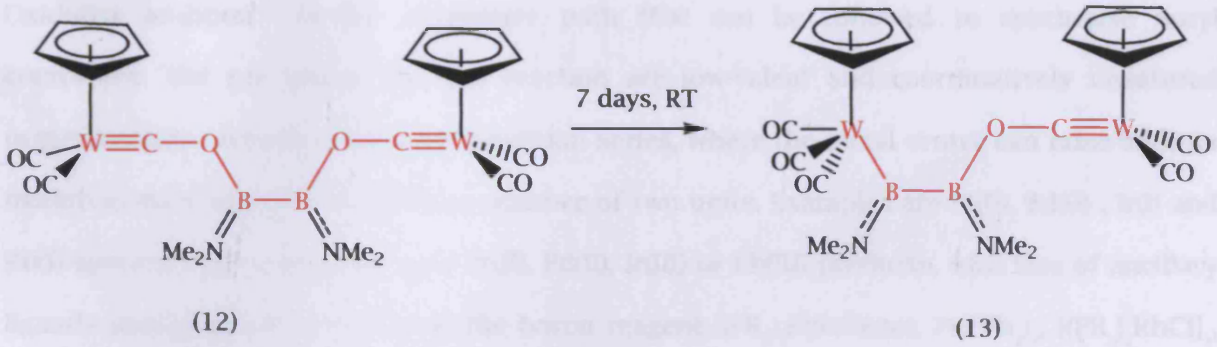

Scheme 6 – Conversion of bis(oxycarbyne) (12) to a mixed species carbyne-boryl (13)

Base-stabilised boryls can also be prepared via salt elimination, in this case starting from a Lewis base adduct of a suitable boron-containing species:

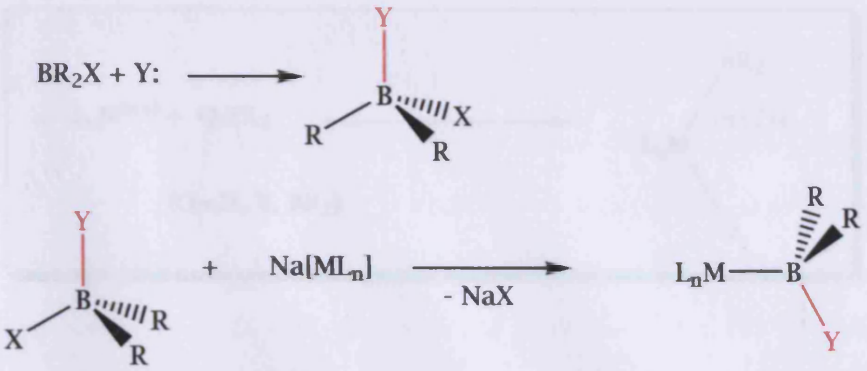

Scheme 7 - Synthesis of a base-stabilised boryl complex

This is an alternative method to the photolytic preparation of the iron complex 5 depicted in Scheme 2. An important fact about these syntheses is that the base must be added *before* the preparation of the complex, because an addition of base to a solution of boryls $L_nM\text{-}BR_2$ typically leads to decomposition rather than to a base-stabilised product[3a,3b,3e].

Oxidative addition[14] is the alternative path that can be followed to synthesise boryl complexes. The precursors for this reaction are low-valent and coordinatively unsatured organometallics typical of the late transition series, where the metal centre can raise both its oxidation state and its coordination number of two units. Examples are Pt(0), Pd(0) , Ir(I) and Rh(I) species, which can easily give Pt(II), Pd(II), Ir(III) or Rh(III) products, with loss of ancillary ligands preceding coordination of the boron reagent: $(PR_3)_2Pt(ethene)$, $Pt(PPh_3)_4$, $[(PR_3)_2RhCl]_2$, etc. Ligand dissociation to generate a highly reactive intermediate can also be achieved, for example, by irradiation of a less reactive precursor complex. This technique has been used to perform oxidative addition reactions on middle transition metals (Nb, Ta, Mo, W, Fe). A variety of bonds have proved amenable to oxidative addition in this way (e.g. B-B, B-H, B-X, B-Si and B-Sn), thereby giving access to a large number of complexes containing one, two or even three boryl groups. However, the boron-boron bonds of diborane(4) derivatives and boron-hydrogen bonds of boranes have been exploited most readily. Some examples are illustrated in Scheme 8.

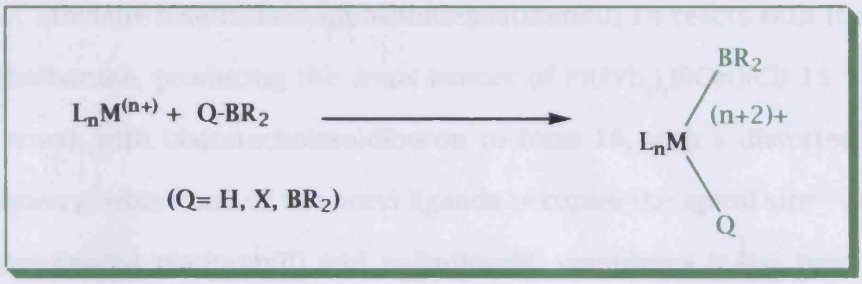

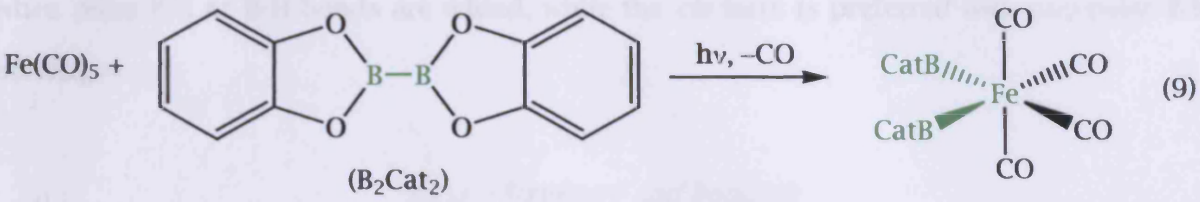

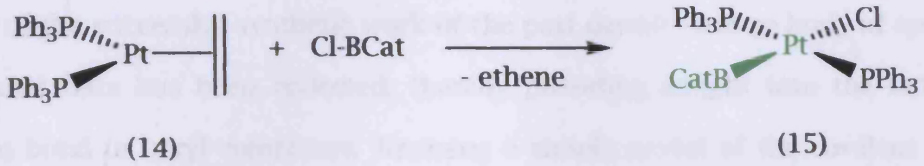

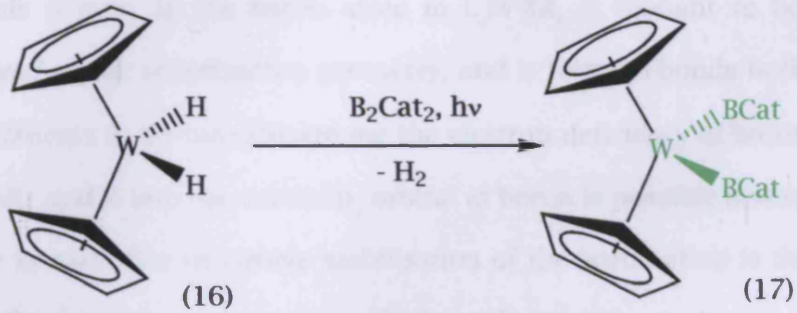

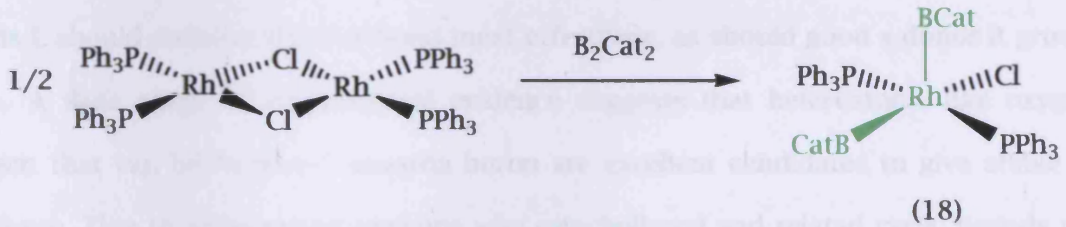

Scheme 8 – Examples of oxidative addition

The iron derivative 9, $(CO)_4Fe(BCat)_2$ can be obtained via oxidative addition of B_2Cat_2 to the reactive $[Fe(CO)_4]$ unit, generated *in situ* by irradiation of iron pentacarbonyl[15]. Similar reactivity is reported for the tungstenocene hydride Cp_2WH_2 16, which is turned into $[Cp_2W]$ upon UV irradiation, with a vacant coordination site on tungsten that is readily occupied by

boryl ligands[10]. Ethylene bis-(triphenylphosphine)platinum(0) 14 reacts with the B-Cl bond of B-chloro-catecholborane, producing the *trans* isomer of $Pt(PPh_3)_2(BCat)(Cl)$ 15[14a]. The dimeric $[RhCl(PPh_3)_2]_2$ reacts with bis(catecholato)diboron to form 18, with a distorted square-based pyramidal geometry, where one of the boryl ligands occupies the apical site[14c]. In the square-planar four-coordinated platinum(II) and palladium(II) complexes it has been noticed that, because of the *trans*-effect of the substituents, the *trans* isomer is the most stable product when polar B-X or B-H bonds are added, while the *cis* form is preferred with non-polar B-B bonds.

1.1.3 - Structure and bonding

As a result of the successful synthetic work of the past decade, a large body of spectroscopic and structural data has been collected, thereby providing insight into the nature of the metal-boron bond in boryl complexes. Applying a simple model of the covalent bonding in these compounds (Figure 4), the boron atom in L_nM–BR_2 is thought to be sp^2 hybridised, showing a *trigonal planar* coordination geometry, and it forms σ-bonds both with the metal M and the substituents R. To compensate for the electron deficiency at boron, competitive *π-donation* from ML_n and R into the vacant p_z orbital at boron is possible (assuming that the M-BR_2 plane is the xy one). The electronic stabilisation of the boron atom is therefore strongly affected by both the metal fragment and the substituents on boron itself. Generally speaking, late transition metals (more electron-rich than the early ones) with good σ-donor ligands L should stabilise the M-B bond most effectively, as should good π donor R groups at boron. A wide range of experimental evidence suggests that heteroatoms like oxygen or nitrogen that can be "π-bases" towards boron are excellent candidates to give stable boryl complexes. This to some extent explains why catecholboryl and related cyclic ligands are so widespread, while other ligands still represent a small minority.

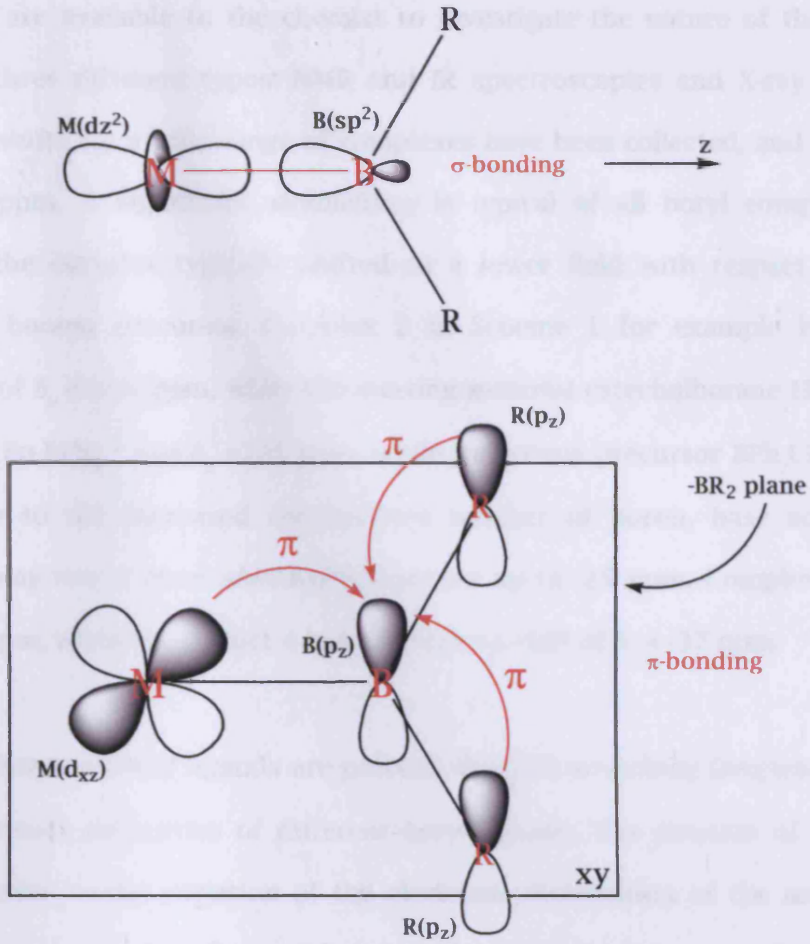

Figure 4 – Bonding in transition metal boryl complexes

For base-stabilised boryl complexes, the hybridisation at boron is sp^3, and the coordination geometry is tetrahedral, like in all the four-coordinate boron compounds. The extra-stabilisation in this case is provided by the Lewis base Y: , which donates its lone pairs to the boron orbitals of suitable symmetry.

The M-B bond in boryl complexes can be considered to be mainly covalent, with a little electrostatic contribution deriving from the polarisation $M^{\delta-}$-$B^{\delta+}$. It is thermodynamically much more stable than the corresponding metal-carbon bonds in alkyl complexes L_nM-CR_3 with respect to homolytic dissociation. In spite of this, the M-B bond is fairly reactive, and indeed many complexes are quite labile, being readily susceptible to nucleophilic attack with subsequent cleavage and degradation. In other words, boryl complexes are often *kinetically unstable*, especially with respect to nucleophiles.

The tools that are available to the chemist to investigate the nature of the M-B bond are essentially of three different types: NMR and IR spectroscopies and X-ray diffraction. ^{11}B-NMR chemical shifts for a wide range of complexes have been collected, and they vary in the range 24-141 ppm. A significant *deshielding* is typical of all boryl complexes, with the resonance of the complex typically shifted to a lower field with respect to that of the corresponding borane precursor. Complex 2 in Scheme 1 for example has a measured chemical shift of δ_B =32.8 ppm, while the starting material catecholborane HBCat has δ_B =28 ppm. Complex Fp-BPh_2[17] has δ_B =121 ppm, while its borane precursor BPh_2Cl resonates at δ_B =61 ppm. Due to the increased coordination number of boron, base adducts of boryl complexes display much more *shielded* resonances up to -25 ppm. Complex 5 in scheme 2 has δ_B = -25.1 ppm, while the adduct 4 has a measured shift of δ_B = -37 ppm.

In molecules where carbonyl ligands are present, IR ν(CO) stretching frequencies are used to gauge the electronic properties of different boryl ligands. The position of such bands are extremely sensitive to the variation of the electronic distribution of the molecule. When a better σ-donor is attached to the metal centre, the metal itself is more electron-rich, and a part of this electron density is transferred into the π* MO of CO. This causes a reduction of C-O bond order and of the related stretching frequency. The opposite trend is observed for a good π-acceptor ligand. A number of structural and spectroscopic observations imply that boryl ligands are stronger σ donors than their alkyl or hydride counterparts[3c]. Thus a (η^5-C_5H_5)$Fe(CO)_2$ (Fp) complex containing a boryl ligand with no π acceptor properties at all might be expected to show somewhat lower carbonyl stretching frequencies than the analogous alkyl complex. That most Fp boryl complexes display ν(CO) wave numbers similar to, or *slight in excess of*, those of Fp alkyls attests to an (albeit minor) π acceptor role. Such role is obviously "tuned" in a various way by the nature of the substituents R on BR_2. As a consequence, regular trends in the variation of ν(CO) of families of similar complexes are not easily found[30].

X-ray diffraction is the most powerful of the three techniques mentioned, because, besides providing the definitive atomic connectivity, it also gives precise geometrical data (bond

lengths and angles) that can be used to infer extra information about the nature of the bonds present in the molecule. As a general trend, the early-middle transition metals give a M-B distance that is longer than the sum of the atomic radii, while late transition series give a M-B distance that is shorter, indicating the presence of a higher degree of π bonding. The final relative position of the $-BR_2$ moiety with respect to the ML_n fragment is determined by *both electronic and steric factors*. An example is the family of compounds of general formula $(\eta^5\text{-}C_5L_5)Fe(CO)_2(BR_2)$, where L can be either hydrogen or methyl, and the boryl fragment contains different substituents. The electronic factors would suggest that, according to the MO scheme of the fragments, all the possible geometries are stable, because it is always possible to have a stabilising interaction between boron and iron, no matter what the dihedral angle θ is (θ is defined as the angle C_5L_5(centroid)-Fe-B-R, refer to figure 5). Hence, the final real geometry is determined mainly by steric hindrance of the R substituents and the L groups on the cyclopentadienyl ring, or by crystal packing forces. The combination of the two effects gives rise to a wide range of values for θ, going from ca. 8° to 90° [17].

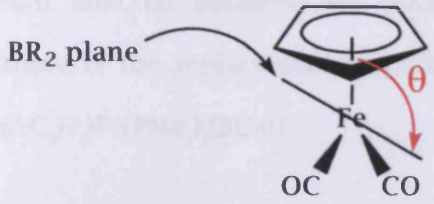

Figure 5 – Definition of the dihedral angle θ

1.1.4 – Chemistry of boryl complexes and applications in homogeneous catalysis: hydroboration /diboration of olefins and alkane activation

Following the discovery of catalytic activity by transition metal boryl complexes in olefin hydroboration, studies of the fundamental reactivity of these organometallics have become more numerous. Their chemistry is diverse, and there are three main modes of reactivity: (i) reactions involving *the metal centre;* (ii) reactions occurring *at the boryl ligand itself*, with retention of the M-B bond; and (iii) reactions involving the *M-B bond*.

(i) - *Reactions involving the metal centre.* The first category mainly involves ligand exchange processes that do not cleave the M-B bond. The ligands L of the fragment ML_n can be replaced by phosphines or other Lewis bases like CO, in some cases with concomitant increase of the coordination number of the metal (ligand addition rather than substitution). This pathway can be used as an alternative synthetic path to particular complexes, and in some cases offers a route to make a metal-boryls which are otherwise inaccessible. Thus, substitution of monodentate phosphines with a bidentate (chelating) one has been used to generate derivatives of the general formula *cis*-$(PR_3)_2Pt(BR_2)_2$[18]:

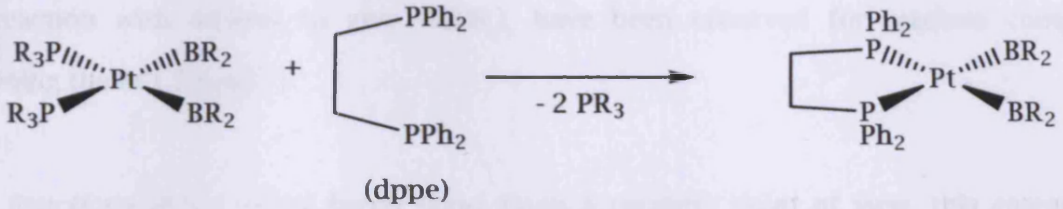

Scheme 9 - Ancillary ligand exchange on boryl complexes

In this case the product could also be obtained via oxidative addition of $R_2B\text{-}BR_2$ to Pt(dppe)(ethene). Another example is the replacement of carbonyl ligands in Fp-BCat with PMe_3 upon irradiation, to get $(\eta^5\text{-}C_5H_5)Fe(PMe_3)_2(BCat)$[19].

(ii) - *Reactions that occur at the boryl ligand.* Reactions that occur at the boron centre without breakage of the M-B bond are rare in comparison to other modes of reactivity, and they have been the subject of investigation of this research group[30]. Thus the synthesis of the first cationic borylene complex 27 (scheme 25, pag.26) and of "asymmetric" boryl complexes $L_nM\text{-}BR_1R_2$, starting from the corresponding haloboryl $L_nM\text{-}BRX$ have been demonstrated.

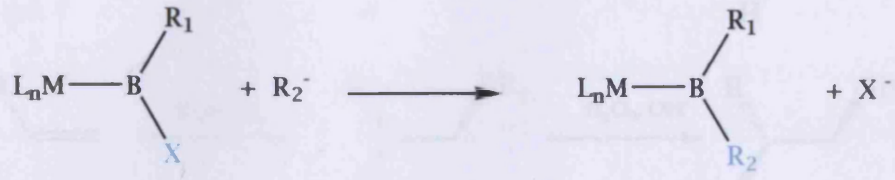

Scheme 10 - Substitution at boron

As already been mentioned, the metal-boron bond in boryl systems is labile and tends to be cleaved even under mild conditions; this to some extent rationalises the limited number of examples of reactions falling into this category. The presence of halide substituents (which can be easily displaced by a range of different nucleophiles) helps the substitution chemistry at boron to take place. Since some examples of this chemistry are also the subject of a part of the present thesis, see section 3.3.4 for further discussion. In general this kind of reaction happens when the groups R on boron are not efficient enough at stabilising its vacant p orbital (i.e. they are not very good π donors). Hydrolysis to $-B(OH)_2$, alcoholysis to $-B(OR)_2$ and reaction with amines to give $-B(NR_2)_2$ have been observed for osmium complexes containing the BCl_2 ligand[20].

(iii) - *Reactions at the metal boron bond.* From a catalytic point of view, this category of reaction is the most interesting, because it is in part due to the lability of the metal-boron bond that it is possible to use these complexes as homogeneous catalysts in fundamental organic transformations. *Hydroboration* of carbon-carbon multiple bonds is an addition of an $H\text{-}BR_2$ molecule, while *diboration* is an addition of a $R_2B\text{-}BR_2$ unit[21]. The uncatalysed reaction is regioselective (anti-Markovinkov direction, with the $-BR_2$ group attached to the less substituted carbon atom), stereoselective (with a *cis*-addition due to the presence of a cyclic four-centre intermediate) and reversible. The resulting organoboron compound can then be oxidised with hydrogen peroxide in basic conditions to get the corresponding mono- or dialcohol. These alcohols are in turn employed as starting materials for other fine organic chemicals (ketones, aldehydes, etc...).

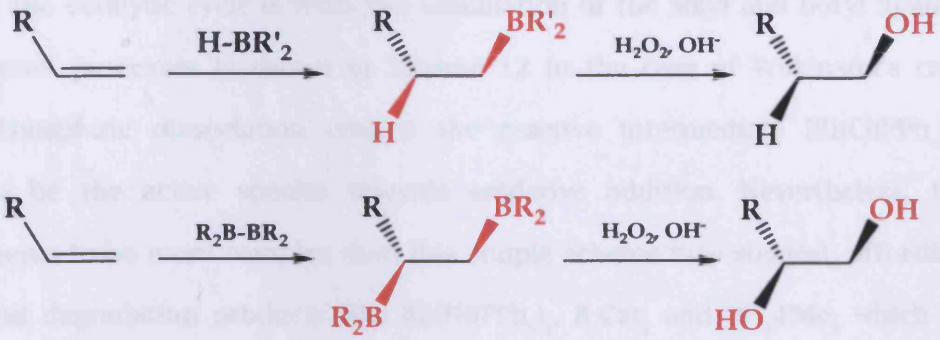

Scheme 11 - Hydroboration and diboration of olefins

Organoboron compounds are useful starting materials themselves, for example in Suzuki-Miyaura palladium-catalysed carbon-carbon bond formation between aryl or vinyl boronate esters and aryl or vinyl halides[22]:

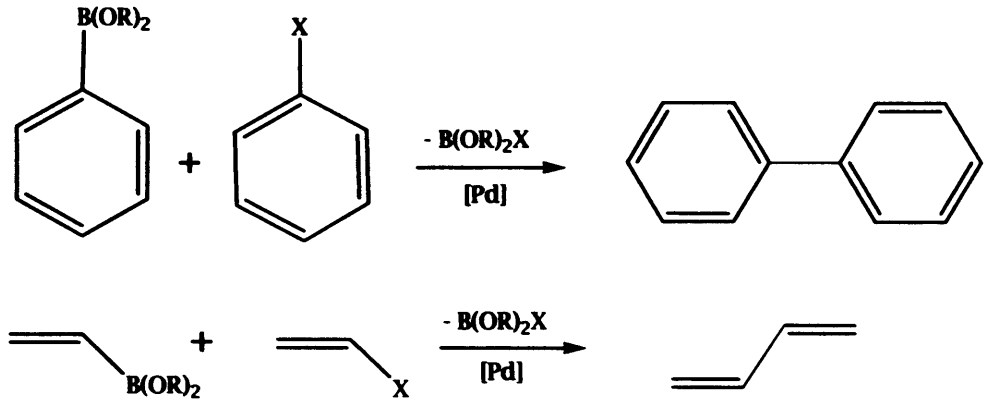

Scheme 12 - Cross coupling reactions with organoboron reagents

If hydroboration is controlled by a metal boryl complex, chemo-, regio- and even stereoselectivity can be different from the uncatalysed one. In the case of 5-hexen-2-one for example the C=C bond is preferentially hydroborated, whereas both functional groups (C=C and C=O) are attacked in the uncatalysed reaction[23]. The presence of a catalyst also lowers the temperature that is needed for hydroboration to occur, thus, more thermally sensitive species can be used. The general mechanism is thought to consist of oxidative addition of the B-H bond to the transition metal (and formation of an hydrido-metal boryl complex), coordination of the olefin to a vacant site and subsequent insertion into the M-H or the M-B bond, yielding a metal alkyl complex. The final step that produces the organoborane product and closes the catalytic cycle is reductive elimination of the alkyl and boryl ligands. One of several overall processes is shown in Scheme 12 in the case of Wilkinson's catalyst and HBCat[24]. Phosphine dissociation creates the reactive intermediate $[RhCl(PPh_3)_2]$ that is thought to be the active species towards oxidative addition. Nevertheless, the overall reaction seems to be more complex than this simple scheme may suggest, affording a series of side- and degradation products like $Rh(H)(PPh_3)_3$, B_2Cat_3 and $BH_3.PMe_3$ which have been identified via NMR[23,24].The reaction also generates other side-products from competitive β-

hydride elimination and *multiple bond isomerisation* (the latter being catalysed by the complex $Rh(H)(PPh_3)_3$).

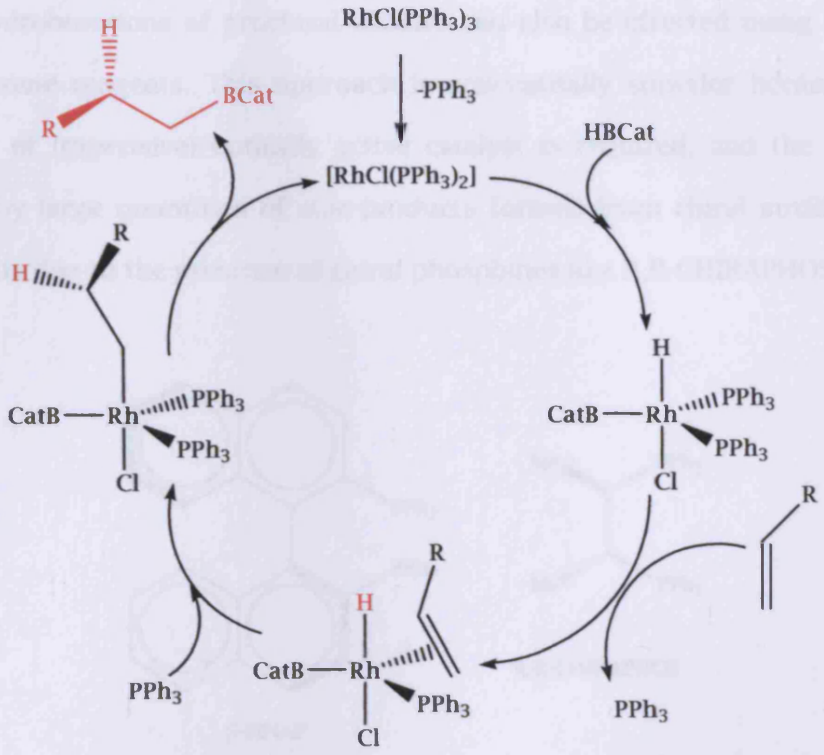

Scheme 13 - Homogeneous catalysis of hydroboration with Wilkinson's catalyst

Stereoselectivity can be induced via two different approaches, depending on the nature of the starting materials: if an optically active borane is used to induce handedness in the substrate *a reagent-controlled diastereoselectivity* is achieved. A typical borane that is used in this case is diisopinocamphenylborane (Ipc_2BH).

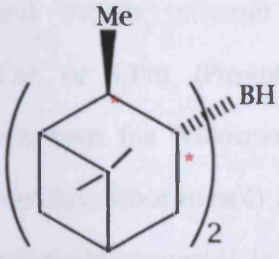

Figure 6 - Diisocamphenylborane

The reaction of this borane with Z-alkenes gives boranes of one diasteromeric series in preference to the other, and they can be converted to enantiomerically enriched alcohols via oxidation.

Asymmetric hydroborations of prochiral alkenes can also be effected using *chiral catalysts* and achiral borane reagents. This approach is conceptually superior because only a very small quantity of (expensive) optically active catalyst is required, and the product is not contaminated by large quantities of side-products formed from chiral auxiliaries. Chirality on the catalyst is due to the presence of chiral phosphines like R,R-CHIRAPHOS or S-BINAP:

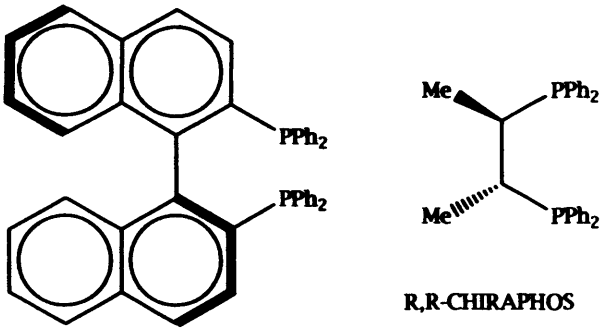

Figure 7 - Chiral phosphines

Regioselectivity is primarily a consequence of the steric demands of the metal; preferential formation of *anti-1,3*-diols in the catalysed hydroboration/oxidation of cyclohexenols is an example[2-9].

The platinum complexes $Pt(PPh_3)_4$ and $Pt(PPh_3)_2$(ethene) have been studied as catalysts for the diboration of alkynes with B_2Cat_2 or B_2Pin_2 (Pin=pinacolato= $OCMe_2CMe_2O$)[2-9a], with a mechanism that is similar to the one seen for Wilkinson's catalyst. The final product is a bisborylalkene, and the use of tetraaryloxydiboranes(4) as starting materials instead of the less stable (but more reactive) tetrahalodiboranes(4) is achieved as a result of the extra-stabilisation and subsequent activation offered by the coordination to the metal atom. The stereochemistry for bis(boryl)alkenes is always *cis*, probably because of the

insertion/reductive elimination mechanisms which give *syn* addition. While diboration of alkynes does not generate noticeable quantities of side products, diboration of alkenes competes with β-hydride elimination as shown in Scheme 14, and a mixture of different products is obtained, depending on the catalyst precursor employed.

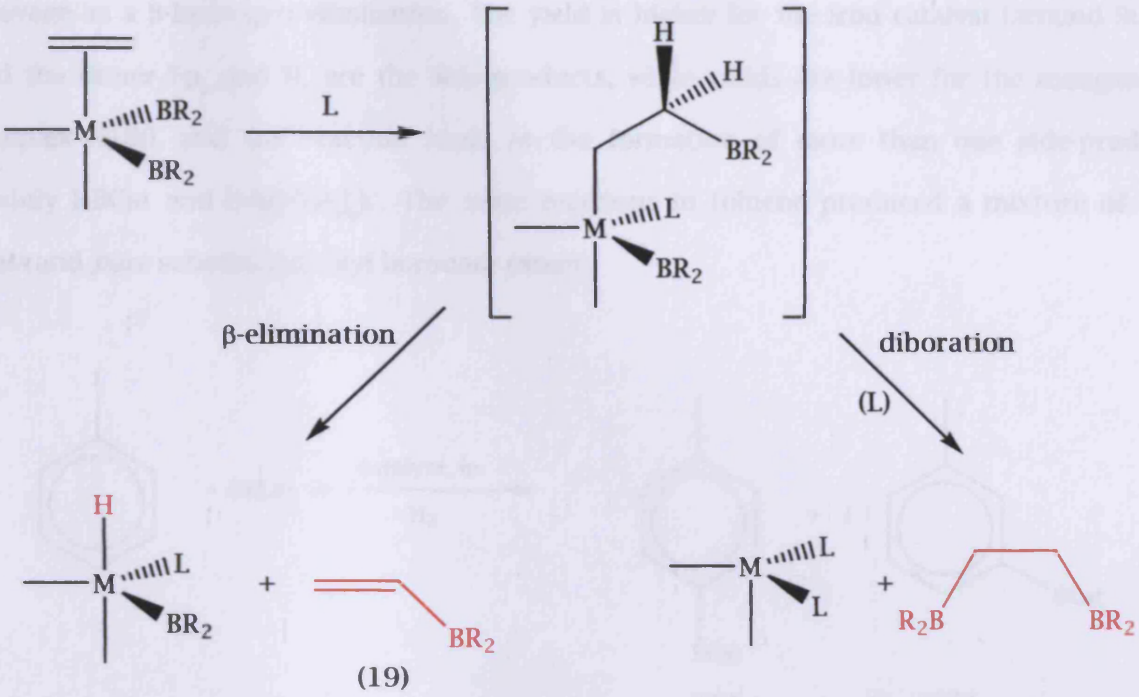

Scheme 14 - Competitive reactions: diboration vs. β-elimination

The resulting vinylorganoboryl 19 can undergo a series of successive insertions and β-eliminations, and, when there are no more β-hydrogens left, a final reductive elimination produces a *tris*-BR_2 compound. The design of a selective catalyst in this case is essential, and the issue involves finding systems that are electron-rich enough to oxidatively add B-B bonds while at the same time speeding up reductive elimination with respect to β-hydride elimination. During the last three years new rhodium (I) phosphine complexes or phospine-free platinum(0) catalysts which give very high yields for diboration have been developed[25b-e].

Besides metal-mediated hydro- and diboration, there is another very important application of these complexes in catalysis: the *activation of the C-H bonds of alkanes, alkenes and arenes*. Photolysis of certain boryl complexes in the presence of the organic substrate leads

to C-H activation with the formation of the corresponding borylated hydrocarbon. Complexes like $Mn(CO)_5(BCat)$ and FpBCat can convert benzene into PhBCat in high yields upon irradiation for 6 hours[26,19a]. Mechanistic studies have revealed that the reaction is initiated by a photochemical cleavage of a metal-bound carbonyl ligand, followed by coordination of benzene and its insertion into the metal-boryl bond, followed by C-H bond cleavage as a β-hydrogen elimination. The yield is higher for the iron catalyst (around 90%), and the dimer Fp_2 and H_2 are the side-products, while yields are lower for the manganese complex (50%), and the reaction leads to the formation of more than one side-product (mainly HBCat and $[Mn(CO)_5]_2$). The same reactions in toluene produced a mixture of the *meta* and *para* substituted tolyl boronate esters:

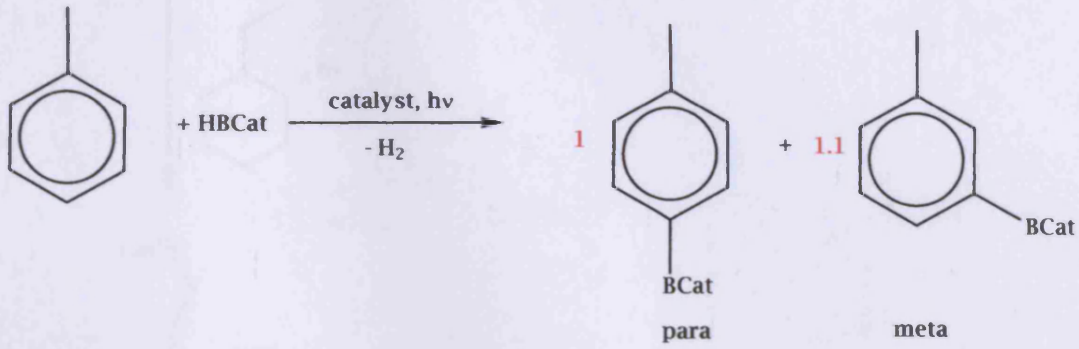

Scheme 15 – Photolytic activation of toluene

The *ortho* position is not reactive, presumably because of the steric hindrance offered by the methyl group during the coordination to the metal centre. The esters can be converted to the corresponding alcohols by oxidation, and the overall conversion of benzene to phenol for example is 70%, or the one of toluene to *m*- and *p*-cresol is 65%. When the substrate is an alkene, the corresponding vinyl boronate ester is formed in a 90% yield, with only a 10% of the saturated product being observed:

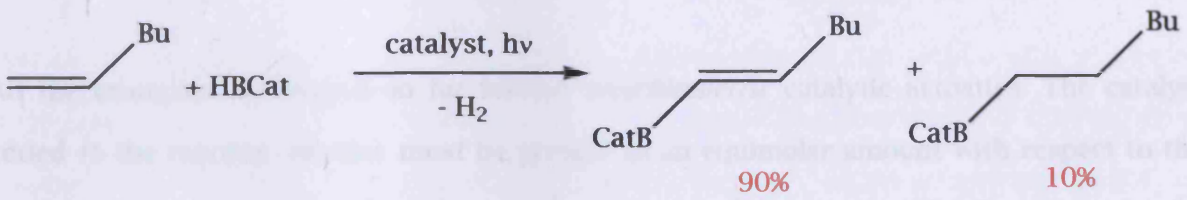

Scheme 16 – 1-hexene activation

When it comes to alkanes, the result is even more impressive, because there are very few examples of molecules that can both activate and functionalise saturated hydrocarbons. The tungsten complex $Cp^*W(CO)_3(BCat')$ ($Cp^*=C_5Me_5$, $Cat'=1,2\text{-}O_2\text{-}3,5\text{-}Me_2C_6H_2$) is extremely successful in functionalising the *terminal position* of alkanes like pentane or ethylcyclohexane[19], with high regioselectivity for the terminal position:

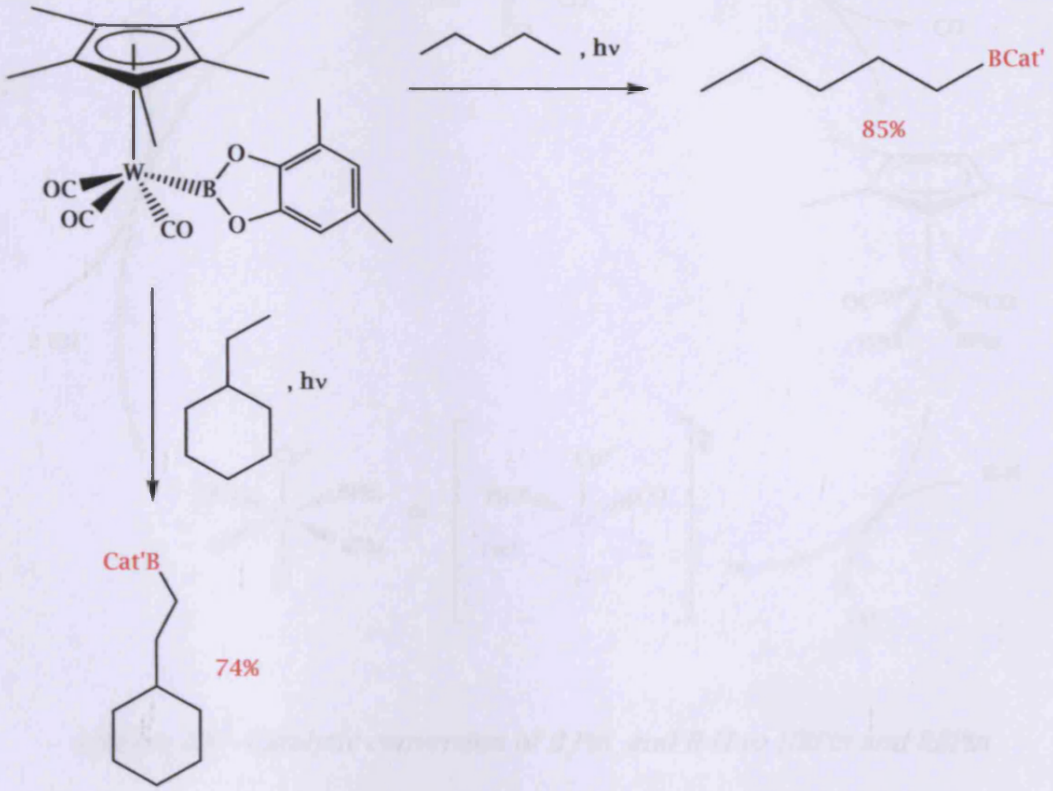

Scheme 17 – Stoichiometric alkane activation by $Cp^*W(CO)_3(BCat')$

Blocking of the carbon sp^2 positions on the catechol ligand and on the Cp ring with methyl groups seems to improve the selectivities, by removing competing sites for functionalisation chemistry. In a specific group of the transition series the general trend says that the heavier the metal the higher the selectivities, because heavier elements of the same group are less reactive (a synonym of more selective).

All the examples mentioned so far involve *stoichiometric* catalytic activities. The catalyst added to the reaction mixture must be present in an equimolar amount with respect to the substrate, because it cannot be regenerated at the end of the process. The first example of a photochemical *catalytic* process is the rhenium system discovered by Hartwig in 1999[27]:

$Cp^*Re(CO)_3$ is used for the reaction of B_2Pin_2 and pentane or methylcyclohexane, with conversions between 85 and 95%. In Scheme 18 the catalytic cycle is reported.

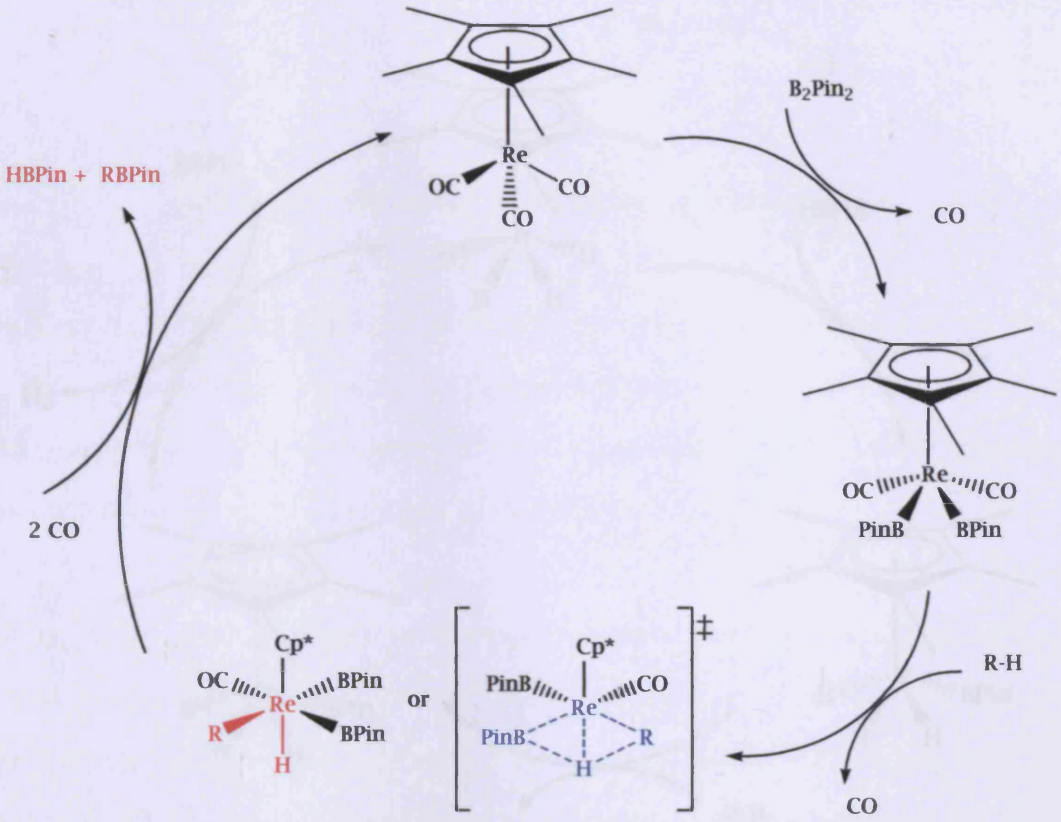

Scheme 18 – Catalytic conversion of B_2Pin_2 and R-H to HBPin and RBPin

The proposed mechanism consists of photochemical cleavage of a Re-CO bond and oxidative addition of the boron reagent to rhenium, followed by activation and functionalisation of the alkane. The transition state could be either a Re(V) intermediate obtained by a "complete" oxidative addition of the R-H bond or a σ bond metathesis, where the formal oxidation state of rhenium is still +3, with an agostic interaction of the four atoms Re, C, H and B at the same time. Final reductive elimination yields the final products observed. At the end of the process the active species is regenerated and it is *not* lost. Only very recently (2001) Kawamura and Hartwig[28a] have discovered a catalytic system that works with a *thermal* activation instead of a photochemical one, which makes use of iridium(V) hydrido boryl complexes like $Cp^*Ir(H)_4$. Thermolysis of this molecule at 80°C in the presence of HBPin and octane or benzene leads to 1-octyl(BPin) or Ph(BPin). In Scheme 19 the supposed catalytic

cycle is reported. In 2002 new iridium (I) systems with 2,2'-bipyridine ligands that can borylate arenes at room temperature have been discovered[28b-c], and mechanistic DFT studies on alkane and arene activation have been published between 2003 and 2004[28d-f].

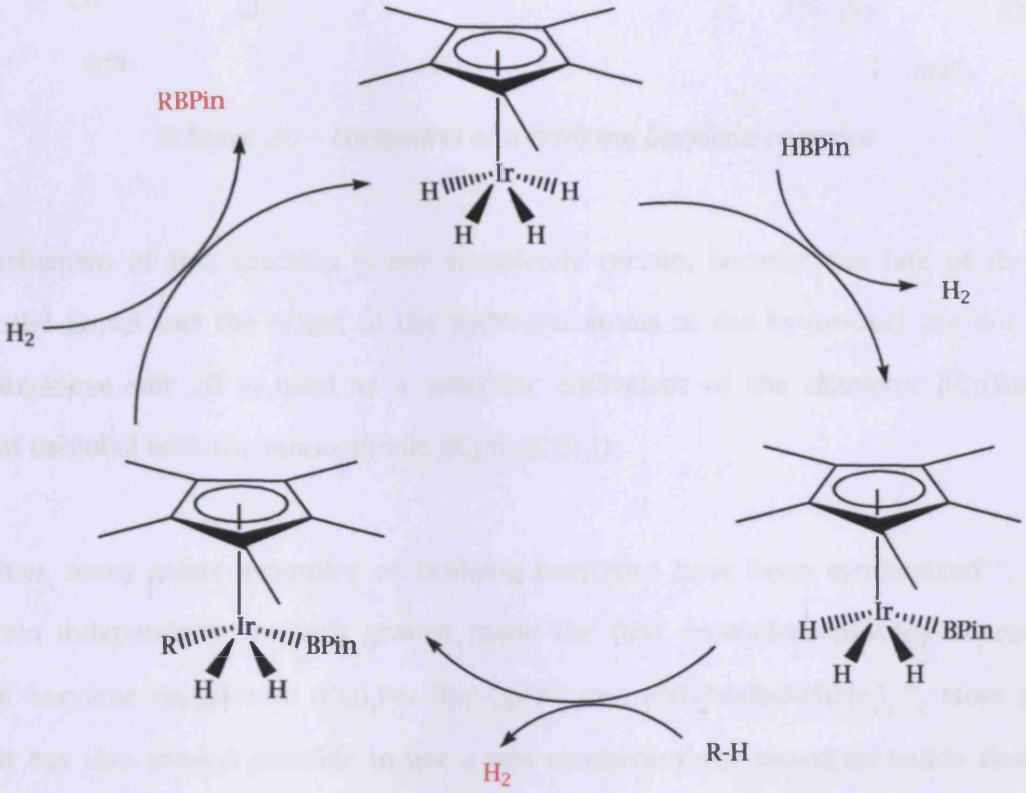

Scheme 19 – Iridium-mediated conversion of HBPin and RH to RBPin and H_2

1.2 – Transition metal – borylene metal complexes [29]

1.2.1 – Historical overview

The very first examples of borylene complexes were also reported in the 1960s[4], however, as in the case of boryl complexes, without structural evidence. ^{11}B NMR spectroscopic data coming from these early studies are at odds with more recent work, thus casting doubt on the proposed constitutions. The only derivative that is mentioned in Schmid's original review is $(CO)_4Fe{=}B(NMe_2)$; no more complexes were reported until 1995, when Braunschweig[30] determined the structure of 22, a new manganese species containing a *bridging* $B(NMe_2)$ fragment derived from a diborane(4) starting material:

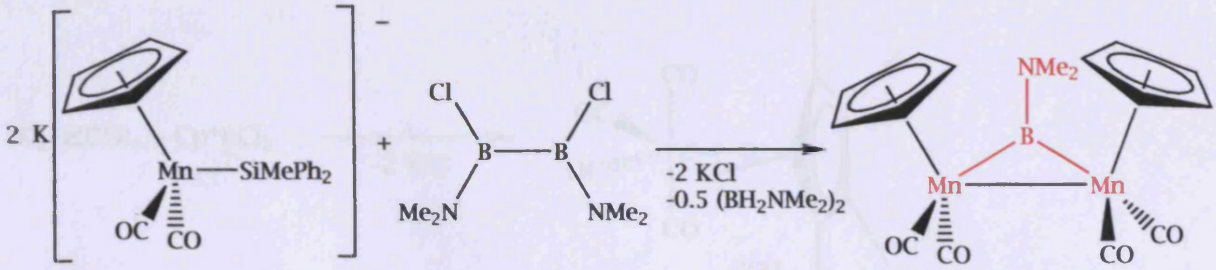

(20) (21) (22)

Scheme 20 – Formation of a bridging borylene complex

The mechanism of this reaction is not completely certain, because the fate of the metal-bound silyl group and the origin of the hydrogen atoms in the by-product are not known. The manganese salt 20 is used as a synthetic equivalent of the *dianionic* $[(Cp)Mn(CO)_2]^{2-}$ fragment (isolobal with the monoanionic $[(Cp)Fe(CO)_2]^-$).

Since then, many other examples of bridging borylenes have been synthesized[31], and, in 1998, two independent research groups made the first crystallographically characterised terminal borylene complexes: $(CO)_4Fe{\leftarrow}B(\eta^5\text{-}Cp^*)$[32] and $(CO)_5W{=}B{=}N(SiMe_3)_2$[33]. More recently (2003) it has also proved possible to use a new synthetic route based on halide abstraction to produce the first *cationic* terminal borylene[34]: $[(Cp^*)(CO)_2Fe{=}B(Mes)]^+$.

1.2.2 – Synthetic pathways to borylene metal complexes

The salt elimination pathway used for boryl complexes can also be applied to borylene synthesis, but a change of the anion charge or of the stoichiometry is needed:

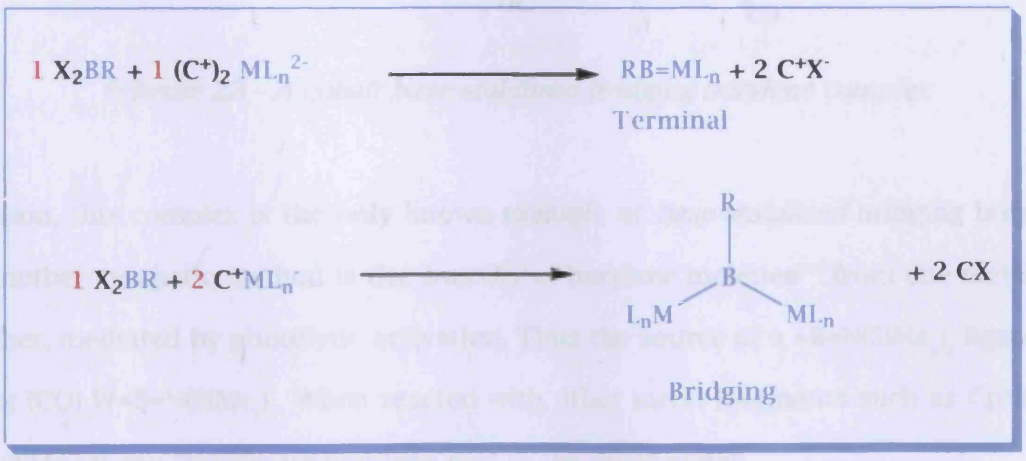

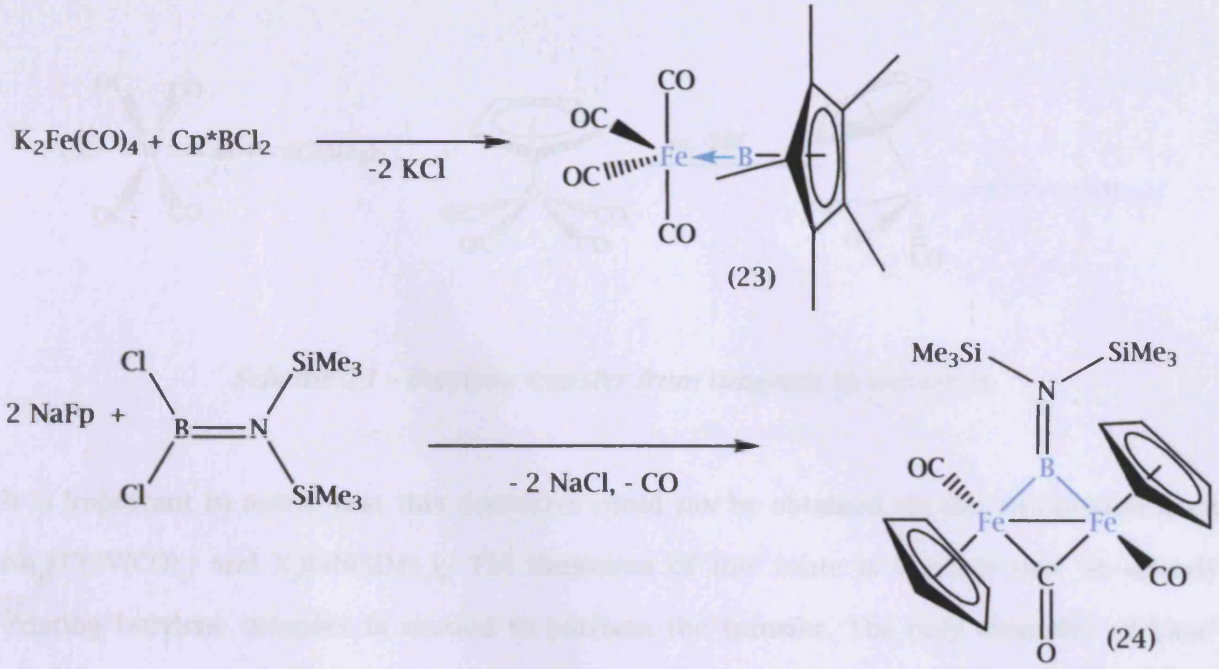

Scheme 21- Examples of borylene complexes

Starting from a dianionic transition metal salt and a dihaloborane (in a 1:1 stoichiometry) a terminal borylene like 23 is the expected product, while if the starting material is monoanionic and a 1:2 stoichiometry is adopted, a bridging species like 24 should result. These syntheses are of a very general kind, but there are also special cases where this pattern is not followed, such as 22 in Scheme 20 and the use of $Co_2(CO)_8$ as the metal source[35]:

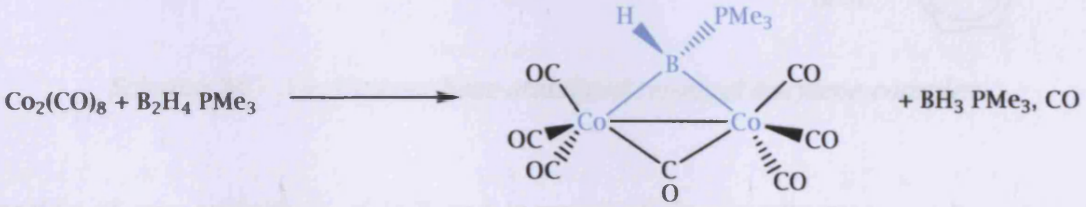

Scheme 22 - A cobalt base-stabilised bridging borylene complex

In addition, this complex is the only known example of *base-stabilised* bridging borylene to date. Another synthetic method is the *transfer* of borylene moieties[36] from one metal center to another, mediated by photolytic activation. Thus the source of a $=B=N(SiMe_3)_2$ ligand is the complex $(CO)_5W=B=N(SiMe_3)_2$. When reacted with other metal fragments such as $CpV(CO)_4$ or $Cr(CO)_5(NMe_2)$ it can transfer its borylene part to the other metal:

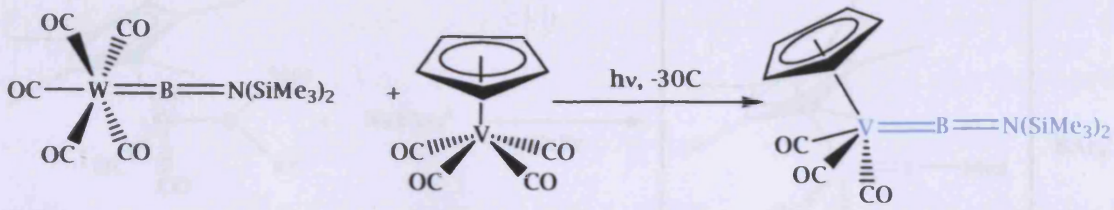

Scheme 23 - Borylene transfer from tungsten to vanadium

It is important to notice that this derivative could *not* be obtained via salt elimination from $Na_2[(Cp)V(CO)_3]$ and $X_2B{=}N(SiMe_3)_2$. The limitation of this route is the fact that an already existing borylene complex is needed to perform the transfer. The only examples of base-stabilised terminal borylenes are Roper's osmium complexes $Os(=BNHC_9H_6N)(Cl)(X)(CO)(PPh_3)_2$ (X=Cl, I)[37], which feature the 8-aminoquinoline ligand chelating at boron. The second nitrogen atom present on the organic ligand can act as a Lewis base, thus providing an *intramolecular* stabilisation:

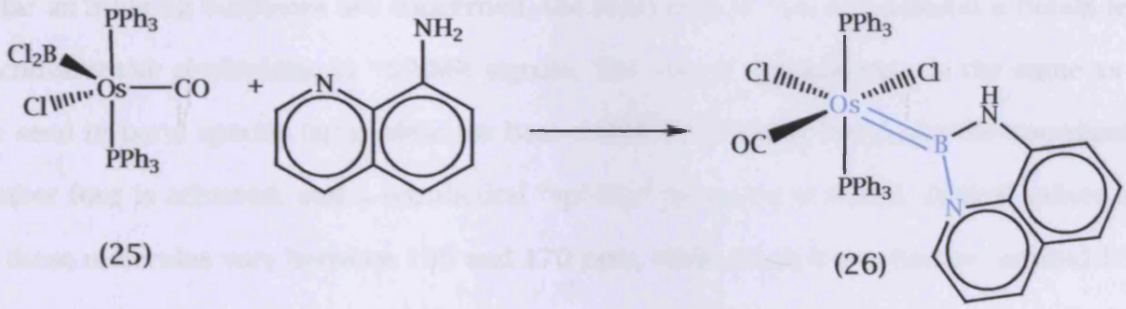

Scheme 24 - An osmium base-stabilised terminal borylene complex

Elimination of one equivalent of HCl and increase of the coordination number at osmium leads to the formation of the borylene, with the ring nitrogen of aminoquinoline donating its lone pair to the boron atom.

Finally, this research group has extended the halide abstraction technique, used by Tilley and co-workers to produce base-free silylene complexes[38], to prepare the first cationic borylene complex, starting from an asymmetric haloboryl precursor[39]:

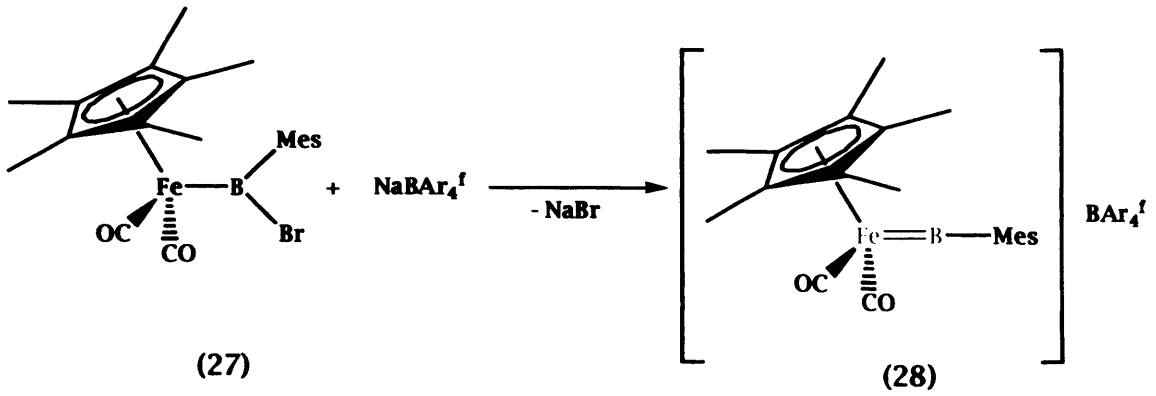

(27) (28)

Scheme 25 - Bromide abstraction to form a cationic terminal borylene

The bromide anion is extracted, and the final cation is isolated in conjunction with the large non-coordinating counter-ion [BAr_4^f]. Steric shielding offered by the Cp* ring is also needed to obtain a stable salt; the comparable reaction with less bulky NaFp instead of NaFp* or with a phenyl ring instead of mesityl as the borylene substituent does *not* work.

1.2.3 - Structure and bonding

As far as bridging borylenes are concerned, the formation of two metal-boron σ bonds leads to *considerable deshielding* in ^{11}B-NMR signals. The overall hybridisation is the same as the one seen in boryl species (sp^2), while for base-stabilised bridging borylenes the coordination number four is achieved, and a tetrahedral "sp^3-like" geometry is found. Typical values of δ_B for these molecules vary between 100 and 170 ppm, while much lower figures (around 15-20 ppm) are related to the base-stabilised ones, presumably because of the usual shielding coming from the extra electrons of the Lewis base. Structural studies reveal that in supported bridging borylenes the M-B-M triangle is isosceles, with M-B and M-M bond lengths in the expected range for corresponding single bonds.

In terminal borylene complexes it can be assumed that the hybridisation of boron in a linear M=B-R moiety is of sp type, with two pure p orbitals that can feature in additional interactions with both R and M orbitals of suitable symmetry. Since very little is known about the nature of the metal-boron bond in these species (mostly because of the lack of examples), several computational studies have been carried out recently (see section 1.3.5) to

shed light on the problem. In particular, the results of the calculations show that these organometallics should have high thermodynamic stability due to the good σ donor and π acceptor properties of the BR ligand. However, low kinetic stability has been predicted for uncoordinated borylene ligands due to high polarity and a small HOMO-LUMO gap. The σ donation and π back-donation after coordination to a metal are not balanced, and a *build up of positive charge* at the boron is the result. Consequently, nucleophilic attack at boron is likely to occur. Two possible strategies for enhancing the stability of borylene complexes have been advanced: either steric shielding of the boron atom by bulky substituents (like Cp* or $N(SiMe_3)_2$) or electronic stabilisation by incorporation of a strongly π donor R substituent (like NR_2). Obviously, the proportion of σ and π contributions on the M=B bond depends on the behaviour of the group R: if it is a strong π donor the amount of π electron density in the M-B bond will be lower, and vice-versa. Part of this thesis deals with the theoretical investigation of terminal borylene complexes, both cationic and neutral.

1.2.4 - Reactivity of borylene metal complexes

In agreement with several computational studies on bridging borylenes[47], investigations of reactivity show that these complexes react with nucleophiles only very slowly. Stability to air and moisture is the consequence. In Scheme 26 there is a short summary of all the reactions performed on complex $[(Cp)Mn(CO)_2]_2(\mu\text{-BCl})$ made by Braunschweig[59]. Treatment of the reactive chloroborylene with protic reagents like primary amines, alcohols and water affords the corresponding amino-, alkoxy- or hydroxyborylenes (29, 30, 31), with retention of the M-B bonds. It is important to stress the fact that this behaviour is very rare indeed, as the M-B bond is usually labile under such conditions.

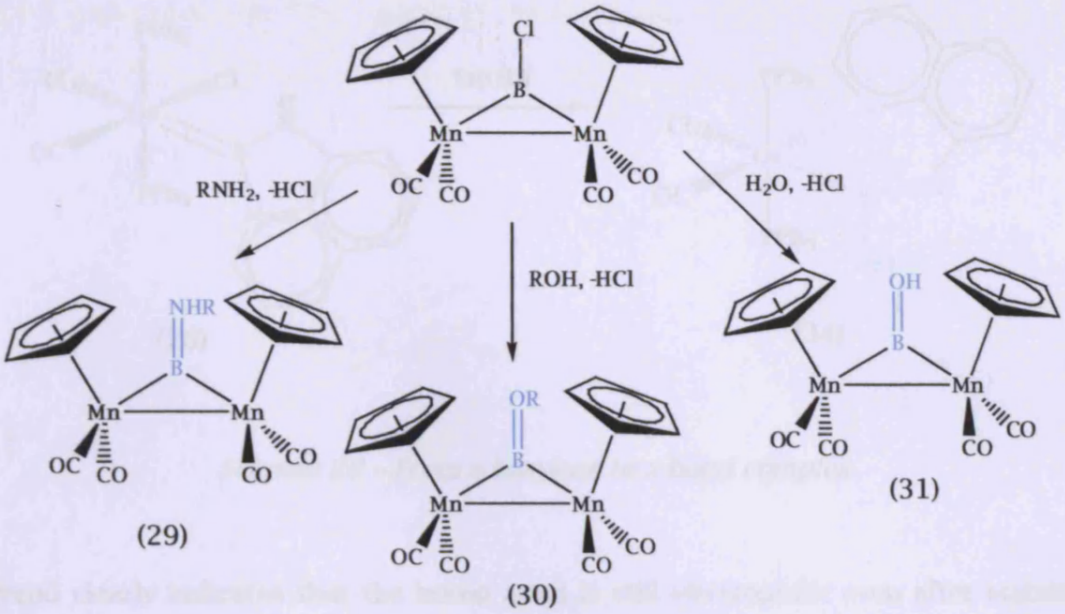

Scheme 26 - Reactivity of a chloroborylene complex

Another example of bridging borylene reactivity is the photolysis of $Fp_2(BMes)$, leading to CO loss and formation of an additional CO bridge and a new Fe-Fe single bond[140]:

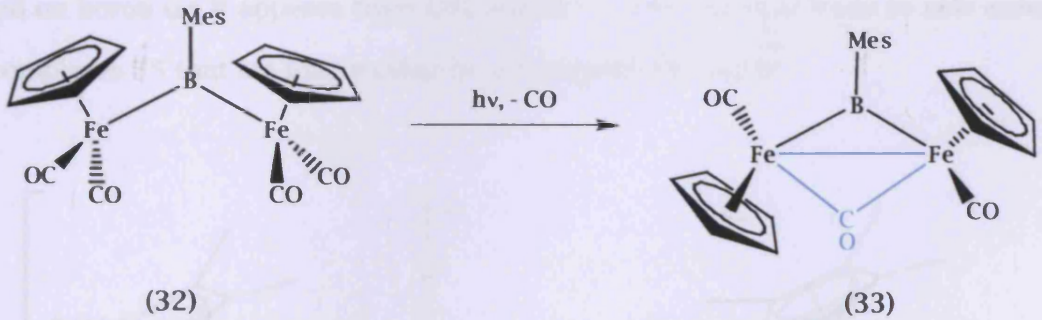

Scheme 27 - Photolysis of a bridging borylene complex

The chemistry of terminal borylenes is still virtually unexplored, and, apart from a photochemically induced intermetal borylene transfer (already discussed as synthetic method to get terminal borylenes, see section 1.2.2), very few examples have been reported. One is provided by Roper, who performed some ligand substitution reactions on the osmium base-stabilised terminal borylene 26 (Scheme 24). Treatment with ethanol lead to the amino(ethoxy) boryl complex 34, where the quinoline nitrogen atom moves from the boron to the metal centre:

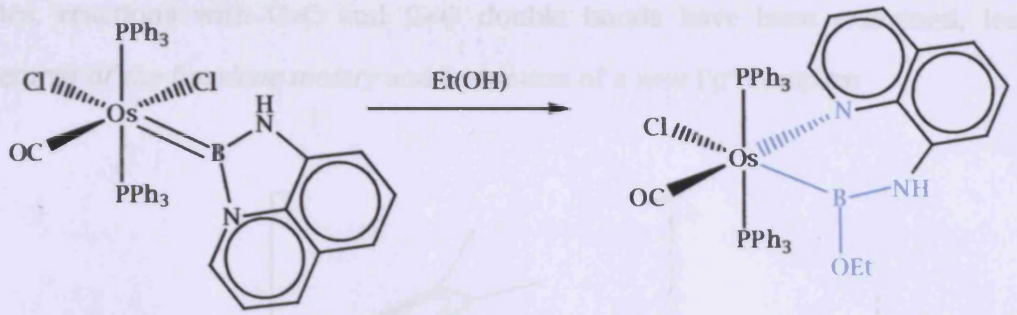

(26) (34)

Scheme 28 - From a borylene to a boryl complex

This trend clearly indicates that the boron atom is still electrophilic even after stabilisation of a coordinated Lewis base, as was predicted by a theoretical study.

Another example to be mentioned in this section is the addition/substitution chemistry of the cationic [Fp*=BMes]$^+$ 28, reported by this research group in 2003 and 2004[30]. Reactivity towards nucleophiles proceeds via *addition at the M=B bond*, and the boron centre is even more electrophilic than the one present in neutral borylenes, due to a net positive charge localised on boron (as it appears from DFT studies[34]). This reaction leads to new asymmetric boryl complexes 35 that are inaccessible via other synthetic routes.

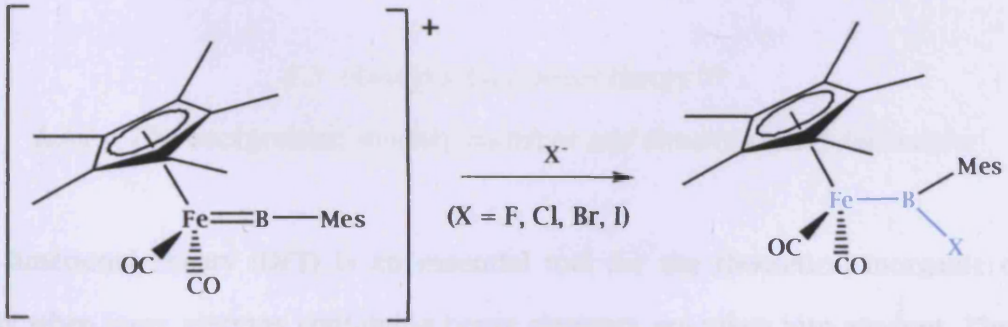

(28) (35)

Scheme 29 - Synthesis of asymmetric boryl complexes

In addition, given the similarities in electronic structure between this complex and cationic Fischer carbene complexes, and the known reactivity of such carbenes towards unsatured

molecules, reactions with C=C and C=O double bonds have been examined, leading to *displacement of the borylene moiety* and formation of a new Fp* complex:

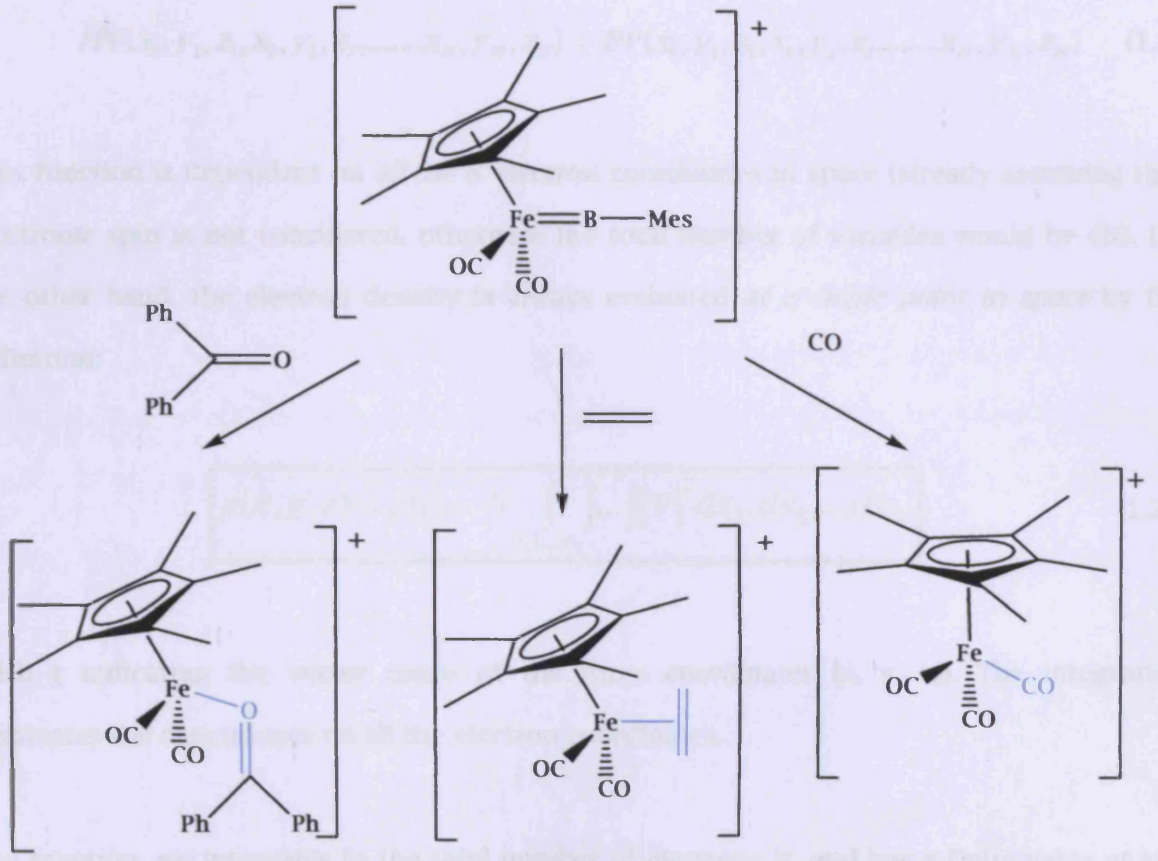

Scheme 30 – Reactivity of the cationic borylene 28 towards nucleophiles

1.3 – Density functional theory [41]

1.3.1 – The background: density matrices and density matrix formalism

Density functional theory (DFT) is an essential tool for the theoretical inorganic chemist, especially when large systems containing heavy elements are taken into account. The reason for this is can be understood if we compare the DFT approach with the traditional wavefunction-based Hartree-Fock methods. The basic idea of DFT is the use of a three-variable only electron density functional to determine the total energy of a poly-electronic system instead of a 3N variable (wave)function (where N equals to the number of electrons).

In fact, *ab initio* methods always deal with a wave function Ψ that is the eigenfunction of the Hamiltonian operator H:

$$\hat{H}\Psi(x_1, y_1, z_1, x_2, y_2, z_2, \ldots\ldots x_N, y_N, z_N) = E\Psi(x_1, y_1, z_1, x_2, y_2, z_2, \ldots\ldots x_N, y_N, z_N) \quad (1.1)$$

This function is dependent on *all* the N electron coordinates in space (already assuming that electronic spin is not considered, otherwise the total number of variables would be 4N). On the other hand, the electron density is always evaluated *at a single point in space* by the definition:

$$\boxed{\rho(x, y, z) = \rho(\underline{r}) = N \int_{2,3\ldots N} \int \ldots \int \|\Psi\|^2 dx_2, dx_3, \ldots . dx_N} \quad (1.2)$$

(with $\underline{r}$ indicating the vector made of the three coordinates [x, y, z]). The integration eliminates the dependence on all the electron coordinates.

The function $\rho(\underline{r})$ integrates to the total number of electrons N, and has a finite value at any atomic nucleus, indicated with $\rho(0)$. In the neighbourhood of a nucleus there is always a mathematical singularity in the density owing to the necessity of avoiding the electron-nucleus electrostatic attraction becoming infinite. This is sometimes called the *cusp condition*:

$$\left[\frac{\partial}{\partial r_\alpha}\rho(r_\alpha)\right]_{r\alpha=0} = -2Z_\alpha\rho(0) \quad (1.3)$$

(with r_α indicating the distance of the electron from the nucleus α of total charge Z_α).

If we consider the product of the wavefunction and its complex conjugate

$$\|\Psi_N\|^2 = \Psi_N(\underline{r}_1, \underline{r}_2, \ldots \underline{r}_N)\Psi_N^*(\underline{r}_1, \underline{r}_2, \ldots \underline{r}_N) \quad (1.4)$$

that appears in the definition of the electron density, it represents the probability density (i.e. the probability per volume unit) of finding the electrons at the location $\underline{r}_1$, $\underline{r}_2$, $\underline{r}_3$,... in the quantum state defined by Ψ. It is possible to give a more general description of a quantum state by changing the set of Cartesian coordinates in the first term:

$$\Psi_N(\underline{r}'_1,\underline{r}'_2,...\underline{r}'_N)\Psi^*_N(\underline{r}_1,\underline{r}_2,...\underline{r}_N) = \rho_N(\underline{r}'_1,\underline{r}'_2,...\underline{r}'_N,\underline{r}_1,\underline{r}_2,...\underline{r}_N) \tag{1.5}$$

This entity is of a more general kind than the previous one, and the two sets of independent variables $\underline{r}`_1$, $\underline{r}`_2$... and $\underline{r}_1$, $\underline{r}_2$...can be thought as two sets of indices associated to a numerical value. In other words, the numbers ρ_N are the elements of a square matrix, called the *density matrix*. If we take the diagonal elements of this matrix, where $\underline{r}`_i = \underline{r}_i$ they represent the original probability density distribution ($\|\Psi\|^2$, equation 1.4). 1.5 can be viewed as the coordinate representation of a *density operator*:

$$\hat{\rho}_N = |\Psi_N\rangle\langle\Psi_N| \tag{1.6}$$

Its trace (the sum of the diagonal elements of the matrix ρ_N representing the operator $\hat{\rho}_N$) equals to 1, and for the calculations of the expectation values of a generic quantum mechanical operator Ô it is possible to write:

$$\langle\hat{O}\rangle = tr(\hat{O}\hat{\rho}_N) = \int\Psi^*(\underline{r}^N)O\Psi(\underline{r}^N)d\underline{r}^N \tag{1.7}$$

where the superscript N simply indicates all the variables of Ψ, and it is assumed that Ψ itself is already normalised ($\|\Psi\|^2$ integrates to one all over space). Obviously, $\hat{\rho}_N$ is a projection operator, carrying the same information as the N-electron wave function Ψ_N. Using these mathematical conventions, it is possible to re-write the classical expressions for expectation values of the operators. In particular, since the terms appearing in the Hamiltonian are either "one-electron" or two-electron" operators, the formulae could be

systematically simplified by integrating the product (1.5) over N-1 or N-2 of its variables. This leads to the idea of a *reduced density matrix of order p*, defined as follows:

$$\rho_p(\underline{r}'_1,\underline{r}'_2,\ldots\underline{r}'_p,\underline{r}_1,\underline{r}_2,\ldots\underline{r}_p) = \binom{N}{p} \int_{p+1\to N} \int \rho_N(\underline{r}'_1,\underline{r}'_2,\ldots\underline{r}'_p,\underline{r}_{p+1},\underline{r}_{p+2},\ldots\underline{r}_N,\underline{r}_1,\underline{r}_2,\ldots\underline{r}_p,\ldots\underline{r}_N)d\underline{r}_{p+1}\ldots d\underline{r}_N \tag{1.8}$$

The integration over (N-p) variables lowers the order of ρ_N from N to p. For our purposes only the reduced matrices of order 1 and 2 are needed:

$$\rho_1(\underline{r}'_1,\underline{r}_1) = N \int_{2\to N} \ldots \int \Psi(\underline{r}'_1,\underline{r}_2,\underline{r}_3\ldots\underline{r}_N)\Psi^*(\underline{r}_1,\underline{r}_2,\underline{r}_3\ldots\underline{r}_N)d\underline{r}_2\ldots d\underline{r}_N \tag{1.9}$$

$$\rho_2(\underline{r}'_1,\underline{r}'_2,\underline{r}_1,\underline{r}_2) = \frac{N(N-1)}{2} \int_{3\to N} \ldots \int \Psi(\underline{r}'_1,\underline{r}'_2,\underline{r}_3\ldots\underline{r}_N)\Psi^*(\underline{r}_1,\underline{r}_2,\underline{r}_3\ldots\underline{r}_N)d\underline{r}_3\ldots d\underline{r}_N \tag{1.10}$$

The second order reduced matrix ρ_2 normalises to the total number of electron pairs, while the first order ρ_1 normalises to the number of electrons. For local one-electron operators, i.e. operators that are acting only on one electron at one time (which represent the vast majority in molecular physics), the expectation value formula in terms of the corresponding density matrix is:

$$\left\langle \widehat{O}_1 \right\rangle = \int [O_1(\underline{r}_1)\rho_1(\underline{r}_1\underline{r}'_1)]_{\underline{r}_1=\underline{r}'_1} d\underline{r}_1 \tag{1.11}$$

(keeping (1.7) in mind), while, for two-electron operators the expectation value formula is

$$\left\langle \widehat{O}_2 \right\rangle = \int [O_2(\underline{r}_1,\underline{r}_2)\rho_2(\underline{r}_1,\underline{r}_2,\underline{r}'_1,\underline{r}'_2)]_{\substack{\underline{r}_1=\underline{r}'_1 \\ \underline{r}_2=\underline{r}'_2}} d\underline{r}_1 d\underline{r}_2 \tag{1.12}$$

again referring to (1.7). The change of variables from $\underline{r}_i'$ to $\underline{r}_i$ must be done *after* the application of the operator but *before* the integration. If we apply all these general equations

to the specific case of the operator H, the final expression for its expectation value (*the electronic energy*) is:

$$E[\rho] = \left\langle \widehat{H} \right\rangle = \int [-\frac{\nabla^2}{2} \rho_1(\underline{r}', \underline{r})]_{\underline{r}'=\underline{r}} d\underline{r} + \int v(\underline{r}) \rho(\underline{r}) d\underline{r} + \iint \frac{\rho_2(\underline{r}_1, \underline{r}_2)}{|\underline{r}_1 - \underline{r}_2|} d\underline{r}_1 d\underline{r}_2 \quad (1.13)$$

The first term represents the electronic kinetic energy, the second the nuclear-electron potential energy and the third the electron-electron potential energy. Thus, the whole expression can be written as separate functionals of ρ:

$$E[\rho]=T[\rho]+V_{en}[\rho]+V_{ee}[\rho] \quad (1.14)$$

As a result of this new formalism, the total electronic energy of a multi-electron system is now expressed as a functional of ρ instead of a function of Ψ. This is exactly the basic idea of the DFT approach. Since the electron density is in turn a function of the electronic coordinates, the energy is said to be a *functional*, the word used in mathematics to define a complex function whose independent variable is another function.

Density matrices assume a very simple form when they are derived from a single determinant like in the case of Hartree-Fock (HF) approximation. Without going into the details of the mathematical treatment, if a Slater determinant is taken as wave function describing the system, and the secular problem is solved following the same path as in HF theory (that is to find the ρ_1 and ρ_2 that minimise the energy $E[\rho]$, according to the variational principle), the final expression for the HF energy of a closed shell system is:

$$E_{HF}[\rho_1] = \int [-\frac{\nabla^2}{2} \rho_1(\underline{r}_1', \underline{r}_1)]_{\underline{r}_1'=\underline{r}_1} d\underline{r}_1 + \int v(\underline{r}) \rho(\underline{r}) d\underline{r} + \frac{1}{2} \iint \frac{\rho(\underline{r}_1)\rho(\underline{r}_2)}{|\underline{r}_1 - \underline{r}_2|} d\underline{r}_1 d\underline{r}_2$$
$$- \frac{1}{4} \iint \frac{\rho_1(\underline{r}_1, \underline{r}_2)\rho_1(\underline{r}_2, \underline{r}_1)}{|\underline{r}_1 - \underline{r}_2|} d\underline{r}_1 d\underline{r}_2 \quad (1.15)$$

which can be shortened like this:

$$E[\rho] = T[\rho_1] + V_{ne}[\rho] + J[\rho] - K[\rho_1] \tag{1.16}$$

The first two terms are identical to the ones described in (1.14), while the electron-electron interaction V_{ee} is split into two different terms. *J[ρ]* describes the classical Coulomb repulsion energy, while *K[ρ]* is the exchange term that also appears in the HF theory. However, since the HF method is deliberately approximate, because of the choice of a single determinant only to represent the *exact* poly-electronic wave function, also the DFT version of the HF equations will be approximate. The problem is related to the treatment of electron exchange and correlation, which include all the deviations from the classical (simplified) model of *non-interacting electrons*. Exchange is already considered in the HF approach, owing to the presence of the term *K[ρ]* which "swaps" electron 1 with electron 2, but correlation is ignored.

1.3.2 - The Hohenberg-Kohn existence and variational theorems.

In 1964 the two physicists Hohenberg and Kohn rigorously proved that *any external potential v(r)* acting on the electrons is univocally determined by the ground state electron density *ρ(r)*. Although essential for the development of a DFT theory, this theorem is unhelpful in providing any indication of *how to predict* the density of a system. Just as with MO theory, we need a means to optimise our fundamental quantity. Hohenberg and Kohn showed in a second theorem that the density indeed obeys a variational principle exactly like the wave function. For any trial density $\tilde{\rho}(\underline{r})$ we can choose, the ground state energy functional $E[\tilde{\rho}(\underline{r})]$ related to this density is an approximation *in excess* of the real energy:

$$E_0[\rho(\underline{r})] \leq E_v[\tilde{\rho}(\underline{r})] \tag{1.17}$$

This implies that, in order to find the optimal value of ρ, one must find the minimum of the function *E[ρ(r)]*.

1.3.3 -Thomas-Fermi-Dirac and Kohn-Sham energy functionals

Work by Thomas and Fermi dates back to the 1920s, and it has to be regarded as a first attempt to solve the problem of how to use the density rather than the wavefunction. In equation (1.15) there are several reduced density matrices of first order that must be expanded and calculated somehow. In addition, the expression, derived from the HF classic model, does not consider at all the correlation effects between electrons with opposite spin. What Thomas and Fermi did was to ignore these effects completely, and calculate the reduced density matrices in equation (1.15) using the fermion statistical mechanics theory of a non-interacting uniform electron gas. This gas is called "jellium", and it consists of an infinite number of electrons moving in an infinite volume of space, under the effect of a uniformly distributed positive charge (not localised as it is in the presence of the nuclei). Jellium has a constant non-zero density. Under these assumptions, the kinetic energy $T[\rho]$ assumes the simple form:

$$T_{TF}[\rho] = \frac{3}{10}(3\pi^2)^{2/3}\int \rho(\underline{r})^{5/3} d\underline{r} \tag{1.18}$$

while the exchange energy $K[\rho]$ turns to

$$K_D[\rho] = \frac{3}{4}\left(\frac{3}{\pi}\right)^{1/3}\int \rho(\underline{r})^{4/3} d\underline{r} \tag{1.19}$$

The complete expression for the energy functional then becomes:

$$E_{TFD}[\rho] = C_F\int \rho(\underline{r})^{5/3} d\underline{r} + \int \rho(\underline{r}) v(\underline{r}) dr + J[\rho] - C_x\int \rho(\underline{r})^{4/3} d\underline{r} \tag{1.20}$$

with C_F and C_x being the constants coming from (1.18) and (1.19). The subscript D stands for Dirac, since it was Dirac who explicitly calculated it in 1930. Unfortunately, while these

equations now have a relevant historical interest, the underlying assumptions are so inaccurate that they find no use in modern theoretical chemistry. In Thomas-Fermi-Dirac DFT all molecules are unstable relative to dissociation into their constituent atoms.

This model and the related ones developed in the same period constitute a *direct* approach, whereby one tries to find explicit forms for $T[\rho]$ and $V_{ee}[\rho]$. In a trade of simplicity for accuracy, Kohn and Sham invented an ingenious *indirect* approach to the kinetic energy functional in 1965, which is now known as the Kohn-Sham method (KS). They proposed introducing orbitals into the problems in such a way that the kinetic energy can be computed simply to good accuracy, leaving a small residual correction that is handled separately. The main idea is to evaluate the kinetic energy of a system made of N *non-interacting* electrons, for which the related ground state wave function is a "Slater-like" single determinant.

$$T_s[\rho] = \sum_{i=1}^{N} \langle \psi_i | -\frac{\nabla^2}{2} | \psi_i \rangle \tag{1.21}$$

The expression (1.14) is rewritten like this:

$$E[\rho]=T_s[\rho]+V_{en}[\rho]+J[\rho]+E_{xc}[\rho] \tag{1.22}$$

And the defined quantity E_{xc} is the *exchange-correlation functional*, which contains the difference between $T[\rho]$ and $T_s[\rho]$ and the non-classical part of V_{ee}. This time *the treatment is exact*, because nothing is omitted, but the very clever idea of Kohn and Sham was to transfer all the deviations from the classic model into a single term. Nevertheless, the model system has a ground state density that is *exactly the same* as the real system of interest where molecules *do* interact. In a non-interacting system the total values of the (different) energies can be expressed as a sum of individual contributions coming from each individual electron. This permits us to write the KS equations in their monoelectronic *canonical form*:

$$[-\frac{\nabla^2}{2} + v(\underline{r}) + \int \frac{\rho(\underline{r}')}{|\underline{r} - \underline{r}'|} d\underline{r}' + v_{XC}(\underline{r})]\psi_i = \varepsilon_i \psi_i$$

$$\rho(\underline{r}) = \sum_{i=1}^{n} \|\psi_i(\underline{r})\|^2 \qquad (1.23)$$

All the effects of exchange and correlation are contained in the potential $v_{xc}(\underline{r})$. Simplicity of the single equation (1.20) of the TFD method is lost, because now we need to solve N independent equations (one for each electron). To solve the pseudo-eigenvalue equation 1.23 it is necessary to find a suitable form of this term of the Hamiltonian operator. What is done in practice is to derive it from the corresponding energy functional E_{xc} (equation 1.22):

$$v_{XC}(\underline{r}) = \frac{\delta E_{xc}[\rho]}{\delta \rho(\underline{r})} \qquad (1.24)$$

Solving the eigenvalue equations (1.23) leads to the creation of a set of wave functions $\{\psi_i\}$ that can be used to build up the electron density ρ. However, since ρ appears in the definition of the Hamiltonian itself, an iterative SCF approach must be used.

1.3.4 - Local and non-local methods

As described in chapter 1.3.2, Hohenberg and Kohn established that there must be a unique functional of the electron density that provides the ground electronic energy of a molecule. Unfortunately, nothing is said about the mathematical form of this functional, therefore the main challenge in DFT methods is to find a "well-behaved" E_{xc} to put in equation (1.22). The wide range of DFT methods that have developed since the birth of the KS formalism is a proof of the effort made in this direction, to get equations that can reproduce the experimental values as accurately as possible. A lot of different expressions for $E_{xc}[\rho]$ are known, and many more are emerging constantly from the literature, given that this is a very active area of research.

In the *local density approximation* (LDA) it is assumed that the density at a given point is not varying with the cartesian coordinates, as in the case of Thomas-Fermi "Jellium". Expressions of exchange and correlation functionals will show only the density itself, without taking its variations into account. Examples of this category are the Dirac exchange formula (1.19) or the Xα exchange proposed by Slater in 1951[42]. In both cases correlation is neglected. Of course, this is a "perfect world" but unreal, and the assumption of a constant density gives inaccurate results. Improvements over the LDA approach have to consider a non-uniform density: this is known as *gradient corrected approximation* (GGA), where the mathematical expressions used for the functionals contain both the electron density and its derivatives (gradients):

$$E_{XC} = E_{XC}[\rho, \|\nabla\rho\|, \nabla^2\rho...] \tag{1.25}$$

In this category a large number of examples can be found[43], and in here only the Becke88 (B) exchange functional[44] and Lee-Yang-Parr (LYP) correlation functional[45] are quoted, as they have been used for all the calculations shown in this thesis. Becke's functional can be seen as a correction of the local one:

$$E_X^{B88} = E_x^{LDA} - \beta\rho^{1/3}\frac{\left(\frac{|\nabla\rho|}{\rho^{4/3}}\right)^2}{1+6\beta\frac{|\nabla\rho|}{\rho^{4/3}}\sinh^{-1}\left(\frac{|\nabla\rho|}{\rho^{4/3}}\right)} \tag{1.26}$$

where β is a parameter that is determined by fitting to known atomic data. See the reference (45) for the expression of LYP correlation functional. The presence of parameters like β reveals that to a certain extent DFT methods are to be considered *semi-empirical*, even though the starting point is an *ab initio* one, since reference is made to experimental data to parameterise the functional. However, the number of parameters is significantly smaller than for the completely semi-empirical methods.

1.3.5 - DFT case studies on low-valent group 13 element- transition metal complexes [46]

DFT methods are particularly useful when dealing with systems containing transition metals, for the reasons already described in section 1.3.1: the computational effort in a traditional HF approach is proportional to N^4, where N is the number of basis functions used to expand the poly-electronic Ψ. In fact, the presence of the exchange operator K_{ij} in the Fock Hamiltonian forces the evaluation of four-centre integrals. On the other hand, in the KS Hamiltonian there are no exchange terms to be evaluated, and the integrals involved are only two-centred. Thus, the computational effort required to solve the KS equations is only proportional to N^2. In recent years the progresses in synthetic chemistry of transition metal complexes with ligand atoms of the group 13 (B, Al, Ga) has encouraged the parallel development of theoretical tools that can investigate the nature of these M-E bonds. Theory often provides a means to forecast the success or the failure of a synthetic attempt prior to the laboratory work.

Ehlers *et al.* in 1998[47] examined alternatives to the CO ligand in complexes of the general formula $M(CO)_n(AE)$, where AE can be N_2, CO, BF, BNH_2, $BNMe_2$ or BO^-. Results of the theoretical investigation show that BF is a much better σ donor than CO (due to a more extended HOMO on boron), but it is nearly as good as a π acceptor when bound to a transition metal. The consequence is a build up of positive charge at boron, and a metal-boron bond which is highly polarised. Hence, although the M-B bond is thermodynamically stronger then the M-C bond, it is much less kinetically stable. This enhanced polarity upon coordination facilitates nucleophilic attack, especially if there is no steric protection coming from a bulky substituent on boron. BNH_2 or $BNMe_2$ could be a valid alternative to BF, the amino group providing better steric protection (besides offering extra electronic stabilisation to boron via the basic behaviour of nitrogen lone pair). BO^- is a special case, in view of the fact that it bears a negative charge; indeed, figures show that it is a very good σ donor, but it does not have any π acidity at all. Its frontier orbitals have a similar shape to the ones of the other isolobal species, but their energies are much higher, just because of the presence of a negative charge. This situation is unfavourable for interaction with the frontier orbitals of the metal fragment and the M-BO bond is weak. If a bridging coordination mode of the BR

ligand between two metal centres is considered, the presence of a second metallic atom directly linked to boron can restore the balance between σ donation and π acceptance, as it has been shown for the species $Fe_2(CO)_8$(μ-AE) and $Mn_2(Cp)_2(CO)_4$(μ-AE), drawn in Figure 8.

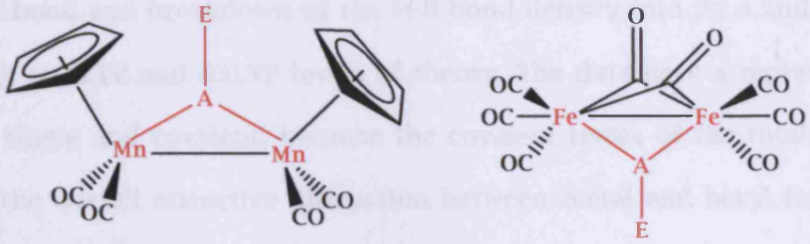

Figure 8 – Study complexes containing the isolelectronic ligands AE in a bridging mode

Giju *et al.* in year 2000[48] carried out DFT calculations using the B3LYP functional on osmium 16 and 18VE complexes $(PH_3)_2(CO)(Cl)Os\text{-}BX_2$ and $(PH_3)_2(CO)_2(Cl)Os\text{-}BX_2$, where the boryl ligand is BH_2, BF_2, $B(OH)_2$, B(OCH=CHO) or BCat. In the cases where a crystal structure was available, comparison of the calculated geometries with the experimental ones has been undertaken. With the $B(OH)_2$ ligand the lowest-energy conformations are those where there is possibility to engage in hydrogen bonding between the boryl hydrogen and the chlorine atom on the metal centre. Barriers of rotation about the Os-B bond are not very high, and they do not seem to change very much for the different boryl ligands. The [Os]-BR_2 bond in both classes of compounds is polarised towards osmium, and its stability is mainly due to X→B π donation rather than Os→B π donation (apart from the case of the BH_2 ligand).

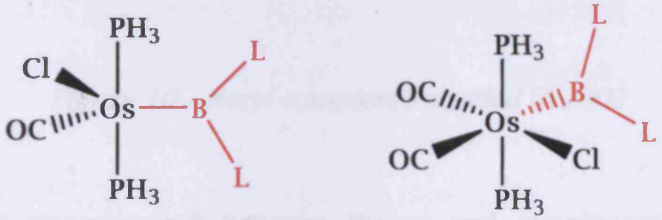

Figure 9 – Five- and six-coordinate osmium boryl model compounds

Work undertaken by Dickinson *et al.* about the analysis of bonding in cyclopentadienyl transition metal boryl complexes was published in Organometallics in 2002[49]. Starting from complexes of general formula $(C_5R_5)M(CO)_2\text{-}BX_2$ (Figure 10), geometry optimisation, comparison of the (available) structural data with the calculated ones, rotational profiles around the M-B bond and breakdown of the M-B bond density into its σ and π contributions were performed, at BLYP and B3LYP levels of theory. The data gave a representation of the $M\text{-}BX_2$ bond as single and covalent, because the covalent terms of the total energy account for ca. 70% of the overall attractive interaction between metal and boryl fragments, with σ donation overwhelmingly predominating over π back-donation, even in the most favourable cases of Fe-B π back-bonding (84%:16% for $(Cp)Fe(CO)_2(BH_2)$ for example). Information coming from the rotational energy profile around the M-B bond confirm the previous data: the rotational barrier is very low, and it represents motion across a very shallow potential energy surface, with the difference in energy for several rotamers being very small. The theoretical work presented in this thesis is a (logical) extension of this, as discussed in chapters 3 and 5.

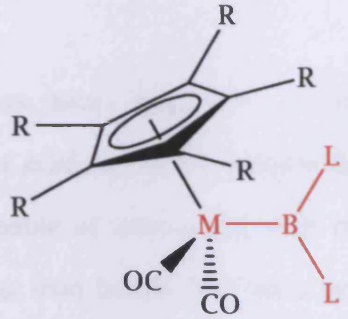

(R=H, Me; M=Fe(0), Co(I), Ru(0))

Figure 10 - Boryl complexes studied in 2002

Another example of "intermixing" between theory and experiment is the case of the compound $(CO)_4Fe\text{-}GaAr^*$ (Ar*=2,6-(2,4,6-tri-isopropylphenyl)-phenyl) made by the Robinson group in 1997[50], which represents the first case of an unsupported M-GaR bond, where R is not a strong π donor. The XRD data reveal a linear Fe-Ga-C(Ph) arrangement and rather short Fe-Ga bond. The authors suggested a triple Fe-Ga bond for this complex, but this idea was dismissed by Cotton and Feng in a later paper[51]. The arguments about the alleged Fe≡Ga

triple bond have been critically examined in a theoretical study by Boehme and Frenking in 1999[52]. They analysed the bonding situation in the model $(CO)_4$Fe-GaPh (Figure 11) using the charge decomposition analysis method (CDA) at the BP86 level of theory. The conclusion is that the classification as single or triple bond is meaningless, since the main contributions to the bond are *ionic* and not covalent. In other words, there is no dispute about the nature of the bond, because there is virtually no (covalent) bond between the two fragments $[Fe(CO)_4]$ and [GaPh].

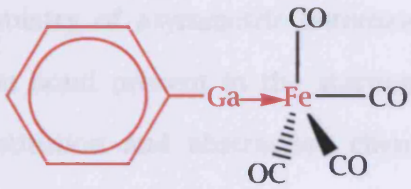

Figure 11 - Model compound for the complex $(CO)_4$Fe-GaAr (refer to text above)*

1.4 - Aims of the project and thesis organisation

The initial work described in this thesis began as a continuation of previous work on the synthesis and characterization of *bridging boryl systems* (boron ligands containing two boryl units on the same molecule capable of interacting with two different metal centers at one time). Prior to this work bridging iron boryls had been synthesised with a central aromatic spacer, derived from 2,5-di(hydroxo)paraquinone [53]. In order to make a comparison of the electronic and structural properties of different bridging boryls, the synthesis and characterization of analogous complexes featuring an *aliphatic* spacer (derived from pentaerythrol) has been undertaken. In chapter 3 the description of the ligand and related iron complexes are developed, together with the aforementioned comparison between the two structures, using both the traditional spectroscopic and structural techniques (multinuclear NMR, IR, X-ray diffraction) and some other previously under-utilised methods (Mössbauer spectroscopy, Raman, cyclic voltammetry). Following this, the target was to make the *terminal* analogue of this species from the corresponding aliphatic terminal boryl ligand, whose syntheses are also described in chapter 3. These analyses bring into play not only

spectroscopic and structural data, but also theoretical calculations (σ and π M-B bond densities and rotational energy barriers around the M-B bond).

The limited number of examples of base-stabilised boryl complexes in the literature[9,54] was the motivation that lead us to attempt the preparation of some complexes belonging to this category, starting from different bases (trimethylphosphine and tetrahyrofuran). Reference to the corresponding "non-stabilised" boryl species could provide additional information about the effect of a Lewis base on the stability of the metal-boron bond. The last part of chapter 3 deals with the chemistry of asymmetric heteroatom-stabilised boron-containing ligands, where the metal-boron bond present in the starting material is not cleaved upon nucleophilic attack. This substitution and abstraction chemistry is relatively new[3f], and, following the path exploited by this research group, new iron derivatives of the oxygen-stabilised *(mesityloxo)boryl* ligand have been prepared and characterised. Comparison with the related nitrogen-stabilised complexes has also been described.

After a detailed analysis of the metathetical pathway to new low-valent boron metal complexes, there has also been a work carried out using oxidative addition chemistry, which represents the contents of chapter 4. In this case both late transition metals (Pt, Rh) and main group metals (In, Sn) have been chosen, using both bridging and terminal ligands. Mechanistic studies of the reaction of $Pt(L)_2$(ethene) and catecholborane HBCat have been investigated, to examine in depth the reaction properties of the related boryl complexes which form during the reaction. Variable temperature NMR (VT-NMR) has been used to try to identify intermediates forming at low temperature, providing extra information about the mechanism of the overall process.

Finally, chapter 5 contains all the results coming from DFT studies on terminal borylene and related gallium-containing complexes. Since very little is known about the nature of the metal-element bond in these new molecules (the available experimental data being scarce), a theoretical prediction of their structural properties and stabilities has been carried out. In complexes of general formula $[(C_5R_5)M(L)_2{=}BY]^+$ each substituent in the molecule has been

systematically varied to see the effects on the total energy and on the relative contribution of σ and π bond density to the M=B double bond.

References for chapter 1

(1) See, for example, *Contemporary Boron Chemistry*, edited by M.G. Davidson, A.K. Hughes, T.B. Marder and K. Wade, Royal Society of Chemistry (2000), pages 197-367.

(2) (a) Herberich G.E., *J. Organomet. Chem.*, 1987, 319, 9; (b) Herberich G.E., *Angew. Chem. Int. Ed. Engl.*, 1970, 9, 805; (c) Herberich G.E., *Chem. Ber.*, 1976, 109, 2382.

(3) General reviews on the subject: (a) Braunschweig H. , Colling M., *Coord. Chem. Rev.*, 223 (2001), 1; (b) Braunschweig H., *Angew. Chem. Int. Ed. Engl.*, 1998, 37, 1786; (c) Irvine G.J., Lesley M.G.J., Marder T., Norman N.C., Rice C.R., Robins E.G., Roper W.R., Whittell G.R., Wright J.L., *Chem. Rev.* 1998, 98, 2685; (d) Wadepohl H. *Angew. Chem. Int. Ed. Engl.*, 1997, 36, 2441; (e) Smith M.R. III, *Prog. Inorg. Chem.* 48 (1999), 505; (f) Aldridge S., Coombs D.L., *Coord. Chem. Rev.* 2004, in press.

(4) Schmidt G., *Angew. Chem. Int. Ed. Engl.*, 1970, 9, 819.

(5) Nöth H., Schmid G., *Angew. Chem. Int. Ed. Engl.*, 1963, 2, 623.

(6) Hartwig J.F., Huber S., *J. Am. Chem. Soc.*, 1993, 115, 4908.

(7) Männig D., Nöth H., *Angew. Chem. Int. Ed. Engl.*, 1985, 24, 878.

(8) Knorr J.R., Merola J.S., *Organometallics* 1990, 9, 3008. Another example published almost at the same time is *fac*-[Ir(H)$_2$(PMe$_3$)$_3$(9-BBN)], appearing in: Baker R.T., Ovenall D.W., Calabrese J.C., Westcott S.A., Taylor N.J., Williams I.D., Marder T.B., *J. Am. Chem. Soc.* 1990, 112, 9399.

(9) Yashue T., Kawano Y., Shimoi M., *Chemistry Letters* 2000, 58.

(10) (a) Braunschweig H., Ganter B., Koster M., Wagner T., *Chem. Ber.* 129 (1996), 1099; (b) Braunschweig H., Koster M., Wang R., *Inorg. Chem.* 38 (1999), 415; (c) Braunschweig H., Koster M., *J. Organomet. Chem.* 588 (1999), 231.

(11) Braunschweig H., Kollann C., Müller M., *Eur. J. Inorg. Chem.* (1998), 291.

(12) Hartwig J.F., He X., *Organometallics* 15 (1996), 5350.

(13) Braunschweig H., Koster M., Klinkhammer K.W., *Angew. Chem. Int. Ed. Engl.*, 1999, 38, 2229.

(14) (a) Clegg W., Lawlor F.J., Lesley G., Marder T.B., Norman N.C., Orpen A.G., Quayle M.J., Rice C.R., Scott A.J., Souza F.E.S., *J. Organomet. Chem.* 550 (1998), 183; (b) Dai C., Stringer G., Corrigan J.F., Taylor N.J., Marder T.B., Norman N.C., *J. Organomet. Chem.* 513 (1996), 273; (c) Clegg W., Lawlor F.J., Marder T.B., Nguyen P., Norman N.C., Orpen A.G., Quayle M.J., Rice C.R., Scott A.J., Souza F.E.S., Robins E.G., Stringer G., Whittell G.R., *J. Chem. Soc., Dalton Trans.*, 1998, 301.

(15) Xe H., Hartwig J.F., *Organometallics* 15 (1996), 400.

(16) Hartwig J.F., Xe H., *Angew. Chem. Int. Ed. Engl.*, 35 (1996), 315.

(17) Hartwig J.F., Huber S., *J. Am. Chem. Soc.* 1993, 115, 4908.

(18) (a) Lesley M.J.G., Nguyen P., Taylor N.J., Marder T.B., Scott A.J., Clegg W., Norman N.C., *Organometallics* 1996, 15, 5137; (b) Curtis D., Lesley M.J.G., Norman N.C., Orpen A.G., Starbuck J., *J. Chem. Soc., Dalton Trans.*, 1999, 1687.

(19) (a) Waltz K.M., Hartwig J.F., *Science*, 1997, 277, 211; (b) Waltz K.M., Muhoro C.N., Hartwig J.F., *Organometallics*, 1999, 18, 3383.

(20) Clark G.R., Irvine J.G., Roper W.R., Wright L.J., *Organometallics*, 1997, 16, 5499.

(21) Pelter A., Smith K., Brown H.C., *Borane Reagents*, Academic Press (1988).

(22) Miyaura N., Suzuki A., *Chem. Rev.* 95 (1995), 2457.

(23) Burgess K., Ohlmeyer M.J., *Chem. Rev.* 91 (1991), 1179.

(24) Burgess K., Van Der Donk W.A., Westcott S.A., Marder T.B., Baker R.T., Calabrese J.C., *J. Am. Chem. Soc.* 1992, 114, 9350.

(25) (a) Marder T.B., Norman N.C., *Top. Catal.* 5 (1998), 63; (b) Nguyen P., Coapes R.B., Woodward A.D., Taylor N.J., Burke J.M., Howard J.A.K., Marder T.B., *J. Organomet. Chem.* 652 (2002), 77; (c) Ishiyama T., Yamamoto M., Miyaura N., *Chem. Comm.*, 7 (1997), 689; (d) Ishiyama T., Miyaura N., *Chem. Rec.* 3(5), 2004, 271; (e) Iverson C.N., Smith M.R., *Organometallics* 1997, 16, 2757.

(26) (a) Waltz K.M., He X., Muhoro C., Hartwig J.F., *J. Am. Chem. Soc.* 1995, 117, 11357; (b) Waltz K.M., Hartwig J.F., *J. Am. Chem. Soc.* 2000, 122, 11358.

(27) Huiyuan C., Hartwig J.F., *Angew. Chem. Int. Ed. Engl.*, 1999, 38, 3391.

(28) (a) Kawamura K., Hartwig J.F., *J. Am. Chem. Soc.* 2001, 123, 8422; (b) Ishiyama T., Takagi J., Miyaura N., Anastasi R.N., Hartwig J.F., *J. Am. Chem. Soc.* 2002, 124(3), 390; (c) Ishiyama T., Takagi J., Hartwig J.F., Miyaura N., *Angew. Chem. Int. Ed.* 2002, 41, 3056; (d)

Tamura H., Yamazaki H., Sato H., Sakaki S., *J. Am. Chem. Soc.* 2003, 125, 16114; (e) Lam W.H., Lin Z.Y., *Organometallics* 2003, 22, 473; (f) Lam W.H., Lam K.C., Lin Z.Y., Shimada S., Perutz R.N., Marder T.B., *Dalton Trans.* 2004, 10, 1556.

(29) General reviews on the subject: (3a, 3b, 3f); (a) Braunschweig H., Colling M., *J. Organomet. Chem.*, 614-615 (2000), 18; (b) Wrackmeyer B., *Angew. Chem. Int. Ed. Engl.*, 1999, 38, 771; (c) Braunschweig H., Colling M., *Eur. J. Inorg. Chem.*, 2003, 393.

(30) Braunschweig H., Wagner T., *Angew. Chem. Int. Ed. Engl.*, 1995, 34, 825.

(31) (a) Braunschweig H., Kollann C., Englert U., *Eur. J. Inorg. Chem.* (1998), 465; (b) Braunschweig H., Kollann C., Klinkhammer K.W., *Eur. J. Inorg. Chem.* (1999), 1523.

(32) Cowley A.H., Lomelì V., Voigt A., *J. Am. Chem. Soc.* 1998, 120, 6401.

(33) Braunschweig H., Kollann C., Englert U., *Angew. Chem. Int. Ed. Engl.*, 1998, 37, 3179.

(34) Coombs D.L., Aldridge S., Jones C., Willock D.J., *J. Am. Chem. Soc.* 125 (2003), 6356.

(35) Shimoi M., Ikubo S., Kawano Y., *J. Am. Chem. Soc.* 120 (1998), 4222.

(36) Braunschweig H., Colling M., Hu C., Radacki K., *Angew. Chem. Int. Ed. Engl.*, 2003, 42, 205.

(37) Irvine G.J., Rickard C.E.F., Roper W.R., Williamson A., Wright L.J., *Angew. Chem. Int. Ed. Engl.*, 2000, 39, 948.

(38) Grumbine S.K., Tilley T.D., Arnold F.P., Rheingold A.L., *J. Am. Chem. Soc.* 116 (1994), 5495.

(39) Braunschweig H., Koster J., *J. Organomet. Chem.* (1999), 588, 231.

(40) Coombs D.L., Aldridge S., Coles S.J., Hursthouse M.B., *Organometallics* 2003, 22, 4213.

(41) (a) Parr R., Yang W., *Density Functional Theory of Atoms and Molecules*, Oxford University Press (1989); (b) Jensen F., *Introduction to Computational Chemistry*, Wiley & Sons, New York (1999); (c) Cramer C.J., *Essentials of Computational Chemistry, Theories and Models, Wiley and Sons*, New York (2002).

(42) Slater J.C., *Advan. Quantum Chem.* 6, 1 (1972).

(43) See, for example: (a) PW86: Perdew J.D., Wang Y., Phys. Rev. B, 1986, 33, 8800; (b) PW91: Perdew J.P., Wang Y., *Phys Rev. B*, 1992, 45, 13244; (c) B3: Becke A.D., *J. Chem. Phys.*, 1993, 98, 5648.

(44) Becke A.D., *Phys. Rev. A*, 1988, 33, 3098.

(45) Lee C., Yang W., Parr R.G., *Phys. Rev. B*, 1988, 37, 785.

(46) Boehme C., Uddin J., Frenking G., *Coord. Chem. Rev.*, 197 (2000), 249.

(47) Ehlers A.W., Baerends E.J., Bickellhaupt F.M., Radius U., *Chem. Eur. J.*, 1998, 4, 210. See also Chapter 5, references (4a) and (4b).

(48) Giju K.T., Bickellhaupt F.M., Frenking G., *Inorg. Chem.* 2000, 39, 4776.

(49) Dickinson A.A., Willock D.J., Calder R., Aldridge S., *Organometallics* 2002, 21, 1146.

(50) Su J., Li X.W., Crittendon R.C., Campana C.F., Robinson G.H., *Organometallics* 16 (1997), 4511.

(51) Cotton F.A., Feng X., *Organometallics* 17 (1998), 128.

(52) Boehme C., Frenking G., *Chem. Eur. J.*, 1999, 5, 2184.

(53) Aldridge S., Calder R.J., Dickinson A.A., Willock D.J., Steed J.W., *Chem. Commun.*, 2000, 1377.

(54) (a) Kawano Y., Yashue T., Shimoi M., *J. Am. Chem. Soc.* 1999, 121, 11744. (b) In the final stages of the preparation of this thesis Braunschweig also published the first example of preparation of a base-stabilised boryl complex *via direct reaction* of a boryl metal complex with a Lewis base: Braunschweig H., Radacki K., Seeler F., Whittell G.R., *Organometallics* 2004, 23, 4178.

2 - Experimental techniques

2.1 - Manipulation of air-sensitive compounds and inert atmosphere techniques [1]

Most of the compounds described in this work are air-sensitive, and, as a result of this, it is essential to employ special laboratory glassware and apparatus that exclude both air and moisture. Schlenk and high vacuum techniques are the ones which meet our needs. Exclusion of the atmosphere during filtration, crystallisation, sublimation, sample transfer and other simple operations is achieved by a special kind of glassware (*Schlenk glassware*). The most common method used to avoid the contact of the sample with air is to create an inert atmosphere with an unreactive gas like nitrogen or argon. Schlenk glassware and syringe techniques allow the handling of solutions and other liquid samples under inert gas, while *glove-box* techniques are more suitable for the handling and storage of solids.

The Schlenk technique utilises a flask which has a standard ground-glass joint and a sidearm with a stopcock, in order to be connected to a vacuum-nitrogen line. Shapes can be different, and besides tubes, solid containers, dropping funnels, fritted funnels, sublimation apparatus and other types of flask are used. See Figure 1.

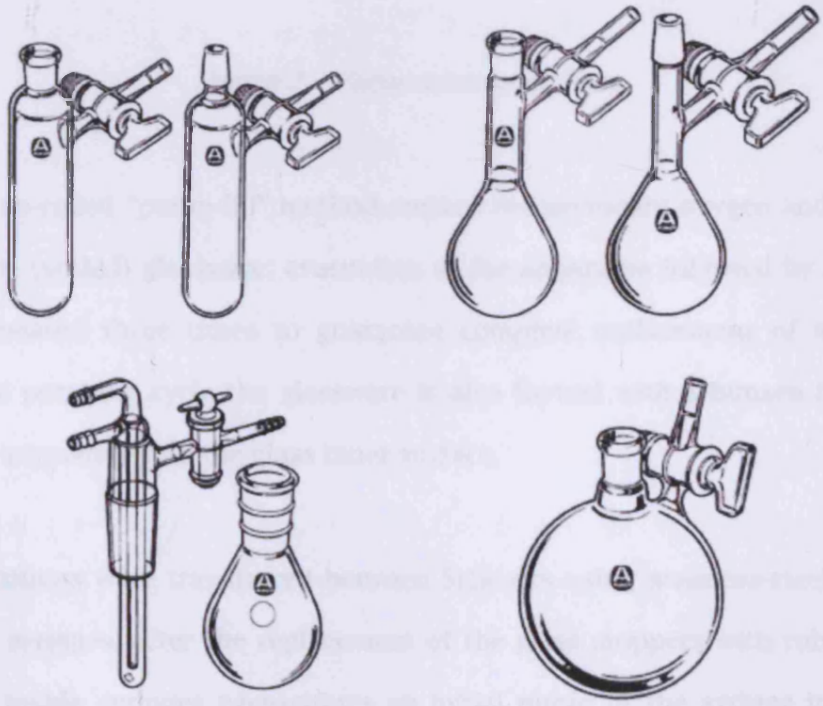

Figure 1 - Schlenk glassware

The vacuum-nitrogen Schlenk line (Figure 2) consists of a Pyrex glass tube featuring a number of two-way stopcocks, which are a convenient means of switching between vacuum and nitrogen (or other inert gas employed). All the joints between different glass parts that form the line are lubricated with silicone grease, to prevent leaking and blocking of the taps. Glassware containing the samples is attached to the stopcocks via a number of heavy walled rubber tubes, and several pieces of apparatus can be purged at once. Evacuation along the line is made by a mechanical vacuum pump in conjunction with a liquid nitrogen trap that freezes volatiles from the line and prevents contamination of the pump oil. A Pirani pressure gauge is attached to the line so that the internal pressure can be monitored over the range 1-10^{-3} Torr. The pure inert gas used (usually argon) is introduced into the line from a cylinder through a scavenger column packed with molecular sieves, to remove any trace of moisture. The whole system is kept under stable pressure conditions by a mercury bubbler attached to the gas outlet.

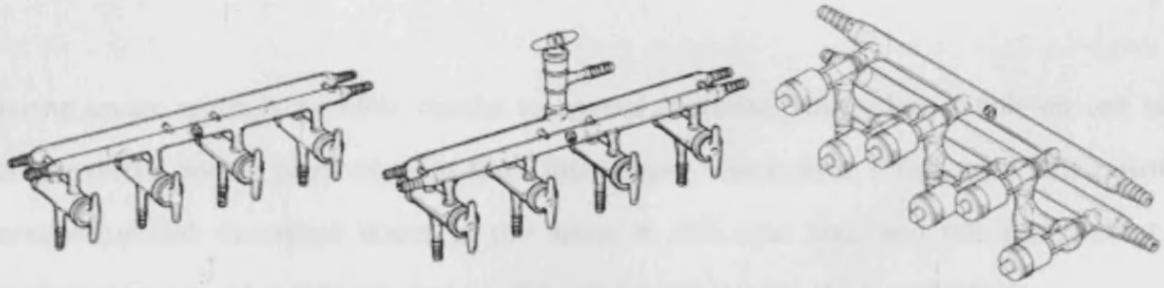

Figure 2 – Vacuum-nitrogen lines

The use of the so-called "pump-fill" method creates the necessary oxygen and moisture free conditions in the (sealed) glassware: evacuation of the apparatus followed by filling with the inert gas is repeated three times to guarantee complete replacement of air with argon. During the final pumping cycle the glassware is also flamed with a Bunsen burner, to help removing water physiorbed on the glass inner surface.

Liquids and solutions were transferred between Schlenks using stainless-steel cannulae and glass or plastic syringes, after the replacement of the glass stoppers with rubber septa. The "dead volume" inside syringes necessitates an initial purge of the syringe itself with inert gas, accomplished by keeping a steady inert-gas flow through the tubing and inserting the

needle through the tube and into the gas stream. The inert gas is "sucked" into the syringe and expelled several times. When cannulae are employed, a pressure differential is maintained to perform the liquid transfer; this differential is created by flowing inert gas into the filled tube and keeping at atmospheric pressure the empty tube with an hypodermic needle:

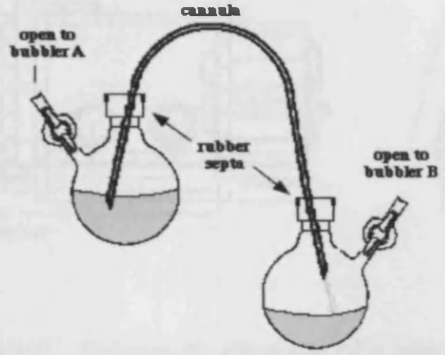

Figure 3 – Liquid transfer under inert atmosphere

Filtering under argon is possible thanks to special cannulae, with a larger hole on one side that is covered with a piece of glass-fibre filter paper sealed with Teflon tape. The positive pressure method described above is the same in this case too, and the supernatant is transferred into another Schlenk, leaving the solid precipitate in the first Schlenk.

Glove boxes (Figure 4) are a straightforward means of handling air-sensitive solids. In its simplest form, it consists of a gas-tight box fitted with a window, a pair of gloves and a transfer port. The entire system is flushed with an inert gas. All the chemicals are introduced in the box via the usual "pump-fill" method applied to the transfer port. The nitrogen (99.9% purity) that flows through the box comes from a cylinder, and it is internally recirculated through catalyst, molecular sieve and solvent scrubbing columns achieving an atmosphere with moisture and oxygen levels of less than 10ppm and 5ppm respectively[2]. In the case of this study a "Saffron Scientific Omega" model glove box was employed.

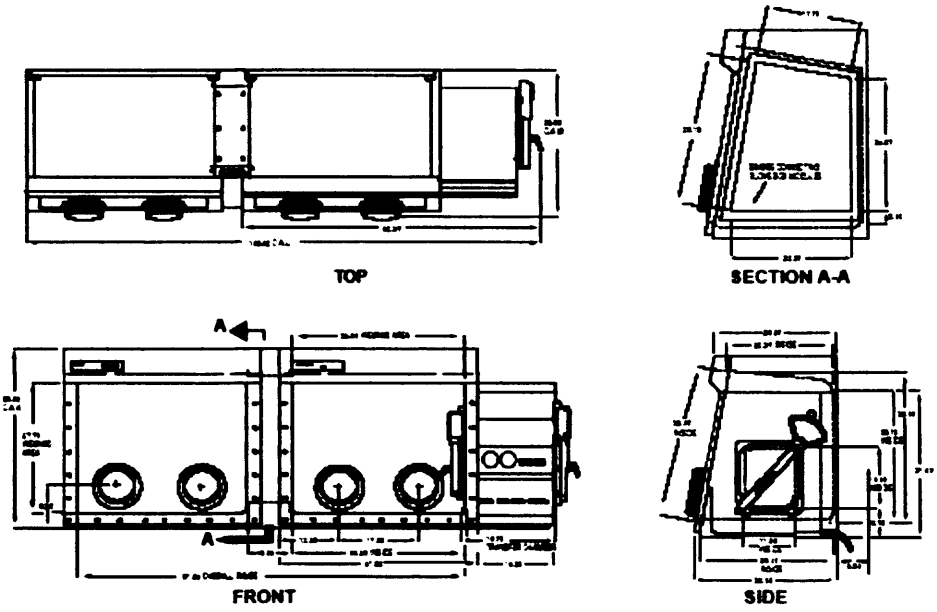

Figure 4 - Schematic drawing of a glove box

In cases where the vacuum provided by the rotary pump is not sufficiently high (as happens for vacuum sublimation or removal of trace solvents from a solid sample), a ***high vacuum line*** is needed. It consists of a Pyrex glass tube incorporating greaseless Young's taps. The combination of a mercury diffusion pump and a normal mechanical pump reduces the internal pressure to 10^{-4} Torr.

2.2 - Purification of solvents [3]

All the solvents used to perform the syntheses described both in the present and the following chapters have been previously dried by refluxing over an appropriate desiccant under an argon atmosphere: for the non-halogenated solvents (toluene, hexane, THF, diethyl ether) sodium or potassium metal in combination with benzophenone are the drying agents of choice. The organic ketone acts as an indicator of the presence of active electrons in solution, because the reaction with the alkali metal produces the intense blue *benzophenone ketyl* radical anion:

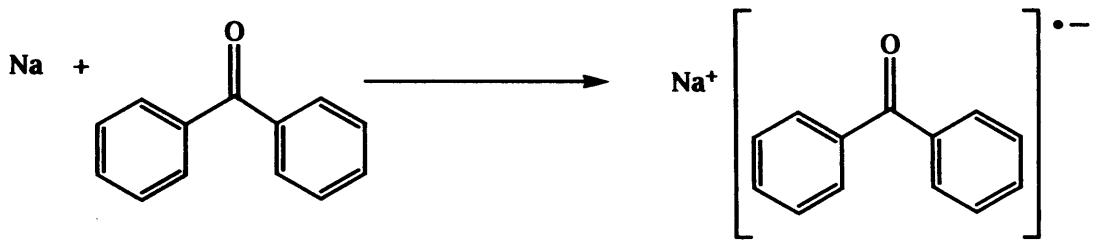

benzophenone ketyl (deep blue)

Scheme 1 - Reaction of sodium with benzophenone

The electron is then transferred to water during the reduction process. For halogenated solvents like dichloromethane reflux under argon over calcium hydride CaH_2 is the optimal solution for purification. Removal of oxygen and other volatile contaminants is achieved either by bubbling argon or nitrogen through the solvent for 15-20 minutes or via several *freeze-pump-thaw* cycles. The latter method consists of pumping on the frozen solid solvent under vacuum, thawing it out in a closed system and repeating the procedure.

As far as the commercial sources of chemicals are concerned, the vast majority of the materials have been used as they were supplied, with no further purification (the quoted purity on the labels is always higher than 97%). If a special treatment is necessary, it is specified in the paragraph describing the related preparation. Deuterated solvents are stored under argon over potassium mirror (benzene-d_6, toluene-d_8) or over flamed-out molecular sieves (chloroform-d, methylene chloride-d_2).

2.3 - Preparation of precursors

2.3.1 - Metallic reagents

Preparation of $Na[(\eta^5\text{-}C_5R_5)Fe(CO)_2]$ ($R_5=H_5$, NaFp; $R_5=Me_5$, NaFp*; $R_5=H_4Me$, NaFp')[41]

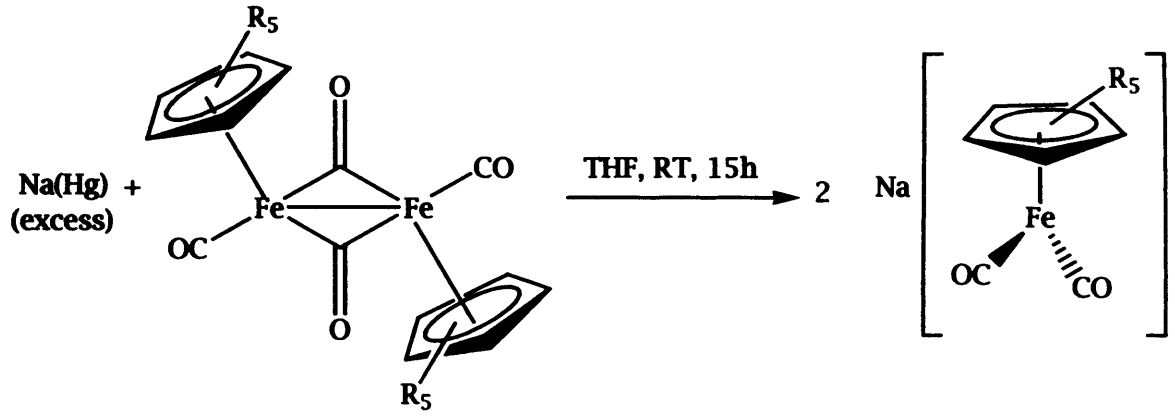

The method described is the same for the three derivatives NaFp, NaFp* and NaFp', therefore the description is given only for the Fp' derivative. Typically, 2 g (5.23 mmol) of the dimeric precursor (commercially available from Aldrich in the case of Fp_2, while Fp'_2 and Fp^*_2 have been made respectively by Dr. Richard J. Calder and Dr. Deborah L. Coombs of Cardiff University) were dissolved in 150 mL of freshly distilled THF, and the solution was transferred via cannula onto sodium amalgam (0.5 g, 4 equiv. of Na). The reaction mixture was stirred overnight, the solution filtered and the solvent removed *in vacuo*, yielding 1.6 g (71.4%) of a dark red-brown powder. Since the presence of coordinating solvents such as THF leads to decomposition of many of the complexes synthesised in this work, it is necessary to remove all the traces of coordinating solvents. This was achieved by washing the product several times with hot toluene and drying by prolonged pumping under high vacuum. Due to its high sensitivity to water and oxygen, no characterising NMR data were obtained for this salt; therefore, it was assumed to be pure for the following synthetic steps, and used without further treatments.

Preparation of $Na[Mn(CO)_5]$ [5]

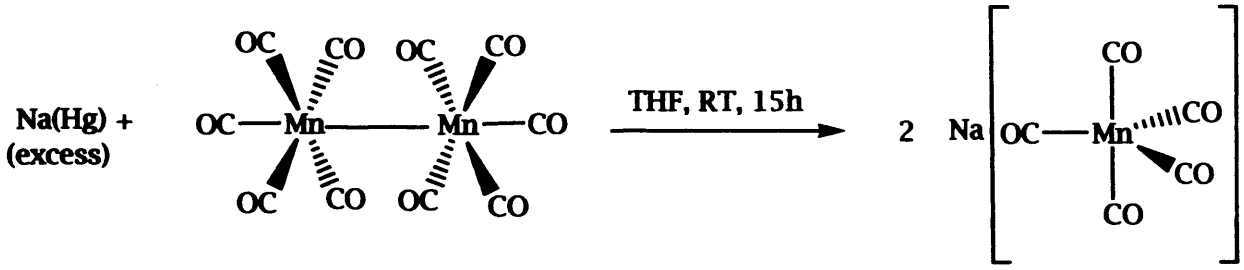

The synthesis is of the same kind as that used for the iron anions. The precursor is $Mn_2(CO)_{10}$, which is commercially available (Aldrich). Dimanganese decacarbonyl (3.8 g, 9.74 mmol) was dissolved in 50mL THF and the solution transferred onto a sodium amalgam (1 g, 4.5 equiv. of Na) at room temperature. The colour of the solution immediately turned from orange to deep green. The mixture was left to react overnight, then filtered. Removal of THF *in vacuo* yielded 3.11 g (71.3%) of a light green powder. In order to remove all traces of THF from the synthesis, the same drying procedure as used for the iron derivative was applied. The salt was taken as starting material in the following syntheses without further purification, taking its purity for granted.

Preparation of $Na[(\eta^5\text{-}C_5H_5)W(CO)_3]$ (NaWp) [6]

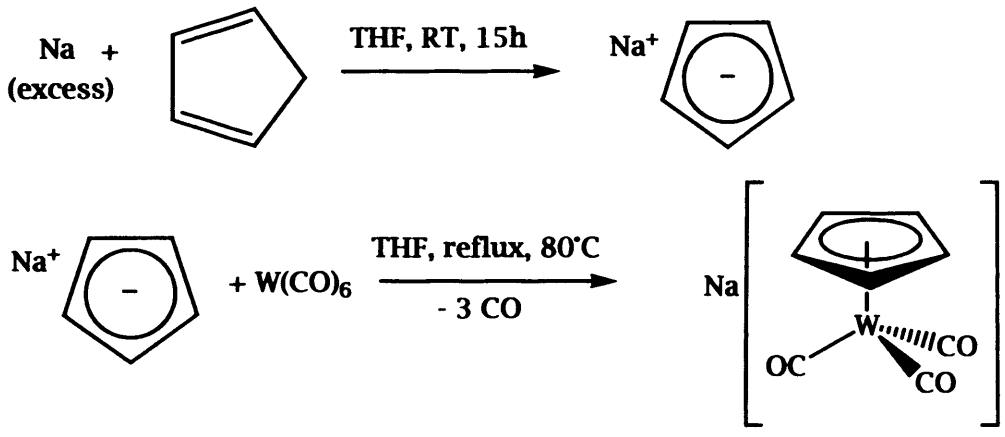

The synthesis requires $Na(C_5H_5)$ as a starting material; this was prepared from cyclopentadiene (C_5H_6) and sodium sand in THF. Sodium metal (35 g, 1.52 mol) was melted in the high-boiling solvent o-xylene (b.p. 147°C) in a Schlenk tube, with vigorous stirring. The xylene was then removed and the sand washed once with THF. After removal of the washing solvent, another fresh 100 mL THF was added, and this suspension was mixed at room temperature over a period of 1 h with a solution of 90 mL of cracked cyclopentadiene (1.34 mol). Strong bubbling was observed, indicating the production of the by-product H_2. When bubbling ceased, the reddish solution was filtered into another Schlenk, and the solvent removed *in vacuo*, to leave 65 g (55.1% yield) of a white powder that was dried under high vacuum and stored in the glove box.

The second step is the reaction of $Na(C_5H_5)$ with tungsten hexacarbonyl. $W(CO)_6$ (3.6 g, 0.01 mol) of (Aldrich) was dissolved in 15 mL THF, and the colourless solution added to a $Na(C_5H_5)$ solution (0.88 g, 0.01 mol) in 15 mL THF. The resulting yellow mixture was refluxed at a temperature of circa 80°C for 8 h. After this time, the dark yellow-orange solution was filtered and the solvent removed with the usual method, leaving a bright yellow solid that was washed with 30 mL toluene and 15 mL hexane and dried under high vacuum for 15 h before being stored in the glove box. Final yield: 2.3 g (63.2%). It was employed as it was in the subsequent syntheses.

Preparation of $K_2Fe(CO)_4$ [7]

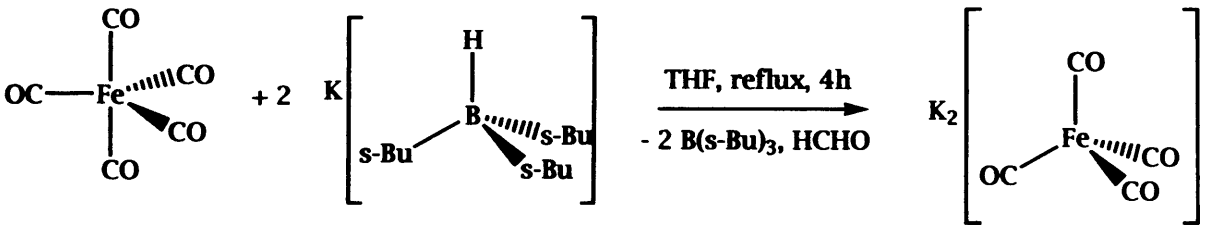

A 0.1 M solution of K-selectride in THF (35 mL, 3.5 mmol) was diluted in 35 mL of fresh THF. $Fe(CO)_5$ (Aldrich, 2.2 mL, 16.7 mmol, 4.8 equiv.) was added with a syringe, and the mixture refluxed for 4 h under argon. After this time, the reaction mixture was cooled and the

precipitate allowed to settle. The red supernatant was removed, and the off-white solid precipitate washed twice with 50 mL portions of hexane and dried under high vacuum for 45 minutes. It was stored in a flame dried round bottom flask in the glove box. Yield: 3.5 g (86.2%). It was used as it was without further purification.

Preparation of $Li[(\eta^5\text{-}C_5H_5)Fe(CO)(PMe_3)]$[8]

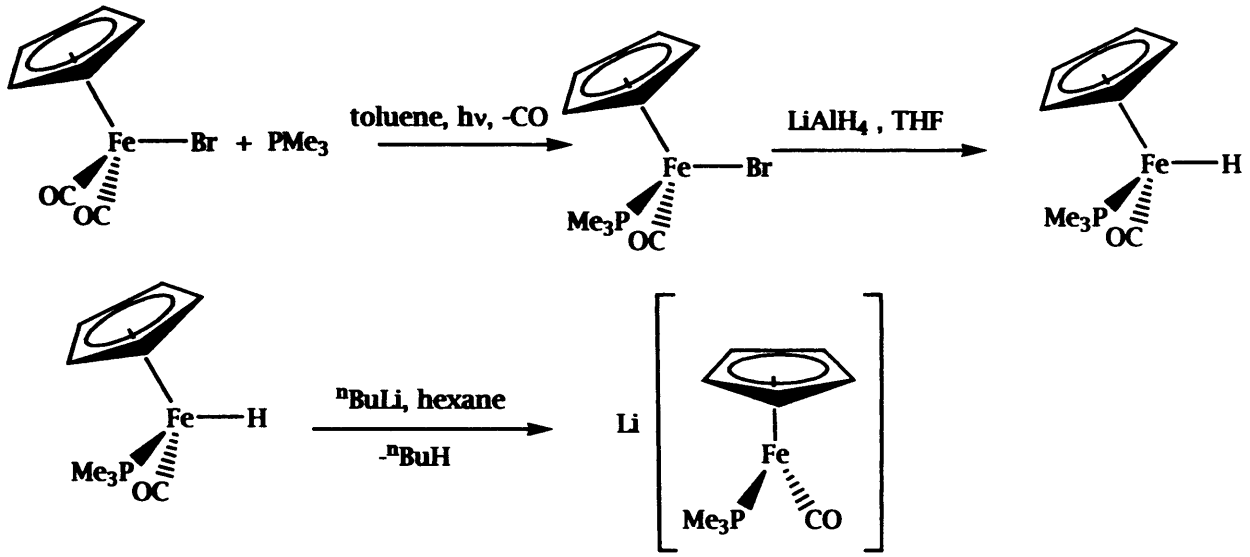

The precursor $(\eta^5\text{-}C_5H_5)Fe(CO)_2Br$ (1.5 g, 5.8 mmol) was dissolved in 150 mL of toluene, and 0.7 mL (6.8 mmol, 1.2 equiv.) of trimethylphosphine (Aldrich) were added to the solution *via* syringe. The mixture was irradiated with a UV-lamp for 15 h, and, after this time, the greenish-brown supernatant was filtered into another Schlenk and the solid residue washed with more toluene (four washings of circa 20 mL each). The washings and the supernatant were combined, and the solvent removed *in vacuo*, to leave pure $(\eta^5\text{-}C_5H_5)Fe(CO)(PMe_3)Br$ as a green solid (yield: 0.35 g, 20%).

In the following step, 0.35 g of $(\eta^5\text{-}C_5H_5)Fe(CO)(PMe_3)Br$ were dissolved in 50 mL THF, and mixed with a solution containing 0.175 g (4.6 mmol, 4 equiv.) $LiAlH_4$ (Aldrich) in 50 mL THF. At room temperature, the mixture was left to react for 15 h. After this time, the excess of reducing agent was decomposed by adding ethanol, until effervescence ceased. The solvent

was then removed *in vacuo*, and the light green solid left sublimed on a Schlenk line, yielding a yellow solid $(\eta^5\text{-}C_5H_5)Fe(CO)(PMe_3)H$ in quantitative yield (0.26 g).

The final step is the abstraction of the iron-bound proton using butyl lithium. The hydride precursor was dissolved in 100 mL of hexane, and 0.72 mL of a 1.6 M solution of n-BuLi in hexane (Aldrich, 1.15 mmol, 1 equiv.) were added by syringe at room temperature. Immediate formation of an orange precipitate was observed, corresponding to the final lithium salt. After 2 h, the supernatant was filtered off, and the solid dried *in vacuo*. Final yield: 0.25 g (92%). The purity of the compounds at each stage was checked *via* ^{31}P NMR, comparing the δ_p values with those reported in the literature.

Preparation of $[RhCl(coe)_2]_2$ [9]

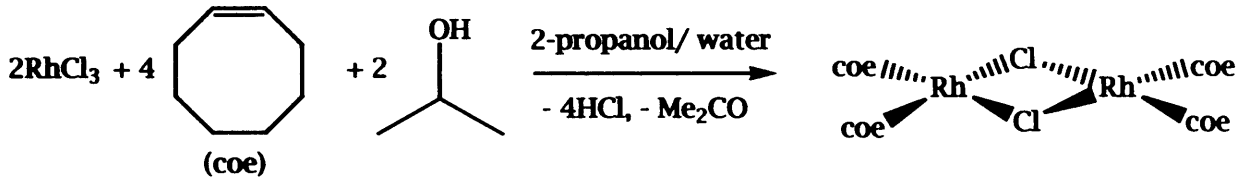

A mixture of 60 mL of 2-propanol and 15 mL of distilled water in a Schlenk was thoroughly degassed with argon for 30 min. $RhCl_3$ (Johnson Matthey, 3 g, 14.4 mmol) was then dissolved in this solvent mixture, and 9 mL (69 mmol, 5 equiv.) of *cis*-C_8H_{14} (Lancaster) were added by syringe. The dark red solution was stirred at room temperature for 35 minutes, then the flask sealed under argon and allowed to stand for one week. During this period, an orange solid precipitated. The supernatant was removed by filtration, and the solid washed once with ethanol (ca. 30 mL). Final drying under high vacuum for 2 h gave 2.52 g (49%) of pure product.

Preparation of $[RhCl(P^iPr_3)_2]_2$ [10]

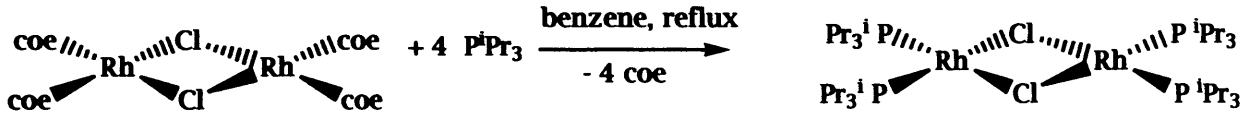

The cyclooctene precursor (0.5 g, 0.7 mmol) was dissolved in 50 mL benzene, and 1 mL of P^iPr_3[11] (5.6 mmol, 8 equiv.) was added by syringe. The reaction mixture changed colour from orange to deep red, and was then brought to reflux for 1.5 h. After cooling to room temperature, the benzene sovent was removed *in vacuo* and the solid residue re-dissolved in ca. 15 mL toluene. The toluene solution was then filtered into a clean Schlenk, concentrated and left at -30°C for two weeks. Over this period, orange crystals of the pure product were precipitated. Further filtration and concentration cycles of the toluene supernatant yielded further product. Total yield: 0.16g (25%). The identity of the product was checked *via* ^{31}P NMR.

Preparation of $[RhCl(PCy_3)_2]_2$ [12]

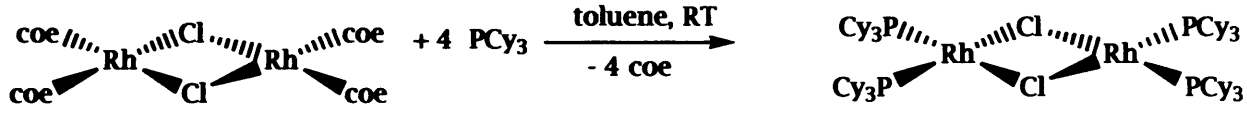

This reaction is akin to that used for the corresponding isopropylphosphine derivative. The precursor (0.44 g, 0.6 mmol) was dissolved in 20 mL of toluene, and 0.7 g (2.5 mmol, 4 equiv.) of PCy_3 (Aldrich) were also dissolved in toluene (20 mL). The two solutions were mixed together at room temperature, causing a colour change to deep red. The mixture was stirred for 15 h, the toluene removed *in vacuo*, and the dark residue washed with hexane (4 x 30 mL). The resulting purple powder was dried under high vacuum for 30 minutes, to yield 0.25 g of final product (30%). Confirmation of the identity of the product came from ^{31}P NMR.

Preparation of In(C_5Me_5)[13]

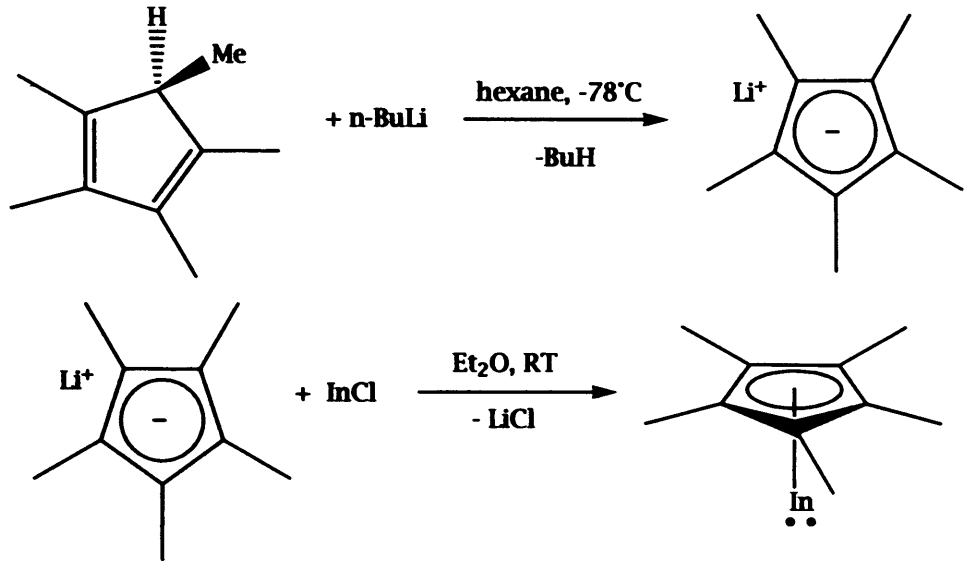

C_5Me_5H (prepared according to the literature method[14], 4 g, 29.3 mmol) of were dissolved in 50 mL of hexane, and the solution cooled to -78°C. A 1.6 M solution of n-BuLi in hexane (Aldrich, 28 mL, 44.8 mmol, 1.5 equiv.) was added by syringe, and the mixture slowly brought back to room temperature. It was then stirred for 15 h, during which time a white prepcipitate formed. The supernatant was filtered to waste, and the solid washed with fresh hexane repeatedly, to eliminate the excess of unreacted butyl lithium. After drying under high vacuum for 30 min., the product $Li(C_5Me_5)$ was transferred to a vial in the glove box. Yield: 2.93 g (70%).

In the subsequent step, 2.93 g of $Li(C_5Me_5)$ were re-dissolved in 40 mL diethyl ether, and the solution added to a suspension of InCl (Johnson Matthey, 2.9 g, 19.3 mmol) in 100 mL diethyl ether. The mixture turns immediately from bright yellow to grey, due to the formation of metallic indium as a by-product. After a further 15 h at room temperature, the yellow supernatant was filtered into another Schlenk and combined with washings of the grey solid residue. The solvent was then removed at -10°C, and the resulting yellow solid residue transferred to a sublimation apparatus. Sublimation at 55°C under high vacuum yielded 2.34 g (48%) of pure product. Since $(C_5Me_5)In$ is extremely reactive towards oxidising agents, it was stored in a previously flamed Schlenk at -30°C.

Preparation of stannocene $SnCp_2$

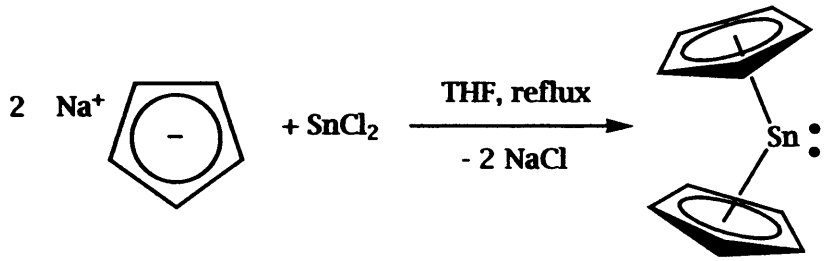

For this compound, the original preparation of Fischer (1956) has been followed[15]. $SnCl_2$ (Aldrich, 6 g, 31.6 mmol) was suspended in 100 mL THF. A solution containing 5.7 g $Na(C_5H_5)$ (64.7 mmol) in 50 mL THF was added to the suspension, and the mixture refluxed for 15 h at 80°C. After this time, the solvent was removed *in vacuo*, and the white solid residue sublimed at 100°C under high vacuum. Final yield: 0.7 g (9%).

Preparation of $Pt(PPh_3)_2(ethene)$[16]

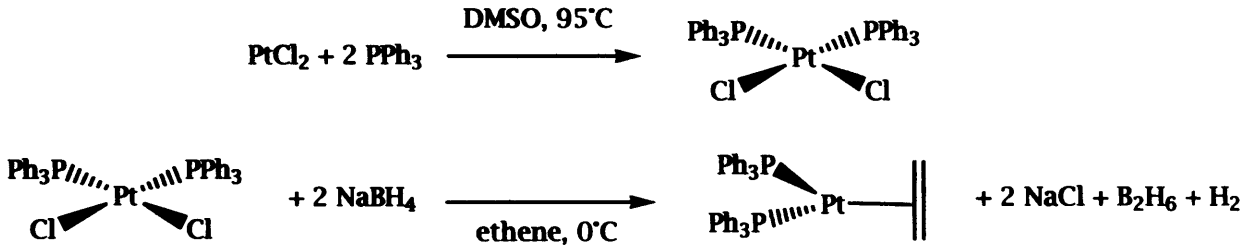

$PtCl_2$ (Johnson Matthey, 2g, 7.5 mmol) was dissolved in 50 mL of hot dimethyl sulphoxide (95°C), and 4 g of PPh_3 added (Aldrich, 15.3 mmol, 2 equiv.). The solution mixture was maintained at 95°C for 30 min., then cooled to room temperature and diluted with 30 mL of degassed ethanol. A white precipitate formed on cooling. The Schlenk was cooled to 0°C and the contents allowed to settle overnight. After this period, the supernatant was removed, and the solid washed with small portions of EtOH and Et_2O. Final drying under high vacuum yielded 6.5 g of white product (quantitative). Purity was checked *via* ^{31}P NMR.

In the next step, 4 g of the phosphine complex (5.1 mmol) were suspended in 50 mL ethanol and 50 mL dichloromethane (both solvents having been previously degassed with ethene for 15 min.). The suspension was cooled to 0°C, and, 0.95 g $NaBH_4$ (Lancaster, 25 mmol, 5 equiv.) added in three portions. Vigorous bubbling was observed during the addition. The temperature was kept at 0°C for a further 10 min. after the last addition of reducing agent. After this time the Schlenk was warmed to room temperature and ethene bubbled through the solution for 30 min. An additional 100 mL of EtOH were added, and the mixture allowed to settle overnight. The off-white solid formed was separated from the supernatant and washed with EtOH, water and finally Et_2O, before a final drying under high vacuum. Yield: 2.5 g (67%). All solvents employed in the last synthesis had been degassed with ethene prior to use. Once more, the identity and purity of the product were confirmed by ^{31}P NMR data.

Preparation of (dppe)Pt(ethene) [16]

The same method described in the previous section also is applicable with chelating phosphines. The first part, involving the preparation of $Pt(dppe)Cl_2$, gives final yields of around 80%. It is extremely important to use the exact stoichiometry (1:1), because, in the presence of an excess of dppe the salt $[Pt(dppe)_2]Cl_2$ also formed[17]. Bis-(dppe) platinum dichloride is a very stable molecule, and it does not lose its ligands even after a prolonged reflux in toluene. As a consequence, it is not possible to get the mono-dppe complex from the bis-dppe one.

The second step, reduction under ethene atmosphere, was best performed in a mixture of THF and EtOH (2:1) as solvents, instead of CH_2Cl_2/EtOH, because the final product is much more soluble in ethanol than the corresponding PPh_3 derivative. After the reduction step using $NaBH_4$, the orange supernatant was kept and the solvent removed *in vacuo*. The orange-brown residue was washed with water and ether, and dried. The final yield was around 55%. An alternative synthetic pathway to $Pt(dppe)Cl_2$ makes use of K_2PtCl_4 as starting material:

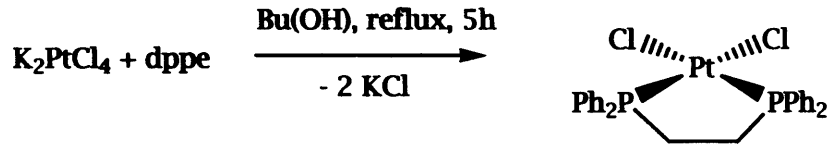

K_2PtCl_4 (Johnson Matthey, 0.5 g, 1.2 mmol) was suspended in 50mL of degassed 1-butanol, then 0.48 g of dppe (Aldrich, 1.2 mmol, 1 equiv.) were added to the suspension. The mixture was refluxed for 5 h under argon. During this time, a white solid precipitated. The supernatant was then filtered to waste, and the solid washed once with EtOH and once with diethyl ether. Final drying *in vacuo* yielded 0.33 g of pure $Pt(dppe)Cl_2$ (yield 41%). In this synthesis the yield is rather low, and the first method is therefore to be preferred. The ^{31}P NMR data found were consistent with those appearing in the literature.

Preparation of $Pt(PPh_3)_4$ (tetrakis-(triphenylphospino)platinum(0)) [18]

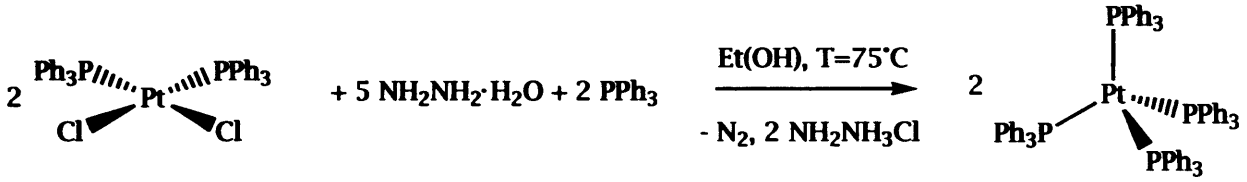

PPh_3 (7.6 mmol, 2 g, 3 equiv.) and $Pt(PPh_3)_2Cl_2$ (2 g, 2.5 mmol) were dissolved in 20 mL of freshly distilled and degassed ethanol, then the solution was warmed to 75°C. The white suspension immediately turned yellow upon addition of 1 mL of hydrazine monohydrate (Avocado, 20.6 mmol, 8.4 equiv.). After 1 h stirring at 75°C, the reaction mixture was brought back to room temperature slowly. After settling overnight, the yellow solid was filtered off and washed twice with ethanol, the first time at around 60°C, the second at room temperature. After one additional hexane washing, the solid was dried *in vacuo*. Yield: 2.1 g (67%). Purity was confirmed by comparison with the literature ^{31}P NMR data.

2.3.2 - Boron-containing ligands

Preparation of $HBO_2C_6H_2O_2BH$ [19]

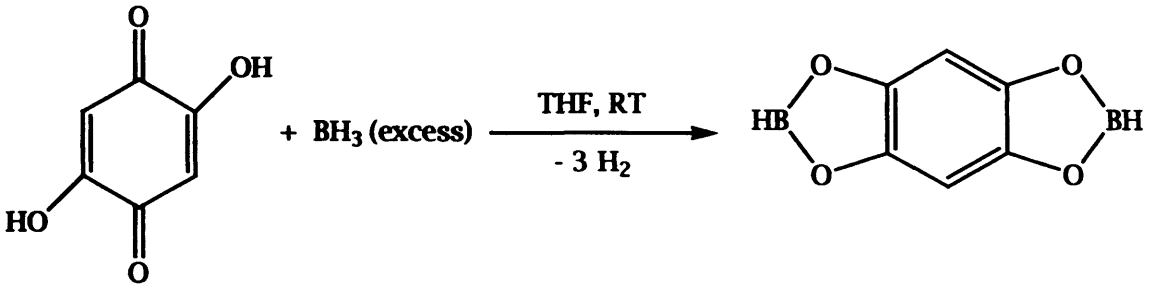

2,5-dihydroxy-para-quinone (Aldrich, 5 g, 35.7 mmol) was dissolved in 50 mL of THF. The solution was added to 150 mL of a 1M solution of BH_3.THF adduct in THF (Aldrich, 150 mmol, 4.2 equiv.) at room temperature. The mixture was stirred for 15 h, then volatiles removed *in vacuo* at 0°C, leaving a dark yellow solid. Sublimation at 60°C and 10^{-4} Torr onto a cold finger kept at -30°C (acetone-dry ice) gave a white pure crystalline product in 29% yield (1.64 g).

Preparation of (tmg)BCl [20]

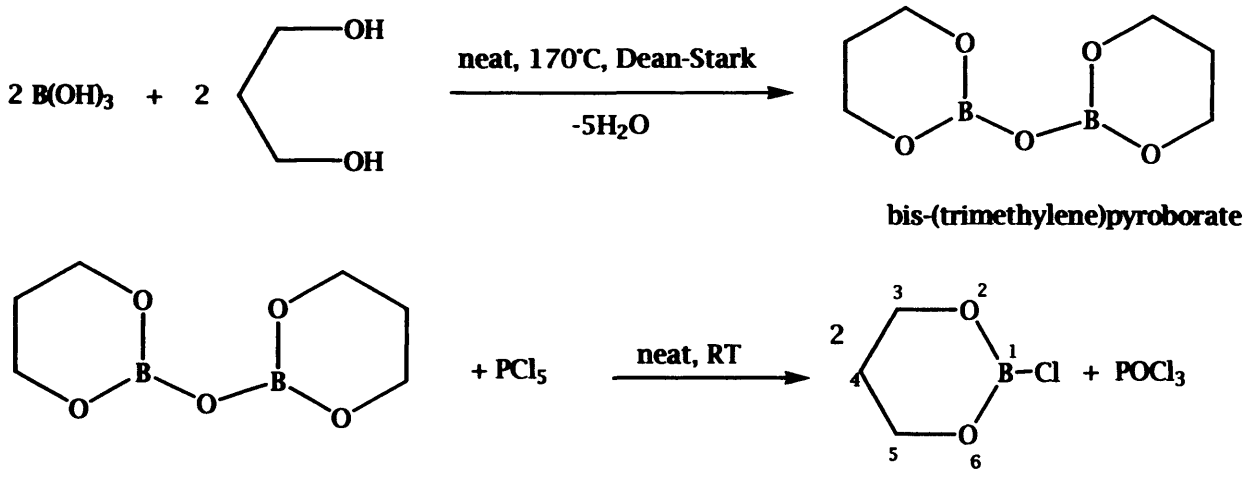

The starting material 1,3-propanediol (trimethyleneglycol, BDH Chemicals Ltd., 12 mL, 0.17 mol) was reacted with boric acid (Aldrich, 10g, 0.17 mol, 1 equiv.). The neat mixture was then

warmed to 170°C for 12 h in a Dean-Stark apparatus, to remove the water by-product. After the overnight condensation, the final residue was distilled under reduced pressure (15 Torr), to allow the collection of final traces of water. The orange oil left after the "distillation" process was the pure bis-(trimethylene)pyroborate. Yield: 13.6 g (90%). It is air-stable. The ^{11}B and ^{1}H NMR data are also reported in this section, because they were absent in the literature. ^{1}H NMR (300 MHz, $CDCl_3$, 21°C), δ 1.80 (2H, br, CH_2 of C(4)), δ 3.90 (4H, br, CH_2 of C(3) and C(5)). ^{11}B NMR (96 MHz, $CDCl_3$, 21°C), δ 15.8.

The pyroborate (10.2 g, 54.8 mmol) was then treated with 11.4 g of PCl_5 (Aldrich, 54.8 mmol, 1 equiv.) at room temperature and under an argon atmosphere. The reaction was always carried out using neat reagents. The mixing process is exothermic, and immediately after mixing a yellow liquid formed, which turned to dark purple after 2 h stirring. The liquid mixture was then fractionally distilled under reduced pressure (15 Torr), initially at a temperature of 60°C (to collect the by-product $POCl_3$, which boils at T=21°C at p=15 Torr) and finally at T=90°C, to collect the less volatile colourless borane (tmg)BCl. Yield: 2.8 g (21%). A "standard" toluene 0.46M solution was prepared, by dissolving the neat ligand in 50 mL of freshly distilled and degassed toluene, for further use. The complete set of NMR data (absent in the literature) is reported for this compound: ^{1}H NMR (300 MHz, $CDCl_3$, 21°C), δ 1.90 (2H, quintet, $^{3}J_{H\text{-}H}$=5 Hz, CH_2 of C(4)), δ 4.00 (4H, t, $^{3}J_{H\text{-}H}$=5 Hz, CH_2 of C(3) and C(5)). ^{13}C NMR (76 MHz, $CDCl_3$, 21°C), δ 26.5 (*C*(4)), δ 64.1 (*C*(3), *C*(5)). ^{11}B NMR (96 MHz, $CDCl_3$, 21°C), δ 22.8.

Preparation of 9-chloro-9-BBN [21]

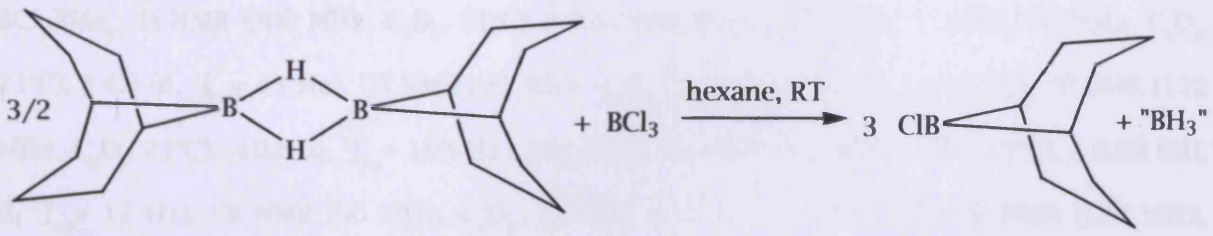

9-BBN dimer (Aldrich, 1.42 g, 5.8 mmol) was dissolved in 150 mL of distilled and degassed hexane, and 8 mL of a 1M solution of BCl_3 in heptane (Aldrich, 8 mmol) was added by syringe. After 12 h stirring at room temperature, the hexane solution was filtered off and the solvent removed *in vacuo*, together with the excess of BCl_3. During the solvent removal the temperature was kept at 0°C, to prevent loss of the (volatile) product. Its purity was checked *via* ^{11}B NMR. The residue was re-dissolved in 100mL of fresh toluene, to prepare a 0.12M "standard" solution (stored under argon) for further use.

Preparation of $BX_3 \cdot PMe_3$ (X=Cl, Br)[22]

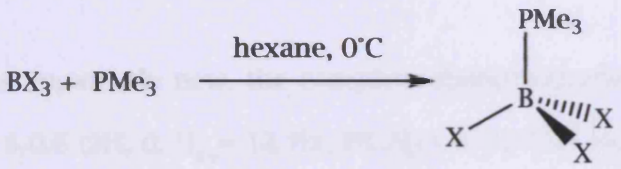

A 1M solution of BCl_3 in heptane (Aldrich, 20 mL, 20 mmol) was diluted with an additional 20 mL of hexane, and the solution cooled to 0°C. 1.5 mL of trimethylphosphine (14.5 mmol) were added in one aliquot by syringe; immediately a white precipitate started to come out of the clear solution. The reaction mixture was stirred for a further 1 h, while warming slowly to room temperature. Filtration of the supernatant and washing with fresh hexane (twice), followed by final drying under high vacuum for 1 h provided 2.5 g of the product (65% yield). The same procedure was used to make the BBr_3 derivative, starting from 2 mL of neat BBr_3 (Aldrich, 21.1 mmol) and 2.2 mL PMe_3 (21.2 mmol). The product is again a white solid. Final yield: 6.2 g (90%). Since the characterization that appears in the literature is not complete, in here the set of multinuclear NMR data is reported:

$BCl_3 \cdot PMe_3$: ^1H NMR (300 MHz, C_6D_6, 21°C), δ 0.57 (9H, d, $^2J_{H-P}$= 12 Hz). ^{13}C NMR (76 MHz, C_6D_6, 21°C), δ 4.6 (d, $^1J_{C-P}$= 43 Hz). ^{11}B NMR (96 MHz, C_6D_6, 21°C), δ 2.0 (d, $^1J_{B-P}$= 163 Hz). ^{31}P NMR (122 MHz, C_6D_6, 21°C), -10.8 (q, $^1J_{P-B}$= 163 Hz). $BBr_3 \cdot PMe_3$: ^1H NMR (300 MHz, C_6D_6, 21°C), δ 0.63 (9H, d, $^2J_{H-P}$= 12 Hz). ^{11}B NMR (96 MHz, C_6D_6, 21°C), δ -15.0 (d, $^1J_{B-P}$= 158 Hz). ^{31}P NMR (122 MHz, C_6D_6, 21°C), -10.8 (q, $^1J_{P-B}$= 158 Hz).

Preparation of $BCl_2(C_6H_5)$·PMe_3

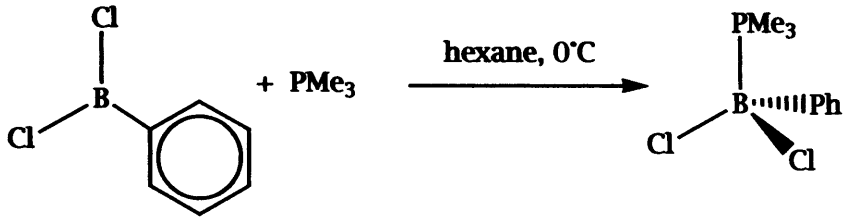

The methodology is the same seen in the previous section, and the product is also a white powder. $(C_6H_5)BCl_2$ (Aldrich, 2 mL, 15.2 mmol) was reacted with 1.6 mL of PMe_3 (15.4 mmol) in 50 mL hexane. Final yield: 3.6 g (quantitative).

Since this compound is apparently new, the complete characterization is reported: ^{1}H NMR (300 MHz, C_6D_6, 21°C), δ 0.6 (9H, d, $^2J_{H\text{-}P}$= 12 Hz, P(C*H*$_3$)$_3$), δ 7.2 (3H, m, *meta* and *para* phenyl C*H*), δ 7.9 (2H, d, *ortho* phenyl C*H*). ^{13}C NMR (76 MHz, C_6D_6, 21°C), δ 5.1 (d, $^1J_{C\text{-}P}$= 41 Hz, P(*C*H$_3$)$_3$), *ortho*, *meta* and *para* phenyl *C* not observed because of the strong solvent peaks, δ 133.2 (d, *ipso* phenyl *C*). ^{11}B NMR (96 MHz, C_6D_6, 21°C), δ 0.9 (d, $^1J_{B\text{-}P}$= 118 Hz). ^{31}P NMR (122 MHz, C_6D_6, 21°C), -12.9 (q, $^1J_{P\text{-}B}$= 118 Hz). IR (KBr disk, cm^{-1}) 3069 m, 2989 m, 2916 m, 2054 w, 1960 w, 1897 w, 1825 w, 1778 w, 1489 m, 1431 st, 1413 st, 1313 m, 1292 st, 1262 m, 1172 m, 1163 m, 1095 st-br, 1034 st-br, 978 st, 951 st, 865 w, 818 st, 765 st, 705 st-br, 653 st, 617 m, 600 st, 481 m. Mass spec. (EI): [M]$^+$: calculated mass 234.0298 a.m.u, measured mass 234.0295 a.m.u.

Preparation of BCl_3·THF [23]

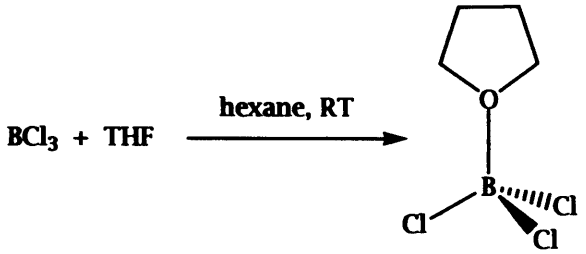

A 1M solution of BCl_3 in heptane (20 mL, 20 mmol) was diluted in 15 mL hexane. To this solution, 10.8 mL (20 mmol) of a 1.85M solution of THF in hexane (prepared by dissolving 15mL THF in 100 mL of hexane) were added at room temperature. A white solid precipitated immediately. After 12 h stirring, the solid was filtered and washed in the usual manner with hexane. Drying under high vacuum for 30 min. yielded 2.82 g of pure product (75%). This adduct, as well as $BCl_2(C_6H_5)$·THF, has to be stored in the freezer at -30°C in a Schlenk, due to its temperature sensitivity. ^1H NMR (300 MHz, $CDCl_3$, 21°C), δ 2.3 (4H, m), δ 4.7 (4H, m). ^{11}B NMR (96 MHz, $CDCl_3$, 21°C), δ 9.2 (s).

Preparation of $BCl_2(C_6H_5)$·THF

This is essentially an identical synthesis to the previous one; the only change is the boron-containing starting material. $(C_6H_5)BCl_2$ (1 mL, 7.6 mmol) was reacted with 4.1 mL of a 1.85M solution of THF in hexane (7.6 mmol). Final yield: 1.13 g (64%). As in the case of $BCl_2(C_6H_5)$·PMe_3, the compound is new; its spectroscopic and mass spectrometry data are included: ^1H NMR (300 MHz, $CDCl_3$, 21°C), δ 2.1 (4H, m, "meta"-CH_2, THF), δ 4.3 (4H, m, "ortho"-CH_2, THF), δ 7.3 and 7.7 (m, aromatic C*H*). ^{13}C NMR (76 MHz, $CDCl_3$, 21°C), δ 25.1 ("meta"-CH_2, THF), δ 75.1 ("ortho"-CH_2, THF), δ 127.7 (*para*-CH), δ 128.5 (*meta*-CH), δ 132.6 (*ortho*-CH), δ 135.1 (*ipso*-C). ^{11}B NMR (96 MHz, $CDCl_3$, 21°C), δ 12.5 (s, br). IR (KBr disk, cm^{-1}) 3077 m, 3051 m, 3020 m, 2960 m, 2908 m, 1965 m, 1912 m, 1900 m, 1829 m, 1781 w, 1601 st, 1575 m, 1558 m, 1494 m, 1392 st-v br, 1179 st, 1087 st, 1025 st, 967 st, 859 st-v br, 694 st-v br, 628 st, 580 st, 470 m. Mass spec. (EI): $[M]^+$: calculated mass 230.0431 a.m.u, measured mass 230.0434 a.m.u.

2.4 - Technical data on the equipment used for characterisation

A wide range of spectroscopic techniques was exploited to characterise the compounds described in this work. In the following section a brief list of the technical features of the various spectrometers is presented.

2.4.1 - Multinuclear NMR

All spectra were measured on a Bruker AM-400 or JEOL Eclipse 300 Plus FT-NMR spectrometer. Residual protons of solvent were used for reference for ^{1}H and ^{13}C NMR, while a sealed tube containing a solution of $[^{n}Bu_4N][B_3H_8]$ in $CDCl_3$ was used as an external reference for ^{11}B NMR. Me_4Sn is the external reference for ^{119}Sn NMR, $CFCl_3$ for ^{19}F NMR and an 85% solution of H_3PO_4 is the external reference for ^{31}P NMR. Samples were prepared by transferral of solution *via* cannula into a Young's NMR tube in a Schlenk which had been previously filled with inert atmosphere using the "pump-and-fill" method.

2.4.2 - IR and Raman

Infrared spectra were recorded on a Nicolet 500 FT-IR spectrometer, each compound pressed into a KBr disk or as a solution in dichloromethane. Disks were prepared in the glove box by compressing a powdered sample with an excess of KBr (dried by heating under high vacuum prior to use). FT-Raman spectra were measured for powdered samples sealed in glass ampoules using a LabRam spectrometer (courtesy of Prof. A.J. Downs, Oxford University Inorganic Chemistry Laboratory).

2.4.3 - Mössbauer spectrometry

Mössbauer spectra were recorded at 77 K on an ES-Technology MS-105 spectrometer with a 135 MBq ^{57}Co source in a rhodium matrix at ambient temperature (courtesy of Dr. David Evans, Department of Biological Chemistry, John Innes Centre, Norwich). Spectra were referenced to a 25 μm iron foil at 298 K. Measurements were in zero field in solid samples ground with boron nitride. Parameters were obtained by fitting the spectra to a Lorenzian function.

2.4.4 - Mass spectrometry

Mass spectra were recorded at the EPSRC National Mass Spectrometry Service Centre, University of Wales, Swansea, and by the departmental service. Perfluorotributylamine and polyethylenimine were used as standards for high resolution EI and CI mass spectra respectively.

2.4.5 - X ray diffraction

Data collection was carried out on an Enraf Nonius Kappa CCD diffractometer (EPSRC Crystallography Service, University of Southhampton) or on a similar instrument housed within the department. Structure solution and refinement were performed by Dr. S.J. Coles (University of Southampton) and Dr. Liling Ooi (Cardiff University).

2.5 - Computational methodology

The calculations performed in this project are all based on density functional methods, and they have been carried out on the Cardiff Computational Group computer resources. These included various SGIs, DEC Alpha (EV5s) and Unix machines. The DFT code ADF 2002.03[25] was the software package of choice for the calculations on the analysis of borylene iron and manganese complexes (and related σ and π M=B bond densities and dissociation energies), while Gaussian03[26] was employed in the calculation of the rotational energy profiles of simple boryls and borylenes around the metal-boron bond. Amsterdam Density Functional program (ADF) uses the Kohn-Sham approach to density functional theory. It has the option of both local density and generalised gradient approximation using a variety of common functionals. Gaussian03 is more of a general piece of *ab initio* software, designed to run different methods ranging in accuracy and corresponding computational cost. These include semi-empirical, Hartree-Fock (including extensions for the treatment of electron correlation) and density functional methods. Gaussian has a wider range of exchange and correlation functionals for use within DFT than ADF.

2.5.1 - STO and GTO basis sets and the frozen core approximation

For the theoretical treatment of molecular orbitals, it is common practice to build them as a linear combination of atomic orbitals, which are chosen as complete basis set (approach called LCAO-MO). The basis functions used in ADF are commonly known as Slater Type Orbitals (STOs). Their general form in polar coordinates is

$$\chi_{STO}(r,\theta,\varphi) = NY_{l,m}(\theta,\varphi)r^{n-1}e^{-\zeta r} \tag{1.1}$$

where N is a normalisation constant, n,l,m are quantum numbers and Y are the spherical harmonics (the solutions coming from the Schrödinger equation of the classical rigid rotor), in the coordinates θ and φ. The functions dependence on the electron-nuclear distance r mirrors the one found in the (exact) solutions of the hydrogen atom. The exponential dependence ensures a rather rapid convergence with increasing number of functions, and the STOs are very "well-behaved" in the region close to the nucleus, in which they have a cusp (the first derivative at r=0 is discontinuous). In order to improve the description of the atomic properties, a *minimum basis set* (i.e. made of the smallest number of functions possible, to contain all the electrons of the neutral atom) can be expanded by adding additional functions with different ζ exponents. This leads to *multiple-zeta* basis sets:

$$\chi_{STO}(\zeta_1,\zeta_2,\ldots\zeta_k) = NYr^{n-1}[e^{-(\zeta_1+\zeta_2+\ldots+\zeta_k)r}] \tag{1.2}$$

Since the chemical bonding occurs only between valence orbitals, this extension of the basis set is usually limited to the outer atomic orbital functions, while a simple single-zeta set is kept for the description of the core orbitals (*split valence basis*). *Polarization functions* are also important to improve the basis set quality: they are higher angular momentum functions that are introduced in order to take into account the "anisotropy" of some physical properties, like the electron distribution along a bond and perpendicular to the bond. *p*-Type orbitals are added to polarize *s* orbitals, while *d*- or *f*-type orbitals polarize *p* orbitals. If a single set of polarization functions (*p*-functions on hydrogen and *d*-functions on heavier

atoms) is added to the "standard" basis, a *singly polarised* set is obtained, while, with the addition of two sets of polarization functions ([*p*+*d*]-functions on hydrogen and [*d*+*f*]-functions on heavier atoms) one gets a *doubly polarised* set. The combination of basis expansion and polarization functions is indicated by typical acronyms: DZP (double-zeta plus (single) polarization), DZ2P (double-zeta plus double polarization), etc...The basis set chosen for the work in this project is always TZ2P (triple-zeta doubly polarized), with the exception of the case of the complex $[(Cp)Fe(PMe_3)_2(BMes)]^+$, where, due to the large system size, it has been reduced to DZP on lighter atoms (carbon and hydrogen).

On the other hand, Gaussian03 makes use of Gaussian type orbitals (GTOs):

$$\chi_{GTO}(r,\theta,\varphi) = NY_{l,m}(\theta,\varphi)r^{(2n-2-l)}e^{-\zeta r^2} \tag{1.3}$$

where the argument of the exponential part is proportional to r^2 instead of r. Gaussian functions are easier to handle in the evaluation of the multicentre integrals that appear in the Schrödinger equation of poly-electronic systems, because the product of two Gaussians centred on two nuclei A, B is itself a Gaussian function centred in the middle point of the A-B line. The computational effort is therefore greatly reduced, but there are also some disadvantages. Unlike STOs, they do not represent properly the behaviour of the wave function in the proximity of the nucleus (where their first derivative is continuous and equal to zero), and they fall off too rapidly from the nucleus compared to the STOs. Thus, the "tail" of the wave function is represented poorly. To compensate for this lack of precision, a larger number of GTOs are required to achieve the same level of accuracy as the STO one, and *contracted basis sets* are normally employed:

$$\sum a_i \chi_{i(PGTO)}$$

$$\chi_{(CGTO)} = \sum_{i}^{k} a_i \chi_{i(PGTO)} \tag{1.4}$$

Here a single *contracted* basis function (CGTO) is the result of a linear combination of k ordinary GTOs (*primitives*, PGTO). The coefficients a_i are then optimised by fitting the

function with the experimental data. The usefulness of contracted basis sets is twofold: (i) – to give a more precise representation of the atomic inner shells, thanks to the possibility of employing several primitives to describe the energetically important but chemically unimportant core electrons; and (ii) – to reduce the overall number of parameters to be optimised with respect to an "uncontracted" set (because all the ζ parameters appearing in each PGTO in the linear combination are kept constant). As in the case of the STOs, special acronyms have been introduced to define the split valence contracted basis sets, whose general form is *k-nlmG*. *K, n, l* and *m* are integers; *k* is the number of PGTOs used to represent the core orbitals, while *n, l* and *m* indicate the number of PGTOs used to represent the valence orbitals (besides giving the information on how many functions the latters are split into: only two numbers *n,l* indicate a double split valence, while three numbers *n,l,m* indicate a triple split valence). The presence of polarization functions is indicated by asterisks (*). The calculations on the rotational barriers around the M-B bond in iron boryls and borylenes shown in this work use a 6-31G** basis set for the lighter atoms (carbon, oxygen, boron and hydrogen): six primitives are used to represent the core orbitals, while the inner part of the valence orbitals is a contraction of three GTOs, and finally the outer part of the valence shell is a single "non-contracted" GTO. Two additional sets of polarization functions are indicated by the two stars at the end, making this basis set very similar to the TZ2P one used in ADF. The basis set for iron is of a different kind, and it is based on the creation of a pseudo-potential to represent the core electrons. It is called LANL2DZ.

In both ADF and Gaussian03 cases the approach of a *frozen core approximation* has been used. The level of frozen core approximation for the atoms of the second period (B, C, N, O, F) was the *1s* orbital, while for the atoms of the third period (Al, P) were the *2p* orbitals, and finally for the atoms of the fourth period (Mn, Fe, Ga) were the *3p* orbitals.

2.5.2 - Exchange and correlation functionals

The mathematical form of the exchange and correlation functionals employed for the analysis has been chosen from the ones available in the ADF and Gaussian packages. In

particular, Becke 88 exchange functional combined with Lee-Yang-Parr correlation functional (BLYP) were the specific choice. BLYP has been proved to be the best E_{xc} from a group of four different functionals (the local density one LDA plus the non-local PW91, LB94 and BLYP) tested in the evaluation of the ionisation energies of the iron atom, giving the closest values to the experimental ones[27].

2.5.3 - Effective core potential (ECP) [28]

In Gaussian03 calculations the basis set chosen for the heavy iron atom is based upon the idea of the pseudo-potential (or effective core potential). For transition elements there is a large number of core electrons that in general are unimportant in a chemical sense. However, it is necessary to give a precise representation of these inner shells, because they account for most of the total electronic energy. In addition, if the core electrons were not represented adequately, a poor description of the valence shell would be a direct consequence, because of a wrong simulaton of the electron-electron repulsion. The creation of a pseudo-potential to mimic the behaviour of the inner shells is in the spirit of semi-empirical methods. The generation of ECPs begins with the definition of the core shell:

First transition series: ...$3s^2\ 3p^6$ = [Ar]

Second series: ...$3d^{10}\ 4s^2\ 4p^6$ = [Kr]

Third series: ... $4d^{10}\ 5s^2\ 5p^6\ 4f^{14}$ = [Xe]$4f^{14}$

Next, an all-electron Hartree-Fock calculation is performed on the atom, to derive a set of numerical valence orbitals $\{\phi_l\}$. This set is the reference for the determination of the pseudo-orbitals $\left\{\tilde{\phi}_l\right\}$, of the general form:

$$\tilde{\phi}_l = r^{(l+3)}(a_0 + a_1 r + a_2 r^2 + a_3 r^3 + a_4 r^4) \qquad (1.5)$$

where l is the orbital quantum number and the five coefficients a_l are determined by imposing five specific restrictions on ϕ: for $r=r_c$ (that is the "critical" radius that divides the

core region from the valence one) the pseudo-orbital and its first three derivatives must match the "authentic" orbital and its three derivatives, and it has to remain normalised.
Once the appropriate form is found, the pseudo-orbitals are fit to Gaussian orbitals using a non linear least squares procedure. These functions are put into the complete Schrödinger equation of the system, and numerical ECPs are found by imposing that the pseudo-orbitals are eigenfunctions of the Hamiltonian *with the same eigenvalues (energies) as the $\{\phi_j\}$ set.* This procedure has been performed on the three transition element series, deriving a complete set of ECPs that are included in Gaussian03.

These potentials provide accurate results in almost all cases, for a small fraction of the computational cost of an all-electron treatment. However, they may diverge from all-electron results in cases where relaxation or correlation effects involve sub valence orbitals (such as the 3s and 3p orbitals for the first transition row). In these cases ECPs can be generated which explicitly treat the outermost core electrons along with the valence electrons, increasing the computational effort but overall still being advantageous with respect to an all-electron calculation.

2.5.4 - Bond dissociation energy and partition of bond energy (ETS)

The bond dissociation energy (BDE) for a given M-B bond in borylene complexes of general formula $[(\eta^5\text{-}C_5R_5)(L)_2M{=}BX]^{n+}$ was calculated by estimating the energy change associated with the cleavage

$$[(\eta^5\text{-}C_5R_5)(L)_2M{=}BX]^{n+} \rightarrow [(\eta^5\text{-}C_5R_5)(L)_2M]^{n+} + [BX]$$

The procedure was to optimise the structure of the whole molecule, then this structure is broken into the two fragments. A single point calculation is then carried out for each fragment in a closed shell configuration (restricted), keeping the nuclei positions fixed, and the resulting fragment MOs are taken as basis sets for another single point calculation of the whole molecule. By doing so, the (negative) value of the bonding energy between the

fragments in the final ADF output is equal to the istantaneous bond dissociation energy (see below), but with the opposite sign (BDE = - ΔE_{int}).

The different contributions to the bond energy were calculated using the energy decomposition scheme called Extended Transition State (ETS), developed by Ziegler and Rauk[29]. This method can be applied to any bonded pair of atoms A-B, where the complex A-B is treated as two distinct ADF fragments, A and B. The total bond energy ΔE is partitioned into four components which are calculated in consecutive steps:

$$\Delta E = \Delta E_{prep} + \Delta E_{\text{int}} \tag{1.6}$$

ΔE_{prep} Is the energy that is necessary to promote the fragments A and B from their equilibrium geometry and electronic ground state to the geometry and state they have in the compound A-B. In the practical calculation, it is simply the difference between a single point energy of A and B (in the geometry of the compound A-B) and the energy of the "relaxed" A and B (that is to say an energy value calculated *allowing relaxation of the nuclear positions*). In all cases examined, there is no difference between a closed shell and an open shell configuration of the fragments; this implies that the electrons in the fragments are already paired in the ground state, and *there is no contribution to ΔE_{prep} deriving from a spin configuration change.*

ΔE_{int} Is the instantaneous interaction energy, which can be further divided into three main components:

$$\Delta E_{\text{int}} = \Delta E_{elstat} + \Delta E_{Pauli} + \Delta E_{orb} \tag{1.7}$$

The first term gives the electrostatic interaction energy between the electronic cloud of one fragment and the nuclei framework of the other, the second term is the repulsive Pauli interaction arising from the fact that electrons with the same spin cannot occupy the same region of space (Pauli exclusion principle for fermions), and the last term is the attractive

orbital interaction, due to the overlap of empty MOs of one fragment with full MOs on the other fragment and vice-versa. The ratio $\Delta E_{elstat}/\Delta E_{orb}$ leads to important information about the "relative importance" of the ionic contributions to the bond respect to the covalent ones. Since ADF decomposes ΔE_{int} automatically into its three constituent parts, this analysis is straightforward, and it does not require any additional software.

2.5.5 - Decomposition of the bond density into symmetry groups: σ and π bond orders

Orbital symmetry plays a crucial role in describing covalent bonding in all areas of chemistry. Bonding interactions can be classified as $\sigma, \pi, \delta, \phi$ depending on the symmetry labels of the interacting orbitals. The starting point of this approach is a work undertaken by Mayer in 1986 [30], re-examined by Bridgeman et al. in 2001[31], where the Mayer bond order B is split into its individual symmetry contributions:

$$B_{AB(Mayer)} = \sum_{\mu \in A} \sum_{\nu \in B} (PS)_{\mu\nu}(PS)_{\nu\mu}$$
$$B^{\Gamma}{}_{AB} = \sum_{\mu \in A} \sum_{\nu \in B} \left(\sum_{\Gamma} PS^{\Gamma}{}_{\mu\nu} \right) \left(\sum_{\Gamma} PS^{\Gamma}{}_{\nu\mu} \right) \qquad (1.8)$$

where Γ refers to an overlap between basis functions of a particular symmetry (for a definition of the matrices P and S vide infra). The overall bond order will be a sum over all the symmetry species:

$$B_{AB} = \sum_{\Gamma} B^{\Gamma}_{AB} \qquad (1.9)$$

To quantify and calculate the degree of σ and π bonding between two atoms the optimised structures were re-orientated so that the bond of interest was aligned along the z-axis. A bonding analysis was then carried out following the approach discussed below to give contributions to the bonding density segregated according to the symmetry of the atomic orbitals involved. The one-electron wave functions ψ_i used to represent the density in these

DFT calculations are formed *via* linear combinations of M atomic basis functions χ (LCAO-MO approach):

$$\psi_i = \sum_k^M c_{ik}\chi_k \tag{1.10}$$

where c_{ik} is the coefficient that gives the "weight" of the contribution of the k^{th} basis function in building the i^{th} molecular orbital. The density ρ is then given by summation over the occupied orbitals of the one-electron densities:

$$\rho = \psi^*\psi = 2\sum_i^{N/2}\sum_l^M c^*_{il}\chi^*_l\sum_k^M c_{ik}\chi_k = 2\sum_{l,k}^M \chi^*_l\chi_k\sum_i^{N/2} c^*_{il}c_{ik} \tag{1.11}$$

where N is the total number of electrons, considering only a closed shell case for simplicity. When this expression is rearranged as shown, it is possible to define two square matrices with dimension M. The first is normally referred to as the *density matrix* P (different from the density matrix described in the introduction, despite the identical names), and its components depend only on the coefficients c, while the second, the *overlap matrix* S, depends on the basis set and the geometry of the molecule:

$$\rho = 2\sum_{l,k}^M S_{lk}P_{kl} \tag{1.12}$$

Since the basis set consists of atom centered functions, P and S will contain contributions which are wholly centered on a given atom, and some others which come from the overlap of functions centered on *different* atoms. This latter part is the one that describes the bonding interactions between atoms. If we focus only on the functions centered on a pair of atoms A and B, the idea of *bonding density A-B* is straightforward:

$$\rho_{AB} = 2\sum_{l\in A}\sum_{k\in B} S_{lk}P_{kl} \tag{1.13}$$

derived from the Mayer bond order (1.8) by summing only the relevant contributions (from A and B). As a consequence of the orientation of the bond A-B of interest along the z-axis, the different atomic orbitals on both A and B can be grouped into different symmetries: for example, p_z, s and d_{z2} will be of a σ type, while p_x, p_y, d_{xz}, d_{yz} will be of a π type, etc... Thus, equation (1.13) can be further sub-divided:

$$\rho_{AB} = 2\sum_{l\in A}^{\sigma}\sum_{k\in B}^{\sigma} S_{lk}P_{kl} + 2\sum_{l\in A}^{\pi}\sum_{k\in B}^{\pi} S_{lk}P_{kl} + 2\sum_{l\in A}^{\delta}\sum_{k\in B}^{\delta} S_{lk}P_{kl} + \ldots \qquad (1.14)$$

The decomposition of the molecular orbital representation of the density to create a bonding density is not unique, hence, to ensure the reliability of our analysis, we also considered a bonding density analysis proposed by Mayer, where the matrix product is calculated first, and the elements of this matrix product are subsequently selected according to the AOs of interest:

$$\rho_{AB} = 2\sum_{l\in A}^{\sigma}\sum_{k\in B}^{\sigma} (PS)_{kl} + 2\sum_{l\in A}^{\pi}\sum_{k\in B}^{\pi} (PS)_{kl} + 2\sum_{l\in A}^{\delta}\sum_{k\in B}^{\delta} (PS)_{kl} + \ldots \qquad (1.15)$$

The data produced by ADF, i.e. the elements of S and P matrices, are used by a tailor-made C program written by Dr. Anthony Dickinson of Cardiff University Theoretical Chemistry group, called *ADF_Reader*[27]. This program first reads the symmetrized fragment orbitals in the ADF output file (SFOs) which are "suitable" linear combinations of fragment orbitals (the *atomic* orbitals, since the initial fragments of choice are the single atoms). These are assigned symmetry labels used to partition the bond. Next, the density matrix P is calculated and combined with the overlap matrix S, to derive the Mayer bond order. Finally, the partitioning of the bond into symmetry contributions is performed (equation (1.14)). The script has been previously tested on molecules ranging from small organic and inorganic species (H_2, CO, CO_2, HCN, ethane, ethylene, acetylene) to organometallics containing transition metals (derivatives of $Fe(CO)_5$), using minimal and reasonably sized triple-zeta

basis sets. In general, it has been inferred that the strength and the efficiency of the analysis comes from a *relative comparison* of similar systems with one another more than from individual absolute values.

2.5.6 – Calculation of the energy barriers for rotation of boryl and borylene ligands around the metal-boron bond.

Energy profiles for rotation of a boryl or borylene ligand around the metal-boron bond in complexes of general formula $[(\eta^5\text{-}C_5R_5)(CO)_2Fe{=}B(Mes)]^+$ or $[(\eta^5\text{-}C_5R_5)(CO)_2Fe\text{-}B(O_2R)]$ can be calculated by referring to the *dihedral angle* (indicated with the Greek letter θ), defined as the angle between the plane containing the atoms Cp(centroid)-Fe-B and the plane containing the atoms B-C(1)-C(2) in the case of the borylene substituent =B(Mes), or the O-B-O plane in the case of the boryls $-B(O_2R)$ (Figure 5).

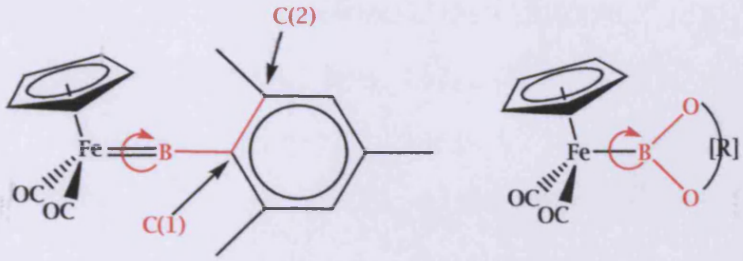

Figure 5 – Reference atoms to define the dihedral angle θ

The complex structure derived from the crystallographic experimental data is firstly optimised in Gaussian03, and the resulting output geometry (and related electronic energy) is taken as a starting point. A series of 10 different optimisations is carried out sequentially, by varying θ in steps of 10°. Relaxation is allowed at every point, under the single constraint of a fixed interplane angle. The relative energy differences between the various conformers are then plotted in a bidimensional graph versus the corresponding θ values, thus allowing for a more intuitive representation of the energy barrier (evaluated as the difference between the highest and the lowest energy point on the graph).

Due to the high computational effort required to run several geometry optimisations, these calculations have been performed by a cluster of processors called Helix (www.helix.cf.ac.uk). The Helix cluster consists of 72 worker nodes, plus a head node that connects the cluster to the rest of the world and manages the cluster itself. Overall, the cluster includes 146 processors, 110 GB of RAM and more than 7 TB of storage. Additional technical information about Helix can be found on the URL above.

(1) Shriver D.F., *The manipulation of air-sensitive compounds*, Mc.Graw Hill, New York (1969).

(2) Saffron Scientific Equipment Ltd., glove box operation manual.

(3) Perrin D.D. and Armarego W.L.F., *Purification of Laboratory Chemicals*, Pergamon Press, New York (1988).

(4) (a) King R.B. and Pannell K.H., *Inorg. Chem.*, 1968, 7, 1510; (b) Clegg W., Compton N.A., Errington R.J. and Norman N.C., *J. Chem. Soc., Dalton Trans.*, 1988, 1671.

(5) King R.B., *Organometallic Syntheses*, Volume 1, Academic Press, New York (1965), p.149.

(6) Fisher E.O., *Inorg. Synth.*, 1963, 7, 136.

(7) Gladysz J.A. and Tom W., *J. Org. Chem.*, 43 (1978), 2279.

(8) (a) Treichel P.M. and Komar D.A., *J. Organomet. Chem.*, 206 (1981), 77; (b) Waltz K.M., Muhoro C.N., Hartwig J.F., *Organometallics* 1999, 18, 3383.

(9) Van Der Ent A., Onderdelinen A.L., *Inorg. Synth.* 1973, 14, 93.

(10) (a) Busetto C., Alfonso A., Maspero F., Perego G., Zazzetta A., *J. Chem. Soc., Dalton Trans.* (1977), 1828; (b) Binger P., Haas J., Glaser G., Goddard R., Krüger C., *Chem. Ber.* 1994, 127, 1927.

(11) Cowley A.H. and Mills J.L., *J. Am. Chem. Soc.* (1969), 2915.

(12) (a) Van Gaal H.L.M. and Van Den Bekerom F.L.A., *J. Organomet. Chem.*, 134 (1977), 237.

(13) Beachley Jr. O.T., Blom R., Churchill M.R., Faegri Jr. K., Fettinger J.C., Pazik J.C., Victoriano L., *Organometallics*, 1989, 8, 346.

(14) Fendrick C.M., Schertz E.A., Mintz E.A., Marks T.J., *Inorg. Synth.*, 1992, 29, 193

(15) Fisher E.O., Grubert H., *Z. Naturforsch. Teil B*, 11, 423 (1956).

(16) (a) Stang P.J., Halton B., *J. Organomet. Chem.*, 388 (1990), 215; (b) Camalli M., Caruso F., *Helvetica Chimica Acta*, 73 (1990), 2263.

(17) Winzer A. and Griebel R., *Z. Chem.*, 15 (1975), 411.

(18) Malatesta L. and Cariello C., *J. Chem. Soc.*, 2323 (1958).

(19) Aldridge S., Calder R.J., Cunningham M.H., Malik K.A.M., Steed J.W., *J. Organomet. Chem.* 614-615 (2000), 188.

(20) (a) Mehrotra R.C. and Srivastava G., *J. Chem. Soc.* 1962, 1032; (b) Singh O.P., Mehrotra R.C., Srivastava G., *Synth. React. Inorg. Met.-Org. Chem.*, 21(5), 717 (1991).

(21) Brown H. and Kulkarni S.U., *J. Organomet. Chem.*, 168 (1979), 281.

(22) Sisler H.H., Mathur M.A., *J. Inorg. Nucl. Chem.* (1977), 39, 1745.

(23) (a) Young D.E., Mc. Achran G.E., Shore S.G., *J. Am. Chem. Soc.*, 1966, 88, 4390; (b) Hagedorn H.F., Gallaway G.L., *Journal of the Scientific Laboratories*, Denison University (OH), USA, 1968, 49, 77.

(24) Kira M., Sato K., Sakurai H., *J. Am. Chem. Soc.*, 1988, 110, 4599.

(25) *ADF2002.03* was obtained from SCM, Theoretical Chemistry, Vrije Universiteit, Amsterdam, Netherlands, http://www.scm.com. (a) G. te Velde, F.M. Bickelhaupt, S.J.A. van Gisbergen, C. Fonseca Guerra, E.J. Baerends, J.G. Snijders and T. Ziegler, *J. Comput. Chem.*, 2001, 22, 931. (b) C. Fonseca Guerra, J.G. Snijders, G. te Velde, and E J Baerends, *Theor. Chem. Acc.*, 1998, 99, 391.

(26) *Gaussian 03, Revision B.04*, M.J. Frisch, G.W. Trucks, H.B. Schlegel, G.E. Scuseria, M.A. Robb, J.R. Cheeseman, J.A. Montgomery, Jr., T.Vreven, K.N. Kudin, J.C. Burant, J.M. Millam, S.S. Iyengar, J. Tomasi, V. Barone, B. Mennucci, M. Cossi, G. Scalmani, N. Rega, G.A. Petersson, H. Nakatsuji, M. Hada, M. Ehara, K. Toyota, R. Fukuda, J. Hasegawa, M. Ishida, T. Nakajima, Y. Honda, O. Kitao, H. Nakai, M. Klene, X. Li, J.E. Knox, H.P. Hratchian, J.B. Cross, C. Adamo, J. Jaramillo, R. Gomperts, R.E. Stratmann, O. Yazyev, A.J. Austin, R. Cammi, C. Pomelli, J.W. Ochterski, P.Y. Ayala, K. Morokuma, G.A. Voth, P. Salvador, J.J. Dannenberg, V.G. Zakrzewski, S. Dapprich, A.D. Daniels, M.C. Strain, O. Farkas, D.K. Malick, A.D. Rabuck, K. Raghavachari, J.B. Foresman, J.V. Ortiz, Q. Cui, A.G. Baboul, S. Clifford, J. Cioslowski, B.B. Stefanov, G. Liu, A. Liashenko, P. Piskorz, I. Komaromi, R.L. Martin, D.J. Fox, T. Keith, M.A. Al-Laham, C.Y. Peng, A. Nanayakkara, M. Challacombe, P.M.W. Gill, B. Johnson, W. Chen, M.W. Wong, C. Gonzalez and J.A. Pople, Gaussian, Inc., Pittsburgh PA, 2003.

(27) Dickinson A.A., Ph.D. Thesis, Cardiff University, 2003.

(28) Hay P.J. and Wadt W.R., *J. Chem. Phys.*, 82(1), 1985, 270.

(29) Ziegler T. and Rauk A., *Theor. Chim. Acta* 1977, 46, 1.

(30) Mayer I., *Int. J. Quantum Chem.*, 29 (1986), 477.

(31) Bridgeman A.J., Cavigliasso G., Ireland L.R., Rothery J., *J. Chem. Soc., Dalton Trans.* 2001, 2095.

3 - New metal-boryl complexes synthesised via metathesis

3.1- Introduction

The importance of boryl complexes as intermediates in transition metal catalysed hydroboration/diboration and in hydrocarbon activation has been the driving force for considerable research interest, which has been vigorous since the early 1990s. While the reactivity of transition metal boryl complexes has provided the impetus for much research effort, there has also been considerable interest in determining the fundamental ligand properties of boryl systems through a combination of spectroscopic, crystallographic and computational approaches. Ultimately a better understanding of the nature of the metal boron interaction may help provide insight into the underlying reasons for the unusual reactivity of such systems. Predominantly, however, such studies have focussed on monodentate boryl ligands (often BCat, $BO_2C_6H_4$) adopting a terminal mode of coordination with respect to the metal centre, with alternative ligand types (*e.g.* bridging, chelating, base-stabilised) being almost totally ignored. Consequently we have sought to expand the coordination chemistry of these highly topical ligand systems.

In section 3.3.1 the structural properties of a dinuclear boryl complex of iron derived from *pentaerythritol* are described, together with a comparison with the parent bridging species derived from 1,2,4,5-tetrahydroxybenzene. The analysis has been carried out with the aid of both "traditional" techniques (multinuclear NMR, FT-IR, XRD) and some others that were previously under-utilised in this field (DFT, electrochemistry, Mössbauer and FT-Raman). Section 3.3.2 describes the structure and bonding properties of an analogous terminally bound boryl complex, derived from *1,3-propanediol*, and the related comparisons that can be made both with the bridged species and with the terminal aromatic parent compound (featuring the catecholboryl ligand BCat). DFT-calculated rotational energy profiles around the iron-boron bond have been calculated and compared with information coming from spectroscopic and X-ray diffraction data. In order to understand how the metal-boron bond changes upon coordination of a Lewis base on boron, the preparation of new examples of *base-stabilised boryl complexes* of iron has been attempted. These are described in section 3.3.3.

The last part of the chapter (section 3.3.4) includes the substitution and abstraction chemistry of new boranes *(MesO)*BX_2 (X=Cl, Br). These have been used to derive asymmetric boryl complexes L_nM-B(OMes)(X) and further substitution products L_nM-B(OMes)(ER). Halide abstraction reactions on L_nM-B(OMes)(X) have been attempted to prepare the cationic terminal borylene $[L_nM{=}B(OMes)]^+$ (as its BAr^f_4 salt). All of the species appearing in this chapter have been synthesised using the salt elimination pathway, which is the "common theme" that links all the different sections together.

3.2 - Syntheses

Preparation of $(Me_3SiOCH_2)_4C$

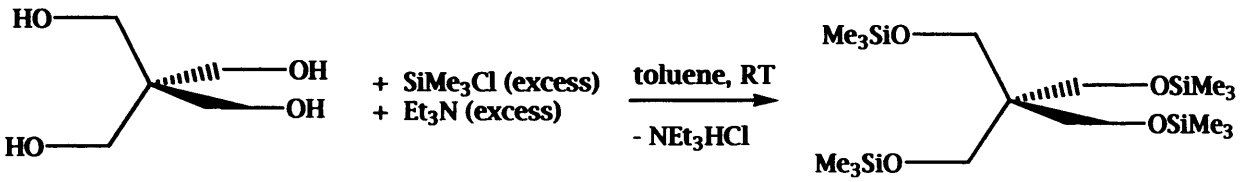

(1b) (2b)

Pentaerythritol 1b (Avocado, 5.4 g, 39.7 mmol) was suspended in toluene (100 cm^3) and 10 equiv. of trimethylsilyl chloride (Aldrich, 50 cm^3, 397 mmol) and 10 equiv. (55.3 cm^3, 397 mmol) of triethylamine (Aldrich) were then added by syringe to the rapidly stirred reaction mixture. After 12 h at room temperature the supernatant toluene solution was separated from the $(Et_3NH)Cl$ precipitate by filtration. The precipitate was washed with toluene (2 x 50 cm^3) and the combined washings reduced to dryness *in vacuo* yielding a colourless oil (*ca.* 70 % yield). Examination of the product at this point by ^1H and ^{13}C NMR revealed it to be > 99 % pure and no further purification was therefore attempted. $(Me_3SiOCH_2)_4C$ 2b was characterised by ^1H and ^{13}C NMR, IR and CI mass spectrometry (including exact mass determination). ^1H NMR (400 MHz, C_6D_6, 21°C), δ 0.14 (36H, s, $Si(CH_3)_3$), 3.70 (8H, s, $C(CH_2)_4$). ^{13}C NMR (76 MHz, C_6D_6, 21°C), δ -0.7 ($Si(CH_3)_3$), 47.3 ($C(CH_2)_4$), 59.9 ($C(CH_2)_4$). IR (neat, cm^{-1}): 2959 m, 2919 m, 2876 m, 1475 m, 1402 w, 1304 w, 1249 st, 1172 m, 1074 st, 909 st, 883 st, 747 m, 728 m, 694 m. Mass spec. (CI): $[M+H]^+$ = 425 (100 %), exact mass (calculated) *m/z* 425.2395, (observed) 425.2394.

Preparation of Spiro-[ClBO$_2$(CH$_2$)$_2$]$_2$C

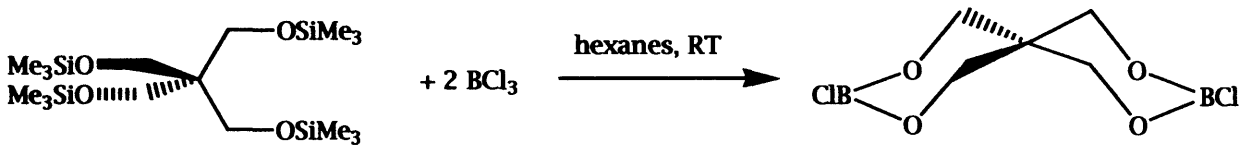

(2b) (3b)

To a solution of 11.7 g (27.6 mmol) of 2b in hexanes at room temperature was added dropwise by syringe 2 equiv. of BCl_3 (55 cm^3 of a 1.0 M solution in heptane (Aldrich), 55 mmol). The reaction mixture was warmed to 55°C and stirred for 12 h, after which the white precipitate so formed was separated from the supernatant solution by filtration, washed with hexanes (3 x 30 cm^3) and dried *in vacuo*. The crude material was then recrystallized from toluene to give 3b as a white microcrystalline solid in yields of up to 86 %. It was characterised by ^{1}H, ^{13}C and ^{11}B NMR, IR and EI mass spectrometry. ^{1}H NMR (400 MHz, C_6D_6, 21°C), δ 2.90 (8H, s, C(C*H*$_2$)$_4$). ^{13}C NMR (76 MHz, C_6D_6, 21°C), δ 35.2 (*C*(CH$_2$)$_4$), 65.1 (C(*C*H$_2$)$_4$). ^{11}B NMR (96 MHz, C_6D_6, 21°C), δ 23.1. IR (KBr disk, cm^{-1}): 2963 m, 2908 w sh, 1490 m, 1436 m, 1374 m, 1262 st, 1097 st, 1021 st, 864 w, 801 st. Mass spec. (EI): $[M]^+$ = 225 (weak).

Preparation of *Spiro-[(η^5-C$_5$H$_3$)Fe(CO)$_2$BO$_2$(CH$_2$)$_2$]$_2$C*

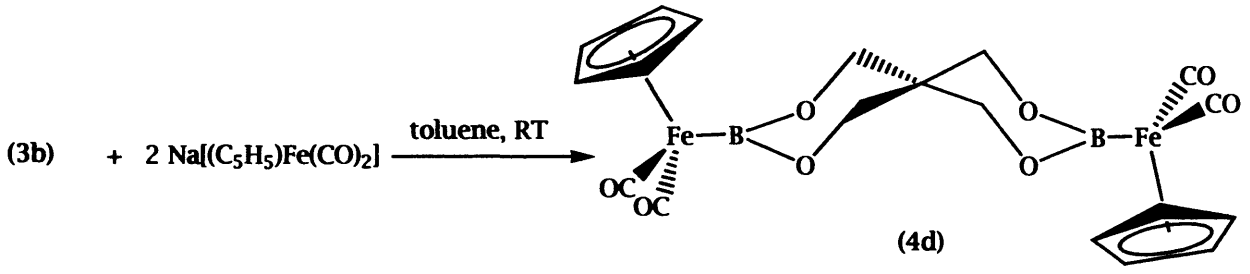

(4d)

A toluene solution of 3b was added to the (dry) NaFp salt in a 1:2 stoichiometry, and the mixture was stirred for 12 h. The solution turned from colourless to red. It was then filtered to remove the NaCl formed during the reaction, concentrated to one third of the original volume and cooled at -30°C for 48 h, giving 4d as a pale-creamy coloured powder. ^{1}H NMR

(400 MHz, C_6D_6, 21°C), δ 3.56 (8H, s, C(CH_2)$_4$), δ 4.26 (10H, s, η^5-C_5H_5). ^{13}C NMR (76 MHz, C_6D_6, 21°C), δ 36.6 (*C*(CH_2)$_4$), 65.7 (C(*C*H_2)$_4$), 83.3 (η^5-C_5H_5), 216.0 (CO). ^{11}B NMR (96 MHz, C_6D_6, 21°C), δ 45.3. IR (KBr disk, cm^{-1}) ν(CO) 1998 st, 1932 st. Mass spec. (EI): $[M\text{-}CO]^+$ = 480 (weak), expected isotopic distribution for 2 B, 2 Fe atoms, fragment ion peaks at *m/z* 452 (30 %), 424 (weak) and 396 (20 %) corresponding to sequential loss of the three remaining CO ligands. Crystals suitable for X-ray diffraction were grown by layering a toluene solution with hexanes. Yields of the pale yellow crystalline material were typically of the order of 40 %.

Preparation of Spiro-[(η^5-C_5H_5)Fe(CO)(PMe_3)$BO_2(CH_2)_2]_2C$

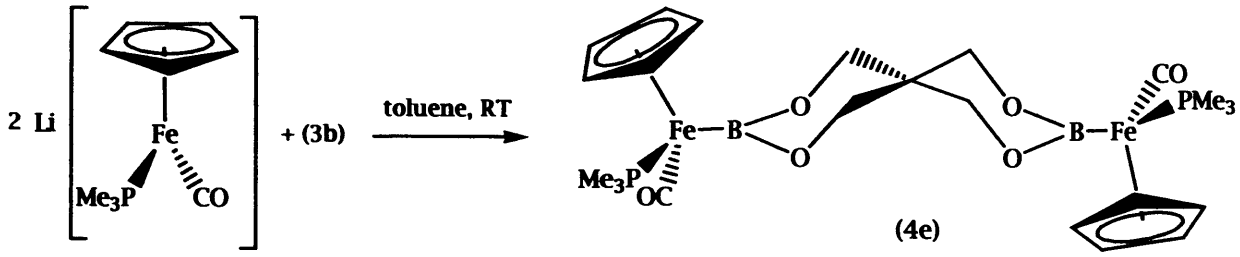

(4e)

The preparation is analogous to that used for the Fp derivative. A solution of 3b was added to the orange metal salt suspension at room temperature. The colour of the reaction mixture turned to green. It was left to react for 3 d, then the liquid phase was filtered into another Schlenk and the solvent removed *in vacuo*. The yellow-greenish solid residue was washed with hexane (3 x 30 mL) and finally dried under high vacuum for 30 min. Unfortunately, the NMR inspection of this powder (C_6D_6) revealed that it is a mixture of the expected 4e and the iron hydride [(η^5-C_5H_5)Fe(CO)(PMe_3)]H. Nevertheless, a complete set of multinuclear NMR data for 4e has been obtained: ^{1}H NMR (300 MHz, C_6D_6, 21°C), δ 1.1 (18H, d, $^2J_{H\text{-}P}$= 9 Hz, PMe_3), δ 3.6 (8H, s, C(CH_2)$_4$) δ 4.3 (10H, s, η^5-C_5H_5). ^{13}C NMR (76 MHz, C_6D_6, 21°C), δ 21.6 (d, $^1J_{C\text{-}P}$= 29Hz, PMe_3), δ 36.4 (s, *spiro-C*), δ 65.4 (s, C(CH_2)$_4$), δ 80.6 (s, η^5-C_5H_5) (carbonyl C not observed). ^{11}B NMR (96 MHz, C_6D_6, 21°C), δ 49.7 (s). ^{31}P NMR (122 MHz, C_6D_6, 21°C), δ 41.4 (s).

Attempted preparation of Spiro-[Mn(CO)$_5$BO$_2$(CH$_2$)$_2$]$_2$C

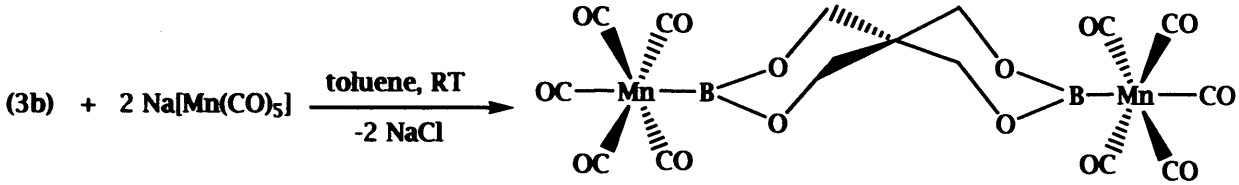

If sodium manganese pentacarbonylate is used as the metal fragment, the corresponding complex 5 is obtained. However, due to its extreme instability, this molecule could not be isolated; every crystallisation attempt led to the isolation of a powder that is a mixture of the expected product and (unknown) decomposition products, at δ_B=17-18 ppm. ^{11}B NMR (96 MHz, C_6D_6, 21°C), δ 44.2.

Preparation of [(η^5-C_5Me_5)Fe(CO)$_2$][B(tmg)]

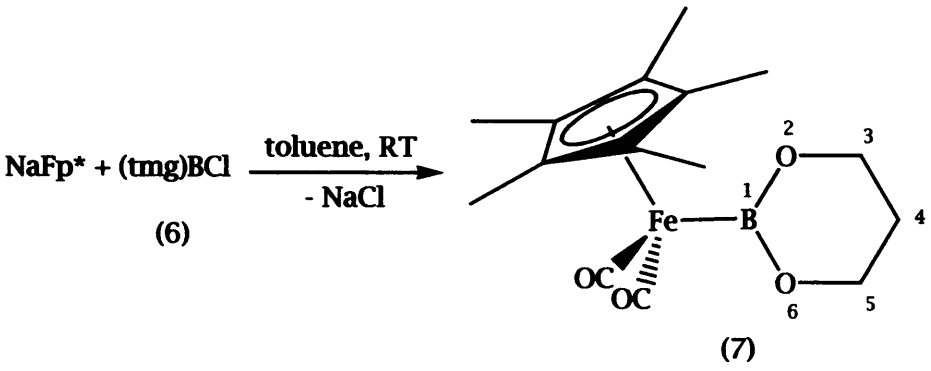

NaFp* (0.25 g, 0.92 mmol) was suspended in 40 mL of toluene, and a 0.46M solution of 6 in toluene (2 mL, 0.92 mmol) was added at room temperature. The mixture turned deep red, and it was left to react overnight. After that time, it was filtered and the solvent pumped away. The solid residue was extracted with 3 x 15 mL portions of hexane, the washings combined and concentrated to 15 mL. 12 h at -50°C yielded pale yellow crystals of 7 (typically around 35%). ^{1}H NMR (300 MHz, C_6D_6, 21°C), δ 1.4 (2H, br, CH_2 from ligand C(4)), δ 1.7 (15H, s, η^5-C_5Me_5), δ 3.6 (4H, br, CH_2 from ligand C(3) and C(5)). ^{13}C NMR (76 MHz, C_6D_6, 21°C), δ 9.8 (η^5-C_5Me_5) δ 28.0 (ligand C(4)), δ 62.8 (ligand C(3) and C(5)), δ 94.2 (η^5-C_5Me_5). ^{11}B

NMR (96 MHz, C_6D_6, 21°C), δ 47.0. IR (KBr disk, cm^{-1}) ν(CO) 1971 st, 1910 st. Mass spec. (EI): $[M]^+$: calculated mass 332.0877 a.m.u, measured mass 332.0882 a.m.u.

Following the same methodology the Fp derivative was also prepared, but, due to the fact that this complex is an oil which is difficult to obtain pure, only NMR data were collected: Fp-B(tmg) (8): ^1H NMR (300 MHz, C_6D_6, 21°C), δ 1.3 (2H, quintet, $^1J_{H-H}$=5 Hz, CH_2 of ligand C(4)), δ 3.6 (4H, t, $^1J_{H-H}$=5 Hz, CH_2 from ligand C(3) and C(5)), δ 4.3 (5H, s, η^5-C_5H_5). ^{13}C NMR (76 MHz, C_6D_6, 21°C), δ 28.1 (ligand C(4)), δ 62.9 (ligand C(3) and C(5)), δ 83.2 (η^5-C_5H_5), δ 216.2 (*C*O). ^{11}B NMR (96 MHz, C_6D_6, 21°C), δ 45.1.

Attempted preparations of $[(\eta^5\text{-}C_5R_5)Fe(CO)_2][BClX \cdot THF]$ *(R=H, Me; X=Cl, C_6H_5)*

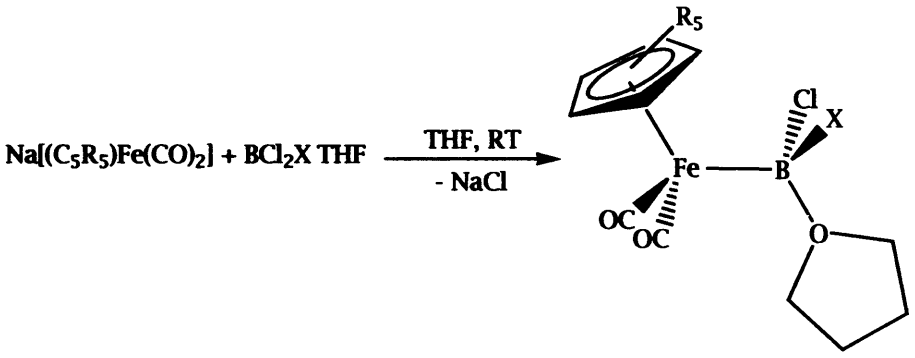

The case with R=H and X=Cl is described, all other syntheses being analogous. NaFp (0.3 g, 1.5 mmoles) was dissolved in 20 mL THF, and an analogous solution prepared containing 0.28g of BCl_3.THF (1.5 mmoles). The two solutions were mixed together at room temperature, and left to react for 15 h. The resulting red solution was filtered and the THF removed *in vacuo*. The solid residue was re-dissolved in hexane, the solution filtered again, concentrated to 15 mL and finally stored at -50°C overnight. $[(\eta^5\text{-}C_5H_5)Fe(CO)_2][BCl_2.THF]$ (9): ^{11}B NMR (96 MHz, C_6D_6, 21°C), δ 58.9. IR (THF/hexane solution, cm^{-1}) ν(CO) 1950 st, 1996 st. $[(\eta^5\text{-}C_5H_4Me)Fe(CO)_2][BCl_2.THF]$ (10): ^{11}B NMR (96 MHz, C_6D_6, 21°C), δ 59.2.

In the case of the trimethylphosphine adducts, of general formula *[(η^5-C_5R_5)Fe(CO)$_2$][BClX$_3$·PMe$_3$]* no reaction was observed leading to the generation of Fe-B bonds, the mixture always providing decomposition products in which the base is still attached to the boron atom (see the discussion section for more details).

Preparation of (MesO)BX$_2$ (X=Cl, Br)

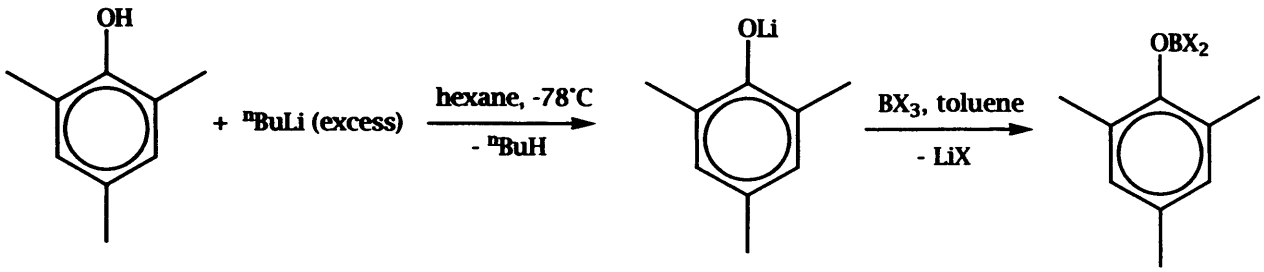

Freshly sublimed mesitol (2,4,6-trimethylphenol, Aldrich, 4.6 g, 33.8 mmol) was dissolved in 300 mL of hexane. The solution was cooled to -78°C, and 25 mL of a 1.6 M heptane solution of n-butyl lithium (Aldrich, 40 mmol) were added. After the addition, there was immediate formation of an off-white precipitate. The mixture was left to react at room temperature overnight, the contents allowed to settle and the hexane supernatant filtered off to waste. The solid product was washed with more fresh hexane (300 mL) and dried under high vacuum for 45 min. Yield: 4.27g of MesOLi (91%). Next, the lithium salt was reacted in a 1:1 stoichiometry either with a 1 M heptane solution of BCl_3 (Aldrich) or with neat BBr_3 (Aldrich), in toluene, to obtain the desired haloborane in quantitative yield. These were stored as stock toluene solutions of known molarity, to be used for the complex syntheses. (MesO)BCl_2 (11): ^{11}B NMR (96 MHz, toluene solution, 21°C), δ 31.1. In this specific case, it has been proved impossible to isolate the pure compound, since attempts to remove the solvent completely *in vacuo* cause decomposition of the ligand itself, shifting the equilibrium:

$$2\ (MesO)BCl_2 \rightleftharpoons (MesO)_2BCl + BCl_3$$

presumably by removal of the volatile BCl_3. Hence, attempted removal of solvent yields a mixture containing (MesO)BCl_2 (δ_B 31.1) and $(MesO)_2BCl$ (δ_B 22.3), with the BCl_3 being pumped away with the solvent.

(MesO)BBr_2(12): ^{1}H NMR (300 MHz, C_6D_6, 21°C), δ 1.7 (3H, s, *para*-CH_3), δ 1.9 (6H, s, *ortho*-CH_3), δ 6.3 (2H, s, aromatic H). ^{13}C NMR (76 MHz, C_6D_6, 21°C), δ 16.1 (*para*-CH_3), δ 20.3 (*ortho*-CH_3), δ 126.6 (*para* aromatic C), δ 129.3 (*meta* aromatic C), δ 134.1 (*ortho* aromatic C), δ 149.9 (*ipso-C*). ^{11}B NMR (96 MHz, C_6D_6, 21°C), δ 26.7. The compound is an oil, therefore its purification is difficult. The same problem of equilibrium shifting is also present in this case: (MesO)BBr_2 rearranges to $(MesO)_2BBr$ (δ_B 23.2) and BBr_3, but the process is slower than that of the chloro derivative, BBr_3 being less volatile than BCl_3.

Preparation of [(η^5-C_5R_5)Fe(CO)$_2$][B(OMes)X] (R=H, Me; X=Cl, Br)

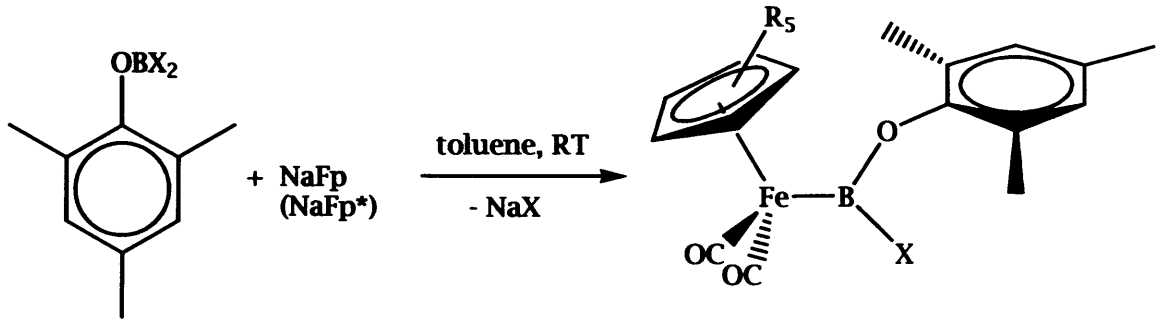

[(η^5-C_5H_5)Fe(CO)$_2$][B(OMes)Cl] (13): NaFp (1g, 5 mmol) was suspended in 15 mL of toluene, and 41.6 mL of a 0.12 M solution of 11 in toluene (5 mmol) were added *via* syringe at room temperature. The solution turned deep red, and it was left to react for 3 h. After that time, toluene was removed *in vacuo* and the solid residue was extracted with 3 x 20 mL portions of hexane. The washings were concentrated to 15 mL and cooled to -50°C overnight. Repeated cycles of "filtration-concentration-cooling" of this hexane solution (decomposition product Fp_2 precipitates out first, and the complex afterwards) finally yielded 0.62 g (35%) of crystalline 13. ^{1}H NMR (300 MHz, C_6D_6, 21°C), δ 2.1 (3H, s, *para*-CH_3), δ 2.3 (6H, s, *ortho*-CH_3), δ 4.2 (5H, s, η^5-C_5H_5), δ 6.7 (2H, aromatic C*H*). ^{13}C NMR (76 MHz, C_6D_6, 21°C), δ 17.0 (*ortho*-CH_3), δ 20.5 (*para*-CH_3), δ 84.7 (η^5-C_5H_5), δ 127.6 (*para-C* mesityl), δ 129.2 (*meta-C* mesityl), 132.7 (*ortho-C* mesityl), 152.3 (*ipso-C*), δ 214.1 (*C*O). ^{11}B NMR (96 MHz, C_6D_6, 21°C), δ 61.5. IR (KBr disk, cm^{-1}) ν(CO) 1940 st, 2002 st. Mass spec. (EI): $[M]^+$: calculated mass 358.0225 a.m.u, measured mass 358.0236 a.m.u.

$[(\eta^5\text{-}C_5Me_5)Fe(CO)_2][B(OMes)Cl]$ (14): Following an analogous route, and starting from NaFp* and 11 as precursors, the Fp* derivative 14 was prepared and obtained as pale yellow crystals after two "filtration-concentration-cooling" cycles of a hexane solution. The final yields were of the same order of magnitude as the ones of the Fp complex (35%). ^{1}H NMR (300 MHz, CD_2Cl_2, 21°C), δ 1.9 (15H, s, $\eta^5\text{-}C_5(CH_3)_5$), δ 2.1 (3H, s, *para*-$CH_3$), δ 2.2 (6H, s, *ortho*-CH_3), δ 6.8 (2H, aromatic CH). ^{13}C NMR (76 MHz, CD_2Cl_2, 21°C), δ 9.9 ($\eta^5\text{-}C_5(CH_3)_5$), δ 17.0 (*para*-$CH_3$), δ 20.4 (*ortho*-$CH_3$), δ 96.5 ($\eta^5\text{-}C_5(CH_3)_5$), δ 127.7 (*para*-*C* mesityl), δ 128.8 (*meta*-*C* mesityl), δ 129.2 (*ortho*-*C* mesityl), δ 132.6 (*ipso*-*C* mesityl), δ 217.8 (*C*O). ^{11}B NMR (96 MHz, CD_2Cl_2, 21°C), δ 63.7. IR (KBr disk, cm^{-1}) ν(CO) 1925 st, 1971 st.

$[(\eta^5\text{-}C_5H_5)Fe(CO)_2][B(OMes)Br]$ (15): The precursors in this case were 12 and NaFp, providing the product as a non-crystalline powder. ^{1}H NMR (300 MHz, C_6D_6, 21°C), δ 2.1 (3H, s, *para*-CH_3), δ 2.3 (6H, s, *ortho*-CH_3), δ 4.2 (5H, s, $\eta^5\text{-}C_5H_5$), δ 6.7 (2H, s, aromatic CH). ^{13}C NMR (76 MHz, C_6D_6, 21°C), δ 17.1 (*ortho*-CH_3), δ 20.5 (*para*-CH_3), δ 85.1 ($\eta^5\text{-}C_5H_5$), (*para*-aromatic *C* obscured by the C_6D_6 signal), δ 129.3 (*meta*-aromatic *C*), δ 132.9 (*ortho*-aromatic *C*), δ 153.2 (*ipso*-*C*), δ 213.8 (*C*O). ^{11}B NMR (96 MHz, C_6D_6, 21°C), δ 59.3. IR (KBr disk, cm^{-1}) ν(CO) 1961 st, 2015 st. Mass spec. (EI): $[M\text{-}CO]^+$: calculated mass 373.9771 a.m.u, measured mass 373.9781 a.m.u.

Preparation of $[(\eta^5\text{-}C_5H_5)Fe(CO)_2][B(OMes)(OAr)]$ (Ar=p-(t-Butyl)phenyl)

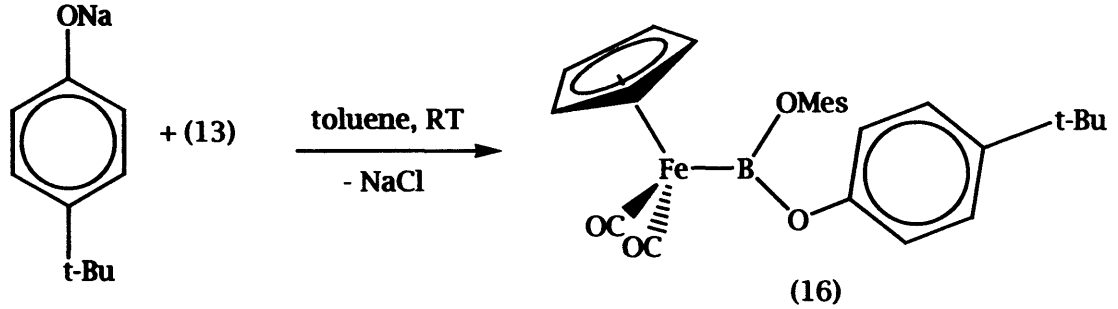

(16)

Complex 13 (0.13 g, 0.36 mmol) was dissolved in 10 mL of toluene, and the solution added to a suspension of $Na[OC_6H_4(^tBu)]$ (courtesy of Dr. Simon Aldridge, Cardiff University, 0.062 g, 0.36 mmol) in 10 mL of toluene. The mixture was stirred at room temperature for 3 d, and

after that time toluene was removed and residue extracted with 2 x 20 mL of hexane. The washings were concentrated to 15 mL and cooled to -50°C overnight, to yield colourless crystalline 16 quantitatively. ^{1}H NMR (300 MHz, C_6D_6, 21°C), δ 1.2 (9H, s, C(C*H*$_3$)$_3$), δ 2.1 (3H, s, *para*-C*H*$_3$), δ 2.4 (6H, s, *ortho*-C*H*$_3$), 4.2 (5H, s, η^5-C$_5$*H*$_5$), δ 6.9 (2H, s, aromatic C*H* from Mesityl), δ 7.0 (2H, s, *meta*-C*H* from aryl substituent), δ 7.2 (2H, s, *ortho*-C*H* from aryl substituent). ^{13}C NMR (76 MHz, C_6D_6, 21°C), δ 15.4 (*ortho*-*C*H$_3$), δ 18.6 (*para*-*C*H$_3$), δ 29.4 (C(*C*H$_3$)$_3$), δ 32.0 (*C*(CH$_3$)$_3$), δ 80.9 (η^5-*C*$_5$H$_5$), δ 119.1 (*para-C* from aryl substituent), δ 124.1 (*meta-C* aryl), *para-C* mesityl obscured by the C_6D_6 signal, δ 127.2 (*ortho-C* from aryl), δ 129.6 (*meta-C* mesityl), δ 143.6 (*ortho-C* mesityl), δ 150.1 (*ipso-C* aryl), δ 151.4 (*ipso-C* mesityl), δ 213.3 (*C*O). ^{11}B NMR (96 MHz, C_6D_6, 21°C), δ 47.4. IR (KBr disk, cm^{-1}) ν(CO) 1944 st, 2006 st. Mass spec. (EI): [M-CO]$^+$ *m/z* 444 (weak), fragment ion peak at *m/z* 416 corresponding to loss of the remaining CO ligand ([M-2CO]$^+$).

Preparation of [(η^5-C$_5$H$_5$)Fe(CO)$_2$][B(OMes)(SC$_6$H$_5$)]

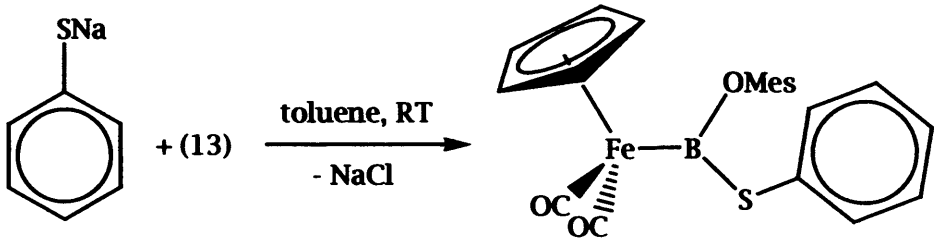

(17)

The boryl precursor 13 (0.1 g, 0.28 mmol) was dissolved in 10 mL of toluene, and 0.05 g (0.42 mmol, 1.5 equiv.) of sodium thiophenolate (courtesy of Dr. Deborah Coombs, Cardiff University) were also dissolved in 10 mL of toluene. The iron complex solution was added to the salt suspension, and the mixture stirred for 2 d at room temperature. After that time, the starting material had converted completely into the final substitution product 17, on the evidence of the ^{11}B NMR spectrum. Toluene was removed *in vacuo*, and the solid residue extracted with 2 x 15 mL portions of hexane. The hexane solution was filtered, concentrated and cooled to -50°C overnight, to yield colourless crystals of 17. ^{1}H NMR (300 MHz, C_6D_6, 21°C), δ 2.1 (3H, s, *para*-C*H*$_3$), δ 2.2 (6H, s, *ortho*-C*H*$_3$), 4.2 (5H, s, η^5-C$_5$*H*$_5$), δ 6.6 (2H, s, aromatic

C*H* from Mesityl), δ 6.9 (3H, m, *meta+para*-C*H* from aryl substituent), δ 7.4 (2H, m, *ortho*-C*H* from aryl substituent). ^{13}C NMR (76 MHz, C_6D_6, 21°C), δ 17.0 (*ortho*-CH_3), δ 20.5 (*para*-CH_3), δ 83.7 (η^5-C_5H_5), δ 126.7 (*para-C* of the SPh ring), δ 127.6 (*para-C* of the Mesityl ring), δ 128.3 (*meta-C* of the SPh ring), δ 129.2 (*meta-C* of the Mesityl ring), δ 132.4 (*ortho-C* of the Mesityl ring), δ 134.4 (*ortho-C* of the SPh ring), δ 134.8 (*ipso-C* of the SPh ring), δ 152.8 (*ipso-C* of the Mesityl ring), δ 214.6 (*C*O). ^{11}B NMR (96 MHz, C_6D_6, 21°C), δ 69.1. IR (KBr disk, cm^{-1}) ν(CO) 1930 st, 1996 st. Mass spec. (EI): $[M\text{-}CO]^+$ calculated mass 404.0699 a.m.u, measured mass 404.0700 a.m.u.

Attempted preparation of $[(\eta^5\text{-}C_5H_5)Fe(CO)_2][B(OMes)(O^tBu)]$

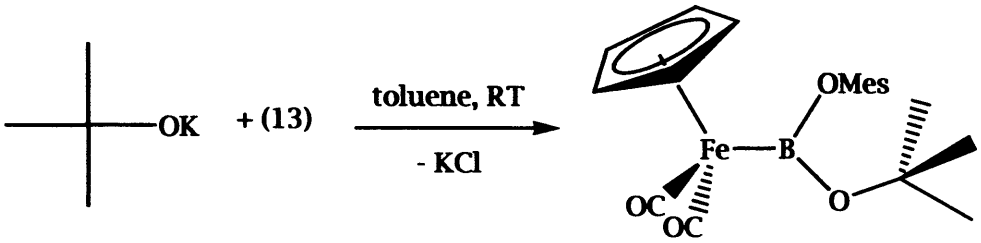

(18)

Using an analogous approach, substitution of the chlorine atom of 13 with a t-butoxy group was attempted. After stirring for 2 d at room temperature 18 decomposes to a product which gives a ^{11}B resonance at δ_B=18 ppm, without even reaching a complete conversion of the starting material. ^{11}B NMR (96 MHz, toluene solution, 21°C), δ 45.9.

Preparation of $[(\eta^5\text{-}C_5H_5)Fe(CO)_2][B(OMes)(F)]$

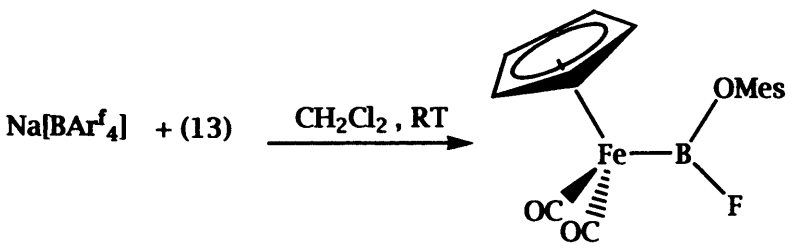

(19)

Complex 13 was further reacted with the halide abstraction agent $Na[BAr'_4]$. 13 (0.14 g, 0.39 mmol) was dissolved in 15 mL of dichloromethane. The mixture was then added to a suspension of 0.35 g $Na[BAr'_4]$ (0.39 mmol) in 15 mL of dichloromethane at room temperature. After one night stirring, the orange solution turned deep red. Reaction was complete, judging from the ^{11}B NMR spectrum, and all the starting material was consumed. The CH_2Cl_2 was pumped away, and the solid residue extracted with hexane (2 x 20 mL). The concentrated and cooled (-50°C) hexane solution yielded an oily red material, which was analysed by NMR and IR, confirming it as compound 19: ^1H NMR (300 MHz, C_6D_6, 21°C), δ 2.1 (3H, s, *para*-C*H*$_3$), δ 2.3(6H, s, *ortho*-C*H*$_3$), 4.2 (5H, s, η^5-C$_5$*H*$_5$), δ 6.7 (2H, s, aromatic C*H* from Mesityl). ^{13}C NMR (76 MHz, C_6D_6, 21°C), δ 17.0 (*para*-*C*H$_3$), δ 20.4 (*ortho*-*C*H$_3$), δ 83.4 (η^5-*C*$_5$H$_5$), δ 129.3 (*meta+para-C* of mesityl), δ 132.2 (*ortho-C* of mesityl), δ 134.7 (*ipso-C* of mesityl). ^{11}B NMR (96 MHz, C_6D_6, 21°C), δ 45.7 (d, $^1J_{B\text{-}F}$= 181 Hz). ^{19}F NMR (283 MHz, C_6D_6, 21°C), δ -9.1 (partially collapsed quartet). IR (C_6D_6 solution, cm^{-1}) ν(CO) 1954 st, 2013 st.

3.3 - Discussion of results

3.3.1 - Bridging boryls: a comparison between aliphatic and aromatic spacers

Dinuclear complexes featuring metal centres linked *via* bridging boryl ligands can be synthesised in yields of 50-60 % according to the general synthetic route outlined in Scheme 1:

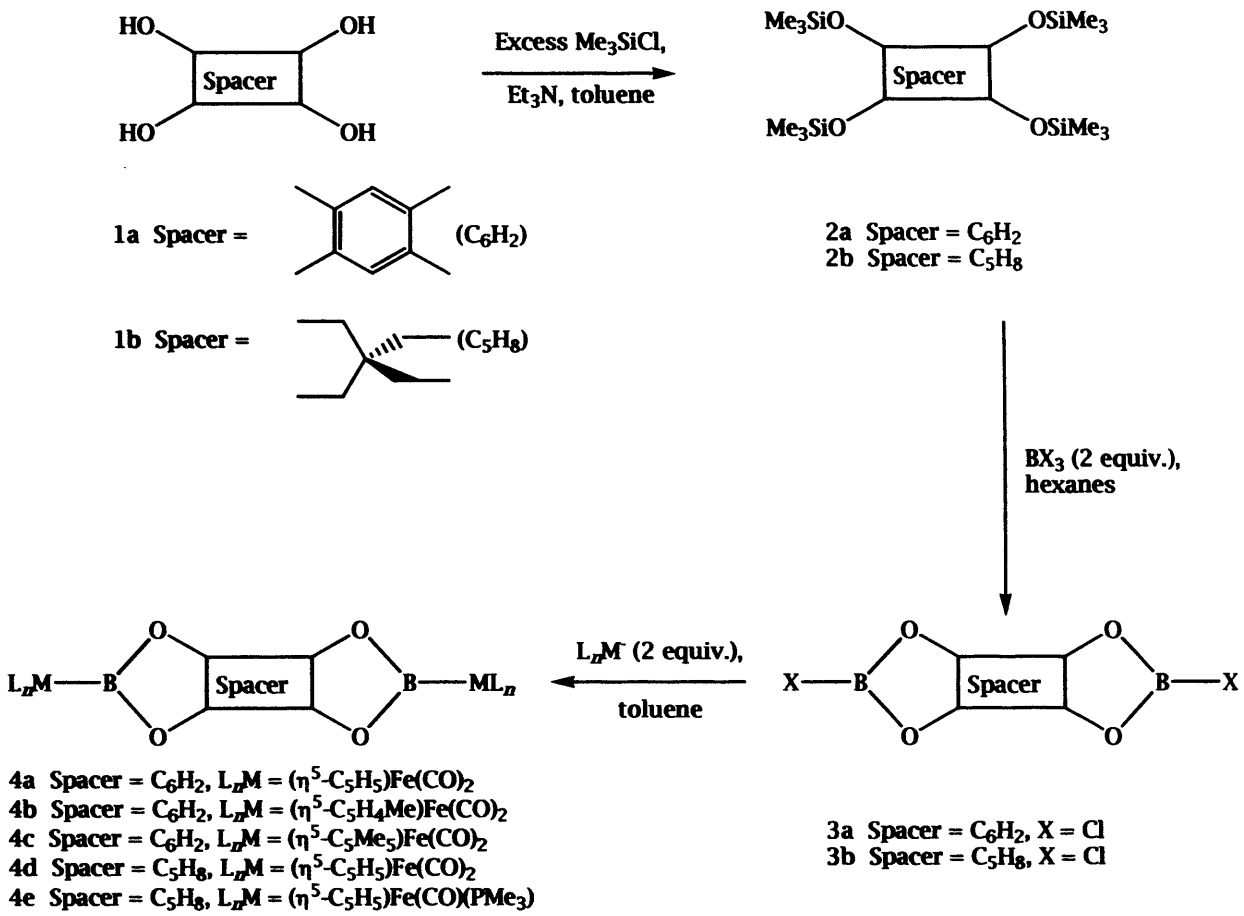

Scheme 1 - Bridging boryl complexes

This methodology can be applied both to unsaturated bridging 'spacer' groups such as those based around a 1,2,4,5-tetrasubstituted benzene framework, and also to saturated aliphatic systems such as the *spiro* species derived from pentaerythritol precursors. The bifunctional boron halide reagents (3a, 3b) required in the final metathesis step are most conveniently prepared from trimethylsilyl-substituted precursors (*i.e.* 2a, 2b) which are freely soluble in the non-polar organic media employed. By contrast, direct synthesis from polyhydroxy species and boron trichloride, for example, suffers from low yields resulting from the difficulty in adequately drying compounds such as 1a and 1b (water is always present in the lattice). Not unexpectedly, dinuclear species 4a-e are significantly less soluble in organic media than their mononuclear counterparts, with those containing unsaturated spacer groups (4a-c) being less soluble than those such as 4d-e containing saturated bridging units.

Single crystals of metal complexes 4a, 4b and 4d suitable for X-ray crystallography proved to be accessible by layering with hexanes of concentrated solutions in either dichloromethane (4a, 4b) or toluene (4d). In each case the molecular structure consists of two piano stool (η^5-C_5H_5)Fe(CO)$_2$ fragments linked in μ-(η^1, η^1) fashion by a bridging boryl ligand. The molecular structure of 4d is reported in Figure 1. The most significant bond lengths (Å) and angles (°) of 4a and 4d are in Table 1. 4a and 4b were made by Dr. Richard Calder.

Table 1 - Bond lengths (Å) and angles (°) for 4a and 4d

	4a	4d
Fe - B	1.971(2)	2.030(5)
B - O(ligand)	1.406(2)	1.369(6)
Fe - C(carbonyl)	1.751(2)	1.743(5)
Fe(1) - Cp (centroid)	1.721(2)	1.722(6)
C(CO) - Fe - C(CO)	93.97(8)	95.1(2)
O(lig) - B - O(lig)	109.15(14)	121.2(4)
O(lig) - B - Fe	121.94(12) 125.79(13)	118.7(3) 120.2(3)
O(lig) - B - Fe - Cp(cd)	82.2(1)	43.5(3)
Fe(1) - C(10) - Fe(1')		130.4(4)

The molecular structure of 4d is bent [∠Fe(1)-C(10)-Fe(1')=130.4(4)°] reflecting the conformation of the six-membered chelate rings, and in particular the angle [132.3(5)°] between the planes defined by C(9), C(10), C(11) and O(3), B(1), O(4).

Of particular interest is the significantly longer Fe-B bond length found in 4d [2.030(5) Å] compared to those found in 4a [1.971(2) Å], 4b [1.973(2) Å] and in the terminally bound BCat analogue (η^5-C_5H_5)Fe(CO)$_2$BCat [1.959(6) Å][1]. The latter three compounds all feature five-membered BO_2C_2 chelate rings in which *conjugation* of the appropriate symmetry lone pairs of the oxygen centres [*e.g.* O(1) and O(2) in 4a] into the aromatic ring system is possible. In the case of 4d, however, no such conjugation is possible, and as a consequence O→B π

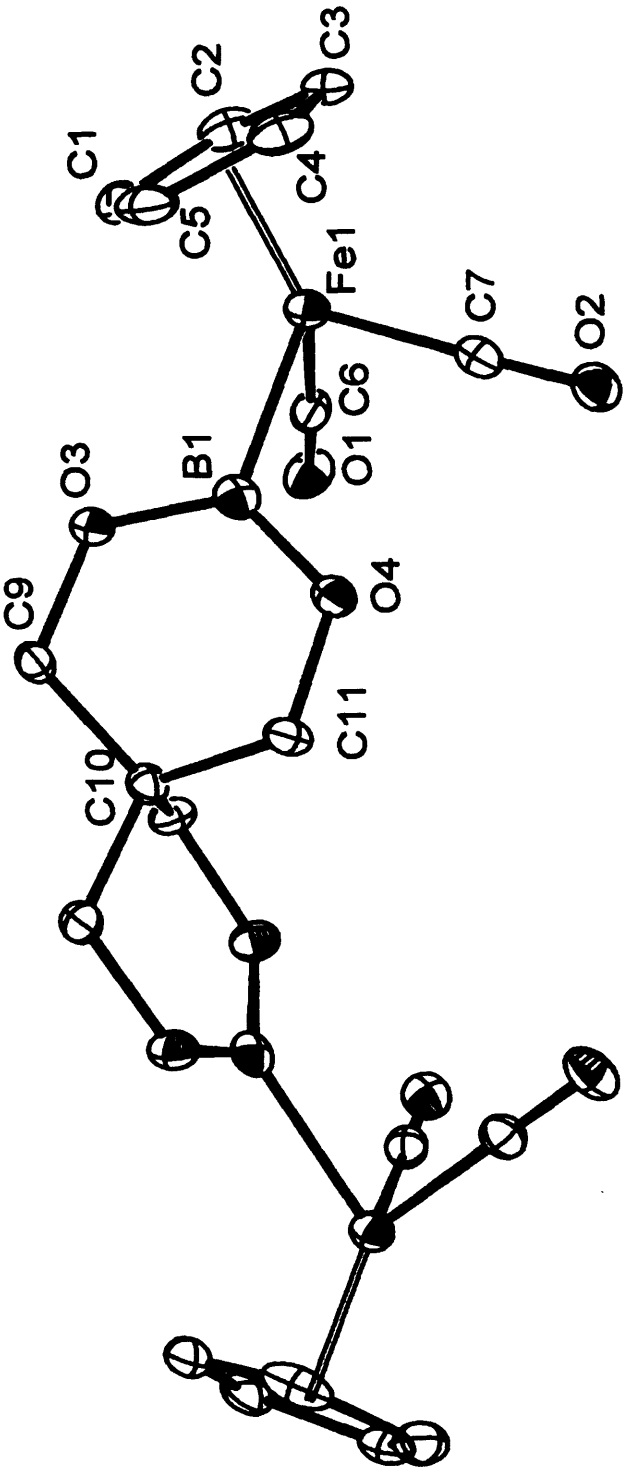

Figure 1 *- Molecular structure of spiro-[(η^5-C_5H_5)Fe(CO)$_2$BO$_2$(CH_2)$_2$]$_2$C,* ***4d****. ORTEP ellipsoids drawn at the 50% probability level; hydrogen atoms omitted for clarity.*

donation is likely to be more significant. This in turn renders the boryl boron centre less π acidic, and consequently *the extent of π back donation from the iron centre is reduced.* Hence, the Fe-B distance in 4d is similar to that found in $[(\eta^5\text{-}C_5H_4Me)Fe(CO)_2]_2B_3ClN_3H_3$ [mean 2.043(1) Å [2]] and $(\eta^5\text{-}C_5Me_5)Fe(CO)_2B(NMe_2)Cl$ [2.027(5) Å [3]] where little if any π back bonding is thought to exist. A further consequence is that the B-O distances in 4d [mean 1.365(5) Å] are significantly shorter than those found in 4a [1.406(2) Å] or 4b [1.408(2) Å].

For systems of the type $(\eta^5\text{-}C_5H_5)Fe(CO)_2X$, ^{57}Fe Mössbauer spectroscopy offers an extensively used alternative to crystallographic methods to probe the electronic properties of a ligand X[4]. In general, a decrease in the Mössbauer effect isotope shift (i.s.) corresponds to an increase in the s electron density at the iron nucleus. Such an increase usually results from the presence of a ligand (X) which has good σ donor or π acceptor properties[4].

The ^{57}Fe Mössbauer spectra of the dinuclear complexes 4a and 4d at 77 K are reproduced in Figure 2:

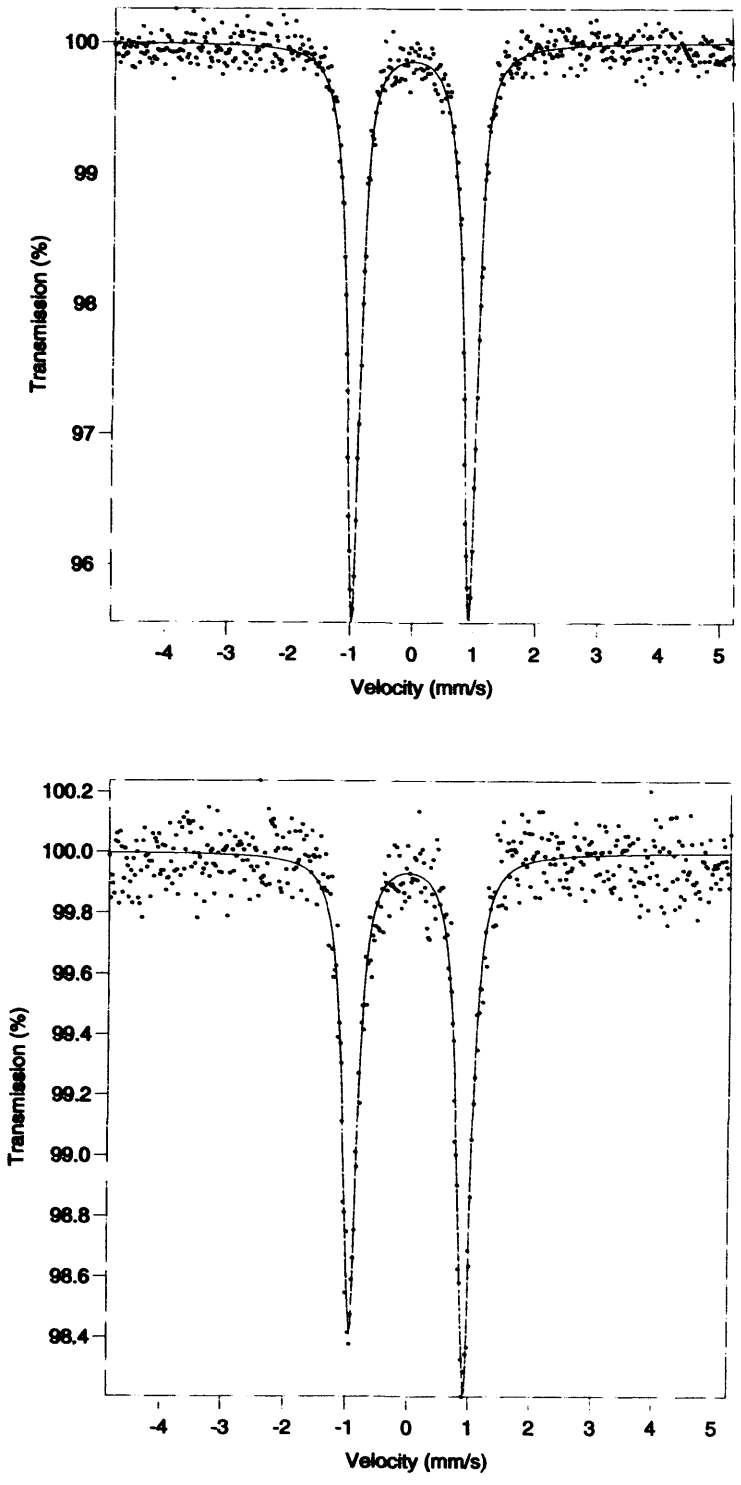

Figure 2 - Mössbauer spectra of 4a and 4d

Their associated spectral parameters are listed in Table 2, along with those for related Fe complexes containing good σ donor or good π acceptor ligands.

Table 2 - Mössbauer parameters for different iron complexes

Complex	Isomer shift / mm s^{-1}	Quadrupole splitting / mm s^{-1}	ν (CO) / cm^{-1}	Reference
4a	0.02	1.91	2006, 1954	This work
4d	0.00	1.86	1998, 1932	This work
$(\eta^5\text{-}C_5H_5)Fe(CO)_2Br$	0.22	1.88	2045, 1999	This work
$(\eta^5\text{-}C_5H_5)Fe(CO)_2Br$	0.23	1.87	2045, 1999	4b
$(\eta^5\text{-}C_5H_5)Fe(CO)_2CN$	0.07	1.90	2060, 2015	4b
$(\eta^5\text{-}C_5H_5)Fe(CO)_2SCN$	0.19	1.81	2050, 2005	4b
$(\eta^5\text{-}C_5H_5)Fe(CO)_2SiMe_3$	0.05	1.77	1996, 1944	4c
$(\eta^5\text{-}C_5H_5)Fe(CO)_2CH_3$	0.08	1.76	2010, 1958	4c
$(\eta^5\text{-}C_5H_5)Fe(CO)_2B_5H_8$	0.04	1.84	2005, 1947	4d

For reference purposes, the spectrum of $(\eta^5\text{-}C_5H_5)Fe(CO)_2Br$ was also measured and spectral parameters were found to be in good agreement with those reported previously.[4b] The very low values of the isomer shifts for both 4a (0.02 mm s^{-1}) and 4d (0.00 mm s^{-1}) are comparable to those reported for complexes containing either good π acceptor ligands (*e.g.* CN^-, 0.07 mm s^{-1} [4b]), or for those containing good σ donor ligands (*e.g.* $SiMe_3$, 0.05 mm s^{-1} and CH_3, 0.08 mm s^{-1} [4c]). That the bridging boryl ligands in 4a and 4d fit into the latter category as giving low isomer shifts due to strong σ donor rather than strong π acceptor properties is confirmed by analysis of the IR data listed in the same table. The low carbonyl stretching frequencies found for 4a and 4d (2006, 1954 and 1998, 1932 cm^{-1}, respectively) are clearly more consistent with strong σ donor properties [*c.f.* 2010, 1958 and 1996, 1994 cm^{-1} for $(\eta^5\text{-}C_5H_5)Fe(CO)_2CH_3$ and $(\eta^5\text{-}C_5H_5)Fe(CO)_2SiMe_3$, respectively[4c]] than with an appreciable π acceptor role [2060, 2015 cm^{-1} for $(\eta^5\text{-}C_5H_5)Fe(CO)_2CN$]. Indeed, it is noticeable how similar are both Mössbauer and IR spectral parameters for 4a and 4d to those reported for $(\eta^5\text{-}C_5H_5)Fe(CO)_2B_5H_8$.[4d] This complex contains a $(\eta^5\text{-}C_5H_5)Fe(CO)_2$ fragment terminally bound to a

four-coordinate boron centre, which by implication must have little or no π acceptor properties.[4d]

An additional piece of information that is in agreement with the structural and spectroscopic data reported is DFT bond density analysis. Decomposition of the iron-boron total bond density into its σ and π components has been performed with the *ADF_Reader* script. The ratios found for the terminal analogues of 4a and 4d [i.e. the complexes (η^5-C_5H_5)Fe(CO)$_2$(BCat) and (η^5-C_5H_5)Fe(CO)$_2$B(tmg) respectively] are 87.8% : 12.2% and 90.1% : 9.9%, thus providing further evidence that the π contribution is small in each case and that the complex with the aromatic spacer has a marginally greater Fe-B π interaction than in the aliphatic case.

By contrast, FT-Raman and electrochemical probes of boryl complexes 4a-d have proved to be less informative. Raman spectra of the four dinuclear complexes show little variation, strong features in the region 520-530 cm^{-1} in each case being assigned to Fe-B stretching modes. Interestingly, however, the analogous stretching vibration for the more Lewis acidic pentafluorophenyl substituted derivative (η^5-C_5H_5)Fe(CO)$_2$B(C_6F_5)$_2$ is found at 577 cm^{-1} [5].

Electrochemical methods have been used to great effect to assess the possibility for communication between metal centres through bridging ligand systems. Consequently, it was hoped that cyclic voltametry (CV) measurements for complexes 4a-c might indicate whether communication between metal centres through bridging boryl ligands was possible. CV measurements for all four dinuclear complexes (including complex 4d containing a comparative saturated spacer group) were unfortunately complicated by problems of irreversibility, which were only partially alleviated by the use of bulkier ligand systems (η^5-C_5Me_5 *vs.* η^5-C_5H_5), glassy carbon electrodes or low temperature. Consequently it proved impossible to definitively assign spectra and therefore to use electrochemical methods as a probe of the electronic structure of these systems.

Attempts to make complexes with different metal fragments were less successful: in the case of $Na[Mn(CO)_5]$ a peak at δ_B= 44 ppm is observed, and no peak of the starting material is found (δ_B=23 ppm). The conversion is complete, but the solid obtained by cooling concentrated toluene or hexane solutions is a mixture of the (supposed) boryl 5 and one by-product at δ_B=17 ppm (possibly coming from a partial hydrolysis of the ligand, yielding a molecule like HO-B(spacer)B-OH, whose chemical shift can be similar to that of boric acid $B(OH)_3$ (δ_B = 18 ppm)).

3.3.2 – Terminal analogues: a comparison between aliphatic and aromatic boryl ligand substituents

Synthesis of ligand precursor 3b *via* preliminary functionalisation with trimethylsilyl groups proved to be difficult to accomplish cleanly. Experiments conducted on neopentyl glycol (2,2-dimethyl-1,3-propanediol) showed that, while this first step gives good yields (around 80%) and leads to the expected product, the second step is not as clean as the first one; the reaction appears not to reach completion. After warming to 60°C for 12 h, the situation is unchanged. In the case of BCl_3, for example, three different peaks are observed in the ^{11}B NMR spectrum of the hexane solution mixture: δ_B=45 ppm (BCl_3), δ_B=31 ppm (presumably the intermediate 20, *c.f.* (MesO)BCl_2 δ_B=31 ppm) and δ_B=23 ppm (21, *c.f.* (tmg)BCl δ_B=22.8 ppm). A similar situation also occurs for BBr_3 or BF_3.

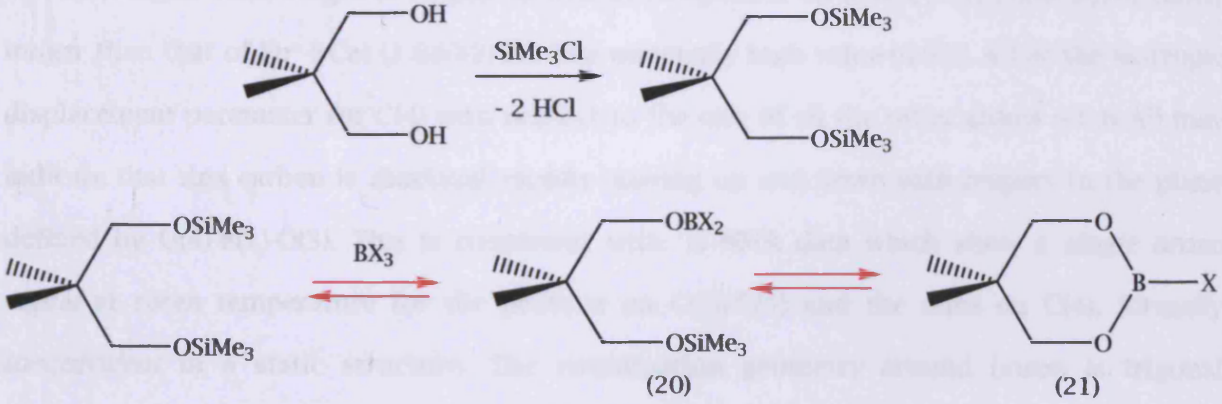

Scheme 2 – Equilibrium reactions of (Neop)BX (21).

Thus, the ligand precursor 6 was prepared cleanly with a different approach, using $B(OH)_3$ as starting material (Chapter 2, section 2.3.2). Reactions of 6 with different metal fragments were tried, but only in the case of the Fp* complex was a crystalline material obtained. The structure of Fp*-B(tmg) 7 is analogous to that of its bridged counterpart; Table 3 lists the most significant structural features, together with comparative data from the related compound Fp*-BCat made by Hartwig *et al.* in 1999[6]. Figure 3 shows the crystal structure of 7.

*Table 3 - Bond lengths (Å) and angles (°) for 7 and Fp*BCat*

	7	Fp*-BCat
Fe - B	2.024(4)	1.980(2)
B - O(ligand)	1.357(5)	1.404(3)
Fe - C(carbonyl)	1.737(4)	1.749(3)
Fe - Cp (centroid)	1.72(8)	1.72(1)
C(CO) - Fe - C(CO)	95.43(19)	96.3(1)
O(lig) - B - O(lig)	121.1(3)	108.8(2)
O(lig) - B - Fe	119.9(3) 118.9(3)	126.8(2) 124.4(2)
O(lig) - B - Fe - Cp	92.9	26.7

The iron-boron bond length is similar to that of compound 4d (2.030(5) Å), and significantly longer than that of Fp*-BCat (1.980(2) Å). The unusually high value (0.923 $Å^2$) of the isotropic displacement parameter for C(4) with respect to the one of all the other atoms (<0.6 $Å^2$) may indicate that this carbon is *fluxional*, rapidly moving up and down with respect to the plane defined by O(4)-B(1)-O(3). This is consistent with ^1H NMR data which show a *single broad signal* at room temperature for the protons on C(3)/C(5) and the ones on C(4), formally *inequivalent* in a static structure. The coordination geometry around boron is trigonal planar, with all the bond angles close to 120°, as expected for tri-coordinated boron.

Information coming from IR and NMR spectroscopies reveals that *the extent of π donation Fe→B is smaller for the ligand B(tmg) than that of the ligand BCat*, exactly as in the case of

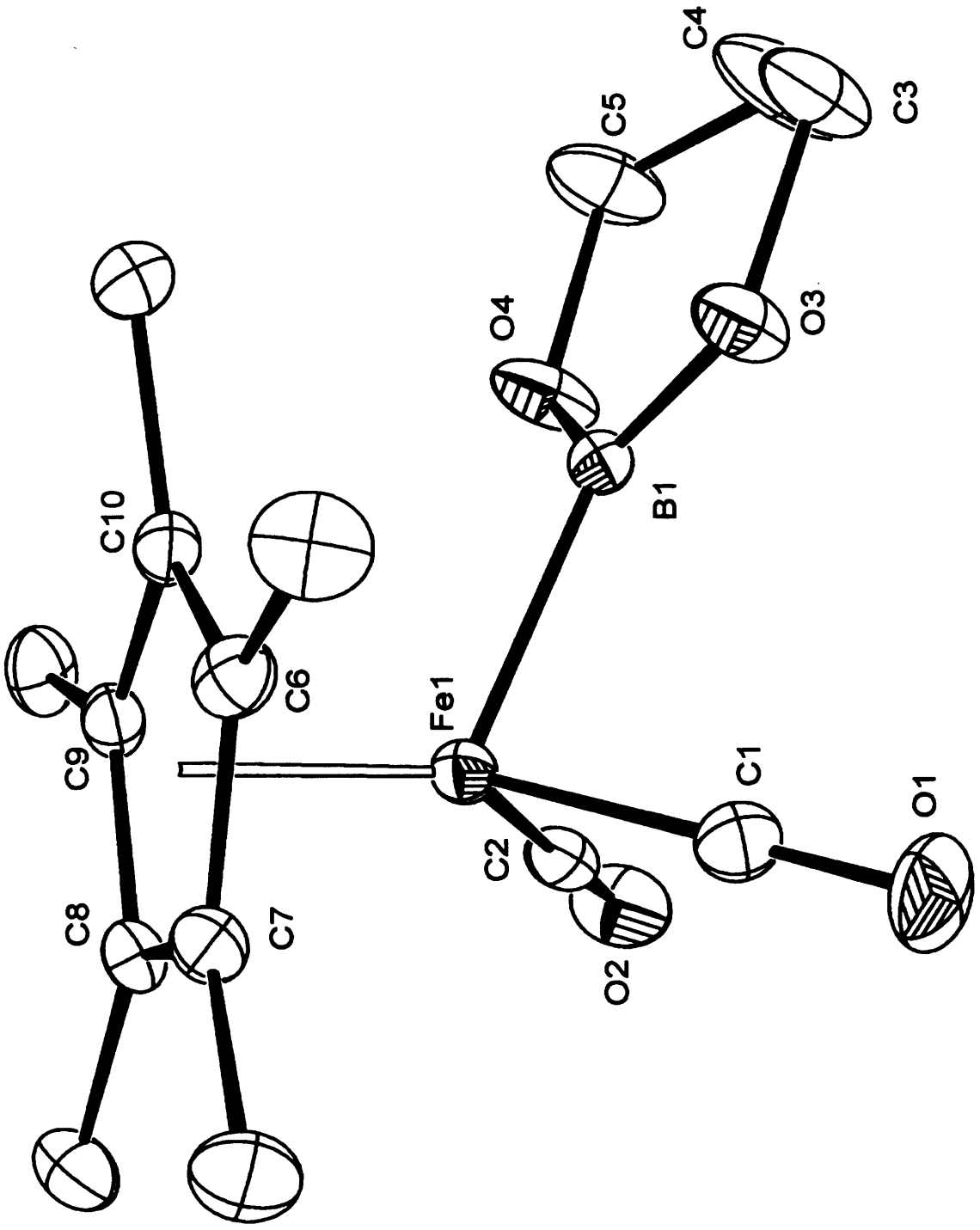

***Figure 3** - Molecular structure of (η^5-C_5Me_5)Fe(CO)$_2$[B(tmg)], 7. ORTEP ellipsoids drawn at the 50% probability level; hydrogen atoms omitted for clarity.*

their bridging analogues. IR ν(CO) frequencies of Fp*-BCat (1996, 1940 cm^{-1} [6]) are higher than those of Fp*-B(tmg) (1971, 1910 cm^{-1}), and the ^{11}B NMR signal of 7 (δ_B=47 ppm in C_6D_6) is more upfield than that of Fp*-BCat (δ_B=54 ppm in C_6D_6 [6]), implying that the boron atom in 7 is more electron-rich than in Fp*-BCat. However, this excess of electron density comes from the oxygen atoms of the ligand and not from the metal centre.

In order to complement the experimental data, a set of DFT calculations has been carried out on these systems to determine the energy barrier of rotation of the B(tmg) and BCat ligands around the Fe-B single bond. The three examples considered are: 7, 8, and Fp-BCat. The results are exemplified by Figure 4, showing the variation of the relative energies of the different conformers with the dihedral angle θ for 7. For a definition of θ refer to section 2.5.6.

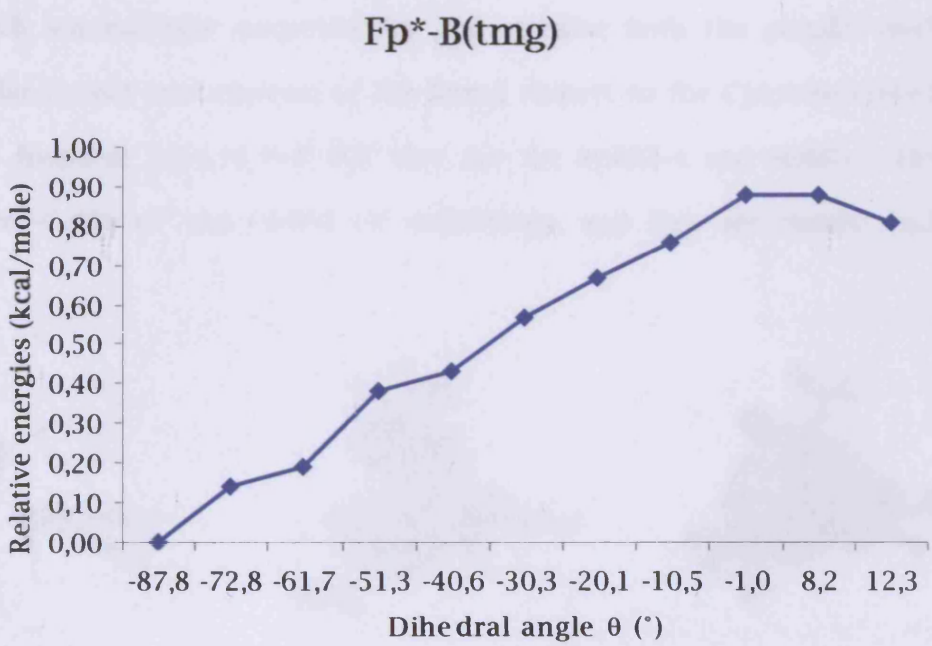

Figure 4 - Rotational profile of complex 7 Fp-B(tmg)*

As a general feature, in all cases the rotational barriers are very small, as expected for a predominantly single σ bond, and mirroring the results obtained in other similar studies[7]. The starting point is the crystal structure (previously optimised with Gaussian), apart from

the case of 8, where the structure is obtained from the bridged structure of complex 4d by formally cutting it into half and adding hydrogens on C(10) (see Figure 1), since the structure of the actual compound is not available. The effects of sterics and electronics can be gauged by examining the rotational barriers for Fp*-B(tmg), Fp-B(tmg) and Fp-BCat (0.88, 0.21 and 0.68 kcal/mole respectively). Compared to model complex Fp-B(tmg) higher barriers are obtained for the bulkier Fp* derivative and for the more π acidic BCat complex. It should be noted that the rotational barrier in such systems is *not* a direct measure of π bond strength (due to the presence of mutually perpendicular orbitals on the [Fp] fragment, *vide infra*), but merely the *difference in π bonding between the θ=0° and θ=90° orientations.*

The MO scheme of the two fragments (fragment molecular orbitals, FMO) derived from homolytic cleavage of the Fe-B bond shows the existence of two filled orbitals on the metal centre which are mutually perpendicular and stabilise both the parallel (θ=0°) and the perpendicular (θ=90°) conformation of the ligand respect to the Cp(centroid)-Fe-B plane. In the radical fragment $[(\eta^5\text{-}C_5H_5)Fe(CO)_2]^\bullet$ they are the SOMO-4 and SOMO-5 FMOs, whose energies are -5.848 eV and -5.954 eV respectively, and they are mainly made of d(Fe) orbitals:

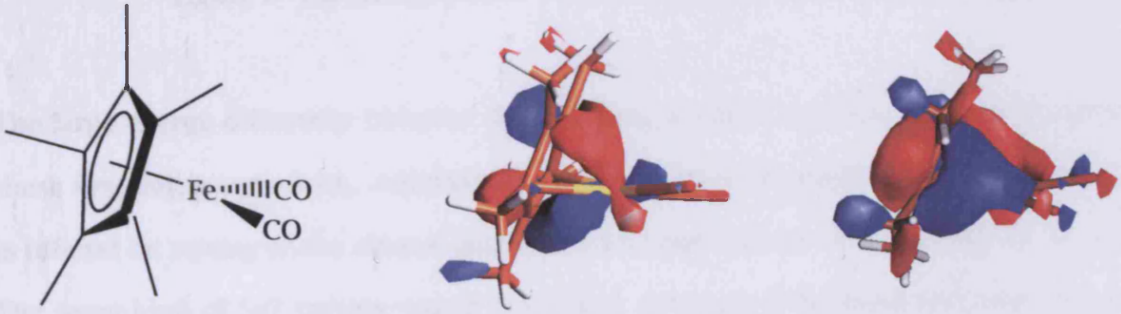

Figure 5 - Calculated SOMO -4 and SOMO -5 of the fragment $[(\eta^5\text{-}C_5H_5)Fe(CO)_2]^\bullet$

The ligand empty FMOs which can overlap with these FMOs are SOMO+3 in [BCat]• and SOMO+2 in [B(tmg)]•. They are mainly of p(B) and p(O) character: their energies are -0.521 eV for [BCat]• and +0.088 eV for [B(tmg)]•:

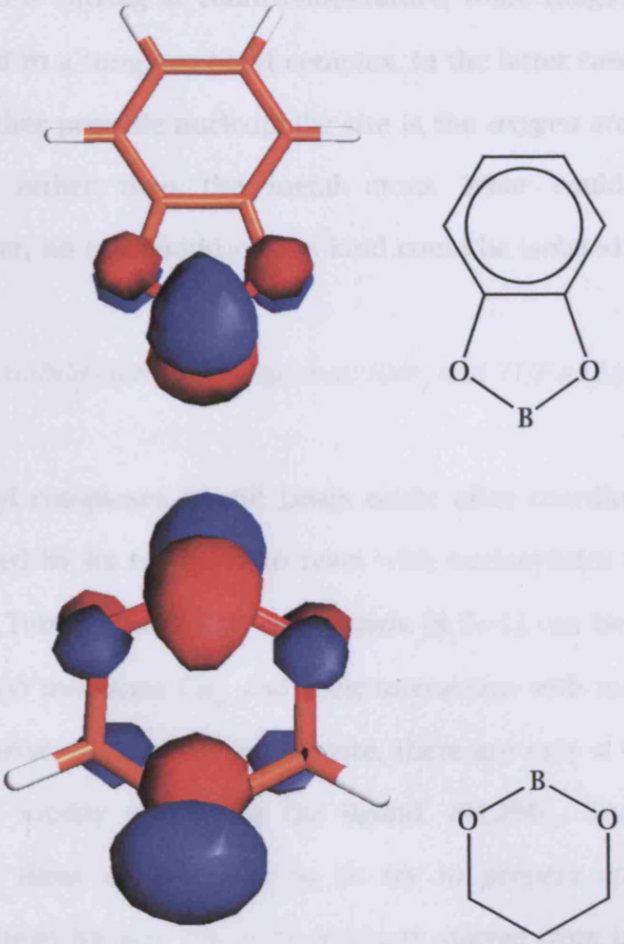

Figure 6- Calculated SOMO +3 of [BCat]• and SOMO +4 of [B(tmg)]•

The large energy difference between the two sets of FMOs explains why the π interaction in these systems is very weak. Additionally, the possibility of stabilising all ligand orientations is offered by *mixing* of the almost degenerate MO pair (SOMO -4 and SOMO -5) on the metal. The same kind of MO pattern would have been obtained if the bond had been broken in an heterolytic way, that is $[(\eta^5\text{-}C_5H_5)Fe(CO)_2]^-$ and $[L]^+$ (according to the results of the calculation of Mulliken charges, the boron atom always brings a positive charge, while the metal is negative). In that case the π interaction would have involved the HOMO(-n) of the metal with the LUMO(+n) of the ligand fragment (backbonding M→L), but the conclusions would have been identical[8].

When it comes to different transition metals, attempts to make complexes with the terminal ligand 6 were all unsuccessful: $Na[Mn(CO)_5]$ gave only decomposition products at δ_B=17.6

ppm in toluene after 20 h stirring at room temperature, while tungsten fragments Na[(η^5-C_5R_5)W(CO)$_3$] did not lead to a tungsten boryl complex. In the latter case there is evidence in the literature[9] that another possible nucleophilic site is the *oxygen atom* of the CO ligands in the Wp fragment, rather than the metal atom. What could be obtained is a boryloxycarbyne. However, no compound of this kind could be isolated in the case of ligand 6.

3.3.3 - Base-stabilised boryl complexes: PMe_3 and THF as Lewis bases

The boron atom in boryl complexes is still Lewis acidic after coordination to a transition metal, as is demonstrated by its tendency to react with nucleophiles (which generally also cleave the M-B bond)[10]. Tetrahedral boron compounds [R_3B←L] can be thought of as being isostructural to tetra-alkyl methanes CR_4, and their interaction with metals can be taken as *models to study the activation of methane*. To date, there are only a very few examples of base-stabilised boryls[11], mostly containing the ligand -BH_2.PMe_3. The importance of the practical application of these species lead us to try to prepare some new derivatives, containing *halogenated* boryl ligands. The first attempts started from trimethylphosphine as a Lewis base, forming adducts with BCl_3 and BCl_2Ph. Unfortunately, while it is relatively easy to get the corresponding starting materials as pure compounds, all the reactions of BCl_3.PMe_3 and BCl_2Ph.PMe_3 with transition metal anions failed. The aim was the formation of base-stabilised boryls and borylenes *via* the usual salt elimination:

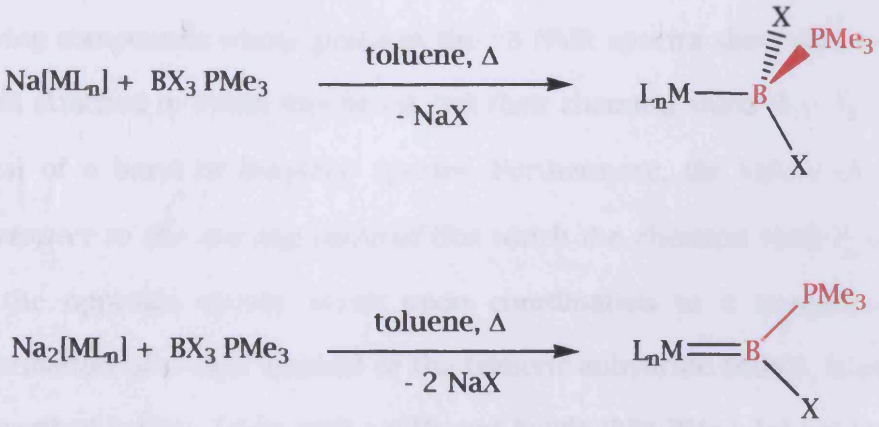

Scheme 3 - Salt elimination as a route to base-stabilised boryl and borylene complexes

Reactions of BCl_3.PMe_3 with both $Na_2Fe(CO)_4$.1.5 dioxane (Collman's reagent, Aldrich) and $K_2Fe(CO)_4$ produced no new Fe-B bonds at room temperature, and the situation does not change if the toluene solution is warmed up to 65°C for 5 days. Reaction of BCl_2Ph.PMe_3 with the same salts at T=65°C in toluene gives the same result (only unreacted starting material), and, if a more polar solvent like diethyl ether or THF is used to improve the solubility of the salts, the only result is decomposition of the ligand to phenyl boronic anhydride $(PhBO)_3$ (22, $\delta_B \approx 30$ ppm) and phosphorus containing products such as PMe_3O (δ_P=41 ppm) and $HPMe_3Cl$ (δ_P=29 ppm), presumably coming from side-reactions of trimethylphosphine with water and HCl produced during the formation of the boric anhydride, as shown in Scheme 4.

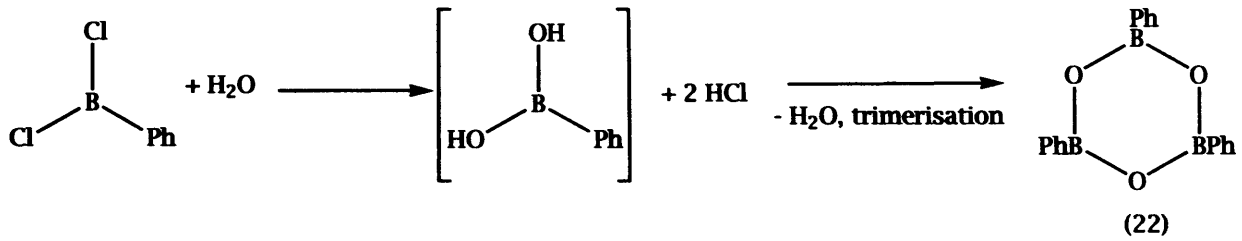

(22)

Scheme 4 - Proposed decomposition pathway for BCl_2Ph

The use of a more soluble $[Fe(CO)_4]^{2-}$ synthon, $(SiMe_3)_2Fe(CO)_4$ (courtesy of Dr. Deborah Coombs, Cardiff University), also results in the formation of no new boryl or borylene compounds, despite the solubility of both starting materials in toluene.

When the starting material is $Na[(\eta^5\text{-}C_5H_5)Fe(CO)_2]$, both BCl_3.PMe_3 and BCl_2Ph.PMe_3 react in the same way, giving compounds whose peaks in the ^{11}B NMR spectra show that in these species the base is still attached to boron (doublets), but their chemical shifts (δ_B= -10, -19, -25 ppm) are *not* typical of a boryl or borylene species. Furthermore, the values of δ_B are moved *upfield with respect to the starting material* (for which the chemical shift δ_B is around +0.6 ppm), while the opposite should occur upon coordination to a transition metal. With BCl_2Ph.PMe_3 formation of a large amount of the trimeric anhydride $(PhBO)_3$ is also noticed, as in the case described before. Trials with a different halide (BBr_3.PMe_3) did not lead to any new results.

The above lack of reactivity underlines the fact that *PMe_3 adducts of boron halides are very stable* and that they do *not* react readily with transition metals, presumably due to electronic and steric saturation of the boron centre.

In order to improve the situation, a different Lewis base was chosen for the second part of this work: tetrahydrofuran (THF). As in the case of trimethylphosphine, the adducts of BCl_3 and BCl_2Ph with THF are white powders that precipitate out of hexane solution. It is essential that THF is *diluted* in hexane before adding it to the Lewis acid, otherwise *polymerisation of the base occurs* if it is added neat. Boron halides are well known catalysts for the polymerisation of ethers, and, in order to avoid this undesired reaction, dilution is required.

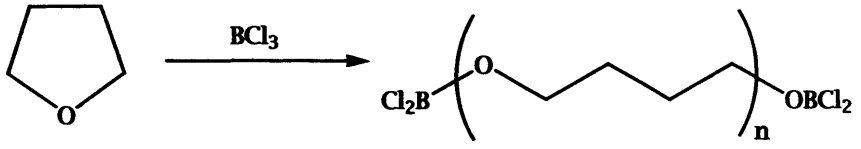

Scheme 5 - Acid catalysed polymerisation of THF

In the case of BCl_3.THF, the crystal structure is also available (Figure 7); upon coordination the hybridisation on boron is sp^3, as confirmed by the mean value of the bond angles around it (109.4°), on a tetrahedral geometry. The B-O distance is 1.51(9) Å , and the mean value of the B-Cl distances is 1.83(9) Å, identical (in the uncertainty interval) to that of free BCl_3 (1.74 Å).

Reactions of this molecule with different iron fragments have been examined, both in toluene and THF as solvents. Collman's reagent or $K_2Fe(CO)_4$ gave only decomposition products at δ_B ca. 17 ppm, while more promising results come from the reaction with $Na[(\eta^5\text{-}C_5H_5)Fe(CO)_2]$. When the reaction is performed in toluene, a mixture of the (supposed) base stabilised complex Fp-BCl_2.THF (9, δ_B=+59 ppm) and the non-stabilised Fp-BCl_2 (δ_B=+90.7 ppm[12]) is obtained. The assignment of these peaks is based on the variation of the ^{11}B chemical shift that occurs upon coordination to the iron centre [*c.f.* the $\Delta\delta_B$ from BCl_3 to Fp-BCl_2 (ca. 45 ppm downfield) with that from BCl_3.THF to the putative Fp-BCl_2.THF (ca. 50 ppm downfield)]. The δ_B value of putative 9 is also more downfield than that found for the

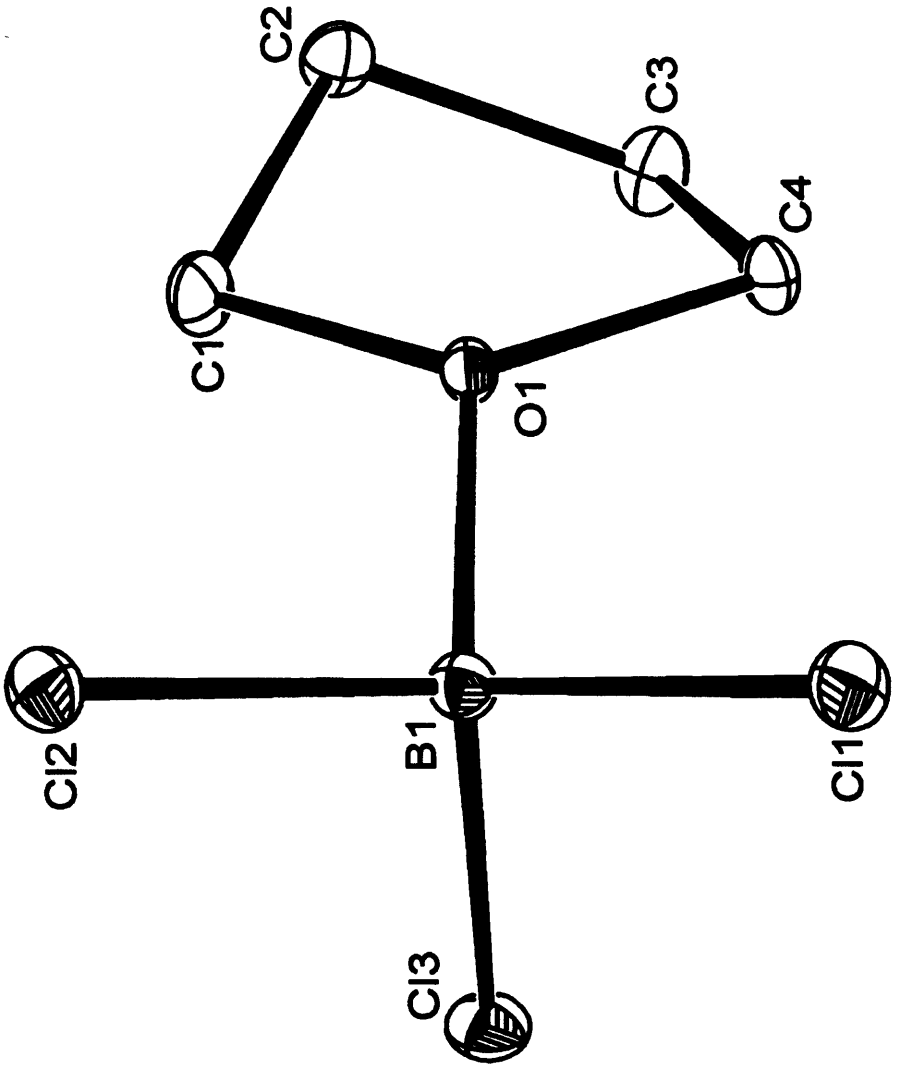

***Figure 7** - Molecular structure of BCl_3.THF. ORTEP ellipsoids drawn at the 50% probability level; hydrogen atoms omitted for clarity.*

corresponding 4-methylpyridine adduct Fp-BCl_2-[NC_5H_4-4-Me][11] (δ_B=18.8 ppm), this reflecting the enhanced electronegativity of oxygen compared to nitrogen, with consequent higher deshielding of the boron atom in 9 than in Fp-BCl_2-[NC_5H_4-4-Me].

The situation is much better when *THF is used both as base and solvent*: in this case only the base-stabilised species forms. Attempts to isolate a pure material were again unsuccessful: removal of THF, re-dissolution in hexane and cooling has always led to a red oil that consists of mixtures of the desired species and decomposition products. Attempts to get a more crystalline product were made, using both Na[(η^5-C_5H_4Me)$Fe(CO)_2$] and Na[(η^5-C_5Me_5)$Fe(CO)_2$], but, while in the first case the product is still oily, in the latter case the reaction does not proceed as expected, leading to decomposition (probably because of the steric hindrance offered by both C_5Me_5 and THF on the boron atom).

If BCl_2Ph.THF and Na[(η^5-C_5H_5)$Fe(CO)_2$] are used as starting materials, the results obtained using THF as solvent are different from the previous case: decomposition occurs, and the excess of Lewis base seems to catalyse the redistribution reaction[13] shown in Scheme 6, at least judging from the boron NMR peaks observed: δ_B=+27.5 ppm and +9 ppm, which can be ascribed to $BClPh_2$.THF and BCl_3.THF respectively [for the former compound *c.f.* the $\Delta\delta_B$ from BCl_3 and BCl_3.THF (ca. 37 ppm upfield) with that from $BClPh_2$[14] and the putative $BClPh_2$.THF (33 ppm upfield)].

$$2\ BCl_2Ph \longrightarrow BCl_3 + BClPh_2$$

Scheme 6 - Ligand redistribution reaction on BCl_2Ph

No ^{11}B signal corresponding to a base stabilised boryl complex is observed. This behaviour could be justified again invoking the steric hindrance of the substituents on boron: the simultaneous presence of a phenyl and a THF group on the same boron atom may preclude its coordination to a Fp fragment. In fact, when the same reaction is done in toluene, the result is a peak at δ_B=+108 ppm, which corresponds to the "unsupported" compound Fp-B(Cl)Ph, where the base on boron has been lost. In order to confirm the identity of this species, the same reaction has been carried out using Na[(η^5-C_5Me_5)$Fe(CO)_2$], yielding a light

yellow crystalline product (40%) from hexane solution at -50°C. Spectroscopic data: ^{11}B NMR (C_6D_6): δ 111.2. ^1H NMR (C_6D_6): δ 1.45 (15H, s, C_5Me_5), δ 7.3 (3H, m, *meta* and *para* C*H* of the aromatic ring), δ 8.2 (2H, m, *ortho*-C*H*). ^{13}C NMR (C_6D_6): δ 9.4 (C_5Me_5), δ 95.7 (C_5Me_5), δ 127.9 (*para*-aromatic *C*), δ 131.0 (*meta*-aromatic *C*), δ 134.0 (*ortho*-aromatic *C*), δ 135.7 (*ipso*-*C*), δ 216.3 (*C*O). IR (C_6D_6): ν(CO) (cm^{-1}) 1993 st, 1934 st. These data match with those of the known compound Fp*-B(Cl)(Ph)[15], thus proving that ***when the solvent is toluene, THF dissociates upon coordination of boron to the iron centre.***

3.3.4 - Substitution and abstraction chemistry of the (mesityloxy)chloroboryl ligand: formation of asymmetric heteroatom-stabilised boryl complexes of iron

In recent work by this research group it has been demonstrated that asymmetric haloboryl complexes $L_nMB(R)X$ are not only readily accessible, but prove to be versatile substrates for boron-centred ***substitution*** chemistry[16], leading to a range of novel bridging borylene and asymmetric boryl complexes. Given that halide (or pseudo-halide) ***abstraction*** from coordinated ligand fragments has previously been used to great effect in the synthesis of low-coordinate or unsaturated group 14 systems[17], a similar methodology applied to haloboryl complexes might offer a versatile new route to terminally bound group 13 diyl complexes. Such an approach proves to be viable, leading to the development of a new route to terminal borylene complexes, and to the first examples of cationic group 13 diyls $[L_nMER]^+$[18]. $[(\eta^5\text{-}C_5Me_5)Fe(CO)_2(BMes)][BAr'_4]$ contains the shortest M-B distance yet reported. Asymmetric haloboryl complexes can be easily prepared following the usual salt elimination path, starting from dihaloboranes and a monoanionic metal fragment. The basic idea of this work was to prepare and characterise new precursors for the preparation of the related terminal borylene complexes *via* halide abstraction. Previous results were obtained for the (Mes)B and (NMe_2)B ligands on iron[19], and a comparison of the novel (MesO)B ligand with these species was to be developed.

Treatment of $(MesO)BX_2$ with the iron fragments $Na[(\eta^5\text{-}C_5R_5)Fe(CO)_2]$ in toluene in a 1:1 stoichiometry provides the desired haloboryl complexes $(\eta^5\text{-}C_5R_5)Fe(CO)_2[B(OMes)X]$ 13 (R=H, X=Cl), 14 (R=Me, X=Cl) and 15 (R=H, X=Br) in moderate yields (ca. 30%). Structural data are

available for the two chloroboryl species 13 and 14, whose structures are reported in Figures 8 and 9. Salient bond lengths and angles are listed in Table 4 for comparison.

Table 4 - Bond lengths (Å) and angles (°) for 13 and 14

	13	14
Fe - B	1.977(4)	1.977(4)
B - O(ligand)	1.350(4)	1.366(4)
B - Cl	1.816(4)	1.831(4)
Fe - C(carbonyl)	1.757(9)	1.755(9)
Fe - Cp (centroid)	1.723	1.725
C(CO) - Fe - C(CO)	95.8(2)	96.7(3)
O(lig) - B - Cl	115.5(3)	114.1(9)
O(lig) - B - Fe	125.2(3)	123.7(0)
Cl - B - Fe	119.4(2)	122.1(1)
O(lig) - B - Fe - Cp(cd)	111.6	87.5

The Fe-B lengths are identical for the two compounds (1.977(4) Å). The boron-chlorine and boron-oxygen distances are slightly longer for the Fp* derivative 14, observations which could be accounted for in terms of either the increased steric bulk or increased electron release of the Cp* fragment. The coordination geometry at boron is close to trigonal planar, and the boryl substituent is orientated almost perpendicular to the Cp(centroid)-Fe-B plane, with deviations from the value θ=90° that are more pronounced for the Fp complex, presumably for steric reasons (the ligand being sterically less hindered and with more rotational freedom).

The variation in the ^{11}B NMR chemical shifts follows the pattern already observed for other boryls: deshielding of the boron nucleus is recorded on going from the ligand precursor (MesO)BX_2 to the related iron complex [*c.f.* $\Delta\delta_B$ between (MesO)BCl_2 and 13 (ca. 30 ppm

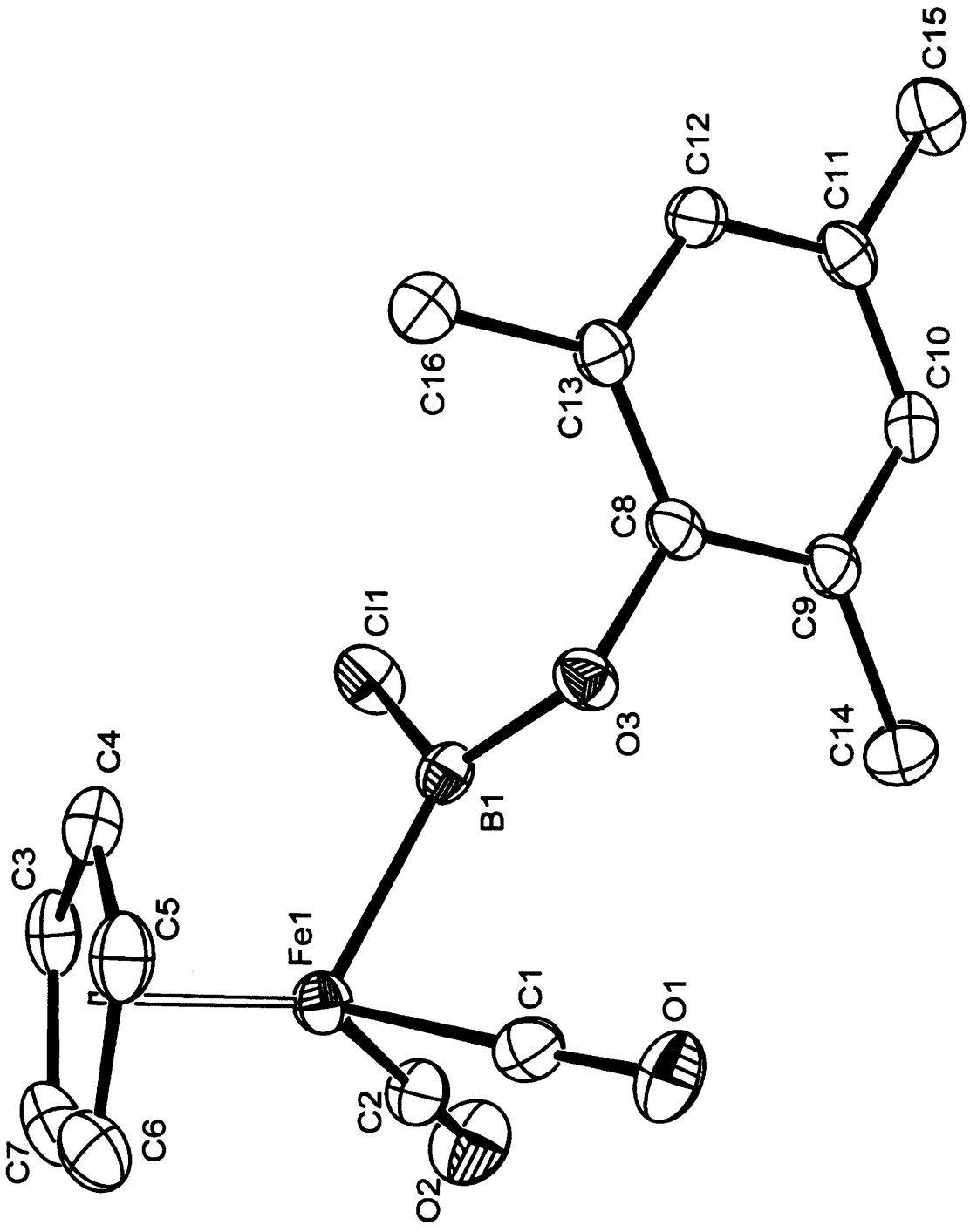

***Figure 8** - Molecular structure of [(η^5-C_5H_5)Fe(CO)$_2$[B(OMes)Cl], 13. ORTEP ellipsoids drawn at the 50% probability level; hydrogen atoms omitted for clarity.*

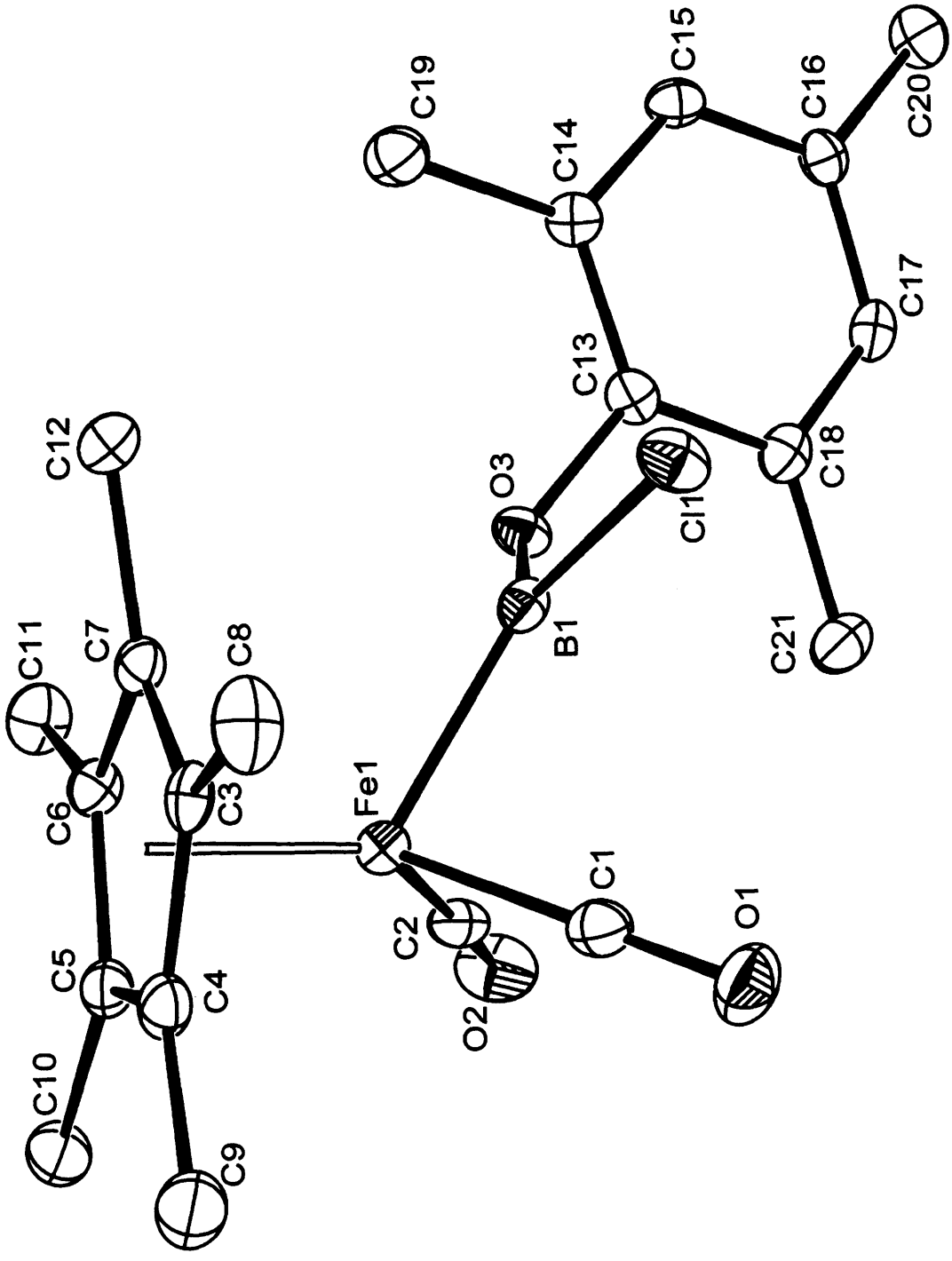

Figure 9 *- Molecular structure of [(η^5-C_5Me_5)Fe(CO)$_2$][B(OMes)Cl], **14**. ORTEP ellipsoids drawn at the 50% probability level; hydrogen atoms omitted for clarity.*

downfield), or between (MesO)BBr_2 and 15 (ca. 33 ppm downfield)]. The IR ν(CO) values reflect the stronger donor capabilities of Cp* with respect to Cp: 1940 and 2002 cm^{-1} for 13, 1925 and 1971 cm^{-1} for 14.

Following the successful preparation and characterisation of the haloboryl starting materials, a series of different substitution reactions was carried out on 13, using different anionic nucleophiles that displace the boron-bound halide, leaving the iron-boron bond intact. The substitution products are new asymmetric boryl complexes, and they have been characterised using conventional spectroscopic and diffraction techniques. Reaction with sodium *para*-t-butylphenolate for example leads to the corresponding B(OMes)(OAr) complex 16. Potassium t-butoxide also reacts in the same fashion, but the resulting asymmetric complex Fp-B(OMes)(O^{t}Bu) (18) is not as stable as 16, and it decomposes over a period of two days at ambient temperature. Sodium thiophenolate gives 17, the first crystallographically characterised example of asymmetric boryl where the boron atom is stabilised by one oxygen atom and one sulphur atom (L_nM-B(OR)(SR')). Its structure is depicted in Figure 10, and Table 5 lists relevant structural data.

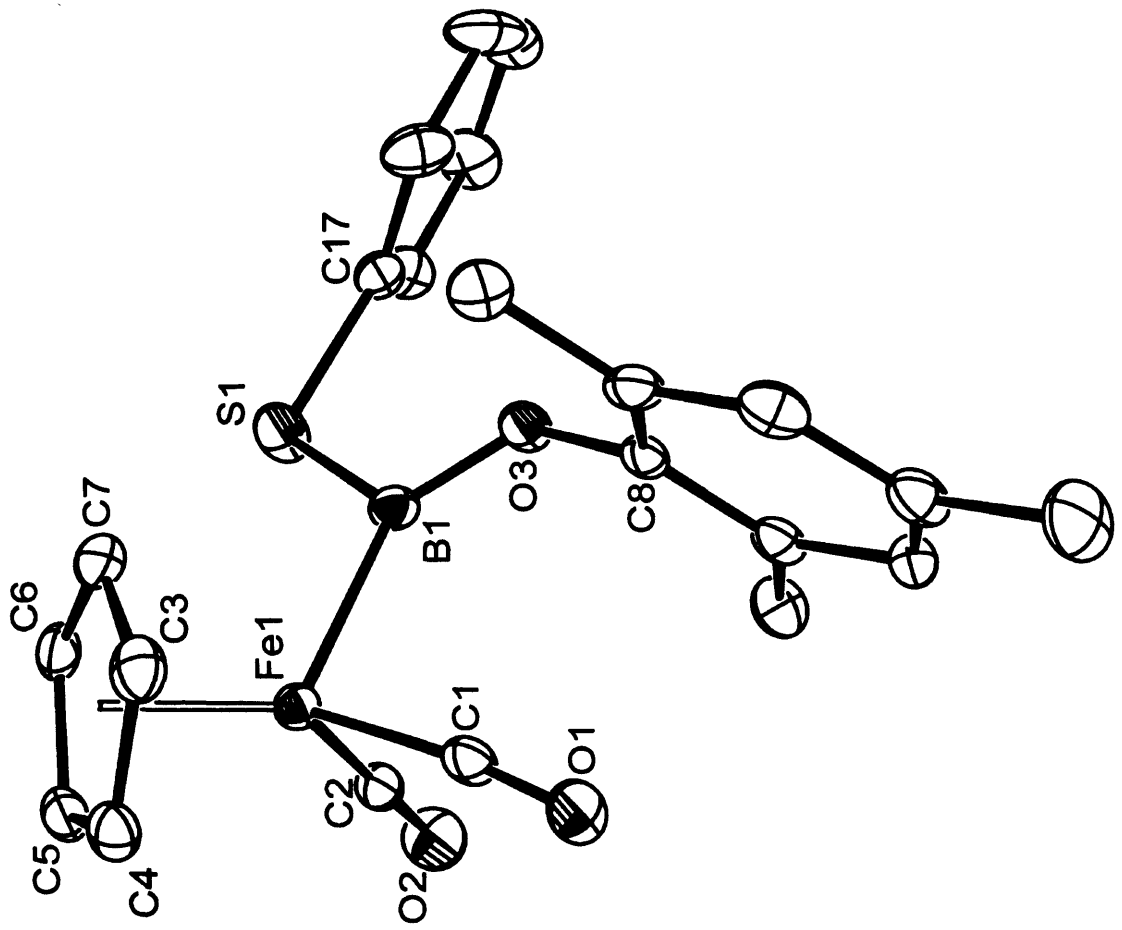

***Figure 10** - Molecular structure of $[(\eta^5\text{-}C_5H_5)Fe(CO)_2[B(OMes)(SPh)]$, 17. ORTEP ellipsoids drawn at the 50% probability level; hydrogen atoms omitted for clarity.*

Table 5 - Bond lengths (Å) and angles (°) for 17

	17
Fe - B	2.034(4)
B - O(ligand)	1.349(5)
B - S	1.848(4)
Fe - C(carbonyl)	1.742(9)
Fe - Cp (centroid)	1.731(2)
C(CO) - Fe - C(CO)	92.7(0)
O(lig) - B - S	114.2(9)
S - B - Fe	113.6(9)
O(lig) - B - Fe	132.0(1)
O(lig) - B - Fe - Cp(cd)	124.2

The metal-boron bond is significantly longer than in the precursor 13, as might be expected on both steric and electronic grounds. The boron-oxygen bonds are almost identical, and the mesityl and phenyl aromatic rings in the ligand are less or more perpendicular to each other.

In the ^{11}B NMR chemical shifts, the resonances are moved *upfield* with respect to the chloride starting material if a second oxygen substituent is present, while they are moved *downfield* by a sulphur nucleophile (*c.f.* δ_B=61.5 ppm for 13, δ_B=69.1 ppm for 17 and δ_B=47.4 ppm for 16). This effect can be attributed to the different balance between inductive and resonance effects in the two chalcogenides. Nevertheless, π effects normally dominate on influencing the values of the ^{11}B chemical shifts, and, for boron, oxygen is a better π-donor than sulphur[20].

The last step in studying the reactivity of asymmetric haloboryl complexes was to attempt the halide abstraction using $Na[BAr_4^f]$, since the same synthetic methodology has proved to be successful in the case of the (mesityl)haloboryl ligand[18]. Reaction with the Fp derivative did not form the expected borylene though, but the *fluoroboryl* complex 19 presumably

resulting from reaction of the putative borylene 23 with the anion $[BAr_4^f]^-$. The final product is always the same, both at ambient and at low temperature, and no intermediate is observed by multinuclear NMR.

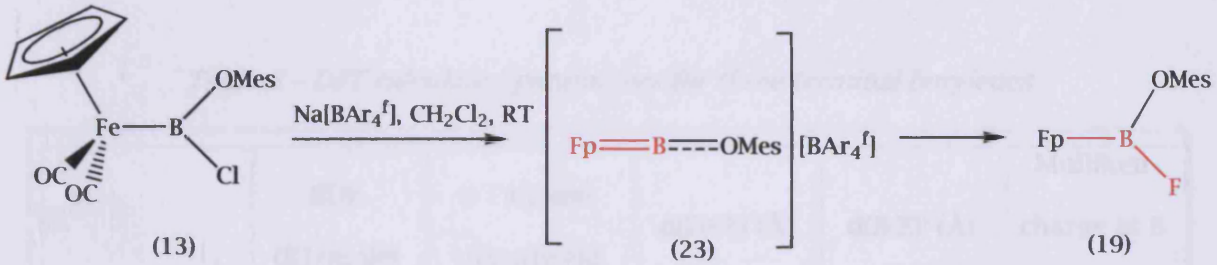

(13) (23) (19)

Scheme 7- Unexpected reactivity of 13 under halide abstraction conditions

One possibility is that the intermediate borylene 23 might form, but it is so unstable that it reacts immediately with its counterion to give the final observed product. The steric shielding offered by the Cp substituent is probably not enough to stabilise the intermediate. (Mesityloxy)borylene 23 is similar in some respects to (dimethylamino)borylene 25, where the isolation of a stable species at room temperature is impossible, but the identity of the product has been confirmed by *trapping the intermediate* at -20°C with [PPN]Cl[19]:

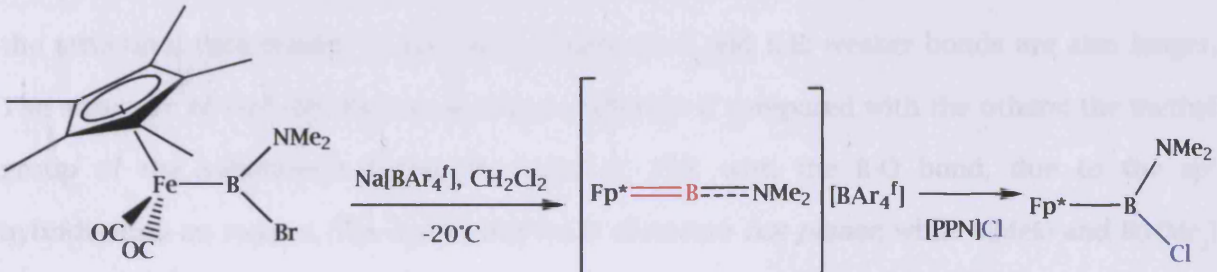

(24) (25) (26)

Scheme 8 - Trapping of an iron dimetyhlaminoborylene (25)

Addition of the anionic nucleophile at boron leads to the chloroboryl final product 26 observed at room temperature.

To examine these related compounds in more depth, some theoretical work on the bond dissociation energies and σ and π Fe=B bond densities of the three species $[Fp^*=B(Mes)]^+$, $[Fp^*=B(OMe)]^+$ and $[Fp^*=B(NMe_2)]^+$ was also carried out, and the most relevant results are summarised in Table 6.

Table 6 - DFT calculated parameters for three terminal borylenes

	BDE (KJ/mole)	σ : π bond density (%)	d(Fe-B) (Å)	d(B-E)[a] (Å)	Mulliken charge at B (e units)
$[Fp^*=B(Mes)]^+$	631	62 : 38	1.843	1.495	+0.4382
$[Fp^*=B(OMe)]^+$	295	72 : 28	1.870	1.278	+0.6504
$[Fp^*=B(NMe_2)]^+$	539	66 : 34	1.869	1.357	+0.5284

[a] E=C for Mes, N for NMe_2 and O for OMe.

As shown, the mesitylborylene ligand offers the most stable M=B bond, while in the case of the (dimethylamino)borylene and (particularly) the (methoxy)borylene ligand the π character is lower and the dissociation easier. The bond density partitioning scheme is consistent with the structural data related to the bond lengths Fe-B and B-E: weaker bonds are also longer. The structure of $[Fp^*=B(OMe)]^+$ is somehow different if compared with the others: the methyl group of the substituent forms an angle of 139° with the B-O bond, due to the sp^2 hybridisation on oxygen. The ligand B(OMe) is therefore *not planar*, while B(Mes) and $B(NMe_2)$ are. The enhanced reactivity towards nucleophiles of the boron atom in $[Fp^*=B(OMe)]^+$ can also be inferred from the value of its Mulliken charge, the highest of the series.

Attempts to make bridging borylenes from the haloborane precursors $(MesO)BX_2$ have also been made: reaction of two equivalents of NaFp with either 11 or 12 in toluene at room temperature gave some evidence of formation of a supposed bridging borylene species 27 at around δ_B=100 ppm, together with a large amount of the boryl complex 13 or 15 {*c.f.*

δ_B=158.0 ppm for [μ-(Mes)B]Fp_2[16a]. $\Delta\delta_B$ between FpB(Mes)Cl and [μ-(Mes)B]Fp_2 is about 47 ppm downfield, and $\Delta\delta_B$ between FpB(OMes)Cl and the putative 27 would be 40 ppm downfield}.

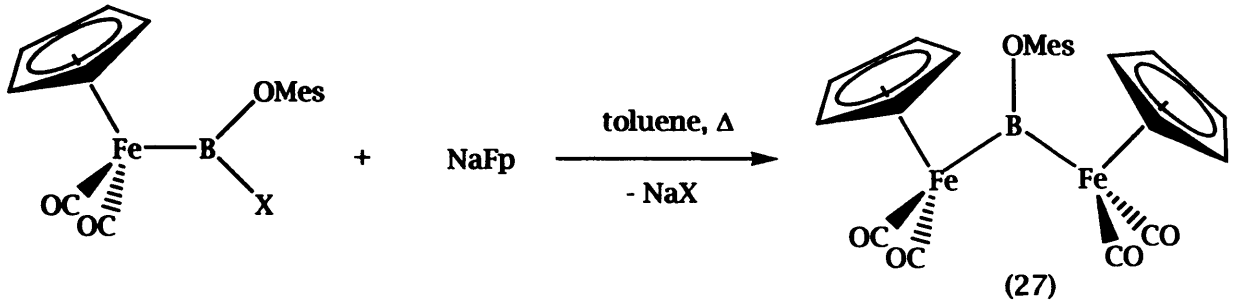

(27)

Scheme 9 - Formation of a bridging borylene with the (MesO)B ligand

When an excess of the metal salt is added (to reach four equivalents in total) and the solution warmed to 55°C for 12h to promote the conversion of the intermediates 13 or 15 to the desired borylene products, the result is merely decomposition of the boryl, without any improvement in yield. Therefore, it was impossible to isolate and characterise this species. At face value, this observation is surprising, especially given that [μ-(Mes)B]Fp_2 is accessible from Fp(BMes)Br [16a]. In the case of the (MesO)B ligand steric hindrance should be less than for (Mes)B, because the bulky mesityl group is further away from the boron centre with the extra oxygen acting as a spacer. On this basis, formation of the bridging borylene should be easier for the (MesO)B ligand, but evidently *electronic effects are more important*. The boron centre in Fp[B(OMes)]X is more electron-rich as a consequence of the Lewis π-basicity of oxygen, thus reducing the reactivity towards further nucleophilic substitutions (by an additional Fp group).

The synthesis of a series of different halides of general formula Fp[B(OMes)(X)] 13, 15, 19 offers the opportunity to investigate the electronic influence of the boron-bound substituents in organometallic boryl complexes. Relevant spectroscopic data for the three complexes are included in Table 7.

Table 7 - Spectroscopic data for haloboryl complexes 13, 15 and 19

	19 (X=F)	13 (X=Cl)	15 (X=Br)
^{11}B NMR δ / ppm	45.7	61.5	59.3
IR ν(CO) / cm^{-1}	1954, 2013	1940, 2002	1961, 2015

There is a feature in common with the analogous series of the mesitylboryl ligand: the marked *upfield shift* of the boron NMR resonance in the fluoro complex, compared to the others {*c.f.* δ_B=113 ppm for Fp[B(Mes)(Br)], δ_B=112 ppm for Fp[B(Mes)(Cl)] and δ_B=90 ppm for Fp[B(Mes)(F)] [19]}. The strong π donor properties of the fluoride substituent are a well known phenomenon, which has also been noticed in the series of boron dihalides $PhBX_2$ (X=F, Cl, Br and I)[21]. The trend in IR ν(CO) frequencies is more difficult to rationalise, because both the π donation and σ withdrawal by the halogen substituent must be taken into account, and *they act in opposite directions*. In a comparison between fluoride and bromide for example, F is a *better π donor* than Br, thus making the whole ligand B(OMes)F a worse π acceptor from iron than B(OMes)Br. On the other hand, B(OMes)F should be a *worse σ donor* than B(OMes)Br. The final observed values are the result of a balance of these two opposing effects, since the former effect should lead to higher electron density at iron for B(OMes)F [over B(OMes)Br], whereas the latter will lead to a reduced electron density.

3.4 - Conclusions

An investigation of bridging and terminal boryl ligands containing an aliphatic backbone (4d and 7) has proved that there is a substantial similarity of chemical properties in the two cases, with no evidence of electronic communication between the two iron centres in the bridged species. In addition, the back-bonding from iron to boron in these molecules as deduced from spectroscopic and structural data appears to be lower than in the analogous aromatic boryl ligands, presumably due to the lack of delocalisation in the spacer itself. In both types of ligand, however, the Fe-B bond is mainly σ in character, with little π contribution.

Attempts to prepare base-stabilised boryl systems via metathesis chemistry are strongly dependent on the nature of the stabilising base. Hence, haloborane precursors featuring a coordinated strongly σ-donor phosphine base (e.g. $RBCl_2{\cdot}PMe_3$) appear unreactive towards boron-centred substitution chemistry. With a weaker donor, such as THF, spectroscopic evidence for the intact base-stabilised complex $(C_5H_5)Fe(CO)_2BCl_2{\cdot}thf$ can be obtained, although the lability of the B-O bond is such that with toluene as the solvent, base-free complexes of the type $(C_5H_5)Fe(CO)_2BClR$ are obtained.

It is possible to perform substitution and abstraction reactions on the novel (mesityloxy)chloroboryl ligand, with a wide range of nucleophiles. This leads to the synthesis of different asymmetric complexes L_nM-B(OMes)(Nu), although attempts to isolate the cationic borylene $[Fp{=}B(OMes)]^+$ led instead to the formation of the fluoroboryl complex $(\eta^5\text{-}C_5H_5)Fe(CO)_2[B(OMes)F]$, presumably via F^- abstraction from the $[BAr'_4]^-$ counterion.

References for chapter 3

(1) Chapter 1, reference (17).

(2) Chapter 1, reference (11).

(3) Chapter 1, reference (31a).

(4) (a) Parish R.V., in *The Organic Chemistry of Iron*, eds. E.A. Koerner v. Gustorf, F.-W. Grevels and Fischler I., Academic Press, 1978, vol. 1. (b) Long G.J.,. Alway D.G and Barnett K.W., *Inorg. Chem.*, 1978, 17, 486. (c) Pannell K.H., Wu C.C. and Long G.J., *J. Organomet. Chem.*, 1980, 186, 85. (d) Goodreau B.H., Orlando L.R., Long G.J. and Spencer J.T., *Inorg. Chem.*, 1996, 35, 6579.

(5) Aldridge S., Al-Fawaz A., Calder R.J., Dickinson A.A., Willock D.J., Light M.E., Hursthouse M.B., *Chem. Comm.* 2001, 1846.

(6) Chapter 1, reference (19b).

(7) Chapter 1, reference (52).

(8) Dickinson A.A., Ph.D. Thesis, Cardiff University, 2002.

(9) (a) Chapter 1, reference (13); (b) Braunschweig H., Klinkhammer K.W., Koster M., Radacki K., *Chem. Eur. J.* 2003, 9, 1303.

(10) Chapter 1, references (3a), (3b) and (3e).

(11) Chapter 1, references (9) and (54).

(12) Aldridge S., Calder R.J., Baghurst R.E., Light M.E., Hursthouse M.B., *J. Organomet. Chem.* 649 (2002), 9.

(13) Similar nucleophile-promoted degradations of borane reagents like HBCat and ClBCat have been previously reported; see, for example: (a) Westcott S.A., Blom H.P., Marder T.B., Baker R.T., Calabrese J.C., *Inorg. Chem.* 1993, 32, 2175; (b) Chapter 4, reference (19).

(14) Wrackmeyer B., *Chem. Ber.* 1976, 109(3), 1075.

(15) Chapter 1, reference (40).

(16) See, for example: (a) Aldridge S., Coombs D.L., Jones C., *Chem. Comm.* 2002, 856; (b) Coombs D.L., Aldridge S., Jones C., *Dalton Trans.* 2002, 3851; (c) Coombs D.L., Aldridge S., Jones C., *Appl. Organomet. Chem.* 2003, 6-7, 356.

(17) See, for example: (a) Grumbine S.K., Tilley T.D., Arnold F.P., Rheingold A.L., *J. Am. Chem. Soc.* 1993, 115, 7884; (b) Mitchell G.P., Tilley T.D., *J. Am. Chem. Soc.* 1997, 119,

11236; (c) Tobita H., Ishiyama K., Kawano Y., Inomata S., Ogino H., *Organometallics* 1998, 17, 789; (d) Mork B.V., Tilley T.D., *Angew. Chem. Int. Ed.* 2003, 42, 357.

(18) Chapter 1, reference (34).

(19) Coombs D.L., Aldridge S., Rossin A., Jones C., Willock D.J., *Organometallics* 2004, 23, 2911.

(20) The same behaviour has been observed in derivatives of the general formula *cis*-$(PPh_3)_2Pt(B\text{-}1,2\text{-}E_2C_6H_4)_2$ (E=O,S); see chapter 1, reference (14a) and (18a).

(21) Nöth H., Wrackmeyer B. in *NMR Basic Principles and Progress*, Diehl P., Fluck E. Kosfeld R. Eds., Springer Verlag, Berlin (1978), vol. 14.

4 - New metal-boryl complexes synthesised via oxidative addition

4.1- Introduction

Oxidative addition represents the main synthetic route to boryl complexes, featuring metals of the late transition series, where the existence of two different stable oxidation states and variable coordination numbers makes this reaction possible. Examples of B-H, B-X, B-Si, B-Sn and B-B bond addition to Rh(I), Ir(I), Pt(0) and Pd(0) complexes are abundant in the literature[1]. The work presented in this chapter seeks to complement the salt elimination studies described in chapter 3, by making use of similar oxidative addition reactions.

Section 4.3.1 discusses the attempts to prepare novel complexes of rhodium and platinum, starting from metallic precursors of different kinds. The boron reagents employed are either bridging ($HBO_2C_6H_2O_2BH$) or terminal [9-chloro-9-BBN, (tmg)BCl, B-bromocatecholborane, (MesO)BX_2 (X=Cl, Br)]. The last part of the section is a mechanistic study on the interaction of catecholborane HBCat with phospino complexes of platinum(0), where a change of the steric and electronic properties of the ancillary phosphine can strongly influence platinum reactivity. The reaction itself is a model of one step in a possible catalytic conversion of HBCat to B_2Cat_2.

Section 4.3.2 groups together all the attempts made to extend the oxidative addition methodology to the main group metals indium and tin, using $(\eta^5\text{-}C_5Me_5)In$ and $Sn(\eta^5\text{-}C_5H_5)_2$. Again, several boron-containing starting materials were examined for oxidative addition chemistry.

Reaction of $[Rh(Cl)(PR_3)_2]_2$ with $HBO_2C_6H_2O_2BH$ (R=^{i}Pr, Cy)

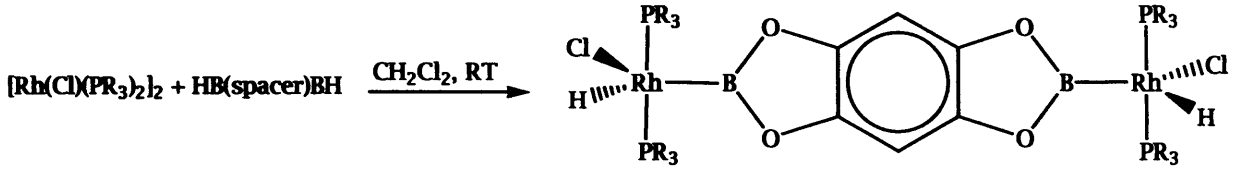

(1,2)

The methodology is described for the triisopropylphosphine complex only, that for PCy_3 being analogous. The dimeric rhodium precursor (75 mg, 0.08 mmol) was dissolved in 15 mL of dichloromethane, as well as 72.8 mg (0.56 mmol, 7 eqvl.) of ligand. The colourless ligand solution was added to the orange solution of the rhodium complex, and the mixture was left to react at room temperature for 15 h. After that time, the colour had changed to light yellow. The dichloromethane mixture was filtered, concentrated and layered with diethyl ether. Cooling at -30°C for three days produced a creamy powder corresponding to the complexes 1 or 2. Unfortunately, the yields were very low and the powder was not pure, containing some unknown decomposition products. Attempts to purify this powder *via* recrystallisation from concentrated dichloromethane solutions were made, but they all failed. The same impure mixture precipitated every time. As a consequence, only some (tentative) NMR data are available: $[Rh(H)(Cl)(P^iPr_3)_2]_2[BCatB]$ (1): ^1H NMR (300 MHz, C_6D_6, 21°C), δ -17.0 (m, hydride). ^{11}B NMR (96 MHz, C_6D_6, 21°C), δ 37 (br). ^{31}P NMR (122 MHz, C_6D_6, 21°C), δ 52.2 (d, $^1J_{P\text{-}Rh}$=107.2 Hz). $[Rh(H)(Cl)(PCy_3)_2]_2[BCatB]$ (2): ^1H NMR (300 MHz, C_6D_6, 21°C), δ -17.2 (m, hydride), δ 1.5 (m, PCy_3), δ 7.0 (s, ligand aromatic C*H*). ^{31}P NMR (122 MHz, C_6D_6, 21°C), δ 40.3 (d, $^1J_{P\text{-}Rh}$=101.2 Hz).

Reaction of 9-chloro-BBN with $Pt(PPh_3)_2$(ethene)

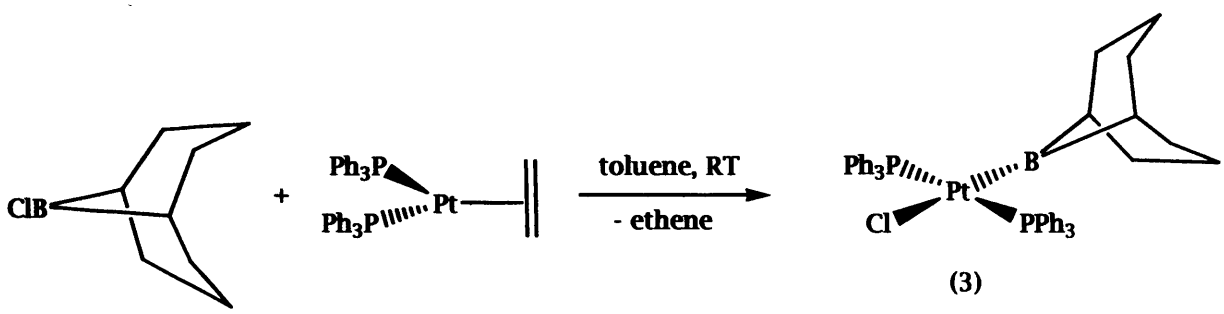

(3)

0.25 g of the platinum precursor (0.33 mmol) were dissolved in 15 mL of toluene, and mixed with 5.7 mL of a 0.059 M solution of ligand in toluene (0.33 mmol, 1 equivalent) at room temperature. After 2 h, the reaction mixture started turning deep red. Removal of toluene *in vacuo* and repeated washing of the solid residue with hexane yielded a dark orange-brown powder, that was dried under high vacuum for 30 min. NMR analysis shows that the expected product 3 is not pure. Recrystallisation attempts from concentrated toluene solutions (3 is not soluble in hexane) were unsuccessful. ^{11}B NMR (96 MHz, C_6D_6, 21°C), δ 87 (br). ^{31}P NMR (122 MHz, C_6D_6, 21°C), δ 29.2 ($^1J_{P\text{-}Pt}$=3010 Hz).

Reaction of $(MesO)BX_2$ with $Pt(PPh_3)_2$(ethene) (X=Cl, Br)

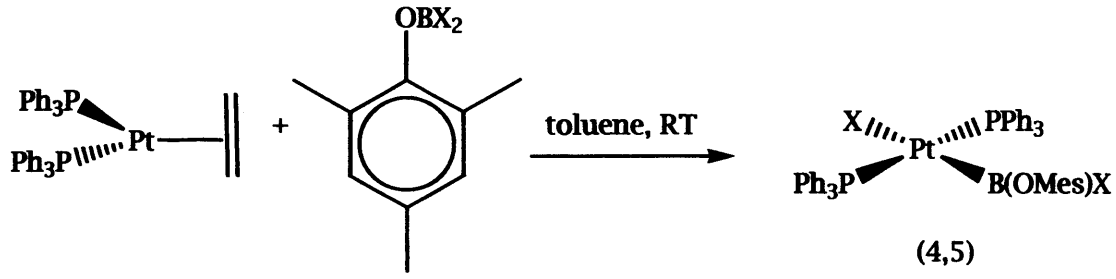

(4,5)

The preparation is similar for the two different haloboranes, therefore only that using $(MesO)BBr_2$ is described. $Pt(PPh_3)_2(CH_2{=}CH_2)$ (0.35 g, 0.47 mmol) was dissolved in 20 mL of toluene, and 1.7 mL of a 0.28 M solution of the boron ligand in toluene (0.47 mmol, 1 equivalent) were added at room temperature. The reaction reaches completion in 2 h, as it could be seen from the ^{31}P and ^{11}B NMR spectra, where the peaks of the starting material disappeared. In both cases, a mixture of the platinum hydride *trans*-$Pt(H)(X)(PPh_3)_2$ and the (supposed) product 4 or 5 was obtained, but all the attempts to precipitate the boryl complex from a concentrated toluene solution layered with hexane were fruitless.

Compounds 4 and 5 are insoluble in hexane; nevertheless, the undesired hydride is always what precipitates out of the layered solution. In the case of (MesO)BCl_2, a ligand redistribution on the boron centre catalysed by free PPh_3 could also be seen from the ^{11}B NMR spectra (see the discussion section). Proposed assignments are the following. *Trans*-Pt[B(OMes)Br](Br)$(PPh_3)_2$(4): ^{31}P NMR (122 MHz, toluene solution, 21°C), δ 23 ($^1J_{P\text{-}Pt}$=3126 Hz). ^{11}B not observed. See discussion section for the chloro-derivative.

Preparation of trans-Pt$(PPh_3)_2$(Cl)[B(tmg)]

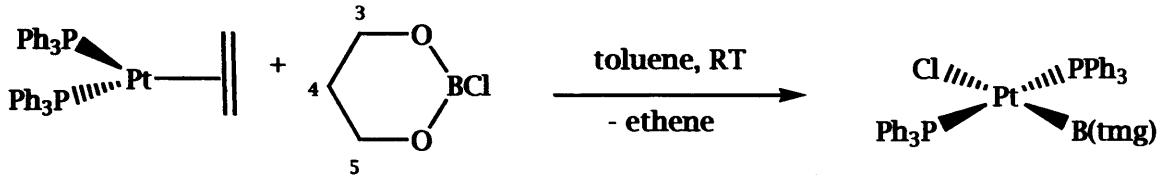

(6)

The platinum precursor (0.6 g, 0.8 mmol) was dissolved in 15 mL of toluene, and 1.7 mL of a 0.46 M solution of (tmg)BCl (0.8 mmol, 1 equiv.) in toluene was added *via* syringe at room temperature. A white precipitate is formed after 30 min. The mixture was left to react for 3 d, and the yellow supernatant was then separated from the solid. The latter was washed twice with hexane (2 x 15 mL). Final drying under high vacuum for 35 min. yielded 0.12 g of pure 6 (18%). ^1H NMR (300 MHz, $CDCl_3$, 21°C): δ 1.9 (2H, quintet, $^3J_{H\text{-}H}$= 5 Hz, C*H*$_2$ of ligand C(4)), δ 2.9 (4H, t, $^3J_{H\text{-}H}$= 5 Hz, C*H*$_2$ of ligand C(3) and C(5)), δ 7.6 (3H, m, *meta* and *para* C*H* of phenyl rings in PPh_3), δ 7.8 (2H, m, *ortho* C*H* of phenyl rings in PPh_3). ^{13}C NMR (76 MHz, $CDCl_3$, 21°C), δ 25.9 (ligand C(4)), δ 61.3 (ligand C(3) and C(5)), δ 128.0 (*para* *C*H of phenyl rings), δ 130.2 (*meta* *C*H), δ 132.8 (*ortho* *C*H), δ 135.0 (*ipso* *C*H). ^{11}B NMR (96 MHz, $CDCl_3$, 21°C), δ 23 (br). ^{31}P NMR (122 MHz, $CDCl_3$, 21°C), δ 26 ($^1J_{P\text{-}Pt}$=3189 Hz). IR (KBr disk, cm^{-1}): 3046 w, 2962 m, 2886 w, 1480 w, 1471 w, 1435 m, 1400 w, 1260 st, 1178 m, 1165 m, 1095 st-br, 862 w, 801 st, 753 m, 694 m, 626 w, 603 m, 523 st, 499 m. Mass spec. (EI): $[M\text{-}Cl]^+$ = 804 (weak), fragment ion peaks at *m/z* 762 ($[M\text{-}Ph]^+$), 754 ($[M\text{-}boryl]^+$), 727 ($[M\text{-}Ph\text{-}Cl]^+$), 719 ($[M\text{-}boryl\text{-}Cl]^+$), 456 ($[M\text{-}Ph\text{-}boryl\text{-}Cl]^+$), 262 ($[PPh_3]^+$).

Preparation of $(Cp^*)In(BCat)_2$ and $(Cp^*)InBr_2$

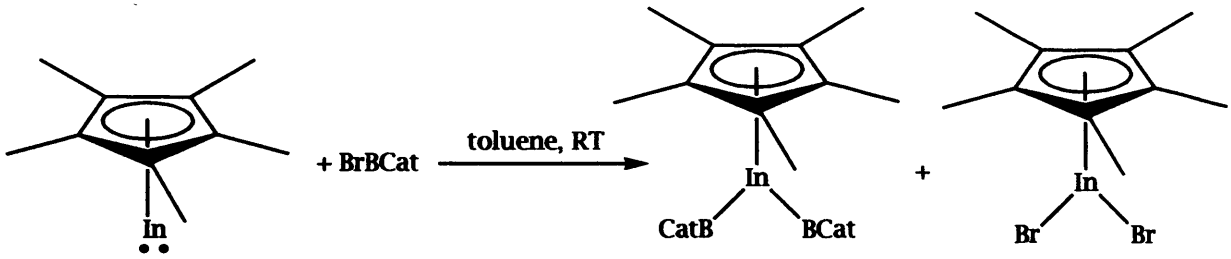

(7) (8)

Cp*In (0.6 g, 2.4 mmol) was dissolved in 25 mL of toluene, and the solution added to 0.48 g of B-bromocatecholborane (2.4 mmol, 1 equiv.) in 25 mL of toluene. Formation of a dark brown precipitate occurred immediately after the mixing, and the supernatant was light yellow. Stirring at room temperature was continued overnight, and the mixture then filtered and the toluene removed *in vacuo*. The solid residue was re-dissolved in 15 mL of hexane, the solution concentrated and cooled to -30°C overnight, yielding a white powder corresponding to a mixture of compounds 7 and 8. Nevertheless, an NMR assignment has been proposed for 7: ^{1}H NMR (300 MHz, C_6D_6, 21°C): δ 1.8 (s, η^5-$C_5(CH_3)_5$), δ 6.7 (m, C*H* of catechol ligand C(4) and C(5)), δ 7.0 (m, C*H* of catechol ligand C(3) and C(6)). ^{13}C NMR (76 MHz, C_6D_6, 21°C), δ 11.4 (η^5-$C_5(CH_3)_5$), δ 59.9 (η^5-$C_5(CH_3)_5$), δ 112.3 (catechol ligand C(4) and C(5)), δ 122.4 (catechol ligand C(3) and C(6)), δ 148.6 (catechol ligand C(1) and C(2)). ^{11}B NMR (96 MHz, C_6D_6, 21°C), δ 34 (br). Mass spec. (FAB): peaks found at *m/z* 490 (7) and 413 (8).

*Reaction of Cp*In with ClBCatBCl*

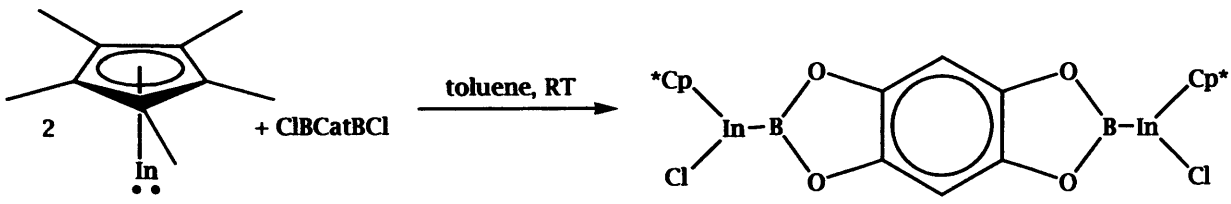

(9)

The indium precursor (0.25 g, 0.1 mmol) were dissolved in 25 mL of toluene, and the solution is added to a solution of 0.12 g (0.05 mmol) of the ligand ClBCatBCl in 25 mL of

toluene. The mixture was left to stir overnight, and after that time a green solid had formed, while the toluene supernatant was light yellow. The reaction could not reach completion over a period of 4 d stirring at room temperature, as judged from the ^{11}B NMR spectra, and, in order to remove the unreacted starting material, toluene was pumped away *in vacuo* and the solid residue washed with hexane. The product 9 and some unknown decomposition products were dissolved into hexane, but not the ligand starting material. Further purification of 9 was attempted *via* precipitation from a concentrated hexane solution cooled at -30°C, unsuccessfully. ^{11}B NMR (96 MHz, toluene solution, 21°C), δ 35 (br).

Preparation of $Cp_2Sn(BCat)_2$ and Cp_2SnBr_2

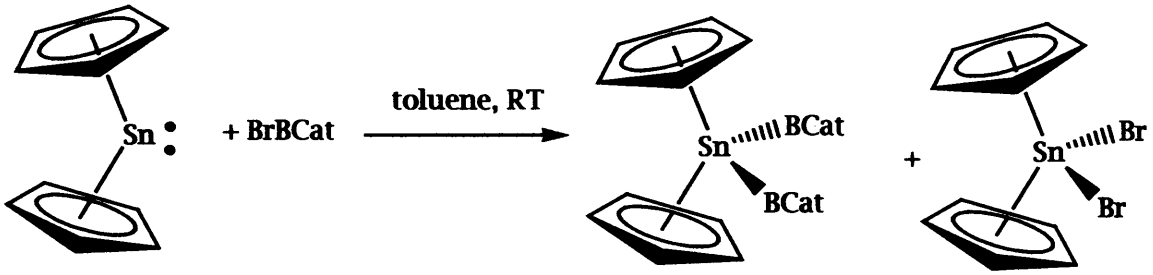

(10) (11)

Stannocene (0.2 g, 0.8 mmol) was dissolved in 25 mL of toluene and mixed to a solution of 0.16 g of B-bromocatecholborane (0.8 mmol, 1 equiv.) in 25 mL of toluene. After 2 h stirring at room temperature, a white precipitate started to form. The reaction proceeded overnight, then, after checking its completion via ^{11}B NMR, the toluene solvent was removed and the solid dried under high vacuum for 45 min. The final NMR and MS analyses revealed that tin reacts in the same way as indium, because this powder was a mixture of the two compounds 10 and 11. Once more, it was not possible to separate 10 from 11 *via* "selective precipitation" from a concentrated toluene or hexane solution. As already done in the indium case, an attempted assignment of the peaks of 10 is reported in here: ^{1}H NMR (300 MHz, C_6D_6, 21°C): δ 5.8 (s, η^5-C_5H_5), δ 6.6 (m, C*H* of catechol ligand C(4) and C(5)), δ 6.8 (m, C*H* of catechol ligand C(3) and C(6)). ^{13}C NMR (76 MHz, C_6D_6, 21°C), δ 111.0 (η^5-C_5H_5), δ 112.3 (catechol C(4) and C(5)), δ 122.5 (catechol C(3) and C(6)), δ 148.4 (catechol C(1) and C(2)). ^{11}B NMR (96 MHz, C_6D_6, 21°C), δ 30 (br). ^{119}Sn δ not observed. Mass spec. (FAB): peaks found at *m/z* 490 (10) and 413 (11).

Variable temperature NMR experiment with $Pt(PPh_3)_2$(ethene) and HBCat

A Young's NMR tube with a d_8-toluene insert was loaded under an inert atmosphere with 0.023 g of the platinum precursor (0.03 mmol). The tube was then cooled to -78°C and 1 mL of a 0.094 M solution of catecholborane in toluene (Aldrich, 0.09 mmol, 3 equiv.) was then added. The mixture was initially kept at -78°C, and slowly warmed to ambient temperature (in steps of 20°C) in the NMR spectrometer, recording the ^{31}P, ^{11}B and ^{1}H spectra at each step. A similar experiment was also carried out with Pt(dppe)(ethene) and HBCat as starting materials, under the same conditions.

4.3 - Discussion of results

4.3.1.1 - Oxidative addition to transition metals: new boryl species of rhodium and platinum

It is known from the literature[2] that rhodium(I) in 14VE organometallics can react with B-H bonds of borane derivatives to form the corresponding hydrido boryl complexes *via* oxidative addition. The extension of this chemistry to new bridging boryl ligands was the starting point for this work. The rhodium(I) starting materials chosen are of general formula $Rh(Cl)(PR_3)_2$, of coordination number 3 (or 4 when dimeric or complexed with N_2), and containing different organic substituents on the ancillary phosphines: $[Rh(Cl)(P^iPr_3)_2]_2$, $[Rh(Cl)(PCy_3)_2]_2$, $Rh(Cl)(PCy_3)_2(N_2)$. These reagents react with the boryl ligand in a similar fashion, with the NMR resonances due to the starting materials slowly disappearing and yielding, among other products, resonances consistent with the expected complexes 1 or 2. Extensive decomposition also occurs, as shown by an intense ^{11}B resonance at δ_B=23 ppm (most likely due to species like HO-BCatB-OH). The only purification process that appeared not to decompose the boryl derivative is recrystallisation from solutions made with non-coordinating solvents (hexane, toluene). Unfortunately, this method tends to lead to co-precipitation of the boryl complexes together with the boronic ester decomposition products. An interesting feature of these species is their *extreme lability*; ^{31}P NMR spectroscopy shows that the product undergoes a B-H reductive elimination when N_2 is vigorously bubbled into the solution, as shown in Scheme 1. In the case of the

isopropylphosphine derivative for example, the intensity of the ^{31}P doublet at δ_P=52 ppm of 1 decreases and the peaks of the starting materials $Rh(P^iPr_3)_2Cl(N_2)$ (δ_P=45 ppm, $^1J_{P\text{-}Rh}$=95 Hz[3]) and $[Rh(P^iPr_3)_2Cl]_2$ (δ_P=62.4 ppm, $^1J_{P\text{-}Rh}$=116 Hz[4]) re-appear on bubbling nitrogen through the solution. This behaviour might explain why it is so difficult to obtain these complexes as pure single compounds, probably because the final oxidative addition product can undergo *reductive elimination readily in solution.*

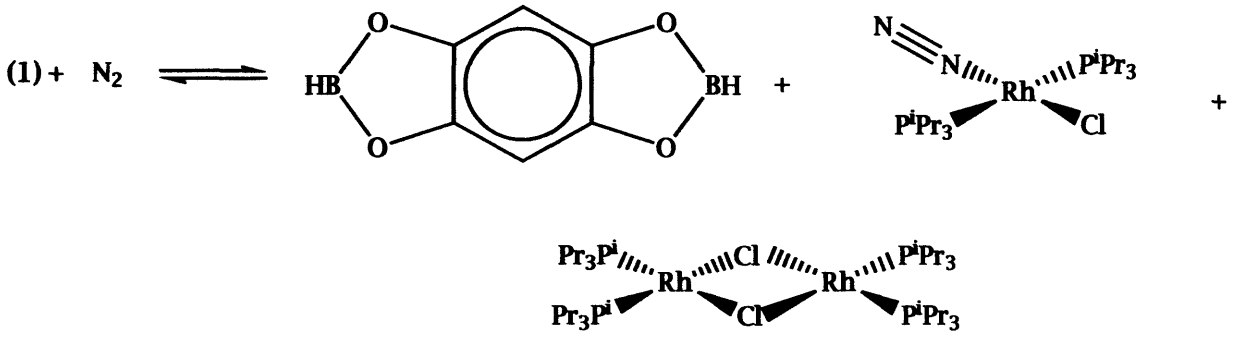

Scheme 1 - Reductive elimination on boryl complex 1

Despite the impossibility to obtain a pure product, it is possible to make some general remarks concerning the NMR data for putative bridged species 1 and the terminal analogue made by Westcott *et al.* in 1991[5]: $Rh(H)(Cl)(BCat)(P^iPr_3)_2$. A collection of the main NMR data for the two species is in Table 1.

Table 1 - Spectroscopic NMR data for two rhodium boryls

	(1)	$Rh(H)(Cl)(BCat)(P^iPr_3)_2$
^{11}B NMR δ (ppm)	37	37.7
^{31}P NMR δ (ppm)	52.2 ($^1J_{P\text{-}Rh}$= 107 Hz)	51.7 ($^1J_{P\text{-}Rh}$= 109 Hz)
^1H NMR δ (ppm)	-17	-17.1

Although the data for 1 are clearly incomplete, the similarities with those reported for the BCat analogue give us some confidence in proposed formulation for 1.

Another transition metal that is known to undergo oxidative addition reactions readily is platinum[1]. The precursor chosen for this work is a 16-valence-electron complex of platinum(0): $Pt(L)_2(\eta^2\text{-}CH_2{=}CH_2)$, where L=$PPh_3$ or $(L)_2$=dppe. It was reacted with different B-X bonds (X=Cl, Br), to try to synthesise the related halo boryl complex. Unfortunately, while most of them seem to show the expected reactivity, purification and isolation of the final platinum boryl proved extremely difficult. In fact, due to their extreme sensitivity to traces of water in the solvents, these complexes decompose to the related platinum *hydride* $Pt(H)(X)(L)_2$, as a consequence of the hydrolysis process. Crystallisation attempts tended to lead to the production of light yellow crystals of the hydride, from a layered solution of the complex. An additional problem is represented by a lack of solubility of the *trans* polar species in apolar solvents like benzene. When a more polar solvent like CH_2Cl_2 or $CHCl_3$ is employed, dissolution is complete, nevertheless the complexes then appear to react either with the solvent itself or with traces of HCl to give the related *platinum(II) dichloride* $Pt(X)_2(L)_2$[6]. The molecular structure of the crystalline *cis*-$Pt(PPh_3)_2Cl_2 \cdot 3CHCl_3$, obtained from a chloroform solution of complex 6 layered with hexane, is reported in Figure 1. Owing to all the aforementioned experimental difficulties, definitive structural results in this section are scarce.

Reaction of $Pt(ethene)(PPh_3)_2$ with 9-chloro-9-BBN in toluene produces 3, whose boron chemical shift is slightly downfield compared to that of the starting material (δ_B=81 ppm), together with a vast amount of the byproduct BBN-O-BBN[7] (δ_B=59 ppm). The ^{31}P signals of 3 are *broad*, implying the presence of the quadrupolar ^{11}B nucleus in the proximity of phosphorus. When a toluene solution of 3 is layered with hexane and cooled to -30°C overnight, the crystals that come out of the solution are the platinum hydride $Pt(H)(Cl)(PPh_3)_2$, judging from its crystallographic cell parameters[8].

Reactions between $Pt(PPh_3)_2$(ethene) and the ligands $B(OMes)X_2$ (X=Cl, Br) have different course, depending on the halogen. With the bromo derivative $B(OMes)Br_2$ initial formation of the expected product 5 occurs, but after 24 h it decomposes to the hydride *trans*-$Pt(H)(Br)(PPh_3)_2$[9] [δ_P=29.7 ppm ($^1J_{P\text{-}Pt}$=2989 Hz), δ_H=-13.7 ppm ($^1J_{H\text{-}Pt}$=1215 Hz, $^2J_{H\text{-}P}$=13 Hz in C_6D_6)]. The chloro ligand $B(OMes)Cl_2$ interacts with platinum, but *ligand redistribution*

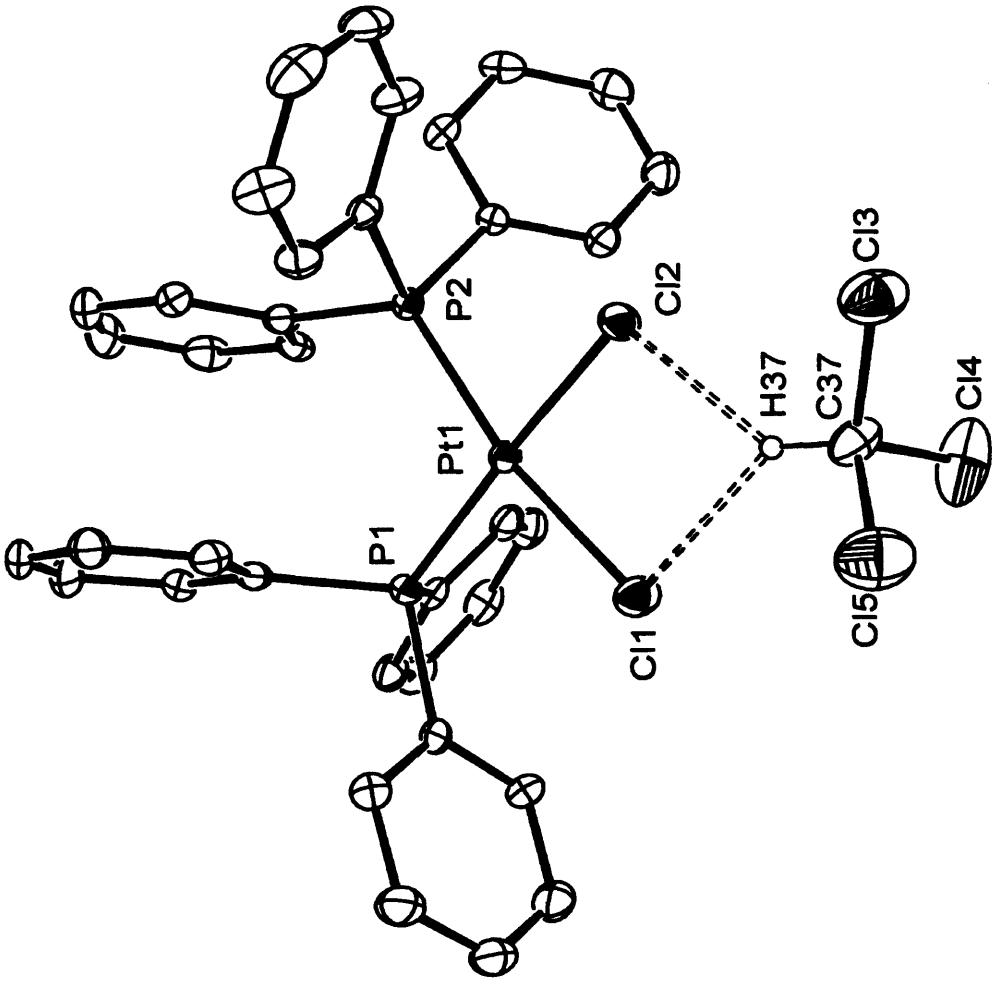

Figure 1 *- Molecular structure of cis-$Pt(PPh_3)_2Cl_2.3CHCl_3$, decomposition product of $Pt(PPh_3)_2Cl[B(tmg)]$ in $CHCl_3$, showing weak hydrogen bonding of one molecule of $CHCl_3$ to the platinum-bound chloride ligands. ORTEP ellipsoids drawn at the 50% probability level; hydrogen atoms (except that attached to C37) and two molecules of $CHCl_3$ omitted for clarity. Salient parameters (Å, °) relating to the hydrogen bonding: Cl(1)-H(37) 2.905, Cl(2)-H(37) 2.635, Cl(1)-C(37) 3.733(4), Cl(2)-C(37) 3.466(4), C(37)-H(37)-Cl(1) 140.6, C(37)-H(37)-Cl(2) 140.6.*

occurs, and free phosphine in solution, presumably labilised from the coordination sphere of platinum, coordinates to the BCl_3 formed, to generate $(MesO)_2BCl$ and $BCl_3{\cdot}PPh_3$. Similar boron substituent redistribution reactions have previously been reported with HBCat and free PPh_3 derived from Wilkinson's catalyst[10].

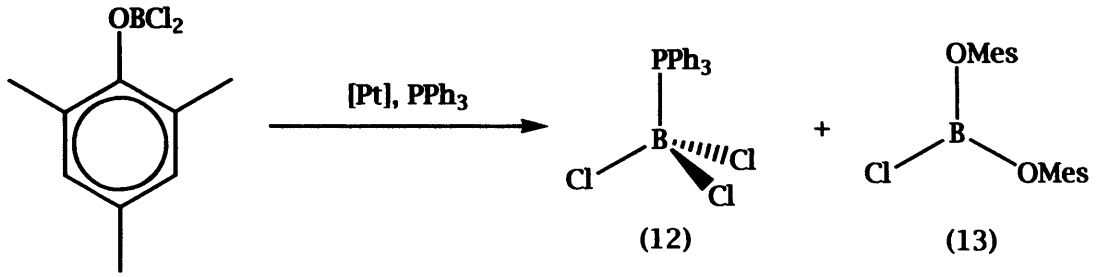

Scheme 2 - Ligand redistribution of $(MesO)BCl_2$ catalysed by platinum

In the ^{11}B spectrum of the toluene solution a sharp doublet is observed at δ_B=3.5 ppm ($^1J_{B-P}$=151 Hz, corresponding to 12[11]) and a broad peak at δ_B=21.6 ppm , compound 13 (see chapter 3, page 91). The phosphine coordinates only to the more electrophilic and less bulky boron centre, *i.e.* that of BCl_3. The presence of two aryloxy substituents in 13 makes the boron atom less electron-deficient and less reactive towards Lewis bases. While the value of the $^1J_{Pt-P}$ coupling constant for the putative platinum(II) boryl 4 is in line with other literature data on similar derivatives like *trans*-$Pt(PPh_3)_2(Ph)(Cl)$ ($^1J_{Pt-P}$=3152 Hz [12]), the value measured for 5 (4650 Hz) is far too high for a platinum(II) species, and it must be ascribed to an unknown phosphine-containing *Pt(0)* molecule.

The only oxidative addition reaction that led to a stable platinum boryl complex was that of the aliphatic ligand (tmg)BCl. Reaction with $Pt(PPh_3)_2$(ethene) gives the corresponding complex 6, which has been characterised spectroscopically. A comparison of 6 with the related species containing the aromatic catecholboryl ligand (*trans*-$Pt(PPh_3)_2$(BCat)Cl, made by Clegg *et al.* in 1998[13]) is possible. Table 2 contains the most relevant NMR chemical shifts for the two species.

Table 2 - NMR spectroscopic data for two platinum boryls

	(6)	$Pt(PPh_3)_2(BCat)Cl$
^{11}B NMR δ (ppm)	23	29
^{31}P NMR δ (ppm)	26 ($^1J_{P\text{-}Rh}$ = 3189 Hz)	23 ($^1J_{P\text{-}Rh}$ = 2869 Hz)

In complex 6 the boron atom is more shielded than in the BCat derivative, showing a trend that is similar to that seen in the iron derivatives Fp*-BCat and Fp*-B(tmg) (see chapter 3, page 105). The aliphatic ligand B(tmg) presumably releases more electron density from its oxygen atoms onto the boron atom than the aromatic ligand BCat does, causing the ^{11}B chemical shift to fall at higher fields. The ^{31}P NMR chemical shift and $^1J_{Pt\text{-}P}$ coupling constant measured for 6 are consistent with a ligand manifold featuring *trans* PPh_3 substituents.

4.3.1.2 - Insights into the interaction of catecholborane with platinum phosphine complexes: mechanistic VT-NMR studies of the conversion of HBCat to platinum bis(boryls)

The key step in all the hydroboration/diboration processes mediated by transition metals is the oxidative addition of the boron species to the metal centre. Substrate activation is thus achieved, and further reactions like ligand rearrangements, insertions, β-hydride eliminations and reductive eliminations can occur, producing the new organoboron species and regenerating the active catalyst. Nowadays the production of organoboron compounds is performed on an industrial scale, since these reagents are very diverse as starting materials in organic synthesis. For diboration in particular, derivatives of diborane(4) 14 are the starting materials.

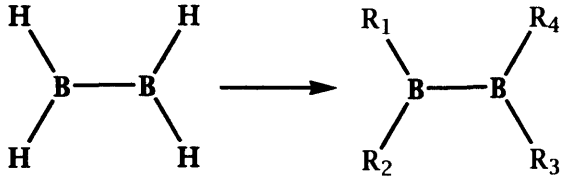

diborane(4) (14)

Scheme 3 - Derivatives of diborane(4)

The groups R can be of various nature, and molecules with both cyclic and terminal substituents have been made[14]. One of the most useful is *bis-(catecholato)diboron* B_2Cat_2 (Figure 2).

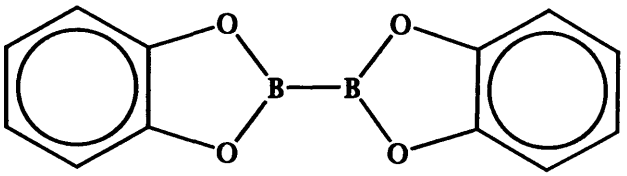

Figure 2 - Bis-(catecholato)diboron

The traditional synthetic route to B_2Cat_2 comes from the early work of Brotherton et al. in the 1960s[15]: it is a multi-step synthesis that starts from boron trichloride and dimethylamine (Scheme 4).

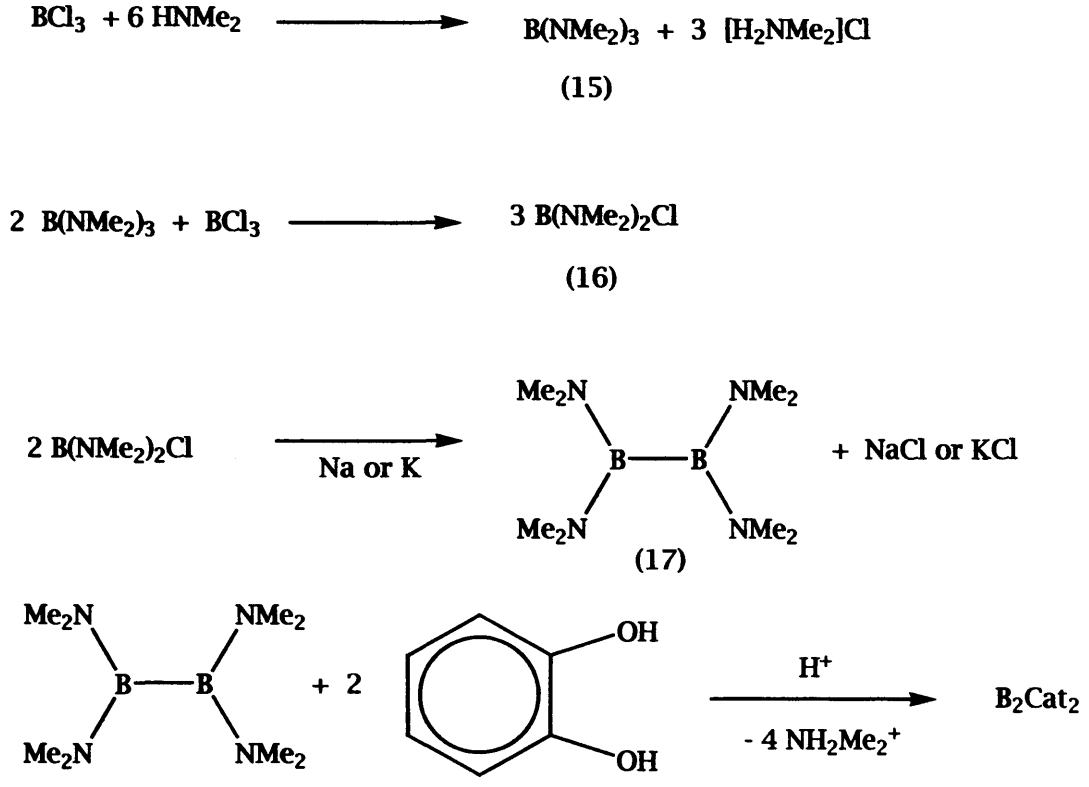

Scheme 4 - Preparation of bis-(catecholato)diboron

In specific cases[14a] it is also possible to obtain the same kind of products by direct coupling of the corresponding chlorocatecholborane derivatives with sodium-mercury amalgam under

controlled conditions. An alternative starting material could be catecholborane HBCat. Molecular dihydrogen would be the by product, after formation of the B-B bond. Sacrificial scavenging of the dihydrogen to improve the thermodynamics of this process may prove advantageous.

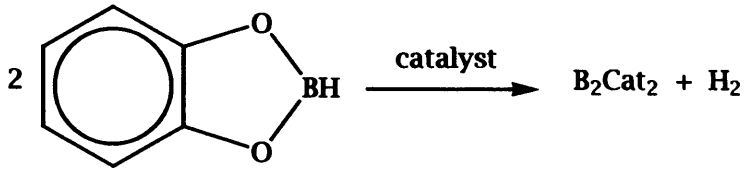

Scheme 5 - Conversion of a B-H into a B-B bond

In principle, this transformation could be mediated by transition metals. This idea is the point from which the present work started. Interaction of HBCat with different platinum precursors has been undertaken, following the reactions *via* multinuclear NMR (both at ambient and low temperature), to achieve a better understanding of the underlying chemistry. The precursors chosen were $Pt(PPh_3)_4$, $Pt(PPh_3)_2(\eta^2\text{-}CH_2{=}CH_2)$ and $Pt(dppe)(\eta^2\text{-}CH_2{=}CH_2)$.

Reaction of $Pt(PPh_3)_2(\eta^2\text{-}CH_2{=}CH_2)$ with HBCat in a 1:1 stoichiometry in toluene provides a light yellow solution mixture, whose colour does not change with time. ^{11}B- and ^{31}P-NMR spectra show that, even after 12h, the only products are B_2Cat_3 (Figure 3, δ_B=21.3 ppm[10]) and unreacted starting material (δ_P=35.1 ppm, $^1J_{P\text{-}Pt}$=3737 Hz[16]).

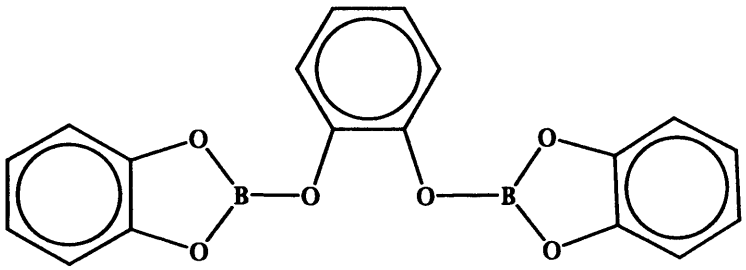

Figure 3 - B_2Cat_3

When an excess of HBCat (3 equivalents) is added to bring the reaction to completion, the starting material disappears, and the final product is the known *bis-boryl cis*-$Pt(PPh_3)_2(BCat)_2$ (19, δ_P=29.7 ppm, $^1J_{P\text{-}Pt}$=1608 Hz[17]). Formation of a bis-boryl from a "monoboryl source" like HBCat implies that *one (or more) intermediates must exist*, on the way to the observed product. If initial B-H oxidative addition occurs then 18 as a possible candidate for such an intermediate:

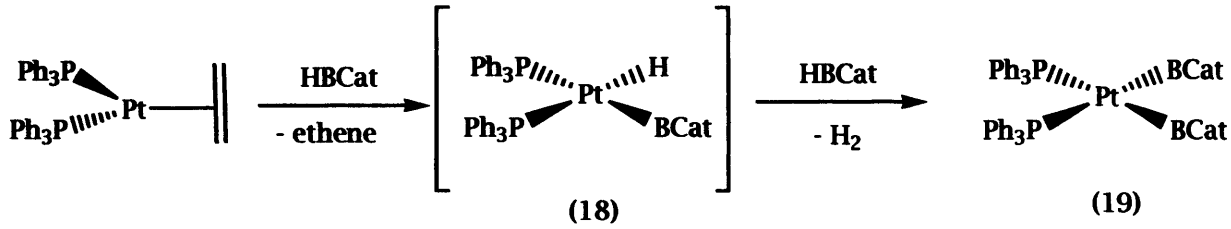

(18) (19)

Scheme 6 - Production of cis-$Pt(PPh_3)_2(BCat)_2$ from catecholborane

Variable temperature NMR has been carried out on the same system, using a toluene-d_8 solution cooled down to -78°C. Slow warming reveals the existence of *two new phosphorus signals* at δ_P=31.2 ppm, $^1J_{P\text{-}Pt}$=2403 Hz and δ_P=34.6 ppm, $^1J_{P\text{-}Pt}$=1602 Hz at -20°C, which gradually disappear to leave only the peaks of the bis-boryl $Pt(PPh_3)_2(BCat)_2$ when the temperature is raised to 25°C. Once more, boron spectra only show the formation of B_2Cat_3, but no other peaks are observed. The proton spectra are not particularly revealing, showing only the very strong signals of the phenyl rings and of catecholborane in the area around δ_H=6-7 ppm. The partially collapsed quartet of the proton bonded to boron in HBCat can be seen as a broad signal centred at δ_H=4.5 ppm. No signals are observed at any point in the hydride region between -5 to -25 ppm. Several parallel experiments have been carried out in order to try to obtain more spectroscopic information about the identity of the intermediate. An initial hypothesis was a *cis asymmetrical* derivative like *$Pt(H)(BCat)(PPh_3)_2$* (18 in Scheme 6). With this idea in mind, attempts to prepare the same molecule in a different manner were made, leading to the results summarised in Scheme 7.

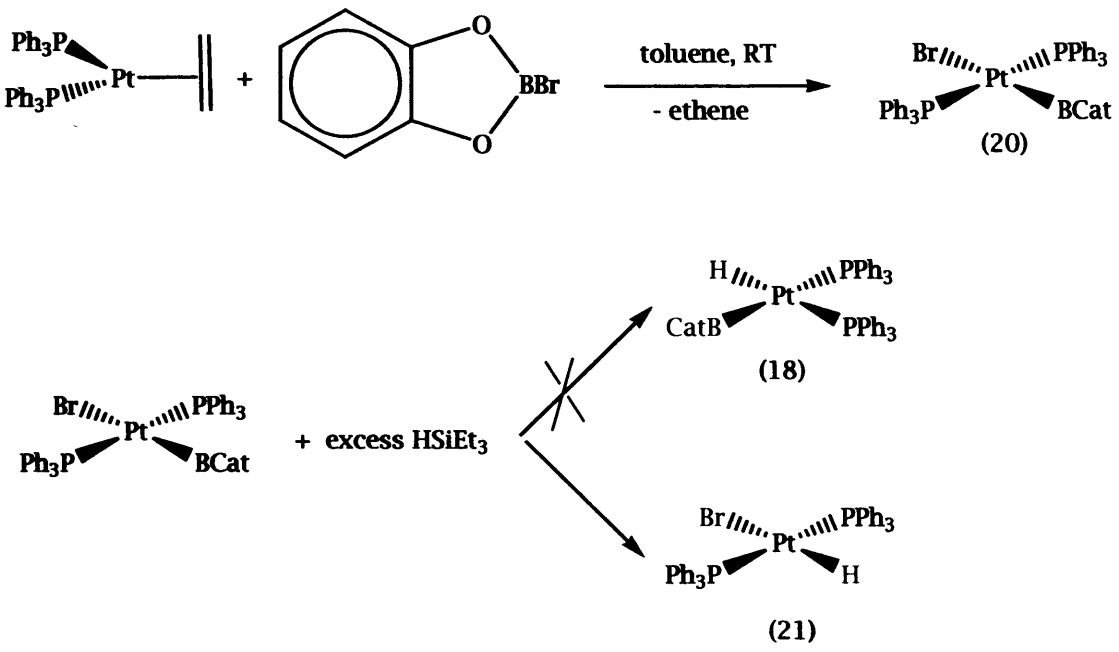

Scheme 7 - Attempted synthesis of 18

The production of the BrBCat adduct 20 (δ_P=23.3 ppm, $^1J_{P\text{-}Pt}$=2849 Hz) according to the literature routes[13] is very straightforward, a white powder precipitates out of a toluene solution obtained by mixing the reagents at room temperature. In the second step, a benzene-d_6 suspension of the bromo compound was treated with an excess of triethylsilane, on an NMR scale. Unfortunately, the use of triethylsilane as a source of hydride yields the alternative product 21[9]. Other attempts were made with more ionic sources of hydride, such as NaH and $LiAlH_4$, but in both cases no reaction seems to occur at all, even after warming at T=55°C, probably because of the limited solubility of these species in benzene. Consequently the synthesis and reactivity of 18, and in particular the possibility of its interconversion to the bis(boryl) 19 could not be investigated.

Another set of experiments was carried out to determine the spectroscopic properties and reactivities of platinum *bis-hydrides* $Pt(H)_2(PPh_3)_2$. Derivatives of this kind could be intermediates which form after a rearrangement of 18 under these particular conditions (Scheme 8).

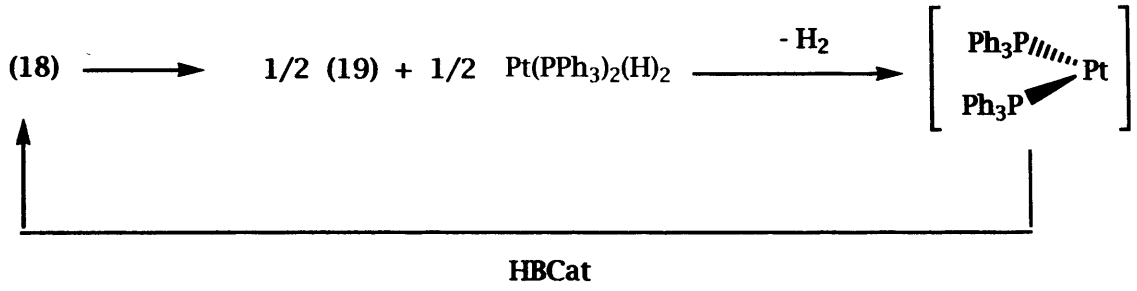

Scheme 8 - Formation of platinum hydrides

In general, two routes are conceivable to prepare bis-hydrides of platinum(II): (i)-reaction of a platinum(0) precursor with H_2 gas and oxidative addition of H_2 to the metal centre; (ii)-reduction of a platinum(II) precursor with an excess of a reducing "hydride-source" agent (normally $NaBH_4$)[18]. Both have been exploited. The results are summarised in Scheme 9.

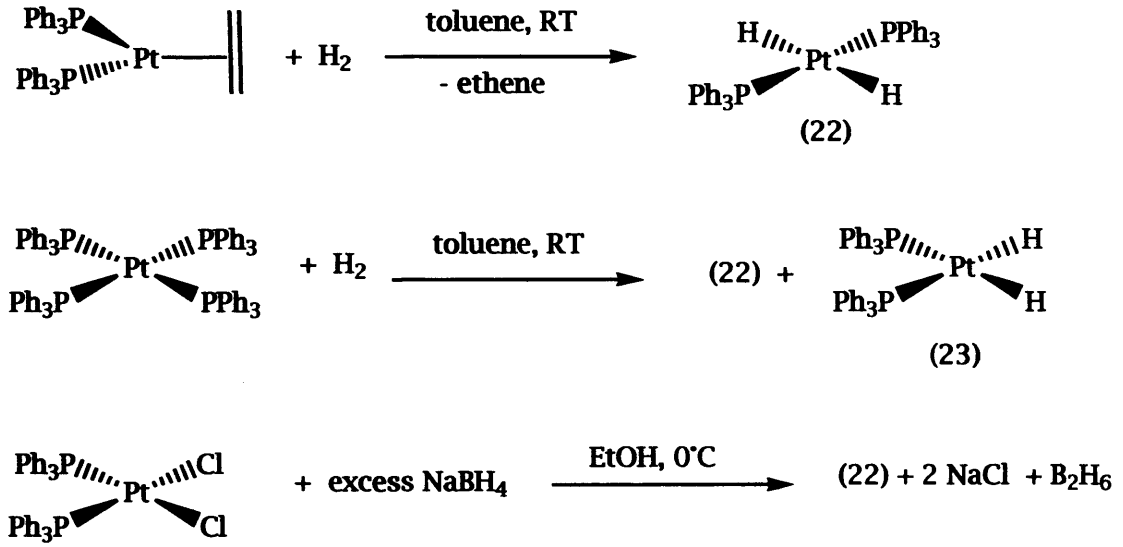

Scheme 9 - Preparations of platinum(II) bis-hydrides

Stereoselectivity is different, depending on the starting material employed. The trans isomer 22 is the most stable, and it forms under all conditions (δ_P=50.9 ppm, $^1J_{P\text{-}Pt}$=4514 Hz in toluene), while the cis isomer 23 forms only from tetrakis-(triphenylphospine)platinum(0) (δ_P=18.2 ppm, $^1J_{P\text{-}Pt}$=4082 Hz in toluene). Clearly, a comparison of these data with those observed for the low temperature intermediate tend to argue against a significant quantity

of either hydride being present in solution. Interestingly, however, mixing of a hexane solution of 22 or 23 with an excess of HBCat in toluene solution at room temperature, yields the same final products as with $Pt(PPh_3)_2$(ethene) as the platinum source (bis-boryl $Pt(PPh_3)_2(BCat)_2$ and B_2Cat_3). In conclusion, the identity of the intermediate detected at low temperature is still unknown, but, as a result of the reactions described in the present section, a bis-hydride complex like 22 or 23 can be definitely ruled out.

The results from the analogous reaction of $Pt(PPh_3)_4$ and HBCat in toluene are also akin to those seen for $Pt(PPh_3)_2$(ethene): in the presence of an excess of catecholborane the bis-boryl $Pt(PPh_3)_2(BCat)_2$ (19) is the final product. In order to avoid the extensive decomposition of the boron reagent catalysed by free PPh_3 in solution, a different platinum(0) complex containing a *chelating* phosphine was employed i.e. Pt(dppe)(ethene). The chelate effect was expected to stabilise this complex to phosphine dissociation. Free phosphine from Wilkinson's catalyst[10,19] has previously been shown to transform HBCat into B_2Cat_3 and $BH_3.PPh_3$. However the observed reaction with catecholborane is very similar to the PPh_3 case: with a 1:1 ratio, two new phosphorus signals can be detected in the ^{31}P NMR spectra, together with a large amount of unreacted starting material at δ_P=54.9 ppm. These two new weak resonances are found at δ_P=40.8 ppm and δ_P=43.9 ppm. The ^{11}B NMR only shows a single broad resonance at $\delta_B \approx 15$ ppm.. When an excess of HBCat is added, bringing the stoichiometric ratio to 3:1, after 12 h stirring at room temperature the ^{31}P NMR of the toluene solution only shows peaks characteristic of the *bis-boryl* complex Pt(dppe)(BCat)$_2$ (δ_P=57.8 ppm, $^1J_{P\text{-}Pt}$=1417 Hz[17]), while in the ^{11}B NMR spectrum a large amount of decomposition product B_2Cat_3 is present (δ_B=21.4 ppm), together with a small amount of unreacted HBCat (δ_B=27.8 ppm), and no other signal is observed. Apparently, even with a chelating bidentate phosphine like dppe ligand dissociation still brings about substantial decomposition of HBcat. In the absence of additional corroborating data it is difficult to attribute the observed peaks in the ^{31}P NMR spectrum definitively to an intermediate species such as *cis-Pt(dppe)(H)(BCat)* (i.e. the dppe analogue of 18). As in the case of triphenylphosphine, no ^{31}P NMR signal for the bis-hydride $Pt(dppe)(H)_2$ around 47 ppm[20] is detected.

Finally, a possible reaction pathway is shown in Figure 4. The formation of a final product like $Pt(L)_2(BCat)_2$ offers some hope for the chemistry outlined in Scheme 5, because further reductive elimination would then produce B_2Cat_2 and regenerate $[Pt(L)_2]$. A better choice of the ligands L may promote reductive elimination, for example by making a *larger* metal ring size with phosphines like dppp (1,3-bis-(diphenylphosphino)propane) or dppb (1,4-bis-(diphenylphosphino)butane), or by bubbling CO in a solution of $Pt(L)_2(BCat)_2$ to displace the boryl ligands with carbon monoxide, to yield B_2Cat_2 and $Pt(L)_2(CO)_2$ [21]. Nevertheless, the use of platinum phosphine complexes to carry out the chemistry proposed in Scheme 5 is unlikely to be widely used, primarily due to the phosphine mediated decomposition of HBCat.

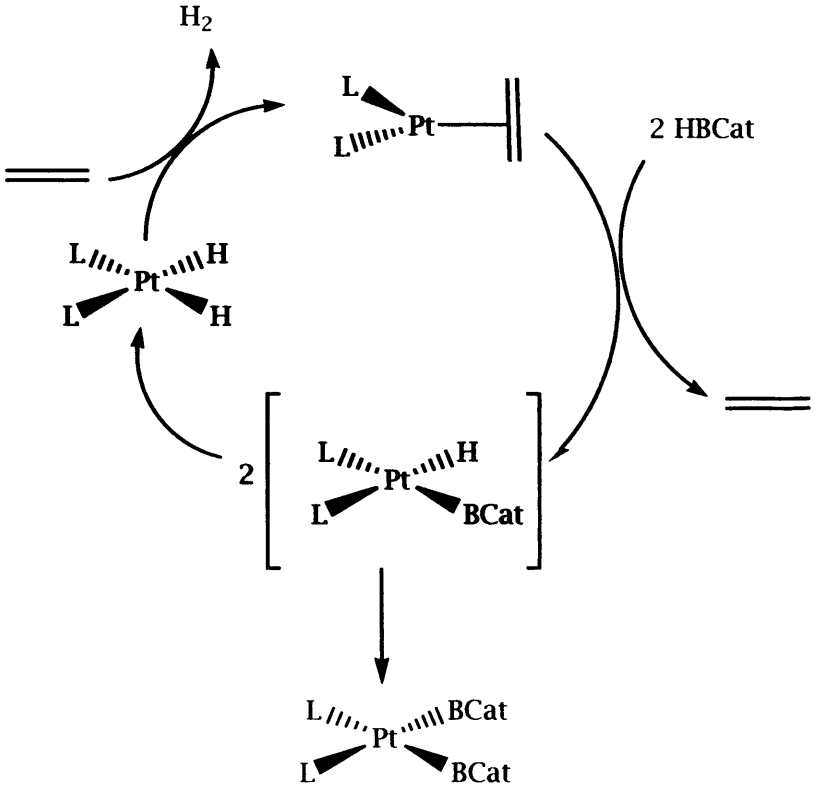

Figure 4 - A possible route to the formation of $Pt(L)_2(BCat)_2$

4.3.2 - Oxidative addition to main group metals: reactivity of indium and tin

An extension of the chemistry of transition metals to group 13 and 14 metals is conceivable, if a suitable organometallic precursor is chosen as starting material[22]. Indium is present

both as indium(I) and indium(III) in its organometallic derivatives, and both oxidation states are stable under appropriate conditions. Our choice was to use (η^5-C_5Me_5)In (Cp*In) as a precursor, which was reacted with different B-Cl, B-Br and B-B bonds.

Reaction of Cp*In with B-bromocatecholborane is immediate. However, the mass spectrometry data (FAB) for the isolated solid product revealed that the expected peak at *m/z* = 449 for [(Cp*)In(Br)(BCat)]$^+$ does not exist; instead, two other peaks whose *m/z* values correspond to the "symmetric" molecules 7 and 8 are observed. On Figure 5(b) the FAB mass spectrum of the white crystalline solid obtained from a hexane solution is reported. Unfortunately, the crystals were not suitable for X-ray diffraction. Separation of 7 and 8 is not easy (attempts were made with recrystallisations from concentrated hexane solutions). However, in the ^{1}H and ^{13}C NMR spectra for the solid dissolved in benzene-d_6 there are no signals corresponding to two different species, but, on the contrary, *only one set of peaks is observed both on the ^{1}H and ^{13}C NMR spectra for the Cp* ligand.* This implies that there must be only one species in solution, and integration of the requisite signals is consistent with the asymmetric species (Cp*)In(Br)(BCat). Presumably this asymmetric species is generated from the bis(bromide) and the bis(catecholboryl) species on dissolution.

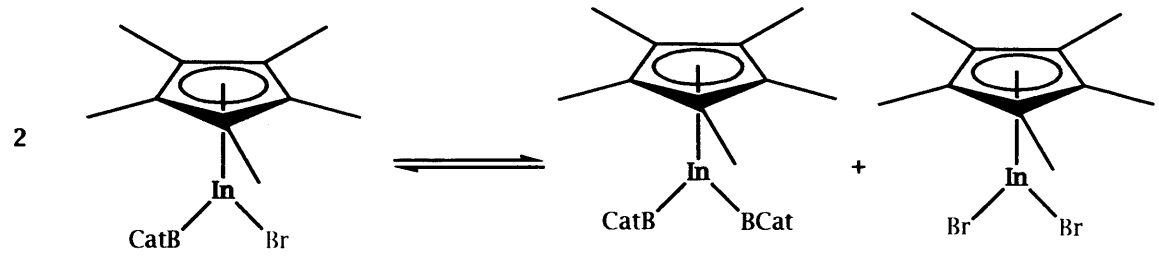

*Scheme 10 - Ligand redistribution in the solid state of Cp*In(Br)(BCat)*

This behaviour would also explain why the purification of the sample is hard. Another possible reaction could be the exchange of Cp* and Br moieties, according to Scheme 11. Neither the mass nor the NMR spectra though show peaks related to those species.

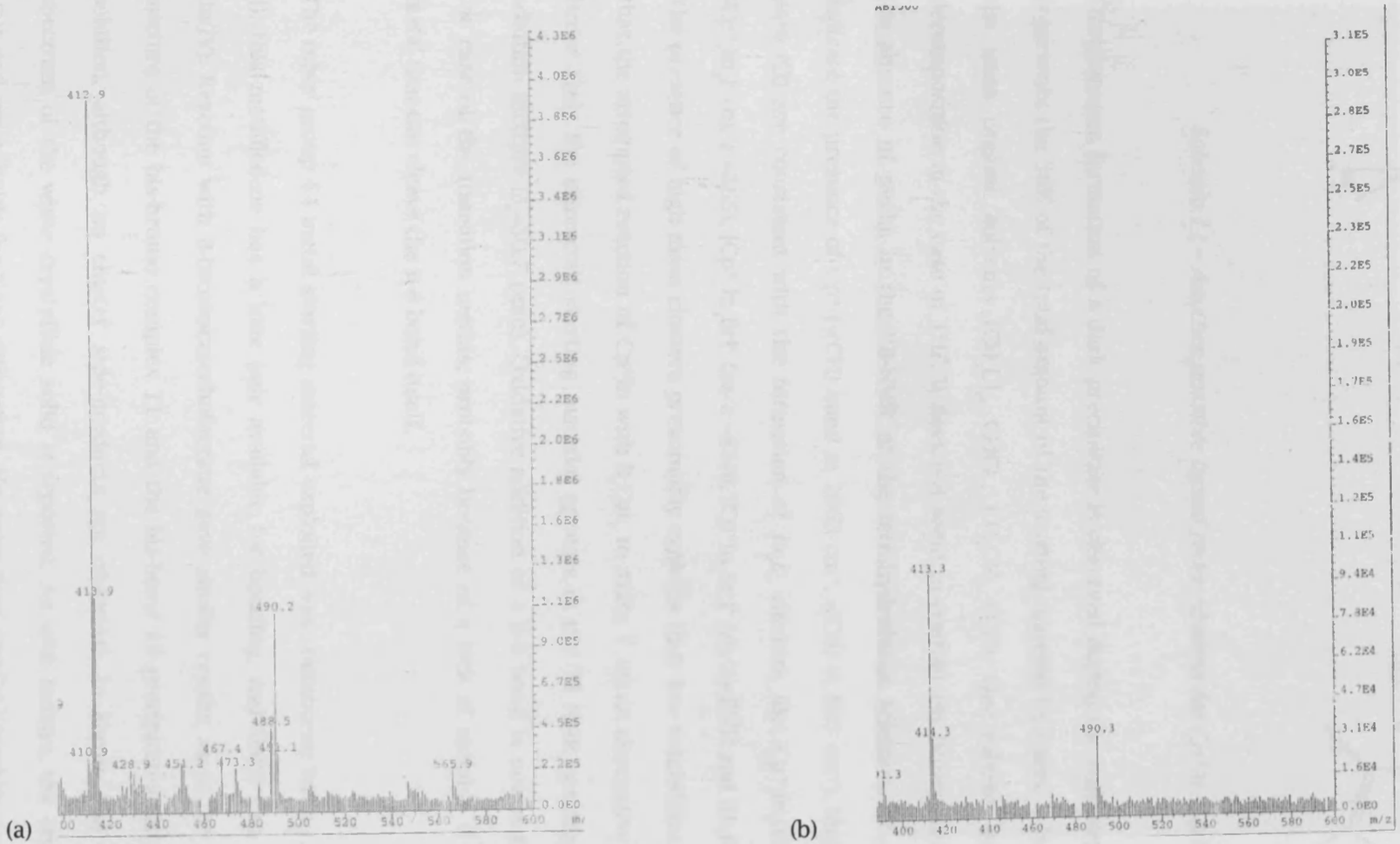

Figure 5 – (a) FAB mass spectrum of the solid mixture of $Cp_2Sn(Br)_2$ (m/z=413) and $Cp_2Sn(BCat)_2$ (m/z=490); (b) FAB mass spectrum of the solid mixture of $(Cp^*)In(Br)_2$ (m/z=413) and $(Cp^*)In(BCat)_2$ (m/z=490).

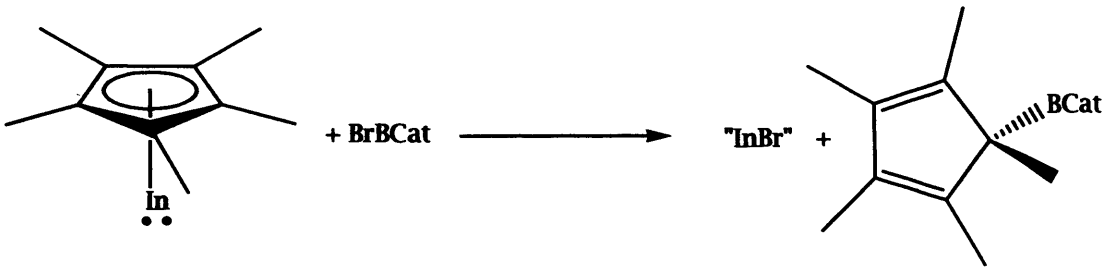

*Scheme 11 - Another possible ligand redistribution for Cp*In + BrBCat*

Simultaneous formation of a dark precipitate is observed during the reaction, and this solid represents the 36% of the total amount of the starting material by mass. It is insoluble in all the main organic solvents (CH_2Cl_2, $CHCl_3$, CH_3CN, Et_2O), the solvent itself leading to decomposition in the case of THF. It does not seem to contain any boron atom, according to the absence of peaks in the ^{11}B-NMR of the tetrahydrofuran solution. IR data (KBr disk) indicate the presence of Cp* (ν(CH) band at 2963 cm^{-1}, γ(CH) at 803 cm^{-1}). Mass spectrometry data (EI) are consistent with the formation of *In_4L_4 clusters*, like $Cp^*_3In_4(OH)$ (*m/z* =882), $[Cp^*_3In_4]^+$ (*m/z* =865), $[Cp^*_2In_4Br]^+$ (*m/z* =810), $[Cp^*In_4Br_2]^+$ (*m/z* =755) and $[In_4Br_3]^+$ (*m/z* =700). The presence of high mass clusters presumably explains their low solubilities. It is intriguing that the attempted reaction of Cp*In with B_2Cat_2 to make 7 *via* an alternative route *does not occur*. Only the unreacted starting material appears in the ^{11}B NMR spectra of the toluene solution mixture (δ_B=30.7 ppm). Oxidative addition of a B-B bond is not as favourable as in the case of the transition metals, probably because of a lack of suitable d orbitals on the metal that can cleave the B-B bond itself.

The other group 14 metal starting material exploited was stannocene $SnCp_2$. As with indium (I), this metallocene has a lone pair available for bonding, and tin(II) can be oxidised to tin(IV). Reaction with B-bromocatecholborane gave similar results as in the indium case: a mixture of the bis-bromo complex 11 and the bis-boryl 10 precipitates out of the toluene solution, although no cluster side-products are observed. In Figure 5(a) the FAB mass spectrum of the white crystalline solid is reported. As with indium, the crystals were too tiny, and not suitable for X-ray diffraction. No more than *one* Cp ligand type can be found in the ^{1}H and ^{13}C NMR spectra; this can be explained by the same ligand redistribution reaction

that has been proposed for indium. What is in solution is not the same as that present in the solid. The reaction of stannocene with B_2Cat_2 under the same conditions *does not occur*, again as in the Cp*In case.

4.4 - Conclusions

Oxidative addition as a route to boryl complexes has proved to be less successful than metathesis, in some case due to problems related to the reversibility of the reaction. Furthermore, some of the platinum chemistry is complicated by several (precedented) side reactions of the labile phosphine ancillary ligands with the borane starting materials, leading to decomposition of the latter. Catalytic conversion of B-H bonds to B-B bonds using catecholborane is therefore not likely to be viable while platinum phosphine precursor complexes are employed. In addition, platinum boryls are extremely sensitive to moisture or halide sources, being transformed into platinum hydrides or chlorides very readily, and therefore making their complete characterisation very difficult for a number of the ligand systems investigated here.

Main group metals indium and tin oxidatively add to B-bromocatecholborane in the same way, but the interconversion of the final product into different species hinders the isolation of a single complex. Yields are also very low.

(1) See, for example: (a) Lu N., Norman N.C., Orpen A.G., Quayle M.J., Timms P.L., Whittell G.R., *J. Chem. Soc., Dalton Trans.* 2000, 4032; (b) Clegg W., Johann T.R.F., Marder T.B., Norman N.C., Orpen A.G., Peakman T.M., Quayle M.J., Rice C.R., Scott A.J., *J. Chem. Soc., Dalton Trans.* 1998, 1431; (c) Ishiyama T., Matsuda N., Murata M., Ozawa F., Suzuki A., Miyaura N., *Organometallics* 1996, 15, 713; (d) Onozawa S., Tanaka M., *Organometallics* 2001, 20, 2956; Iverson C.N., Smith III M.R., *Organometallics* 1996, 15, 5155; (e) Westcott S.A., Marder T.B., Baker R.T., Calabrese J.C., *Can. J. Chem.* 71 (1993), 930; (f) Dai C., Stringer G., Marder T.B., Baker R.T., Scott A.J., Clegg W., Norman N.C., *Can. J. Chem.* 74 (1996), 2026; (g) Nguyen P., Blom H.P., Westcott S.A., Taylor N.J., Marder T.B., *J. Am. Chem. Soc.* 1993, 115, 9329; see also references (14) and (18) of chapter 1 for additional examples.

(2) Chapter 1, reference (14c).

(3) Van Gaal H.L.M., Van Den Bekerom F.L.A., *J. Organomet. Chem.* 134 (1977), 237.

(4) Binger P., *Chem. Ber.* 1994, 127(10), 1927.

(5) Westcott S.A., Taylor N.J., Marder T.B., Baker R.T., Jones N.J., Calabrese J.C., *J. Chem. Soc., Chem. Commun.* 1991, 304.

(6) Scherer O.J., Jungmann H., *J. Organomet. Chem.*, 208 (1981), 153.

(7) Köster R., *Chem. Ber.*, 122 (1989), 1815.

(8) Bender R., Braunstein P., Jud J.M., Dusausoy Y., *Inorg. Chem.* 1984, 23, 4489.

(9) Aldridge S., Coombs D., Jones C., *Acta Crystallogr.*, E59 (2003), m584.

(10) Chapter 1, reference (24).

(11) (a) Muylle E., Van der Kelen G.P., Claeys E.G., *Spectrochim. Acta*, 32A (1976), 1149; (b) Muylle E., Van der Kelen G.P., *Spectrochim. Acta*, 32A (1976), 599.

(12) Mintcheva N., Nishihara Y., Mori A., Osakada K., *J. Organomet. Chem.* 2001, 629, 61.

(13) Chapter 1, reference (14a).

(14) (a) Anastasi N.R., Waltz K.M., Weerakoon W.L., Hartwig J.F., *Organometallics* 2003, 22, 365; (b) Lawlor F., Norman N.C., Pickett N.L., Robins E.G., Nguyen P., Lesley G., Marder T.B., Ashmore J.A., Green J.C., *Inorg. Chem.* 1998, 37, 5282.

(15) Brotherton R.J., McCloskey A.L., Petterson L.L., Steinberg H., *J. Am. Chem. Soc.*, 82 (1960), 6242.

(16) Tolman C.A., Seidel W.C., Gerlach D.H., *J. Am. Chem. Soc.*, 94 (1972), 2669.

(17) Chapter 1, reference (18a).

(18) (a) Malatesta L. and Ugo R., *J. Chem. Soc.* 1963, 2080; (b) Paonessa R.S. and Trogler W.C., *J. Am. Chem. Soc.* 1982, 104, 1138; (c) Shaw B.L. and Uttley M.F., *J. Chem. Soc. Chem. Comm.* 1974, 918.

(19) Coapes R.B., Souza F.E.S., Fox M.A., Batsanov A.S., Goeta A.E., Yufit D.S., Leech M.A., Howard J.A.K., Scott A.J., Clegg W., Marder T.B., *J. Chem. Soc., Dalton Trans.*, 2001, 1201.

(20) Anderson G.K., Lumetta G.J., Siria J.W., *J. Organomet. Chem.*, 434(2), 1992, 253.

(21) Iverson C.N., Smith III M.R., *Organometallics* 1996, 15, 5155.

(22) Housecroft C.E., Sharpe A.G., *Inorganic Chemistry*, Prentice Hall Edition (2001), chapter 18.

5 - DFT studies on transition metal complexes containing low coordinate group 13 ligands

5.1 - Introduction

Transition metal complexes offering the potential for multiple bonding with a main group element have been the focus of considerable research effort[1]. In part, this reflects important synthetic methodologies in which such species have been implicated (e.g. carbene complexes in cyclopropanation and olefin metathesis), as well as vigorously debated issues of structure and bonding. Unlike their group 14 counterparts (e.g. carbenes, $L_nM{=}CX_2$, and silylenes, $L_nM{=}SiX_2$),[2] low-coordinate diyl complexes (L_nMEX) of the group 13 elements (E = B - Tl) are a relatively recent synthetic development[3]. Nevertheless, a number of thorough computational studies have been reported, examining the nature of the metal - group 13 element interaction, in neutral complexes predominantly of the types $(OC)_4FeEX$, $Fe(EX)_5$ and $Ni(EX)_4$[4]. Such studies have probed the effects not only of E and X, but also of ancillary π-acidic carbonyl ligands on the nature of the M-E bond.

Following the synthesis of the first cationic borylene complex $[(\eta^5\text{-}C_5Me_5)Fe(CO)_2{=}B(Mes)]^+$, a detailed theroretical analysis of the metal-group 13 element bond in this and related complexes has been undertaken, in order to shed light on this virtually unexplored field.

Section 5.3.1 discusses the results of an extended DFT study on the aforementioned complex $[(\eta^5\text{-}C_5Me_5)Fe(CO)_2{=}B(Mes)]^+$ and related cationic and neutral half-sandwich diyl systems whose generic structure is reproduced in Figure 1.

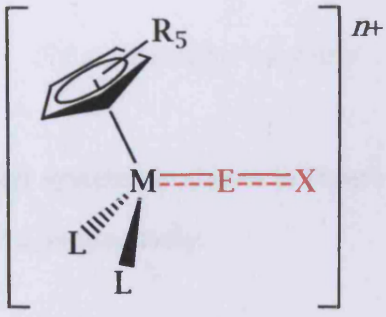

Figure 1 - Model of a terminal group 13 diyl complex

The interest is in defining the nature and scope for variation of the M-E bond by quantifying (i) bond dissociation energies (BDEs); (ii) the ionic and covalent contributions to the instantaneous interaction energy between metal and diyl fragments; (iii) the relative importance of σ and π symmetry covalent terms; and (iv) energetic barriers for rotation about the M-E bond. Of particular interest is a comparison of the bonding situation in cationic diyls $[L_nMEX]^+$ both with their charge neutral analogues and with archetypal group 14 ligand systems {e.g. $[L_nMCO]^+$ and $[L_nMEX_2]^+$ (E = C, Si)}.

Section 5.3.2 reports a theoretical MO analysis of a new dinuclear iron complex containing a "naked" gallium atom symmetrically bridging two different iron centres: $\{[(\eta^5\text{-}C_5Me_5)Fe(CO)_2]_2Ga\}^+$ [5]. This species, which can be thought of as a metalladiyl (L_nMGa:) complex of $[(\eta^5\text{-}C_5Me_5)Fe(CO)_2]^+$, is probably best formulated as a delocalised Fe-Ga-Fe π system incorporating partial Fe-Ga multiple bond character.

Finally, section 5.3.3 presents the optimised geometries, MO analyses and σ and π breakdown of the M-Ga bond density of five different gallium carbene complexes containing metals of the first transition series[6]. Such complexes are formally very similar to heteroatom-stabilised boryl systems and a comparative bonding study is reported.

5.2 - Systems studied: a collection of all the calculated parameters

In this section tables collecting all the experimental and theoretical data are reported. A discussion of the data is then presented in section 5.3.

5.2.1 - Borylene systems

The generic structure of these diyl systems is shown in Figure 1, and structural and bonding data reproduced in Tables 1 and 2, respectively.

Table 1 - Calculated and experimentally determined geometric data for the cationic diyl and related complexes featured in this study.

Compound	M, n[a]	E	X	L	R	Bond lengths / Å				Bond angles and torsions / deg		
						Fe-E	Fe-Cp centroid	Fe-L	E-X	Fe-E-X	L-Fe-L	Torsion[b]
1'[c]	Fe, 1	B	Mes	CO	Me	1.792(8) 1.785(8)	1.738(8) 1.733(8)	1.760(8), 1.768(8) 1.771(8), 1.780(8)	1.491(10) 1.503(10)	178.3(6) 177.4(6)	96.0(3) 96.1(3)	83.0(3) 84.0(3)
1	Fe, 1	B	Mes	CO	Me	1.843	1.849	1.810, 1.812	1.495	177.8	95.2	81.6
2	Fe, 1	B	Mes	CO	H	1.848	1.843	1.812, 1.813	1.487	178.0	94.3	82.0
3	Fe, 1	B	Mes	PMe_3	H	1.798	1.859	2.298, 2.312	1.530	174.9	95.4	81.1
4	Fe, 1	B	C_6F_5	CO	Me	1.813	1.845	1.822, 1.823	1.514	177.9	95.2	82.4
5	Fe, 1	B	$C_6H_3(CF_3)_2$-3,5	CO	Me	1.815	1.852	1.820, 1.822	1.512	179.3	95.4	82.5
6	Fe, 1	B	H	CO	Me	1.776	1.848	1.828, 1.829	1.188	179.6	96.2	[d]
7	Fe, 1	B	NMe_2	CO	Me	1.869	1.841	1.809, 1.811	1.357	175.1	94.9	84.6
8	Fe, 1	B	F	CO	Me	1.835	1.837	1.827, 1.828	1.274	179.2	95.3	[d]
9	Fe, 1	Al	Mes	CO	Me	2.284	1.829	1.805, 1.808	1.942	175.8	95.4	80.7
10	Fe, 1	Ga	Mes	CO	Me	2.309	1.821	1.813, 1.816	1.973	175.3	94.7	82.1

Compound	M, n[a]	E	X	L	R	Bond lengths / Å				Bond angles and torsions / deg		
						Fe-E	Fe-Cp centroid	Fe-L	E-X	Fe-E-X	L-Fe-L	Torsion[b]
11	Mn,0	B	Mes	CO	H	1.811	1.970	1.795 (mean)	1.525	177.9	92.8	80.8
12'[c]	Fe, 1	C	O	CO	Me	1.819 (mean)	1.726(5)	1.819 (mean)	1.145 (mean)	175.7 (mean)	94.2 (mean)	[d]
12	Fe, 1	C	O	CO	Me	1.845 (mean)	1.831	1.845 (mean)	1.147 (mean)	179.4 (mean)	94.0 (mean)	[d]
13	Fe, 1	C	CMe_2	CO	Me	1.829	1.847	1.826, 1.827	1.306	174.1	92.9	86.6

[a] L, M, E, X and *n* defined as in Figure 1. [b] See Figure 5 in chapter 2.5.6 for definition of torsion angle. [c] Data for 1' correspond to the experimental values for the two crystallographically independent molecules in the asymmetric unit.[7] Data for 1 are the corresponding calculated parameters. [d] Not applicable. [e] Taken from reference (8).

Table 2 - Analysis of bonding in complexes 1-13.

Compound	Breakdown of orbital contribution to bond / %		Mayer bond order	BDE (D_o)[a]	ΔE_{int}[a,b]	ΔE_{elstat}[a,b]	ΔE_{orb}[a,b]	ΔE_{Pauli}[a,b]	$\Delta E_{elstat}/\Delta E_{orb}$
	σ	π							
1	62.2	37.5	1.30	147.5	-150.5	-225.7	-153.6	228.2	1.47
2	65.8	33.9	1.28	151.0	-154.1	-224.1	-151.4	221.4	1.48
3	54.9	44.8	1.68	153.0	-159.0	-226.3	-164.7	232.0	1.37
4	59.7	40.0	1.45	136.1	-139.5	-205.4	-153.6	219.5	1.34
5	57.8	41.8	1.41	136.5	-139.4	-207.9	-154.1	222.6	1.35
6	54.9	44.7	1.56	137.7	-140.7	-229.7	-162.2	251.2	1.42
7	66.0	33.7	1.24	125.9	-128.7	-193.9	-131.0	196.2	1.48
8	62.3	37.4	1.30	100.7	-103.1	-149.1	-121.0	167.0	1.23
9	68.6	30.8	1.04	107.1	-111.0	-125.5	-121.7	136.2	1.03
10	66.3	32.8	1.00	101.1	-106.6	-108.9	-108.0	110.9	1.00
11	45.6	54.0	1.49	139.9	-142.0	-227.3	-159.8	245.1	1.42

Compound	Breakdown of orbital contribution to bond / %		Mayer bond order	BDE (D_o)[a]	ΔE_{int} [a,b]	ΔE_{elstat} [a,b]	ΔE_{orb} [a,b]	ΔE_{Pauli} [a,b]	$\Delta E_{elstat}/\Delta E_{orb}$
12	67.7	32.1	1.09	75.5	-78.0	-90.5	-91.5	104.0	0.99
13	64.7	35.1	1.19	114.8	-117.3	-145.4	-119.0	147.1	1.22

[a] All values in kcal mol^{-1}. [b] ΔE_{elstat}, ΔE_{orb} and ΔE_{Pauli} are respectively the contributions to the instantaneous interaction energy (between metal and diyl fragments) due to electrostatic attraction, orbital interaction and Pauli repulsion ($\Delta E_{int} = \Delta E_{elstat} + \Delta E_{orb} + \Delta E_{Pauli}$). The ratio $\Delta E_{elstat}/\Delta E_{orb}$ gives information about the relative importance of ionic and covalent contributions to the M-E bond.[9]

5.2.2. - "Naked" gallium complex $[Fp^*_2Ga]^+$

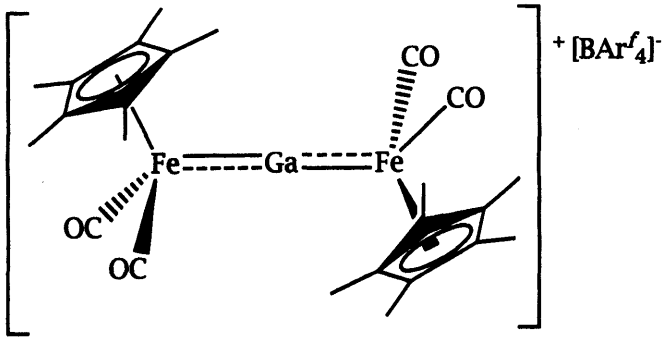

(14)

Table 3 - Calculated and experimentally determined geometric data for 14

$[Fp^*_2Ga]^+$	Bond lengths / Å			Bond angles and torsions / deg			Breakdown of orbital contribution / %		Mayer bond order
	Fe-Ga	Fe-Cp(ct)	Fe-CO	Fe-Ga-Fe	CO-Fe-CO	Torsion[a]	σ	π	
Experimental[b]	2.272(1) 2.266(1)	1.728(3)	1.764(3)	178.99(2)	94.86(13)	84.62(3)			
Calculated	2.337	1.826	1.806	177.93	95.54	86.5	60.7	38.3	0.92

[a] The torsion angle is defined as the angle Cp centroid (1)-Fe(1)-Fe(2)-Cp centroid (2). [b] Data taken from reference (5).

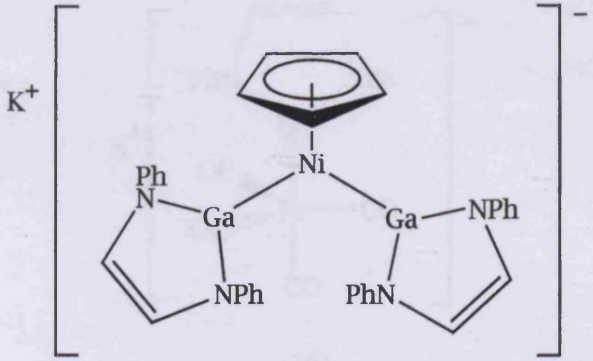

(15)

Table 4 - Calculated and experimentally determined geometric data for 15

$[CpNi(GaX_2)_2]^-$	Bond lengths / Å			Bond angles and torsions / deg			Breakdown of orbital contribution / %		Mayer bond order
	Ni-Ga	Ni-Cp(ct)	Ga-N	Ga-Ni-Ga	N-Ga-N	Torsion[a]	σ	π	
Experimental[b]	2.2196(14) 2.2154(11)	1.719(7)	1.894(5) 1.901(5) x 2 1.900(5)	86.39(4)	87.1(2) x 2	54.3(4)			
Calculated	2.273	1.858	1.858	85.53	84.57	53.8	71.2	27.7	0.91

[a] The torsion angle is defined as the angle Cp(centroid)-Ni-Ga-N. [b] Data taken from reference (6a).

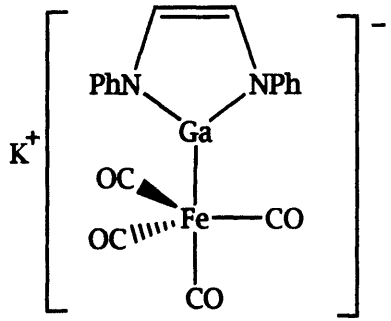

(16)

Table 5 - Calculated and experimentally determined geometric data for 16

$[Fe(CO)_4(GaX_2)]^-$	Bond lengths / Å				Bond angles and torsions / deg			Breakdown of orbital contribution / %		Mayer bond order
	Fe-Ga	Ga-N	$Fe-CO_{ax}$	$Fe-CO_{eq}$	N-Ga-N	$Ga-Fe-CO_{ax}$	$Ga-Fe-CO_{eq}$	σ	π	
Experimental[a]	2.307(1)	1.872(3) 1.882(3)	1.777(4)	1.753(4) 1.758(4) 1.783(4)	88.17(13)	174.13(13)	82.66(12) 87.33(13) 81.04(13)			
Calculated	2.400	1.957	1.810	1.827	84.62	176.93	85.1	79.0	20.1	0.74

[a] Data taken from reference (6b).

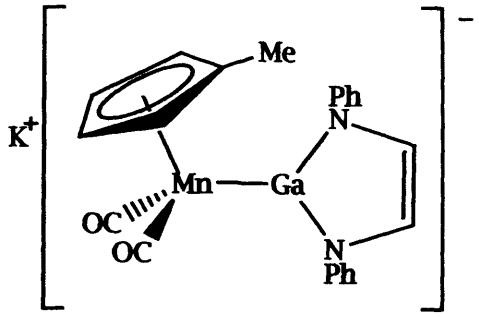

(17)

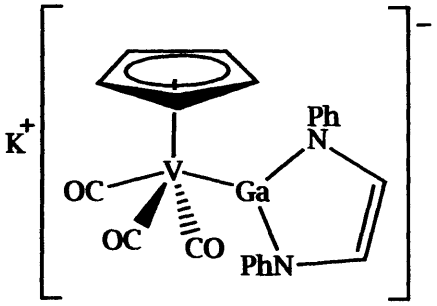

(18)

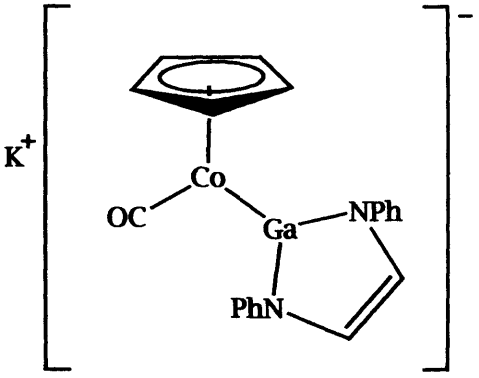

(19)

Table 6 - Calculated and experimentally determined geometric data for 17, 18 and 19

Compound	Bond lengths / Å				Bond angles and torsions / deg			Breakdown of orbital contribution / %		Mayer bond order
(17)	Mn-Ga	Mn-Cp	Ga-N	Mn-CO	CO-Mn-CO	N-Ga-N	Torsion[a]	σ	π	
Exp.[d]	2.3105(9)	1.774(5)	1.902(4) 1.906(4)	1.749(6) 1.752(6)	92.5(3)	85.87(16)	31.3(4)			
Calc.	2.396	1.870	2.012	1.795	92.94	82.86	20.7	81.5	18.2	0.92
(18)	V-Ga	V-Cp	Ga-N	V-CO	CO-V-CO	N-Ga-N	Torsion[b]			
Exp.[d]	2.4618(3) 2.4599(12)	1.939(7)	1.883(5) 1.882(4)	1.893(6) 1.904(8) 1.918(8)	88.5(4)	86.9(2) 86.6(2)	26.9(4)			
Calc.	2.554	2.030	1.984	1.948	90.98	83.25	30.8	86.9	12.5	0.68
(19)	Co-Ga	Co-Cp	Ga-N	Co-CO	CO-Co-Ga	N-Ga-N	Torsion[c]			
Exp.[d]	2.2347(7)	1.709(2)	1.897(2) 1.905(3)	1.677(4)	83.19(13)	86.96(11)	37.8(5)			
Calc.	2.304	1.812	2.002	1.730	87.10	83.37	38.5	71.9	26.8	0.99

[a] The torsion angle is defined as the angle Cp(centroid)-Mn-Ga-N. [b] The torsion angle is defined as the angle Cp(centroid)-V-Ga-N. [c] The torsion angle is defined as the angle Cp(centroid)-Co-Ga-N. [d] Data taken from unpublished work by R. Rose, R. Baker and C. Jones.

5.3 - Discussion of results

5.3.1 - Terminal borylene complexes

(i) - Molecular geometry

The model complexes chosen for this study allow the possibility for significant variation in the nature of the M-E interaction by encompassing (i) R and L substituents of varying electronic and steric properties within the $[(\eta^5\text{-}C_5R_5)ML_2]$ fragment {e.g. $[(\eta^5\text{-}C_5Me_5)Fe(CO)_2(BMes)]^+$ (1), $[(\eta^5\text{-}C_5H_5)Fe(CO)_2(BMes)]^+$ (2) and $[(\eta^5\text{-}C_5H_5)Fe(PMe_3)_2(BMes)]^+$ (3)}; (ii) diyl substituents (X) of widely differing σ and π electronic properties {e.g. $[(\eta^5\text{-}C_5Me_5)Fe(CO)_2(BH)]^+$ (6) and $[(\eta^5\text{-}C_5H_5)Fe(CO)_2(BNMe_2)]^+$ (7)}; (iii) cationic and charge neutral metal systems {e.g. $[(\eta^5\text{-}C_5H_5)Fe(CO)_2(BMes)]^+$ (2) and $(\eta^5\text{-}C_5H_5)Mn(CO)_2(BMes)$ (11)}; and (iv) diyl ligands featuring a range of group 13 elements {e.g. $[(\eta^5\text{-}C_5Me_5)Fe(CO)_2(BMes)]^+$ (1), $[(\eta^5\text{-}C_5Me_5)Fe(CO)_2(AlMes)]^+$ (9) and $[(\eta^5\text{-}C_5Me_5)Fe(CO)_2(GaMes)]^+$ (10)}. The geometries of the carbonyl and vinylidene complexes $[(\eta^5\text{-}C_5Me_5)Fe(CO)_3]^+$ (12) and $[(\eta^5\text{-}C_5Me_5)Fe(CO)_2(CCMe_2)]^+$ (13) were also optimised for comparative purposes. Salient structural parameters for the fully optimised geometries of compounds 1 - 13 are included in Table 1, together with the corresponding experimentally determined parameters for the two independent molecules of $[(\eta^5\text{-}C_5Me_5)Fe(CO)_2(BMes)]^+$ found in the crystal lattice of $[(\eta^5\text{-}C_5Me_5)Fe(CO)_2(BMes)][BAr'_4]\cdot\frac{1}{2}CH_2Cl_2$ (designated 1') and for the $[(\eta^5\text{-}C_5Me_5)Fe(CO)_3]^+$ cation in $[(\eta^5\text{-}C_5Me_5)Fe(CO)_3][BAr'_4]$ (designated 12') [7,10]. A comparison of these parameters for 1 and 1' (and for 12 and 12') allows some conclusions to be drawn regarding the reliability of the computational method used. In general, the agreement between calculated and experimental geometries is very good. Notably, key structural features such as the near linear Fe-B-C unit [$\angle$Fe-B-C_{ipso} = 178.3(6), 177.4(6) (exp.) and 177.8° (calc.), respectively] and the near orthogonal orientation of C_5Me_5 centroid-Fe-C_{ipso} and mesityl planes [torsion, $\angle$centroid-Fe-C_{ipso}-C_{ortho} = 83.0(3), 84.0(3) (exp.) and 81.6° (calc.), respectively] are well reproduced computationally. The near 90° angles between ancillary carbonyl ligands expected for half-sandwich complexes of this type are also well reproduced computationally for both 1' and 12'. In common with previously reported computational studies [11], there is a 2 - 3% overestimate in the lengths of bonds to

iron (Fe-B and Fe-C linkages). Such a discrepancy has been reported to be the result of solid-state effects leading to a shortening of donor/acceptor bonds, accompanied by the general over-estimate of bond lengths by generalized gradient approximation (GGA) methods [4d, 12]. However, previous studies on related iron boryl systems have shown that the DFT method reproduces well the observed *trends* in Fe-B distances, and that no significant improvement in absolute agreement is observed by the use of a higher level of theory (B3LYP rather than BLYP) or of the higher quality Gaussian basis set 6-311++G(d) (B3LYP) [11]. Indeed the very similar bond lengths obtained for model compounds using our standard approach [BLYP (ADF), basis set IV] and the more extensive Gaussian basis set gives us confidence in interpreting the M-E bonding character based on model densities.

In the case of compound 1 both crystallographic and computational studies reveal an orientation of the terminal mesitylborylene (BMes) ligand such that one of the two formally vacant p orbitals at boron could be populated by π back donation from the HOMO of the $[(\eta^5\text{-}C_5Me_5)Fe(CO)_2]^+$ fragment (Figure 2) [13].

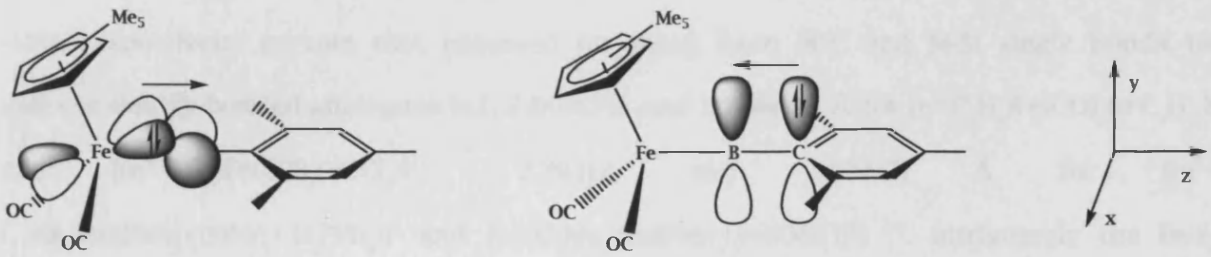

Figure 2

A very similar orientation of the borylene ligand has been determined computationally for the lowest energy conformation of the related vanadium half-sandwich complex $(\eta^5\text{-}C_5H_5)V(CO)_3(BNH_2)$ [14]. In addition, both calculated and experimental structures reveal a significant shortening of the B-C_{ipso} bond [d(B-C_{ipso}) = 1.491(10), 1.503(10) (exp.) and 1.495 Å (calc.)] compared to boryl complexes of the type $(\eta^5\text{-}C_5R_5)Fe(CO)_2B(Mes)X$ [R = Me, X = Br: d(B-C) = 1.569(3) Å; R = H, X = Br: d(B-C) = 1.563(6) Å; R = H, X = O^{t}Bu: d(B-C) = 1.583(3) Å] [15]. Such a bond shortening might be expected not only on the basis of the smaller steric

demands of the BMes ligand [compared to B(Mes)X], but also as a result of population of the second (formally vacant) p orbital at boron as a result of π overlap with the *ipso* carbon of the aromatic ring (Figure 2). A similar phenomenon has been reported by Uddin and Frenking in explaining why Fe→B π back bonding in $(OC)_4FeBPh$ occurs predominantly into the boron p orbital which lies perpendicular to the π system of the phenyl ring, rather than into that which is co-planar with it [9].

Both calculated and experimentally determined Fe-B distances for 1 [1.792(8), 1.785(8) (exp.) and 1.843 Å (calc.)] are significantly shorter than would be expected for a single bond. Thus Fe-B distances of 1.959(6), 2.010(3) and 2.195(14) Å have been reported for $(\eta^5\text{-}C_5H_5)Fe(CO)_2BCat$ (Cat = $O_2C_6H_4$-1,2), $(\eta^5\text{-}C_5Me_5)BFe(CO)_4$ and $(\eta^5\text{-}C_5Me_4Et)Fe(CO)_2BH_2{\cdot}PMe_3$, respectively [16]. The latter compound provides a σ-only single bond point of reference, whereas $(\eta^5\text{-}C_5H_5)Fe(CO)_2BCat$ is thought to feature a small but significant π bonding component; $(\eta^5\text{-}C_5Me_5)BFe(CO)_4$ has been described as featuring a purely σ type B→Fe donor/acceptor interaction. The percentage change in the measured Fe-B bond length for 1 compared to boryl complexes $(\eta^5\text{-}C_5H_5)Fe(CO)_2Bcat$ and $(\eta^5\text{-}C_5Me_4Et)Fe(CO)_2BH_2{\cdot}PMe_3$ (-8.5% and -18%, respectively) mirrors that observed on going from M-C and M-Si single bonds to cationic doubly-bonded analogues {c.f. 2.069(10) and 1.808(12) Å for $(\eta^5\text{-}C_5H_5)Fe(CO)_2(n\text{-}C_5H_{11})$ and $[(\eta^5\text{-}C_5H_5)Fe(CO)_2(=CCl_2)]^+$;[17] 2.381(2) and 2.238(2) Å for $[(\eta^5\text{-}C_5Me_5)Ru(PMe_3)_2(SiMe_2CH_2PPh_3)]^+$ and $[(\eta^5\text{-}C_5Me_5)Ru(PMe_3)_2(=SiMe_2)]^+$} [18]. Intriguingly the Fe-B bond lengths for 1 and 1' are similar to those calculated for the methylborylene complex $MeBFe(CO)_4$ by Macdonald and Cowley (1.794 or 1.806 Å, depending on the basis set used) [12a]. This value is ca. 9% shorter than that calculated for the analogous cyclopentadienylborylene complex $(\eta^5\text{-}C_5H_5)BFe(CO)_4$ and was offered as evidence for a 'modicum' of Fe-B backbonding.

Superficially, the calculated geometries for model compounds 1 - 11 are similar. In each case the orientation of the diyl ligand with respect to the $(\eta^5\text{-}C_5R_5)ML_2$ fragment is such as to give a torsion angle (θ) of ca. 90° (Figure 5, chapter 1.5.6). In addition, a near linear M-E-X unit is found in each case, with the largest deviation from linearity being only ca. 5°. Trends in Fe-E bond lengths are generally reflective of the π donor abilities of the transition metal and X

substituents. Thus, for example, replacement of the strongly π acidic ancillary carbonyl ligands with trimethylphosphines leads to significant shortening of the Fe-B distance {1.798 Å for $[(\eta^5\text{-}C_5H_5)Fe(PMe_3)_2(BMes)]^+$ (3) compared with 1.848 Å for $[(\eta^5\text{-}C_5H_5)Fe(CO)_2(BMes)]^+$ (2)} with concomitant lengthening of the $B\text{-}C_{ipso}$ bond (1.530 Å for 3, c.f. 1.487 Å for 2). Furthermore, the shortened M-B and lengthened B-C distances calculated for the neutral manganese complex $(\eta^5\text{-}C_5H_5)Mn(CO)_2(BMes)$ (11) (1.811 and 1.525 Å, respectively) are as expected on the basis of increased M→B π donation from the manganese centre. A similar shortening of the M-CO bond is found crystallographically on going from $[(\eta^5\text{-}C_5H_5)Fe(CO)_3]^+$ to $(\eta^5\text{-}C_5H_5)Mn(CO)_3$ [values of 1.802(6), 1.831(7) and 1.815(6) for iron; 1.781(2), 1.772(2) and 1.786(2) Å for manganese, respectively[19]]. In a similar fashion, variation in the Fe-B distance as a function of the X substituent can also be rationalized in terms of expected π donor properties of X {e.g. 1.776, 1.813, 1.843 and 1.869 Å for $[(\eta^5\text{-}C_5Me_5)Fe(CO)_2(BX)]^+$ with X = H, C_6F_5, Mes and NMe_2, respectively}, as shown in Figure 3.

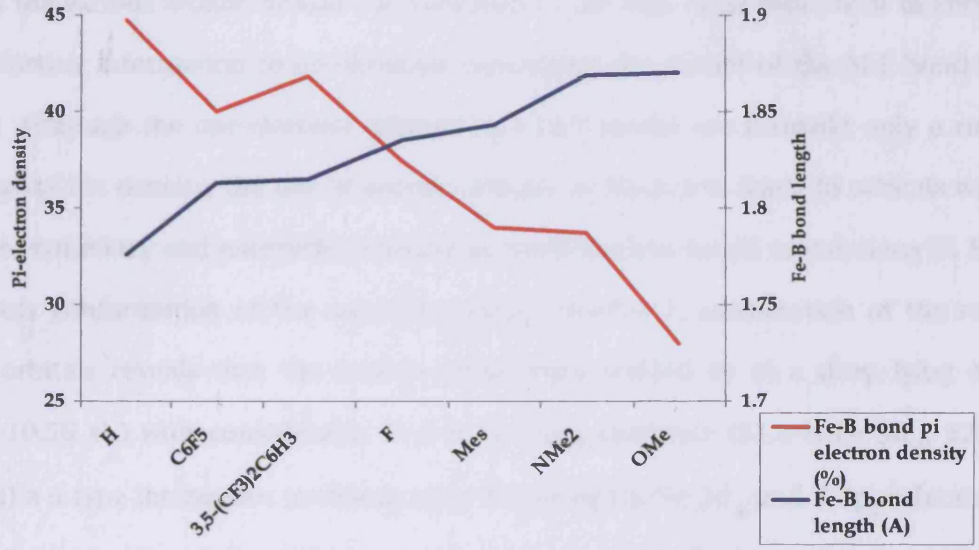

Figure 3 - Graph representing the dependence of the Fe-B bond length and π density as a function of the substituent X in $[(\eta^5\text{-}C_5Me_5)Fe(CO)_2(BX)]^+$

Replacement of the boron atom in 1 by the heavier congener aluminium or gallium leads to a marked increase in the Fe-E bond length {1.843, 2.284 and 2.309 Å for 1, $[(\eta^5\text{-}C_5Me_5)Fe(CO)_2(AlMes)]^+$ (9) and $[(\eta^5\text{-}C_5Me_5)Fe(CO)_2(GaMes)]^+$ (10), respectively}. The calculated increases are slightly greater than might have been expected purely on the basis of the

covalent radii of the elements (0.88, 1.25 and 1.25 Å for B, Al and Ga, respectively[20]), although the Fe-Ga distance for 10, for example, is still significantly shorter than those determined experimentally for the Fe-Ga single bonds in the bridging mesitylgallylene complex $[(\eta^5\text{-}C_5Me_5)Fe(CO)_2]_2GaMes$ [2.432(2) Å] and in the gallyl complex $(\eta^5\text{-}C_5H_5)Fe(CO)_2GaᵗBu_2$ [2.413 Å (mean)][21]. Similar trends in Fe-E bond lengths have been reported by Uddin and Frenking both for homoleptic diyl complexes [e.g. $Fe(EMe)_5$, E = B, Al, Ga] and for species containing ancillary carbonyl ligands [e.g. $(OC)_4FeEPh$]. Thus, bond lengths of 1.782, 2.182 and 2.252 Å were calculated for the axial Fe-E bonds of the homoleptic diyl complexes and distances of 1.803, 2.217 and 2.296 Å for the corresponding linkages in $(OC)_4FeEPh$[9].

(ii) Molecular orbital composition

Analysis of the various atomic orbital contributions to the molecular orbitals of molecules 1-13 allows further information to be obtained concerning the nature of the M-E bond in diyl complexes. Although the one-electron orbitals in a DFT model are formally only a route to construction of the density, the use of atomic orbitals as basis sets leads to orbitals with the same shape, symmetry and energetic ordering as wavefunction based calculations[22]. For the lowest energy conformation of the mesitylborylene complex 1, examination of the relevant molecular orbitals reveals that the Fe-B bond is characterized by (i) a deep lying orbital† (HOMO-7, -10.56 eV) with considerable Fe-B σ bonding character (21.4 % Fe $3d_{z^2}$, 12.8 % B $2p_z$); and (ii) a π type interaction predominantly featuring the Fe $3d_{xz}$ and B $2p_x$ orbitals. Both the HOMO-3 (-9.21 eV) and the HOMO-6 (-9.85 eV) feature significant in-phase contributions from these atomic orbitals (HOMO-3: 17.6 % Fe $3d_{xz}$, 4.9 % B $2p_x$; HOMO-6: 18.1 % Fe $3d_{xz}$, 3.1 % B $2p_x$). The LUMO+3 is the corresponding orbital of predominantly π* character (10.4 % Fe $3d_{xz}$, 35.4 % B $2p_x$). In addition it is possible to identify molecular orbitals [chiefly the HOMO-9 (-10.98 eV) and HOMO-2 (-8.91 eV)] which possess C-B π bonding character characterized by in-phase contributions from the $2p_y$ atomic orbitals of the B and ipso C atoms which lie

† As a point of reference the calculated energies of the HOMO and LUMO for 1 are -8.711 and -5.878 eV, respectively.

perpendicular to the Fe-B π bond. In Figure 4 the calculated HOMO-3 and HOMO-9 are depicted.

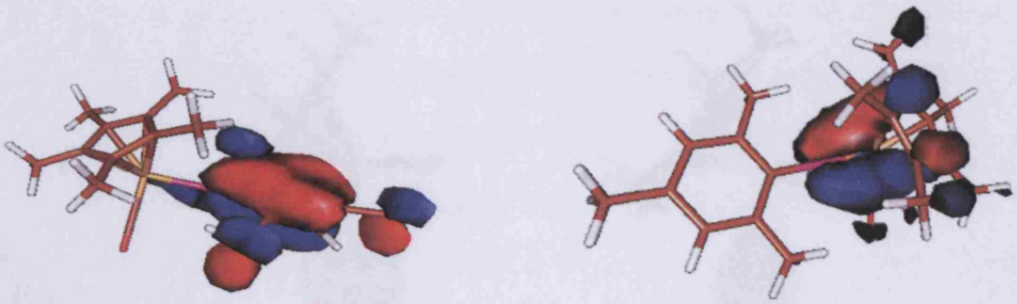

Figure 4 - HOMO-9 (left) and HOMO-3 (right) for [(η^5-C_5Me_5)Fe(CO)$_2$(BMes)]$^+$, showing the in-phase π interactions of the boron atom with adjacent carbon and iron centers.

Analyses of the corresponding molecular orbital descriptions for phosphine ligated complex 3, dimethylaminoborylene 7 and gallanediyl complex 10 allow some comments to be made concerning trends in the nature of the Fe-E bond. Thus, for example, replacement of the ancillary carbonyl ligands with phosphines leads to a greater contribution from the B $2p_x$ atomic orbital to the molecular orbitals of Fe-B π bonding character (12.2 % for 3, 8.0 % for 1). Conversely, significantly diminished contributions from the corresponding p_x orbital to the analogous Fe-E bonding MO are observed for the complexes containing $BNMe_2$ and GaMes ligands (3.8 and 3.4 %, respectively). Such observations conceivably reflect a reduced role for Fe→E back bonding for diyl ligands containing good π donor substituents, or featuring the heavier group 13 elements. A similar comparison of the isoelectronic cationic iron and neutral manganese systems [(η^5-C_5H_5)Fe(CO)$_2$(BMes)]$^+$ (2) and (η^5-C_5H_5)Mn(CO)$_2$(BMes) (11) is consistent with a more significant M-B π interaction for the neutral manganese complex. Thus, the predominant molecular orbital of M-B π bonding character has a greater B $2p_x$ contribution (8.9 % for 11, 7.1 % for 2) and the corresponding anti-bonding molecular orbital has greater metal $3d_{xz}$ character (10.9 % for 11, 10.0 % for 2).

In Figure 5, the π(B-F) bonding orbitals of [(η^5-C_5Me_5)Fe(CO)$_2$(BF)]$^+$ (8) are shown, as an illustrative example of the π interaction between the substituent X and boron, which is particularly strong in this case because of the π-basic behaviour of fluorine. These MOs lie very deep in energy (HOMO-17/HOMO-18); they consist of p(F) (44%) and p(B) (4%), both

along the x and y directions.

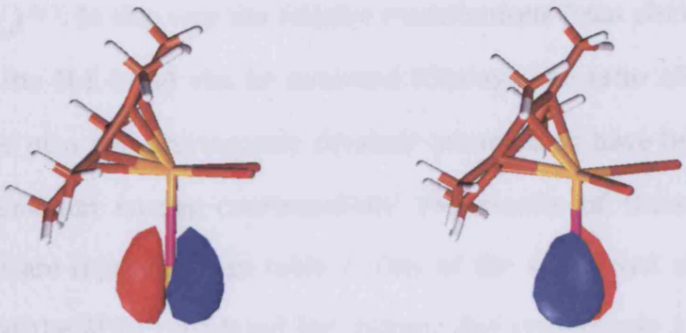

Figure 5 - π(B-F) MO pair in $[(\eta^5\text{-}C_5Me_5)Fe(CO)_2(BF)]^+$. The B-F bond is along the z-axis direction.

This justifies the weak Fe-B π interaction in 8 compared to the one in $[(\eta^5\text{-}C_5Me_5)Fe(CO)_2(BH)]^+$ (6), where the presence of an hydride substituent at boron rules out π stabilization by X in the fragment BX. As a consequence, the Fe-B bond length in 8 (1.835 Å) is longer than in 6 (1.776 Å), and the corresponding Fe-B π bond densities are consistent with the structural data (37.4% and 44.7% in 8 and 6 respectively).

(iii) Bond dissociation energies (BDEs) and energy partitioning scheme

(a) BDEs and analysis of the contributions to ΔE_{int}: As a further aid to the characterization of the M-E bond we have determined bond dissociation energies (D_o, BDEs) for the model compounds 1 - 13, that is the energy change associated with the cleavage reaction generating (independently optimised) metal and singlet diyl fragments:

$$[(\eta^5\text{-}C_5R_5)ML_2(EX)]^{n+} \rightarrow [(\eta^5\text{-}C_5R_5)ML_2]^{n+} + EX$$

In addition we have partitioned the instantaneous interaction energy (ΔE_{int}) between metal and diyl fragments[‡] into attractive terms relating to electrostatic (ΔE_{elstat}) and orbital

[‡] The instantaneous interaction energy, ΔE_{int}, differs from the BDE (D_o) in that it does not take into account the geometric and electronic relaxation that takes place in the isolated components following bond breakage. This relaxation is associated with the energy term ΔE_{prep} such that $-D_o = \Delta E_{int} + \Delta E_{prep}$ [(9)]. In this study values of ΔE_{prep} are calculated typically to be of the order of 3 - 6 kcal mol^{-1}.

components (ΔE_{orb}) and repulsive Pauli terms (ΔE_{Pauli}) in a manner analogous to that used previously in an analysis of charge neutral transition metal diyl and boryl systems ($\Delta E_{int} = \Delta E_{elstat} + \Delta E_{orb} + \Delta E_{Pauli}$)[9,11]. In this way the relative contributions from electrostatic and covalent (orbital) terms to the M-E bond can be assessed (through the ratio $\Delta E_{elstat}/\Delta E_{orb}$). Finally, the relative importance of σ and π symmetry covalent interactions have been assessed for each complex in its minimum energy conformation. The results of these analyses for model compounds 1 - 13 are reproduced in table 2. One of the significant observations based on this analysis is that the BDEs calculated for cationic diyl compounds 1 - 10 are significantly greater than those calculated for the dissociation of similar ligands from charge neutral metal complexes [9]. Thus BDEs of 147.5, 107.1 and 101.1 kcal mol^{-1} are calculated for the cationic boranediyl, allanediyl and gallanediyl complexes 1, 9 and 10, whereas Uddin and Frenking have reported values of 110.3, 73.2 and 61.0 kcal mol^{-1} for the dissociation of very similar EPh ligands from the most stable (axial) isomers of $(OC)_4FeEPh$ (E = B, Al, Ga, respectively)[9]. A comparison of the various components in the energy decomposition analyses for 1 and $(OC)_4FeBPh$ sheds some light on the underlying origins of this effect. The attractive electrostatic and orbital components for the two species are very similar (ΔE_{elstat} = -225.7 and -230.4; ΔE_{orb} = -153.6 and -156.5 kcal mol^{-1}, respectively) and differences in ΔE_{int} are chiefly as a result of the significantly smaller repulsive Pauli term for 1 [ΔE_{Pauli} = +228.2 and +276.6 kcal mol^{-1} for 1 and $(OC)_4FeBPh$, respectively]. The Pauli repulsion term arises from the fact that two electrons with the same spin cannot occupy the same region of space, and effectively corresponds to the four electron destabilizing interaction between two occupied orbitals. The fact that this repulsive term is ca. 50 kcal mol^{-1} smaller for complex 1 is presumably, at least in part, a reflection of its cationic charge (and changes in the degree of localization of that charge on going from reactants to products). Both the slightly longer Fe-B distance in the calculated minimum energy geometry (1.843 *vs* 1.803 Å) and the orbital contraction likely to result from the overall positive charge would be expected to lead to a reduced Pauli repulsive term for complex 1. Consistent with this, the value of ΔE_{Pauli} calculated for the *neutral* manganese complex 11 (which also features a reduced M-B distance of 1.811 Å) is significantly greater than that for isoelectonic cationic iron system 2 (245.1 vs. 221.4 kcal mol^{-1}).

The energy decomposition analyses for model complexes 1, 9 and 10 do, however, reveal several similarities with those reported for the corresponding charge neutral complexes $(OC)_4FeEPh$ (E = B, Al, Ga)[9]. Thus, for both sets of compounds, there is the expected fall in D_o with increasing mass of the group 13 element; the aluminium and gallium diyl complexes also contain significantly less ionic Fe-E interactions than their boron analogues. Thus, the ratio $\Delta E_{elstat}/\Delta E_{orb}$ falls from 1.47 for boranediyl complex 1 to 1.03 and 1.00 for allanediyl 9 and gallanediyl 10, respectively. The observation of a similar trend for $(OC)_4FeEPh$ ($\Delta E_{elstat}/\Delta E_{orb}$ = 1.47, 1.07 and 1.16 for E = B, Al and Ga, respectively) has been attributed to the particularly small magnitude of ΔE_{orb} for the boranediyl complex. This, in turn is thought to reflect the development of an antibonding interaction between the p_z donor orbital of the diyl ligand and the ring-shaped lobe of the Fe $3d_{z2}$ acceptor at short Fe-E distances[9]. The much shorter Fe-E bond length for E = B accentuates this effect for the boranediyl system. In the case of cationic complexes 1 and 9, the very similar absolute values of ΔE_{orb} and ΔE_{elstat} [compared to their neutral analogues $(OC)_4FeEPh$] testify to a similar breakdown of the Fe-B and Fe-Al attractive interactions to those reported by Uddin and Frenking[9]. For gallanediyl complex 10, however, there is a significant increase in the magnitude of the orbital contribution compared to $(OC)_4FeGaPh$ (ΔE_{orb} = -108.0 for 10 vs. -88.2 kcal mol^{-1}) while ΔE_{elstat} remains relatively unchanged (-108.0 vs. -102.3 kcal mol^{-1}). Thus, somewhat counter-intuitively, the electrostatic contribution to Fe-Ga bonding is relatively *less* important in cationic $[(\eta^5\text{-}C_5Me_5)Fe(CO)_2(GaMes)]^+$ than in charge neutral $(OC)_4FeGaPh$.

A similar analysis of the various components of the BDE can be used to compare the ligative properties of isoelectronic boron- and carbon-based ligands. Thus, for example, comparison of the cationic vinylidene-type complexes $[(\eta^5\text{-}C_5Me_5)Fe(CO)_2(CCMe_2)]^+$ (13) and $[(\eta^5\text{-}C_5Me_5)Fe(CO)_2(BNMe_2)]^+$ (7) reveals a markedly stronger metal ligand interaction in the case of the B/N species (125.9 vs. 114.8 kcal mol^{-1} for D_o). For each model complex the magnitudes of the Pauli and electrostatic terms are essentially equal (but of opposite sign) and the trend in D_o (or indeed in ΔE_{int}) effectively mirrors that in ΔE_{orb}. Thus, the magnitude of the orbital component for 7 is calculated to be some 12 kcal mol^{-1} greater than that for 13 (-131.0 *vs* -119.0 kcal mol^{-1}). In a similar fashion, the significantly enhanced binding of the BF ligand in

$[(\eta^5\text{-}C_5Me_5)Fe(CO)_2(BF)]^+$ (8) compared to the isoelectronic carbonyl ligand in $[(\eta^5\text{-}C_5Me_5)Fe(CO)_3]^+$ (12) (100.7 *vs* 75.5 kcal mol^{-1} for D_o) can largely be attributed to the markedly higher value for ΔE_{orb} (-121.0 *vs* -91.5 kcal mol^{-1}). Similar trends in the bond dissociation energies of CO, BF and BNH_2 ligands have previously been reported by Baerends, Hoffmann and co-workers for charge neutral metal complexes, although in common with arylborylene ligands, the absolute magnitudes of the binding energies are significantly smaller than for the cationic complexes reported here[23].

Further examination of the energy decomposition data probes the roles of the metal/ligand fragment and the diyl substituent in determining the nature of the M-E bond. Analysis of the data for 1, phosphine substituted 3, and aminoborylene 7 reveals that in each case the attractive ΔE_{elstat} and repulsive ΔE_{Pauli} terms very nearly cancel out (-225.7 and 228.2 for 1; -226.3 and 232.0 for 3; -193.9 and 196.2 kcal mol^{-1} for 7) and therefore variations in the overall BDE largely reflect changes in the orbital term ΔE_{orb}. Thus BDEs of 147.5, 153.0 and 125.9 kcal mol^{-1} mirror orbital contributions (ΔE_{orb}) of -153.6, -164.7 and -131.0 kcal mol^{-1}, respectively. Such variation in ΔE_{orb} reflects the expected trends in the σ and π properties of the BX ligand and the electronic properties of the metal centre (vide infra). Within this scheme, the calculated dissociation energy for hydridoborylene complex 6 is somewhat anomalous. Compared to mesitylborylene complex 1, a ca. 9.8 kcal mol^{-1} reduction in the overall binding energy is observed, despite a similar value for the ΔE_{elstat} component, and a nearly 10 kcal mol^{-1} enhancement of the orbital contribution. This result can be attributed to a 23.0 kcal mol^{-1} increase in the repulsive Pauli interaction, a factor which almost certainly relates to the much shorter equilibrium Fe-B distance (1.776 vs. 1.843 Å). A very similar argument holds for comparison of isoelectronic iron and manganese systems 2 and 11. Despite small increases in the attractive ΔE_{elstat} and ΔE_{orb} terms for 11, a 23.7 kcal mol^{-1} increase in the repulsive Pauli component is responsible for a lowering of the overall dissociation energy by 7.6 kcal mol^{-1}.

(b) Relative importance of the σ and π components of the orbital interaction: In general the relative contributions from σ and π symmetry covalent interactions to the M-E bond reflect the expected trends in the σ donor / π acceptor properties of the diyl ligand and in the

electronic properties of the metal/ligand fragment. Thus, in comparison to model complex 2, the significance of π back-bonding is enhanced for phosphine ligated 3 (44.8% of the orbital contribution to the bond *c.f.* 33.9 % for 2). The increased π component presumably reflects the absence of competing strongly π acidic carbonyl ligands, and more than compensates for the slight reduction in the absolute magnitude of the σ symmetry orbital component (such that the magnitude of ΔE_{orb} for 3 is 10.1 kcal mol^{-1} greater than that for 1). In a similar fashion, the importance of the π component is enhanced for the charge neutral manganese complex 11, to the extent that in this case it even exceeds the contribution from the σ symmetry component (54.0 *vs* 45.6 %).

Perfluorophenylborylene complex 4 is calculated to have an identical orbital contribution (ΔE_{orb}) to that of mesitylborylene 1 (-153.6 kcal mol^{-1}) with the differing bond population based σ/π breakdown (59.7 : 40.0 *vs* 62.2 : 37.5) presumably reflecting reduced σ donor and increased π acceptor properties for the perfluorinated borylene ligand. In a similar manner the increased value of ΔE_{orb} for BH-ligated 6 is a reflection of the markedly increased π acceptor properties of this ligand compared to BMes. Complexes 7 and 8, containing $BNMe_2$ and BF ligands, respectively, are both calculated to have similar σ/π breakdowns to the parent BMes complex 1. However, both 7 and 8 display markedly reduced overall magnitudes of ΔE_{orb} compared to BMes (-131.0 and -121.0 kcal mol^{-1}, respectively), reflecting the fact that these two ligands are both poorer σ donors *and* poorer π acceptors than BMes. A similar comparison can also be made between 7 and 8 and isoelectronic complexes 12 and 13 containing the carbon donor ligands CO and $CCMe_2$. In each case, the significantly higher BDE for the boron centred ligands can mainly be attributed to the larger magnitude of the ΔE_{orb} term. Given this, together with the fact that the σ:π ratio for the covalent bonding component does not alter markedly between isoelectronic B and C based systems, the clear implication, for these cationic systems at least, is that BF and $BNMe_2$ are both stronger σ donors *and* stronger π acceptors than CO and $CCMe_2$, respectively. Previous computational studies for charge neutral metal complexes have predicted stronger σ donor properties for BX (X = F, NH_2, NMe_2), compared to CO. This has been attributed to the higher energy of the σ donor HOMO orbital and its greater localization on the donor atom for the boron-based

ligands[23,4a,4b]. In addition, BF has previously been reported to be a slightly better π acceptor than CO, again largely due to the greater localization of the LUMO on the more electropositive atom. Similarly, a comparison of the free ligands BNH_2 and CCH_2 reported by Bickelhaupt, Hoffmann and Baerends, revealed a greater localization of the HOMO (σ donor) and LUMO (π acceptor) orbitals on the donor atom in the case of BNH_2.

Among the more intriguing findings from this study is not only that the ΔE_{orb} contribution to the M-E bond becomes proportionally more important for the heavier group 13 elements, but also that relatively minor changes in the σ:π ratio are observed on going from BMes to AlMes and GaMes ligands. Thus, bond population analyses for 1, 9 and 10 yield π contributions of 37.5, 30.8 and 32.8%, respectively. This finding contrasts markedly with the rapid fall-off in the π contribution to the Fe-E bond calculated for $(OC)_4FeEPh$ based on energy decomposition analyses (33.4, 18.0 and 17.2% for E = B, Al and Ga, respectively)[9]. Intriguingly, however, our results are more in line with those derived from charge decomposition analyses of $(OC)_4FeEPh$ reported by Boehme, Uddin and Frenking[24]. This study revealed back-bonding components equal to 47.8, 45.6 and 40.8% for E = B, Al and Ga, respectively. In order to compare directly our bond population σ/π analysis with the energy decomposition and CDA approaches examined by Frenking, we examined the Fe-E bonds in the reference compounds $(OC)_4FeEPh$ (E = B, Al and Ga) by our method. These analyses yielded π contributions of 45.6, 39.5 and 52.0%, respectively. As such, both the absolute magnitude and trends in π bonding as a function of E are more closely related to the results of CDA, rather than energy-based decomposition analyses.

(iv) Rotational profile for complex 1

Previous reports of DFT-based analyses for the crystallographically characterized half-sandwich complex $(\eta^5\text{-}C_5H_5)V(CO)_3BN(SiMe_3)_2$ and the model species $(\eta^5\text{-}C_5H_5)V(CO)_3BNH_2$ have revealed that the orientation of the BNR_2 ligand is influenced both by steric and electronic factors[14]. Thus, for the 'parent' BNH_2 complex a torsion angle θ (∠ centroid-V-N-H) of 90° is calculated for the lowest energy conformer, with that corresponding to θ = 0° being ca. 2.2

kcal mol^{-1} higher in energy. For the sterically more demanding $BN(SiMe_3)_2$ ligand, both DFT optimized and crystallographically determined minimum energy structures feature $\theta \approx 12°$, with the $\theta = 90°$ rotamer being ca. 4.5 kcal mol^{-1} higher in energy.[14] The spatial arrangement achieved at $\theta \approx 12°$ is thought to minimize steric interactions between the silyl methyl substituents and the metal-bound carbonyl ligands. Although energetic barriers to rotation in half-sandwich borylene complexes such as 1 and $(\eta^5\text{-}C_5H_5)V(CO)_3BNR_2$ do not correlate directly with the strength of M→B π backbonding we were interested in determining the energetic preferences for different orientations of the BMes ligand. To this end an energetic profile was calculated for rotation about the Fe-B-C_{ipso} axis, which is reproduced in Figure 6.

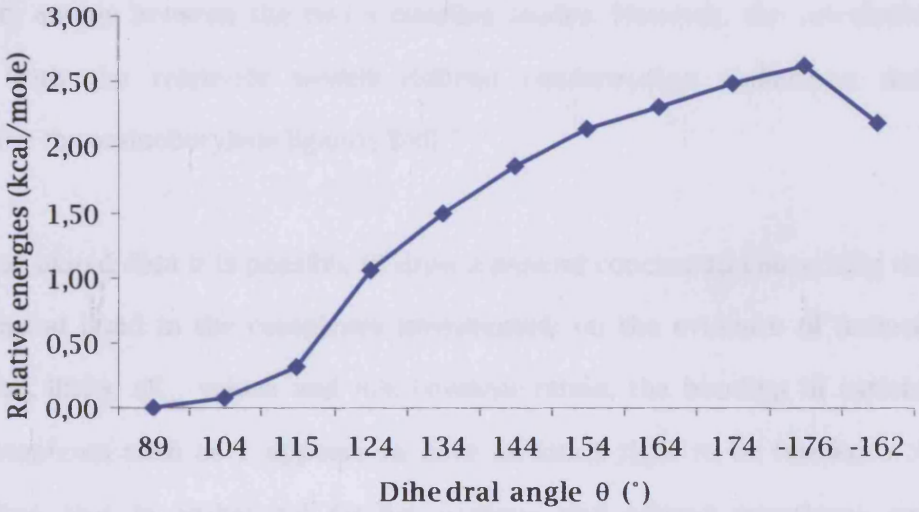

$\Delta E_{rot} = 2.62$ kcal/mole

Figure 6 – Rotational profile for $[(\eta^5\text{-}C_5Me_5)Fe(CO)_2(BMes)]^+$

The lowest energy conformation is calculated to be that corresponding to $\theta = 89°$ (by ADF) or 75.7° (by Gaussian03) i.e. an approximately horizontal orientation. The small discrepancy between the values calculated by the two different methods can be rationalized in terms of the relatively shallow energy profile in the region $60 < \theta < 80°$ (*vide infra*). Both figures are in good agreement with values of 83.0(3) and 84.0(3) determined for the two crystallographically distinct molecules in the asymmetric unit of solid $[(\eta^5\text{-}C_5Me_5)Fe(CO)_2(BMes)][BAr^f_4]$ [7], and can be rationalized both on electronic and steric grounds. The horizontal orientation of the BMes ligand not only minimizes the predominant steric

interaction *i.e.* that between the methyl groups of the (η^5-C_5Me_5) and Mes substituents, but also provides for π donation into the vacant (non mesityl-conjugated) boron 2p orbital from the HOMO of the $[(\eta^5\text{-}C_5Me_5)Fe(CO)_2]^+$ fragment. Hoffmann and co-workers have previously demonstrated that π donation from this a" symmetry orbital (to which the Fe $3d_{xz}$ is a significant contributor, see Figure 2 in this chapter and Figure 5 in chapter 3) is more efficient than that from the perpendicular HOMO-2 of a' symmetry (featuring Fe $3d_{yz}$)[13]. The presence of perpendicular π donor orbitals at the metal centre implies that *some degree of π bonding will be maintained throughout the rotation of the borylene ligand.* For this reason, the barrier to rotation about the Fe-B-C_{ipso} axis is very low (ca. 2.6 kcal mol^{-1}), and as previously stated, offers no real indication of the Fe=B π bond strength, since it is simply the difference in energy between the two π bonding modes. However, the calculated barrier is consistent with the relatively weakly defined conformation preference demonstrated previously for the aminoborylene ligands BNR_2[25].

Given the calculated data it is possible to draw a general conclusion concerning the nature of the metal-ligand bond in the complexes investigated: on the evidence of molecular orbital compositions, BDEs, ΔE_{orb} values and σ/π covalent ratios, the bonding in cationic terminal borylene complexes such as 1 appears to have as much right to be termed a M=E double bond as does that in archetypal Fischer carbene and related complexes such as $[(\eta^5\text{-}C_5R_5)Fe(CO)_2(CCMe_2)]^+$ and $[(\eta^5\text{-}C_5R_5)Fe(CO)_2(CH_2)]^+$. Thus, a bond description solely in terms of donor-acceptor interaction ($RE\rightarrow ML_n$) as the one found in $(CO)_4Fe\rightarrow B(\eta^5\text{-}C_5Me_5)$[16c] is not appropriate.

5.3.2 - A "naked" gallium complex: $[Fp^*_2Ga]^+$

Theoretical bond analysis of compound 14 complements the information coming from crystallographic and spectroscopic experiments, providing additional insight into the nature of the transition metal-gallium bond, a subject of considerable debate in recent years[26]. The nature of the interaction between the ligand and the metal centre in diyl systems $[L_nM(ER)]$, such as $(OC)_4Fe(GaAr)$ [Ar = $C_6H_3(2,4,6\text{-}^iPr_3C_6H_2)_2$-2,6] is a famous example. The description of

superficially similar complexes as being bound via multiple bonds (e.g. $L_nM{=}ER$ or $L_nM{\equiv}ER$) or via donor/acceptor interactions (e.g. $L_nM{\leftarrow}ER$) reflects not only the fundamental questions of structure and bonding posed by such systems, but also the scarcity of structural data available. Although several recent theoretical studies have sought to characterize the metal - group 13 element bond by quantifying its various components[9], experimental validation of these results has been hindered by the paucity of available synthetic routes. Extension of the halide abstraction technique (previously applied by this research group on boryl complexes) to gallium derivatives opens a new route to the preparation of *cationic* unsatured gallium systems such as 14.

(i) - Molecular geometry

The fully optimised geometry [*d*(Fe-Ga) = 2.338, 2.337 Å; ∠(Fe-Ga-Fe) = 177.9°, ∠(Ct-Fe-Fe-Ct) = 86.5°] is consistent with that determined crystallographically (see Table 3). The linear Fe-Ga-Fe unit [∠ Fe(1)-Ga(1)-Fe(1') = 178.99(2)°] is consistent with a two-coordinate gallium centre engaging in no significant secondary interactions (e.g. with the anion)[27]. This geometry is consistent with that found in the only other complex containing a 'naked' bridging gallium atom (*i.e.* $[(\eta^5\text{-}C_5Me_5)Fe(dppe)]Ga[Fe(CO)_4]$[28]) and contrasts with the bent geometry found in base-stabilised analogues[29], such as $[Fp_2Ga{\cdot}bpy]^+$, where *d*(Fe-Ga) = 2.397 Å and ∠(Fe-Ga-Fe) = 132.8°.

(ii) - Molecular orbital compositions

The calculated HOMO and LUMO energies for 14 are -7.944 and -5.627eV respectively, and they are mainly of σ(Fe-Ga-Fe) character, with significant contributions from p_z or s atomic orbitals on gallium and p_z or d_{z2} atomic orbitals on iron. Another deep-lying σ(Fe-Ga-Fe) MO is HOMO -17 [Figure 7; E=-11.604 eV; 45.38% s(Ga), 7.14% d_{z2}(Fe(1)), 7.11% d_{z2} (Fe(2))].

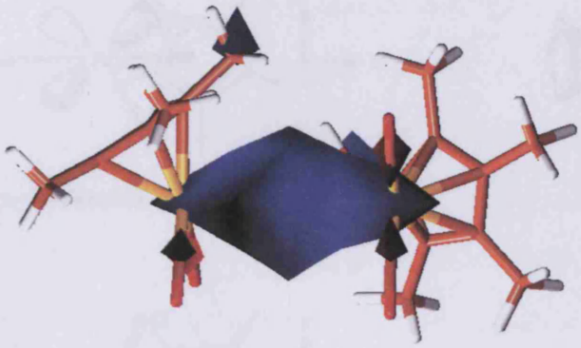

Figure 7 - σ(Fe-Ga-Fe) (orbital HOMO -17) of 14

The (Fe-Ga-Fe) π system consists of *pairs* of nearly *degenerate* orbitals, with components that are both of x and y type. They do *not* possess exactly the same energy because ∠(Fe-Ga-Fe) is *not* exactly 180°. The mixing of x and y coordinates is necessary to achieve optimal stabilization via *simultaneous overlap* of the central gallium atomic orbitals with *both* iron fragments orbitals, which are mutually perpendicular to each other (as shown by the torsion angle close to 90°), as depicted in Figure 8. The resulting molecular orbital is "twisted" around the Fe-Ga-Fe axis, and it is shown in Figure 9. π(Fe-Ga-Fe) are the pair HOMO-5 and HOMO-6 [mean E= -8.9 eV; overall 35% of d(Fe) and 3% p(Ga) components], while π*(Fe-Ga-Fe) are represented by LUMO+1 and LUMO+2 [mean E= -5.2 eV; overall 25% of d(Fe) and 15% p(Ga) components]. While π has very little contribution from gallium, π* is more expanded on the gallium atom (higher percentage of Ga AOs). Finally, σ*(Fe-Ga-Fe) lies at E= -2.5eV, being LUMO+18.

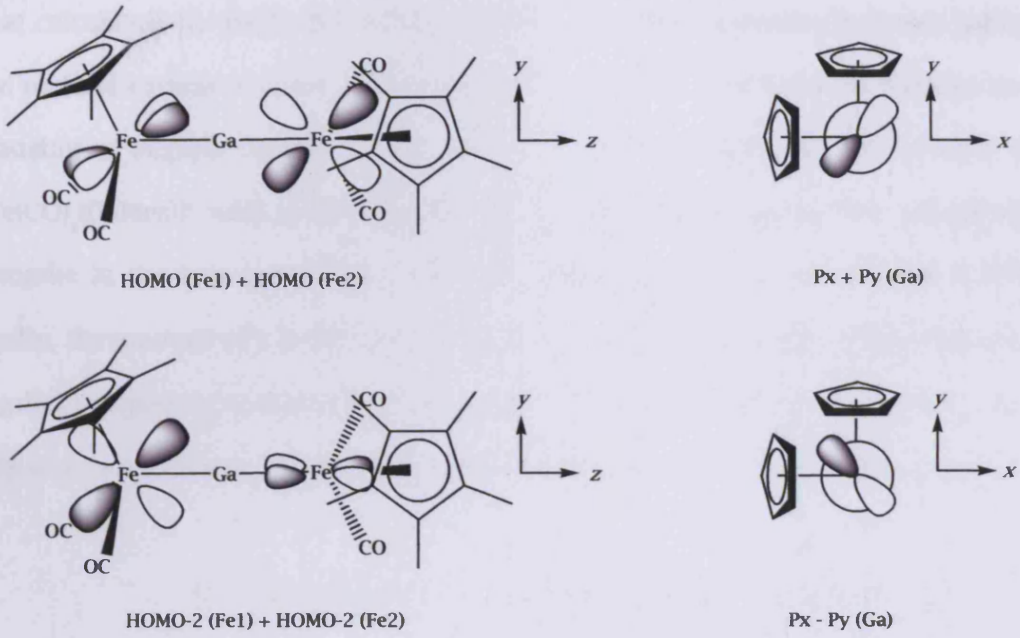

Figure 8 - Mixing of x and y components of the Fe-Ga-Fe π system of 14, generating the "π_x" and "π_y" pair

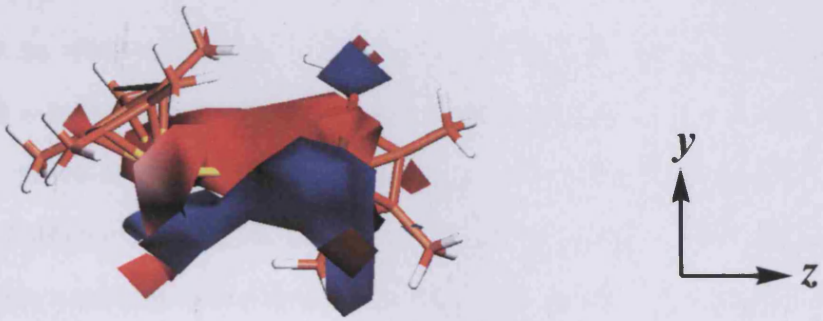

Figure 9 - One of the π(Fe-Ga-Fe) molecular orbitals of 14

(iii) - Bond partitioning analysis

A bond population analysis was carried out to quantify the relative importance of σ and π components to the Fe-Ga covalent interaction using the same method previously applied to the borylene systems described in section 5.3.1 and to boryl complexes of the type $(\eta^5\text{-}C_5R_5)Fe(CO)_2(BX_2)$[11]. This reveals a 61:38 σ:π breakdown of the covalent Fe-Ga interaction {*c.f.* 86:14 for the Fe-Ga single bond in the model compound $(\eta^5\text{-}C_5H_5)Fe(CO)_2GaCl_2$ and a 66:33 breakdown for $[(\eta^5\text{-}C_5Me_5)Fe(CO)_2(GaMes)]^+$}[11,30]. The π component in 14 is slightly higher even

than that calculated for $[(\eta^5\text{-}C_5Me_5)Fe(CO)_2(GaMes)]^+$. The "p-p" π overlap between gallium and the *ipso* mesityl carbon is more pronounced than the "d-p" one between gallium and iron, thus causing a slightly smaller π interaction of gallium with the iron center in $[(\eta^5\text{-}C_5Me_5)Fe(CO)_2(GaMes)]^+$ with respect to 14. This is also confirmed by the calculated Fe-Ga bond lengths in the two cases {*c.f.* 2.309 Å for $[(\eta^5\text{-}C_5Me_5)Fe(CO)_2(GaMes)]^+$ and 2.269 Å for 14}. Finally, the amount of π Fe-Ga bond density in 14 is obviously higher than the one found in the gallyl complex $(\eta^5\text{-}C_5H_5)Fe(CO)_2GaCl_2$, where the Fe-Ga bond σ component is prevalent (partially due to the strong stabilisation of gallium offered by the π-basic chlorine atoms).

5.3.3. - Gallium carbenes of first row transition metals

Anionic gallium compounds of general formula $[:GaX_2]^-$ are isoelectronic with the well-known neutral carbenes $[:CX_2]$. Since the discovery of the first thermally stable N-heterocyclic carbene in 1991[31], this class of ligand has become ubiquitous in the formation of d-block metal complexes[32]. While "Arduengo-type" carbenes are experimentally well established for the group 14 elements carbon, silicon and germanium[33], the isoelectronic anionic species containing a group 13 element are much less common, due in part to the lack of suitable synthetic routes that can provide good yields. Previous theoretical work[34] on the ligand $[E(NH\text{-}CH)_2]^-$ (Figure 10, E=B, Al, Ga, In) has shown that, apart from the case of boron (where 1,2-hydrogen rearrangements occur), all the other group 13 element heterocyclic carbenes should be stable with respect to hydrogen rearrangements, and with a positive charge localised on E (apart from the case E=B), despite the formal overall negative charge of the molecule. In fact, this excess of electron density is *localised* on the more electronegative neighbouring nitrogen atoms.

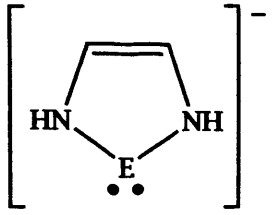

Figure 10 - Model compound for a group 13 element N-heterocyclic carbene

The frontier orbitals of this ligand consist of an a_1 symmetry sp-hybridised HOMO on E plus a b_1 symmetry LUMO made of all the π-system perpendicular to the ring plane (p_z orbitals, if we assume that the ring plane is the xy plane). The HOMO shape (similar to that found in the ordinary N-heterocyclic carbenes) accounts for the strong σ-donor properties of carbenes as ligands in coordination chemistry, while their LUMOs can engage in additional π backbonding interactions with suitable symmetry orbitals on the metal centre.

After the discovery of a facile synthesis of the gallium(I) carbene analogue $[:Ga\{N(Ar)C(H)\}_2]^-$ (Ar=2,6-diisopropylphenyl) by Jones *et al.* in 2002[35], this ligand (as its potassium salt) has been extensively used to prepare transition metal derivatives with several first row elements. Previous DFT studies on iron and nickel complexes[6] based on the charge decomposition analysis (CDA) of Uddin and Frenking[36] have confirmed this hypothesis: the calculated ratio of the two parameters *d* and *b* (which quantify the extent of σ donation and π back-donation respectively) for gallium carbene species (3.40) is essentially identical to the one related to the ordinary carbenes (3.39), thus revealing the analogy between the two systems. Furthermore, these values are much higher than the one found for the carbonyl ligand (1.75), an indication of the prevalence of σ-donation over π-back donation in carbenes compared to carbonyls.

The bond density partitioning approach already used for borylene systems has been applied to five different gallium carbene complexes, to compare the relative contributions from σ and π M-Ga bond densities. The aim is to quantify the extent of π-backbonding M→Ga in each case. Within ADF, due to the large system sizes, the basis set used in this section is DZP (frozen core 1s) only for the lighter atoms (C, H, N, O), while a TZ2P is used for the metal and gallium atoms (both with frozen core 3p).

(i) - Molecular geometry

In all cases the calculated bond lengths and angles are consistent with the experimental ones, as shown in Tables 4-6. The structures of reference are the corresponding $[K(TMEDA)]^+$ salts. The slight overestimation in bond lengths and angles is intrinsic in the computational

method used, as already seen for similar studies[4d,12] and in section 5.3.1. The M-Ga distance is always *smaller* than the sum of the atomic radii, thus indicating some π character of the bond. In addition, this difference increases in going from vanadium to nickel; the extent of π back-donation is higher for the more electron-rich late transition elements. Table 7 collects all the numeric values related to this discussion.

Table 7 - Comparison of geometrical parameters for complexes 15-19

	Σ(atomic radii) / Å	Calc. d(M-Ga) / Å	Δ(%)[a]
V (18)	2.60	2.55	1.9
Mn (17)	2.62	2.40	8.4
Fe (16)	2.51	2.40	4.4
Co (19)	2.50	2.30	8
Ni (15)	2.50	2.27	9.2

[a] Δ has been calculated as {[Σ(atomic radii) - d(M-Ga)]/ Σ(atomic radii)} x 100

If Δ is taken as a parameter to quantify the extent of π bonding M-Ga, the expected trend for complexes 17-19 is observed: the more carbonyl ligands there are, the weaker the π interaction M-Ga is, because of the competition between the gallium carbene and CO as π acceptors. In the case of 15, where no carbonyls are present, the amount of M-Ga π bond density is the highest as possible, while the value for 16 is somehow anomalous. The carbonyl ligands are strong π-acids: they withdraw electron density from the metal center, therefore reducing the extent of π interaction metal-gallium. In complex 16 the Fe-CO axial calculated bond length (1.81Å) is shorter than the Fe-CO equatorial ones (1.83Å). This implies a more extended π character of that M-C bond, due to the excess of electron density on the iron center, provided by the strong σ-donor gallium carbene ligand *trans* to it. In the experimental structure, the observed trend is *opposite* to the calculated one: this is due to an additional interaction of the counterion $[K(TMEDA)]^+$ with the oxygen atom of one of the

equatorial CO groups (d(K-O)=2.626 Å). This interaction is totally neglected in the theoretical calculation, because no counterion is considered.

As already noticed for the boryl neutral analogues (section 3.3.2), the range of torsion angles Cp(centroid)-M-Ga-N displayed in complexes 15-19 is wide, going from 21° (for complex 17) to 54° for complex 15. The same kind of explanation can also be used in here: the final value is determined mainly by steric factors and crystal packing forces. There is a quite good agreement between experimental and calculated values in all cases except from complex 18, where the torsion in the real molecule (31.3°) is much more pronounced than that of the model (20.7°). This may be due to additional interactions between the potassium cation and the π system of one phenyl group on the carbene ligand (mean d(K-C)=3.15 Å). Such an interaction forces the ligand in a specific conformation, while in the calculated structure it is not taken into account. In 15, the much bigger angle found with respect to the other complexes is probably deriving from an "extra-hindrance" of two gallium carbene ligands on the same metal center.

(ii) - Molecular orbital composition

The MO scheme follows a similar pattern in all cases. The cobalt complex 19 will be taken as an example for the discussion. It consists of a deep lying σ(M-Ga) orbital, derived from overlap of the p_z orbitals on gallium and d_{z2} and p_z orbitals on the metal. Depicted in Figure 11 is the HOMO -5 of 19 which has the following composition: 10.15% 4s(Ga), 10% $4p_z$(Ga), 5.51% $3d_{z2}$(Co), 5.12% $3p_z$(Co), 2.96% 4s(Co).

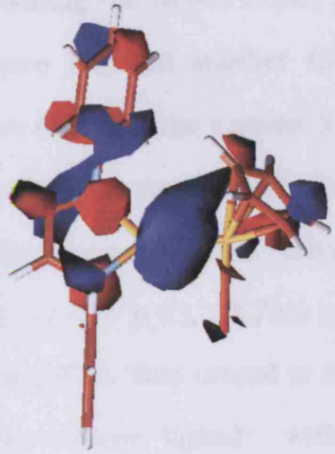

Figure 11 - σ(Co-Ga) (HOMO -5) of the cobalt complex [(Cp)Co(CO)(GaX$_2$)]$^-$ (19). View along the x axis, perpendicular to the carbene ligand plane.

The z axis is set to be coincident with the Co-Ga bond direction, but both the Cp(centroid)-Co and the Co-CO bonds are *not* aligned along the Cartesian x and y axes, because of the angles Cp(centroid)-Co-Ga (130°) and OC-Co-Ga (93°) (Figure 12).

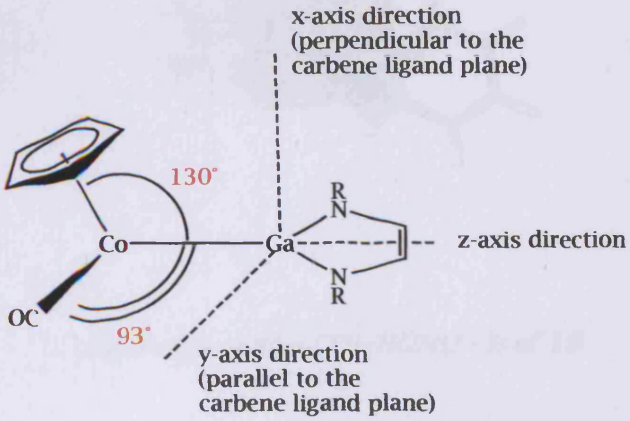

Figure 12 - Relative orientation of the substituents on cobalt in complex 19 with respect to the Cartesian axes

Thus, d orbitals on the metal centre have to *mix* to form an orbital of suitable symmetry to overlap with the p_x/p_y set on the ligand atoms. This justifies the contributions of *several* d orbitals on the metal centre, and the presence of *both* x and y components in the π MOs.

Moving to higher energies, approaching the HOMO-LUMO region, it is possible to identify a π*(Co-CO) orbital (HOMO -3, Figure 13), and another MO of the same symmetry that is formed by the overlap of the p_x set of the of the carbene ligand atoms with d orbitals on the metal centre, thus creating a extended π system M-Ga-N-C (Figure 14). It is bonding N-Ga-Co, but with a nodal plane between the nitrogen and the carbon atoms of the carbene backbone. Its composition is the following: 11.84% p_x(C), 11.79% p_x(N), 10.71% p_x(Ga), 9.72% d_{yz}(Co), 2.05% d_{xy}(Co), 1.78% d_{x2-y2}(Co), 1.1% p_y(Co). This orbital is ideally derived from the overlap of the *empty* LUMO of the gallium carbene ligand[34] with a full "mainly d-type" metallic fragment atomic orbital. Interestingly, in the complex this MO is *full*, thus proving the presence of a M→Ga electronic back-donation.

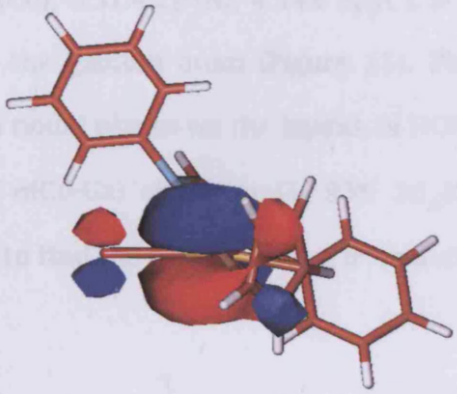

Figure 13 - π(Co-CO) (HOMO -3) of 19*

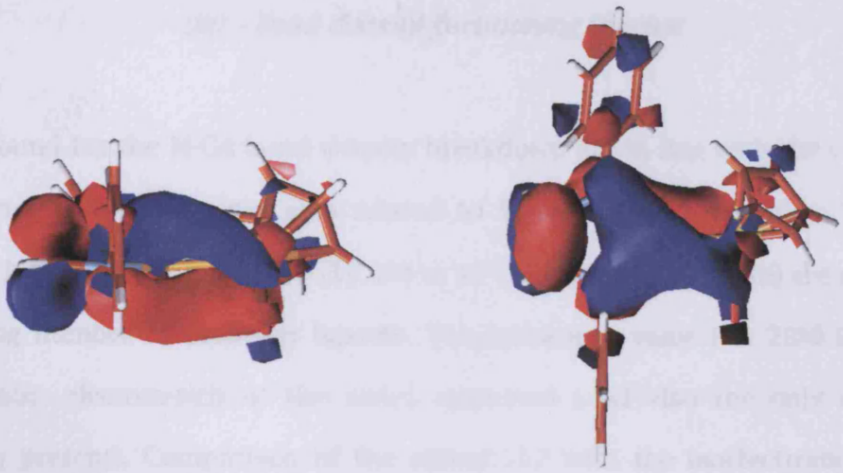

Figure 14 - HOMO -2 of 19: a delocalised Co-carbene π system. Views along the y and x axes respectively. Notice the nodal plane between nitrogens and carbons on the ligand backbone.

The HOMO is again of π symmetry, but in this case there are no contributions on gallium: 30.24% $3d_{yz}$(Co), 13.53% $3d_{xz}$(Co), 6.51% $2p_x$(N), 4.54% $2p_x$(C). It has *two* nodal planes, one of which is exactly containing the gallium atom (Figure 15). The corresponding "completely bonding" π-type MO, with no nodal planes on the ligand, is HOMO - 14, being at much lower energy. LUMO is mainly of σ(Co-Ga) character (17.95% $3d_{z2}$(Co), 12.66% 4s(Ga)), while at higher energies it is possible to find the corresponding σ* and π*(M-Ga) counterparts.

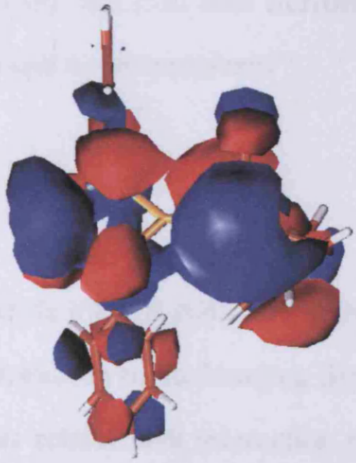

Figure 15 - HOMO of 19. View along the x-axis, perpendicular to the gallium carbene plane.

(iii) - Bond density partitioning scheme

The results found for the M-Ga bond density breakdown are in line with the calculated bond lengths: shorter M-Ga bonds are also related to higher π bond densities. The increasing values of the latters in going from 18 (12.5%) to 17 (18.2%) and 19 (26.8%) are consistent with the decreasing number of carbonyl ligands. The maximum value (ca. 28%) is reported for nickel, the most electron-rich of the series examined (and also the only case where no carbonyls are present). Comparison of the anionic 17 with the isoelectronic neutral gallyl complex $(\eta^5\text{-}C_5H_5)Fe(CO)_2[Ga(OCH)_2]$[37] reveals that the extent of π bond density is higher for the anionic system {18.2% vs. 14.6% found for $(\eta^5\text{-}C_5H_5)Fe(CO)_2[Ga(OCH)_2]$}. As a further confirmation, the calculated Mn-Ga bond length in 17 (2.396 Å) is also smaller than the Fe-Ga one found in $(\eta^5\text{-}C_5H_5)Fe(CO)_2[Ga(OCH)_2]$ (2.434 Å). The presence of a negative charge decreases the HOMO-LUMO gap between the two fragments $[(\eta^5\text{-}C_5H_5)M(CO)_2]$ and $[GaX_2]$, thus raising the extent of π overlap of FMOs of suitable symmetry (higher values for the overlap integrals S_{ij}). Fascinatingly, the Mulliken charges calculated for complexes 17, 18 and 19 are *positive* for the metal centre: +0.2e, +0.5e and +0.9e for Mn, V and Co respectively. In these species the excess of electron density is localised on the nitrogen atoms of the ligand and on the oxygens of the carbonyls. In complexes 15 and 16 the metal is negatively charged: -0.02 and -0.03e for Ni and Fe respectively, the iron case mirroring the results coming from the Mulliken analyisis on the isostructural boryl complexes[11].

5.4 - Conclusions

The DFT analysis of the cationic diyls $[(\eta^5\text{-}C_5R_5)M(L)_2(EX)]^+$ gives a picture of the M=B bond as a [σ+π] double bond, with a π contribution to the bonding density that depends on the nature of R, L and X. In theory, the most robust M=B interaction should occur in the species $[(\eta^5\text{-}C_5Me_5)Fe(PMe_3)_2{=}B(H)]^+$, where the strong phosphine σ donors on iron and the absence of any π interaction between boron and hydrogen simultaneously raise the Fe-B π bond density. Nevertheless, from an experimental point of view, the insignificant steric hindrance offered by the hydride ligand on boron would likely render it highly labile; the steric and electronic

protection afforded by substituents such as Mes and NMe_2 make these synthetically more viable targets.

Aluminium and gallium, like boron, can form bonds to transition metals with appreciable π character, and the use of the same kind of theoretical approach leads to a comparison of the different group 13 donors. Thus the π bond density in complex 14 is of the same order of magnitude of that found for terminal borylenes. In the case of gallium carbenes, the extent of π density M-Ga strongly depends on the number of "competitive" carbonyl ligands on the metal fragment and hence on the d electron availability of the metal itself. Thus, higher π contributions are found for cobalt and nickel in complexes 15 and 19 respectively, even if the absolute values are smaller that those reported for borylenes or 14. In gallium carbenes the M-Ga bond is mainly of σ character (and these ligands are strong σ donors more than π acceptors).

(1) See, for example: (a) Nugent W.A. and Mayer J.M., in *Metal Ligand Multiple Bonds*, Wiley Interscience, New York, 1988; (b) Hendon J.W., *Coord. Chem. Rev.*, 2003, 243, 3. For terminally bound diyl complexes featuring the heavier group 13 elements see, for example: (c) Dohmeier C., Loos D. and Schnöckel H., *Angew. Chem., Int. Ed.*, 1996, 35, 127; (d) Weiss J., Stetzkamp D., Nuber B., Fischer R.A., Boehme C. and Frenking G., *Angew. Chem., Int. Ed.*, 1997, 36, 70; (e) Haubrich S.T. and Power P.P., *J. Am. Chem. Soc.*, 1998, 120, 2202; (f) Jutzi P., Neumann B., Reumann G., Schebaum L.O., and Stammler H.G., *Organometallics*, 1999, 18, 2550; (g) Fischer R.A. and Weiß J., *Angew. Chem., Int. Ed.*, 1999, 38, 2830; (h) Uhl W., Benter M., Melle S., Saak W., Frenking G. and Uddin J., *Organometallics*, 1999, 18, 3778; (i) Linti G. and Schnöckel H., *Coord. Chem. Rev.*, 2000, 206-207, 285; (j) Ueno K., Watanabe T., Tobita H. and Ogino H., *Organometallics*, 2003, 22, 4375.

(2) See, for example: (a) Weidenbruch M., Stilter A., Peters K. and von Schnering H.G., *Chem. Ber.*, 1996, 129, 1565; (b) Grumbine S.K., Mitchell G.P., Straus D.A., Tilley T.D. and Rheingold A., *Organometallics*, 1998, 17, 5607; (c) Mitchell G.P. and Tilley T.D., *J. Am. Chem. Soc.*, 1998, 120, 7635; (d) Mitchell G.P. and Tilley T.D., *Angew. Chem., Int. Ed.*, 1998, 37, 2524; (e) Wanandi P.W., Glaser P.B. and Tilley T.D., *J. Am. Chem. Soc.*, 2000, 122, 972; (f) Mork B.V. and Tilley T.D., *J. Am. Chem. Soc.*, 2001, 123, 9702; (g) Klei S.R., Tilley T.D. and Bergman R.G., *Organometallics*, 2002, 21, 4648; (h) Okazaki M., Tobita H. and Ogino H., *Dalton Trans.* 2003, 493; (i) Glaser P.B., Wanandi P.W. and Tilley T.D., *Organometallics*, 2004, 23, 693; (j) Chapter 2, reference (13).

(3) Chapter 1, references (29c), (32), (33), (36) and (37).

(4) (a) Bickelhaupt F.M., Radius U., Ehlers A.W., Hoffmann R. and Baerends E.J., *New J. Chem.*, 1998, 26, 1; (b) Radius U., Bickelhaupt F.M., Ehlers A.W., Goldberg N. and Hoffmann R., *Inorg. Chem.*, 1998, 37, 1080; (c) Uddin J., Boehme C. and Frenking G., *Organometallics*, 2000, 19, 571; (d) Frenking G. and Fröhlich N., *Chem. Rev.*, 2000, 100, 717; (e) Chen Y. and Frenking G., *Dalton Trans.* 2001, 434; (f) Bollwein T., Brothers P.J., Hermann H.L. and Schwertfeger P., *Organometallics*, 2002, 21, 5236; (g) Chapter 1, references (46), (47) and (52).

(5) Bunn N.R., Aldridge S., Coombs D.L., Rossin A., Willock D.J., Jones C., Ooi L., *Chem. Comm.* 2004, 1732.

(6) (a) Baker R.J., Jones C., Platts J.A., *J. Am. Chem. Soc.* 2003, 125, 10534; (b) Baker R.J., Jones C., Platts J.A., *Dalton Trans.*, 2003, 3673.

(7) Chapter 1, reference (34).

(8) Chapter 3, reference (17).

(9) Uddin J., Frenking G., *J. Am. Chem. Soc.*, 2001, 123, 1683.

(10) Metrical data for $[(\eta^5\text{-}C_5Me_5)Fe(CO)_3]^+$ (12') are taken from the crystal structure of $[(\eta^5\text{-}C_5Me_5)Fe(CO)_3][BAr'_4]$. Brief details of the structure of this cation (as the $[BF_4]^-$ salt) have previously been communicated: McArdle P., MacHale D., Cunningham D., Manning A.R., *J. Organomet. Chem.*, 1991, 419, C18.

(11) Chapter 1, reference (49).

(12) (a) Macdonald C.L.B., Cowley A.H., *J. Am. Chem. Soc.*, 1999, 121, 12113; (b) chapter 1, reference (48).

(13) Schilling B.E.R., Hoffmann R., Lichtenberger D., *J. Am. Chem. Soc.*, 1979, 101, 585.

(14) Chapter 1, reference (36).

(15) Chapter 3, reference (14).

(16) (a) Chapter 1, reference (6); (b) Chapter 1, reference (9); (c) Chapter 1, reference (32).

(17) (a) Crespi A.M. and Shriver D.F., *Organometallics*, 1985, 4, 1830; (b) Hill R.O., Marais C.F., Moss J.R. and Naidoo K.J., *J. Organomet. Chem.*, 1999, 587, 28.

(18) (a) Chapter 1, reference (38); (b) reference (2b) of this chapter.

(19) (a) Gress M.E. and Jacobsen R.A., *Inorg. Chem.*, 1973, 12, 1746; (b) Fitzpatrick P.J., Le Page Y., Sedman J. and Butler I.S., *Inorg. Chem.*, 1981, 20, 2852.

(20) Downs A.J. in *Chemistry of Aluminium, Gallium, Indium and Thallium*, ed. A.J. Downs, Blackie, London (1993).

(21) (a) Yamaguchi T., Ueno K. and Ogino H., *Organometallics*, 2001, 20, 501; (b) He X., Bartlett R.A. and Power P.P., *Organometallics*, 1994, 13, 548.

(22) Stowasser R., Hoffmann R., *J. Am. Chem. Soc.*, 1999, 121, 3414.

(23) Chapter 1, reference (47).

(24) Chapter 1, reference (46).

(25) Chapter 1, reference (33).

(26) Chapter 1, references (49) and (50).

(27) Wehmschulte R.J., Steele J.M., Young J.D. and Khan M.A., *J. Am. Chem. Soc.*, 2003, 125, 1470.

(28) (a) Chapter 1, reference (49); (b) Ueno K., Watanabe T., Tobita H. and Ogino H., *Organometallics*, 2003, 22, 4375.

(29) (a) Ueno K., Watanabe T. and Ogino H., *Appl. Organomet. Chem.*, 2003, 17, 403; (b) Ueno K., Watanabe T. and Ogino H., *Organometallics*, 2000, 19, 5679.

(30) Refer to this chapter, section 5.3.1.

(31) Arduengo A.J. III, Harlow R.L., Kline M., *J. Am. Chem. Soc.* 1991, 113, 361.

(32) See, for example: (a) Herrmann W.A., *Angew. Chem., Int. Ed.*, 2002, 41, 1291; (b) Carmalt C.J., Cowley A.H., *Adv. Inorg. Chem.* 2000, 50, 1.

(33) Arduengo A.J. III, Dias H.V.R., Harlow L., Kline M., *J. Am. Chem. Soc.* 1992, 114, 5530.

(34) Sundermann A., Reiher M., Schoeller W.W., *Eur. J. Inorg. Chem.*, 1998, 305.

(35) Baker R.J., Farley R.D., Jones C., Kloth M., Murphy D.M., *J. Chem. Soc., Dalton Trans.*, 2002, 3844.

(36) Dapprich S., Frenking G., *J. Phys. Chem.* 1995, 99, 9352.

(37) Dickinson A., Ph.D. Thesis, Cardiff University, 2002 (unpublished results).

Appendix 1 - Crystallographic parameters of the new compounds in this work

Spiro-[(η^5-C_5H_5)Fe(CO)$_2$BO$_2$(CH$_2$)$_2$]$_2$C ***(4d, chapter 2)***

Empirical formula	$C_{19}H_{18}B_2Fe_2O_8$
Formula weight	507.66
Temperature	120(2) K
Wavelength	0.71073 Å
Crystal system	Monoclinic
Space group	C2/c
Unit cell dimensions	a = 26.798(2) Å
	b = 6.0907(6) Å β = 108.968(3)°
	c = 12.6373(15) Å
Volume	1950.7(3) Å^3
Z	4
Density (calculated)	1.729 Mg / m^3
Absorption coefficient	1.534 mm^{-1}
F(000)	1032
Crystal	Colourless Plate
Crystal size	0.15 × 0.15 × 0.02 mm^3
θ **range for data collection**	3.22 – 25.01°
Index ranges	$-31 \le h \le 30$, $-6 \le k \le 6$, $-15 \le l \le 13$
Reflections collected	4641
Independent reflections	1649 [R_{int} = 0.0580]
Completeness to θ = 25.01°	95.6 %
Max. and min. transmission	0.9700 and 0.8025
Refinement method	Full-matrix least-squares on F^2
Data / restraints / parameters	1649 / 0 / 141
Goodness-of-fit on F^2	1.089
Final R **indices** [$F^2 > 2\sigma(F^2)$]	$R1$ = 0.0427, $wR2$ = 0.0886
R **indices (all data)**	$R1$ = 0.0732, $wR2$ = 0.1054
Largest diff. peak and hole	0.474 and –0.412 e Å^{-3}

(η^5-C_5Me_5)Fe(CO)$_2$ [B(tmg)] (7, chapter 2)

Empirical formula	$C_{15}H_{21}BFeO_4$	
Formula weight	331.98	
Temperature	180(2) K	
Wavelength	0.71073 Å	
Crystal system	Monoclinic	
Space group	P 21/n	
Unit cell dimensions	a = 13.1516(3) Å	α= 90°.
	b = 8.9576(2) Å	β= 105.1640(10)°.
	c = 14.0546(4) Å	γ = 90°.
Volume	1598.08(7) Å^3	
Z	4	
Density (calculated)	1.380 Mg/m^3	
Absorption coefficient	0.954 mm^{-1}	
F(000)	696	
Crystal size	0.43 x 0.30 x 0.10 mm^3	
Theta range for data collection	2.96 to 27.49°.	
Index ranges	-16<=h<=16, -11<=k<=11, -12<=l<=18	
Reflections collected	18085	
Independent reflections	3649 [R(int) = 0.0990]	
Completeness to theta = 27.49°	99.5 %	
Absorption correction	Semi-empirical from equivalents	
Max. and min. transmission	0.9106 and 0.6844	
Refinement method	Full-matrix least-squares on F^2	
Data / restraints / parameters	3649 / 0 / 191	
Goodness-of-fit on F^2	1.072	
Final R indices [I>2sigma(I)]	R1 = 0.0589, wR2 = 0.1483	
R indices (all data)	R1 = 0.0989, wR2 = 0.1677	
Extinction coefficient	0.0105(19)	
Largest diff. peak and hole	1.084 and -0.682 e.Å^{-3}	

BCl_3.THF (chapters 2 and 3)

Empirical formula	$C_4 H_8 B Cl_3 O$	
Formula weight	189.26	
Temperature	100(2) K	
Wavelength	0.71073 Å	
Crystal system	Monoclinic	
Space group	P21/n	
Unit cell dimensions	a = 7.6075(4) Å	α= 90°.
	b = 10.0398(5) Å	β= 102.10°.
	c = 10.4761(3) Å	γ= 90°.
Volume	782.38(6) $Å^3$	
Z	4	
Density (calculated)	1.607 Mg/m^3	
Absorption coefficient	1.086 mm^{-1}	
F(000)	384	
Crystal size	0.20 x 0.20 x 0.15 mm^3	
Theta range for data collection	2.84 to 27.49°.	
Index ranges	-9<=h<=8, -11<=k<=13, -13<=l<=13	
Reflections collected	4915	
Independent reflections	1774 [R(int) = 0.0405]	
Completeness to theta = 27.49°	99.2 %	
Absorption correction	Scalepack	
Max. and min. transmission	0.8541 and 0.8121	
Refinement method	Full-matrix least-squares on F^2	
Data / restraints / parameters	1774 / 0 / 83	
Goodness-of-fit on F^2	1.075	
Final R indices [I>2sigma(I)]	R1 = 0.0235, wR2 = 0.0548	
R indices (all data)	R1 = 0.0274, wR2 = 0.0559	
Extinction coefficient	0.007(2)	
Largest diff. peak and hole	0.387 and -0.351 $e.Å^{-3}$	

(η^5-C_5H_5)Fe(CO)$_2$[B(OMes)Cl] (13, chapter 3)

Empirical formula	$C_{16}H_{16}BClFeO_3$	
Formula weight	358.40	
Temperature	180(2) K	
Wavelength	0.71073 Å	
Crystal system	Triclinic	
Space group	P -1	
Unit cell dimensions	a = 7.8325(3) Å	α= 81.631(2)°.
	b = 8.0671(3) Å	β= 81.424(2)°.
	c = 13.6886(6) Å	γ= 75.958(2)°.
Volume	824.29(6) Å^3	
Z	2	
Density (calculated)	1.444 Mg/m^3	
Absorption coefficient	1.084 mm^{-1}	
F(000)	368	
Crystal size	0.23 x 0.23 x 0.05 mm^3	
Theta range for data collection	2.93 to 27.49°.	
Index ranges	-9<=h<=10, -10<=k<=10, -16<=l<=17	
Reflections collected	13020	
Independent reflections	3685 [R(int) = 0.0678]	
Completeness to theta = 27.49°	97.4 %	
Absorption correction	Semi-empirical from equivalents	
Max. and min. transmission	0.9478 and 0.7887	
Refinement method	Full-matrix least-squares on F^2	
Data / restraints / parameters	3685 / 0 / 202	
Goodness-of-fit on F^2	1.160	
Final R indices [I>2sigma(I)]	R1 = 0.0516, wR2 = 0.1113	
R indices (all data)	R1 = 0.0913, wR2 = 0.1359	
Largest diff. peak and hole	0.518 and -0.588 e.Å^{-3}	

(η^5-C_5Me_5)Fe(CO)$_2$[B(OMes)Cl] (14, chapter 3)

Empirical formula	$C_{21}H_{26}BClFeO_3$	
Formula weight	428.53	
Temperature	150(2) K	
Wavelength	0.71073 Å	
Crystal system	Triclinic	
Space group	P -1	
Unit cell dimensions	a = 8.3300(3) Å	α= 75.677(2)°.
	b = 8.7470(3) Å	β= 89.5730(10)°.
	c = 14.5400(5) Å	γ= 88.4810(10)°.
Volume	1026.13(6) Å^3	
Z	2	
Density (calculated)	1.387 Mg/m^3	
Absorption coefficient	0.883 mm^{-1}	
F(000)	448	
Crystal size	0.20 x 0.20 x 0.05 mm^3	
Theta range for data collection	3.10 to 27.40°.	
Index ranges	-10<=h<=10, -10<=k<=11, -18<=l<=18	
Reflections collected	15859	
Independent reflections	4575 [R(int) = 0.0912]	
Completeness to theta = 27.40°	98.0 %	
Absorption correction	Semi-empirical from equivalents	
Max. and min. transmission	0.9572 and 0.8432	
Refinement method	Full-matrix least-squares on F^2	
Data / restraints / parameters	4575 / 0 / 252	
Goodness-of-fit on F^2	1.027	
Final R indices [I>2sigma(I)]	R1 = 0.0548, wR2 = 0.0987	
R indices (all data)	R1 = 0.1143, wR2 = 0.1185	
Largest diff. peak and hole	0.392 and -0.650 e.Å^{-3}	

(η^5-C_5H_5)Fe(CO)$_2$[B(OMes)(SPh)] (17, chapter 3)

Empirical formula	$C_{22}H_{21}BFeO_3S$	
Formula weight	432.11	
Temperature	180(2) K	
Wavelength	0.71073 Å	
Crystal system	Monoclinic	
Space group	P 21/n	
Unit cell dimensions	a = 14.4401(4) Å	α= 90°.
	b = 9.7496(3) Å	β= 91.901(1)°.
	c = 14.5657(6) Å	γ= 90°.
Volume	2049.51(12) Å^3	
Z	4	
Density (calculated)	1.400 Mg/m^3	
Absorption coefficient	0.857 mm^{-1}	
F(000)	896	
Crystal size	0.35 x 0.12 x 0.10 mm^3	
Theta range for data collection	3.49 to 27.43°.	
Index ranges	-18<=h<=18, -9<=k<=12, -18<=l<=18	
Reflections collected	12489	
Independent reflections	4272 [R(int) = 0.0699]	
Completeness to theta = 25.00°	99.5 %	
Absorption correction	Semi-empirical from equivalents	
Max. and min. transmission	0.9192 and 0.7535	
Refinement method	Full-matrix least-squares on F^2	
Data / restraints / parameters	4272 / 0 / 253	
Goodness-of-fit on F^2	1.037	
Final R indices [I>2sigma(I)]	R1 = 0.0534, wR2 = 0.1088	
R indices (all data)	R1 = 0.1027, wR2 = 0.1295	
Largest diff. peak and hole	0.398 and -0.520 e.Å^{-3}	

Cis-$Pt(PPh_3)_2Cl_2$. 3 $CHCl_3$ (section 4.3.1)

Empirical formula	$C_{39}H_{32}Cl_{11}P_2Pt$	
Formula weight	1147.63	
Temperature	150(2) K	
Wavelength	0.71073 Å	
Crystal system	Monoclinic	
Space group	P 21/n	
Unit cell dimensions	a = 13.4453(2) Å	α= 90°.
	b = 15.2744(3) Å	β= 91.1660(10)°.
	c = 21.5180(4) Å	γ = 90°.
Volume	4418.21(14) $Å^3$	
Z	4	
Density (calculated)	1.725 Mg/m^3	
Absorption coefficient	3.942 mm^{-1}	
F(000)	2244	
Crystal size	0.20 x 0.18 x 0.15 mm^3	
Theta range for data collection	3.03 to 27.49°.	
Index ranges	-17<=h<=16, -19<=k<=19, -23<=l<=27	
Reflections collected	53201	
Independent reflections	9996 [R(int) = 0.1259]	
Completeness to theta = 27.49°	98.5 %	
Absorption correction	Semi-empirical from equivalents	
Max. and min. transmission	0.5893 and 0.5061	
Refinement method	Full-matrix least-squares on F^2	
Data / restraints / parameters	9996 / 18 / 496	
Goodness-of-fit on F^2	1.051	
Final R indices [I>2sigma(I)]	R1 = 0.0588, wR2 = 0.1137	
R indices (all data)	R1 = 0.1288, wR2 = 0.1355	
Largest diff. peak and hole	2.454 and -1.383 $e.Å^{-3}$	

"Linking of metal centers through boryl ligands: synthesis, spectroscopic and structural characterisation of symmetrically bridged boryl complexes"
Aldridge S., Calder R.J., Rossin A., Dickinson A.A., Willock D.J., Jones C., Evans D.J., Steed J.W., Light M.E., Coles S.J., Hursthouse M.B., *J. Chem. Soc., Dalton Trans.* 2002, 2020.

"Carbonyl analogues? Analysis of Fe-E (E=B, Al, Ga) bonding in cationic terminal diyl complexes by Density Functional Theory"
Aldridge S., Rossin A., Coombs D.L., Willock D.J., *Dalton Trans.* 2004, 2649.

"Fe=B double bonds: synthetic, structural and reaction chemistry of cationic terminal borylene complexes"
Coombs D.L., Aldridge S., Rossin A., Jones C., Willock D.J., *Organometallics* 2004, 23, 2911.

"Fe-Ga multiple bonding? Synthesis, spectroscopic and structural characterization of a transition metal complex containing a cationic two-coordinate gallium centre"
Bunn N.R., Aldridge S., Coombs D.L., Rossin A., Willock D.J., Jones C., Ooi L., *Chem. Comm.* 2004, 1732.

"$(\eta^5\text{-}C_5Me_5)Fe(CO)_2(BOCH_2CH_2CH_2O)$: an organoiron complex containing the (trimethylene glycolato)boryl ligand"
Rossin A., Aldridge S. , Ooi L., *Appl. Organomet. Chem.* 2004, in press.

"Heteroatom stabilised boryl complexes: substitution and abstraction chemistry"
Rossin A., Aldridge S., Coombs D.L., Ooi L., *Organometallics* 2004, submitted.

"Substitution, abstraction and addition chemistry of gallyl and gallylene complexes"
Bunn N.R., Aldridge S., Coombs D.L., Rossin A., Jones C., Willock D.J., *Organometallics* 2004, submitted.